NEW METHODS TO EVALUATE THE EFFECTS OF FOULING IN PROCESS CHROMATOGRAPHY

A thesis submitted to the University of London

for the degree of

DOCTOR OF PHILOSOPHY

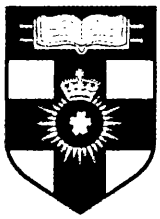

by

Sun Chau Siu

The Advanced Centre for Biochemical Engineering
Department of Biochemical Engineering
University College London
Torrington Place
London WC1E 7JE
United Kingdom

August 2005

ProQuest LLC
789 East Eisenhower Parkway
P.O. Box 1346
Ann Arbor, MI 48106-1346

ABSTRACT

This thesis examines new approaches to evaluate the effects of fouling on process chromatography. Fouling can have a serious, negative impact on the performance of chromatography and considerable effort is normally spent to prevent fouling species reaching the column, or in developing clean-in-place (CIP) protocols of ever increasing complexity to mitigate their effects. Despite this, the knowledge of chromatographic fouling often seems anecdotal, with only a few systematic investigations currently reported in literature. Furthermore, conventional approaches to investigate chromatographic fouling only provide an overall indication of their state. New approaches to investigate fouling at increasingly fine detail are studied in this thesis and provide valuable insights to the mechanism of fouling.

At the whole-column level, the method of frontal analysis was used to determine the effects of fouling a packed bed column (DEAE Sepharose FF) with yeast homogenate. The shape and position of breakthrough curves generated by frontal analysis were used to quantitatively assess the impact of fouling on binding capacity and to qualitatively infer the overall changes in mass transfer properties. In particular, the effects of solids particulate and different modes of applying the fouling stream to the column were examined. Breakthrough curve analysis was also used to investigate the effectiveness of a rigorous CIP procedure in restoring the characteristics of a fouled column.

An extended reverse-flow technique using an acetone tracer was then developed to quantify the dispersive effects of fouling on defined axial sections within a packed bed column, giving more than an overall indication of the fouling condition. The influence of column diameter, bed length and two different header designs on the extent of fouling were examined. The technique allows the band broadening effects due to reversible macroscopic factors, such as flow maldistribution in the flow distributor and inside the packed bed caused by packing heterogeneity, to be separated from irreversible microscopic factors, such as intraparticle diffusion, external fluid film mass transfer and interparticle axial dispersion. It was shown to be a simple, non-destructive method for investigating chromatographic fouling at an intra-column level.

Finally, confocal scanning laser microscopy (CSLM) was proven to be a powerful technique to directly visualise fouling at a single-bead level. A particularly aggressive fouling stream of partially clarified *E. coli* homogenate was used to challenge an anion exchange resin (Q Sepharose FF) in a finite bath, and subsequently in a packed structure under flow conditions. The fouling caused by the material was visualised by fluorescently labelling DNA and host cell proteins in the fouling stream and by measuring the binding capacity and uptake rate for a fluorescently-labelled test protein, BSA. The use of CSLM also allowed the applications of various CIP procedures to be visually followed. The competitive adsorption of whole cells or cell debris and DNA to Q Sepharose FF has also been visualised. Confocal images obtained provide insights to the spatial distribution of key foulant types within a single bead.

This thesis concludes with recommendations for future work which will seek to extend the analysis to situations where fouling occurs in a flow situation by the design of appropriate flow cells and methods of analysis.

To my parents

Dr. T.K. Siu and L.Y. Fong

Perfection is perfectly simple;

fouling things up requires true skill.

– Doug Horton

ACKNOWLEDGEMENTS

On September 24, 2001, my doctoral research formally started. Coming back to academic life after a long period in industry was not an easy task but the decision to come back to UCL has proved to be most fortunate. The PhD process is a complex one that entails an oddly satisfying mixture of frustration and joy. Being in a powerhouse for Biochemical Engineering has certainly made the doctorate journey more inspiring and challenging. Many people have helped me in many ways throughout these past years. The following are friends and colleagues whom I would like to personally thank for their contribution to the success of my research. I am sure there are many others who have helped in other ways that I have forgot to mention. Please pardon the omission and know that I also thank you.

Firstly, I would like to express my deepest gratitude to my supervisor, Professor Nigel J. Titchener-Hooker, who has been truly inspirational. His brilliant knowledge and wisdom have guided me through many difficulties encountered during my research.

For technical and moral support I wish to thank the following people from the department: Jean Aucamp, Dr. Helen Baldascini, BB, Gerard Chan, Sorwar Choudhury, Aloke Dey-Chowdhury, Dr. Roeb García-Arrazola, Alex Graham, Christine Ingram, Jonathan Liau, Jennifer O'Shitu, Victor Topoyassakul and Hekarl Uzir.

Special thanks to Rolf Hjorth and his colleagues at GE Healthcare for their invaluable discussions and hospitality while I was conducting some confocal microscopy work at their company in Uppsala, Sweden.

With great appreciation, I acknowledge my old friends and colleagues at Aventis Pasteur (now Sanofi Pasteur) in Toronto, Canada, especially Dennis Yao, Dr. Teow Koh and Frank Lau who had been superb mentors during my time there before coming to UCL.

Special mention must be made of Vienne Chow for her endless encouragement and patience.

My list would not be complete without thanking my parents, my brother and my sister for their infallible support. All would not have been possible without them.

London – Hong Kong 2005

TABLE OF CONTENTS

LIST OF FIGURES

LIST OF TABLES

1 INTRODUCTION

Process chromatography in the biopharmaceutical industry is concerned with purifying bio-molecules to be efficacious, safe and in abundance for human diagnostic or therapeutic purposes. Due to its excellent resolving power, it continues to be the dominant purification technique in downstream processing. Indeed in order to meet the stringent and exact purification specifications required by regulatory authorities, it is rare to find a bioprocess design that does not incorporate at least one chromatography step and more often at least two. Such requirements place an increasing demand on biochemical engineers to design more efficient, reliable and scalable chromatographic steps. Predictions of chromatography performance are currently rather limited and often require rigorous mathematical analysis (Golshan and Guiochon, 1992; Guiochon et al., 1994; Gu, 1995). These only consider scenarios concerning pure solutes or a mixture of pure solutes, and therefore, may not truly reflect the performance experienced with realistic process streams which contain fouling species that can further complicate the mechanisms governing chromatographic separations. The same criticism may be made at most chromatographic investigations reported in literature. As a result, biochemical engineers often rely on their own experience when trouble-shooting, optimising or scaling up chromatographic processes.

Fouling is a fundamental problem in process chromatography. Many components in process streams contain material that will foul chromatography columns and cause a range of detrimental effects on the separation performance and economics of the chromatographic process step. An important challenge in process design is, therefore, to select the best means of pre-treatment to use so as to minimise fouling as well as designing effective clean-in-place (CIP) protocols to remove significant foulants from the matrix. Overall, though, the knowledge on fouling of chromatography columns often seems anecdotal, with only a few systematic investigations reported in the literature. The following sections will attempt to define chromatographic fouling by highlighting the key foulant types and the effects of fouling as well as discussing relevant process validation and cleaning issues. The final section of this chapter will set out the structure of the remaining chapters of this thesis.

1.1 DEFINITION OF FOULING

Chromatographic fouling may be defined as deleterious effects of process materials on the operating efficiency of chromatographic operation. It is important to realise that fouling may not only have an immediate impact on the chromatographic separation but also a long-term impact on the integrity of the chromatographic matrix. The latter is often time-dependent and process-specific as a result of repeated or prolonged exposure of the matrix to fouling material in the process stream.

1.2 FOULING MATERIAL

A number of components in process feed streams to chromatography columns may cause fouling (Table 1-1).

Particulates/colloids
Cells (> 1 μm)
Cell debris/fragments (< 1 μm)
Protein precipitates (< 1 μm)
Antifoam (surfactant polymers)
Dissolved components
Low molecular mass molecules (MW < 1000)
Amino acids, vitamins, nucleic acids, glucose, metal ions
Buffer salts, additives etc.
Colour and aroma substances
High molecular mass molecules (MW >> 1000)
Proteins, lipoproteins
Polynucleotides (mainly DNA)
Endotoxins

***Table 1-1**: Composition of a typical fermentation or cell culture broth [adapted from Anspach et al. (1999)].*

A qualitative analysis of the components of fermentation broths that can give rise to chromatographic fouling have been presented by Pirotta (1985) and Anspach et al. (1999). Colloidal material such as lipids, cell debris and carbohydrates, as well as soluble components such as contaminant protein and nucleic acids can give rise to this phenomenon. The consequences may include changes in binding capacity (Staby et al., 1998) and separation efficiencies as well as increased pressure drop and loss of bed integrity (Aguilera Soriano et al., 1997).

Brief descriptions of a number of foulants – namely proteins, nucleic acids, lipids, cells, and metal ions – that are commonly found in process feed material to chromatography columns are given below. The list is by no means exhaustive as the composition of a process stream is dependent upon the fermentation/cell culture and the processing prior to the chromatography step.

1.2.1 Proteins

Proteins are among the most abundant biological macromolecules and also extremely versatile in their biological functions, allowing them to be the primary drug class for biologics. They are macromolecules carrying both charged, hydrophilic amino acids and hydrophobic amino acids. Given the right conditions, their multifaceted chemistry allows them to adsorb to all the commonly used matrices. In eukaryotic cells, post-translational modification of proteins gives rise to glycoproteins and lipoproteins. Such modifications are generally on the surface of the tertiary protein structure, and thus may be expected to play a significant role in the interaction with the chromatographic matrix.

Besides the target protein, the process stream may contain proteins from the media components and, especially after cell disruption, host cell proteins (HCPs); both are potentially important fouling species. For example, albumin is often a key media-derived contaminant present in the feed stream during monoclonal antibody purification. Linden et al. (1999) visualised the competitive adsorption of pure human IgG and BSA to an affinity adsorption resin and a cation exchange resin using confocal scanning laser microscopy. It was shown that in equilibrium BSA and IgG were evenly

distributed throughout the affinity adsorbent. However, in the ion exchange adsorbent BSA would bind to the outer regions while human IgG would be displaced to the internal regions. This adsorption pattern contradicts conventional theoretical models of an equal equilibrium distribution of all proteins adsorbed. Importantly, knowledge of the competitive binding kinetics of the target protein and fouling protein was used to design the appropriate contact time of protein mixture and adsorbent to maximise the selectivity.

It is important to remember that the target protein itself may be a potential foulant and cause time-dependent deterioration in column performance under repeated exposure of the matrix to the protein. Tice et al. (1987) studied the effects of repeated loading of a large sample mass of either pure ovalbumin or a pure mixture of ovalbumin and conalbumin on the column lifetime and performance. The central conclusion was that the useful lifetime of a preparative column operated in the non-linear mode is more likely to be determined by irreversibly-adsorbed contaminants then the chemical stability of the sorbent. Additionally, the type of support matrix has only little influence on the column life.

In bioprocess research, much of the work on protein fouling has been done in relevance to membrane filtration. This has been reviewed by Belfort et al. (1994) and Marshall et al. (1993). The mechanisms of protein fouling were studied by Kelly and Zydney (1997). They suggested that proteins in solution can bind to already-adsorbed protein deposits on ultrafiltration membranes through intermolecular disulphide bond formation or hydrophobic interactions, giving rise to secondary fouling. The wider implication of these findings is that the fouling can involve complex foulant-foulant interactions leading to secondary or even multi-layered adsorption. It is reasonable to assume that such mechanisms may also exist in chromatographic fouling.

1.2.2 Nucleic acids

The nucleic acids – deoxyribonucleic acid (DNA) and ribonucleic acid (RNA) – are polyanionic polymers. They can be present in large amounts in the process stream, especially after cell disruption. In conditions of pH > 3 they bind

strongly to anion exchange matrices and so anion exchange chromatography, such as using Q Sepharose FF, are commonly employed to remove contaminant nucleic acids from the process feed stream or used to purify plasmid DNA (Diogo et al., 2005).

In terms of size, nucleic acids are considerably larger than proteins. For example, plasmids (typically < 30 kbp) have a molecular weight 100 to 500 times higher than the average protein. Their large, long structure prevents them from penetrating chromatography beads, thus they bind as a layer to the exterior of the bead (Prazeres et al., 1998; Ljunglof et al., 1999). Genomic DNA (typically 13 – 115 kbp) is usually larger than plasmids.

DNA does not only cause fouling by binding to active sites on the surface of the bead, it also increases dramatically the viscosity of the feed stream. An increased viscosity can lead to an increased pressure drop which may ultimately result in bed compression in packed beds (cf. Section 1.3.4). Feed streams with very high viscosities (> 50 mPa.s) can cause channelling and poor product recovery in expanded bed adsorption (EBA) (Barnfield Frej et al., 1994). The viscosity of the feed stream is often reduced before loading onto an EBA column by dilution and by degrading the nucleic acids with DNase I. Further homogenisation can also reduce the viscosity as DNA is sensitive to shear (Levy et al., 1999).

1.2.3 Lipids

Lipids are a chemically diverse group of compounds that play an important role in biological functions. Fats and oils are the main form of energy storage in many organisms, and phospholipids and sterols make up about half the mass of biological membranes. Their structures can range from amphoteric molecules with hydrophilic heads and hydrophobic tails, to highly hydrophobic steroids. However, the common feature of all lipids is their insolubility in water.

Their structure allows them to interact with chromatographic matrices through hydrophobic and hydrophilic areas. Their smaller molecular size, as compared to proteins, may result in greater diffusivity and access to more of the matrix bead.

Furthermore, biological lipids regularly form bi-layers into which protein can attach; such foulant-foulant interactions further complicates the fouling mechanism.

1.2.4 Whole cells and cell debris

Whole cells and cell debris carry a net negative charge which allows them to bind to chromatographic matrices by electrostatic forces (Shaeiwitz et al., 1989; Feuser et al., 1999; Viloria-Cols et al., 2004). Mannose-containing glycoproteins (mannoproteins) are a major component of cell walls, and it is the phosphate groups in mannoproteins that generate the negative charge normally associated with all microorganisms. Cell debris also carries a negative charge since cell wall fragments retain the basic intact cell wall structure with phosphate groups. Negatively charged cell wall fragments can bind protein under appropriate pH conditions. This was demonstrated by Shaeiwitz et al. (1989) with cell wall debris of *Saccharomyces cerevisiae*.

Feuser et al. (1999) showed that cells and cell debris interact with anion exchange adsorbent to a much greater extent than with cation exchange and affinity adsorbents. Furthermore, they showed that the type of cell is an important factor to the tendency of binding. *E. coli* cells were shown to have the lowest tendency of binding to all matrices while hybridoma cells attached to all the adsorbents except Protein A affinity matrices.

Viloria-Cols et al. (2004) successfully reduced the binding of *E. coli*, *S. cerevisiae* and *L. casei* to an anion exchange resin by coating the resin with agarose. Scanning electron microscopy (SEM) was used to visualise the amount of cell binding before and after coating with agarose. However, the effect of coating the resin on the separation performance was not investigated but proposed as necessary future work.

Chromatographic fouling from whole cells or cell debris is of particular importance to EBA (Barnfield Frej et al., 1994; Feuser et al., 1999; Fernandez-Lahore et al., 1999; Anspach et al., 1999; Smith et al., 2002). Changes in the hydrodynamics of EBA can readily occur in the presence of moderate concentrations of biomass due to

the interaction of biomass and adsorbent (Fernandez-Lahore et al., 1999). However, they may also foul packed bed columns that are employed early in the downstream process train if an appropriate filtration step (e.g., 0.2 μm microfiltration) is not used to clarify the process stream before passing it for downstream processing.

1.2.5 Metal ions

Transition metal ions are largely introduced into the process stream from fermentation media components. An example of the wide range of metal ions added to fermentation broths is given in Table 1-2. Other potential sources of contamination include: impurities in process chemicals, ions that have leached from process equipment and impurities found in process water. However, the last source seems unlikely if high quality water such as water-for-injection (WFI) is used.

Compound	Concentration (g/L)
$CaCl_2 \cdot H_2O$	5
$ZnSO_4 \cdot 7H_2O$	2.46
$MnSO_4 \cdot 4H_2O$	2
$CuSO_4 \cdot 5H_2O$	0.5
$CoSO_4 \cdot 7H_2O$	0.427
$FeCl_3 \cdot 6H_2O$	9.67
H_3BO_3	0.03
$NaMoO_4 \cdot 2H_2O$	0.024

***Table 1-2**: Example of metal compounds added to an E. coli fermentation [from Garcia-Arrazola et al. (2005)].*

Metal impurities in the process stream have been reported to cause progressive discoloration of ceramic hydroxyapatite as the number of chromatographic cycles increased (Shepard et al., 2000). Elemental analysis by inductively coupled plasma optical emission spectrometry (ICO-OES) suggested that the metal ions Mn, Fe, Al, Cd, Ba, Cr and Sn may have caused the discoloration. Regeneration of hydroxyapatite using 0.5 M sodium phosphate followed by 0.5 M sodium hydroxide was unable to remove the metal ions but chromatographic performance did not seemed to be affected by fouling even after 8 -12 loading cycles.

The binding of metal ions to hydroxyapatite have been reported in other studies but for protein purification by the principle of immobilised metal-ion affinity chromatography (IMAC) (Nordstrom et al., 1999; Suen et al., 2004). In fact, IMAC is widely known to be effective for purifying polyhistidine-tagged proteins (Hochuli et al., 1987). Natural proteins can also bind to highly activated IMAC matrices and even in lowly activated supports mild adsorption of large proteins is observed (Pessela et al., 2004). In the context of fouling, binding of metal ions to a chromatographic matrix may, therefore, give rise to further unspecific binding of proteins which may have an effect on the degree of purification.

1.3 EFFECTS OF FOULING

1.3.1 Mass transfer limitations

The kinetic mechanisms underlying chromatography are reasonably well understood and discussed extensively in the literature for fresh chromatographic matrices (Ruthven, 1984; Guiochon, 1994). The adsorption of a solute to a chromatographic bead is governed by three processes: film mass transfer, pore diffusion and adsorption kinetics. (Obviously, adsorption kinetics does not apply in size exclusion chromatography). This adsorption process is illustrated in a simplified fashion in Figure 1-1. The matrix may be visualised as a packed bed of porous beads, so that the total area for adsorption includes both the outer bead surface, and the internal area of the pores. For a solute molecule to be absorbed, two important resistances to mass transfer need to be overcome. Firstly, the molecule must traverse the laminar fluid sub-layer surrounding the bead (the external fluid film resistance).

Having reached the bead surface, unbound molecules must then overcome a resistance to internal diffusion within the bead itself before binding to active sites. The overall rate of adsorption is always controlled by mass or heat transfer resistances, rather than by the intrinsic adsorption kinetics.

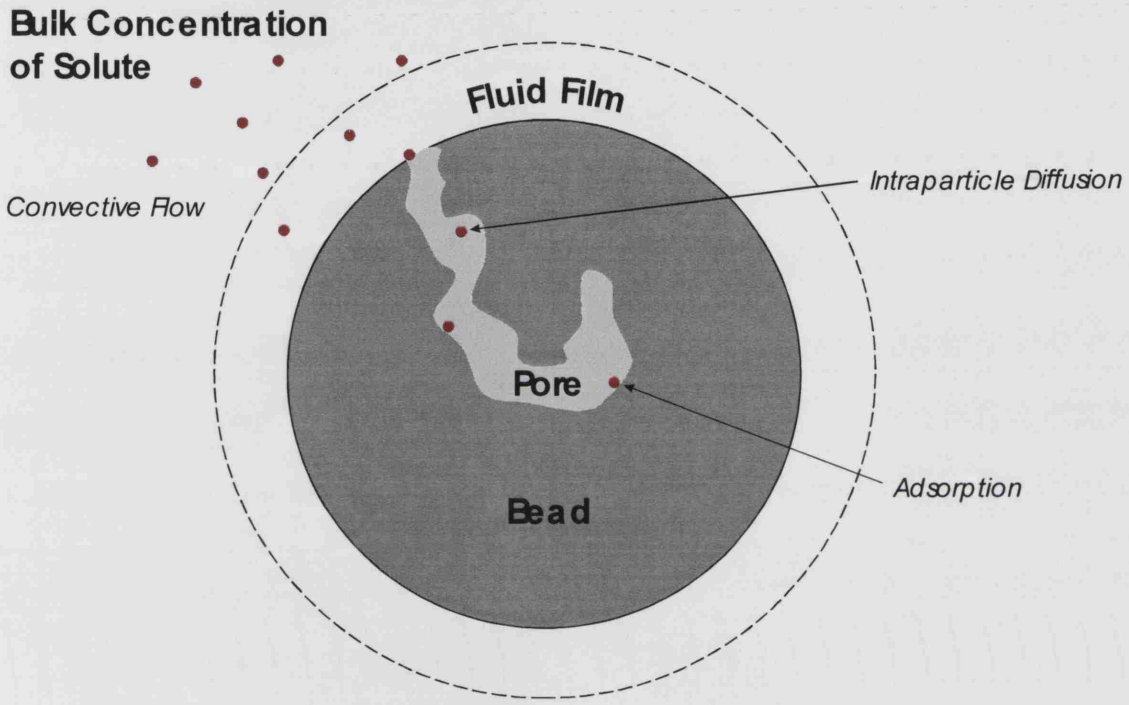

***Figure 1-1**: Transport processes in liquid chromatography.*

The kinetic mechanisms are presumably far more complex in a scenario where fouling exists. Colloidal material may obstruct bead pores, and for large absorbents, narrowing of bead pores due to the presence of bound species has also been suggested as a limiting mechanism to intraparticle diffusion (Linden et al., 1999). Specific binding of some fouling species to adsorption sites both on the bead surface (Feuser et al., 1999; Viloria-Cols et al., 2004) and internal to the pore could alter the capacity of the adsorbent for the target protein and affect the position of the breakthrough curve (Staby et al., 1998).

The accurate modeling of fouled chromatographic processes can prove to be a challenging task (cf. Chapter 2) which reflects the multitude and complexity of the

phenomenon. Fundamental research in mass transfer has led to complex non-linear mathematical models that describe the mass transfer resistances in packed beds with porous adsorbent particles (Liapis, 1990; Carta et al. 1992; Heeter and Liapis, 1996; Meyers and Liapis, 1998 and 1999). However, these models are only relevant to pure single-solute systems and the existing models can not be postulated as being fit under fouling conditions. It must be proved by *a priori* or *a posteriori* methods that the mathematical expressions do indeed represent the physics and chemistry in a fouled system. Clearly, a greater understanding of the detailed mechanisms of fouling is needed before accurate models can be derived, and this definitely presents a challenge to researchers in chromatography.

1.3.2 Capacity and Breakthrough

Direct and systematic investigations on the effect of a realistic process stream on the performance of packed bed chromatography are scarce. The paper by Stably et al. (1998) is noteworthy in that it points out the importance of investigating the effects of fouling on important performance parameters under realistic process conditions.

Staby et al. (1998) confirmed that competitive adsorption of the target protein with fouling species in the process stream will most certainly reduce the binding capacity of the chromatographic matrix. They compared the static and dynamic binding capacities on various ion exchangers of proteins and peptides in culture medium and in pure state. Experiments were carried out in finite bath and packed bed modes. The same pH, flow and residence time, conductivity, temperature, protein concentration, scale and buffers were used in both cases to maintain a fair comparison. As expected, they showed that both the static and dynamic capacity significantly reduced when present in culture/fermentation medium. Moreover, the binding capacity of the target protein/peptide was shown to increase with the purity of the component in the culture/fermentation broth. The breakthrough curves obtained in the presence of culture/fermentation medium was noticeably less sigmoidal-shaped than that for pure components.

1.3.3 Packing and flow heterogeneity

Packing and flow heterogeneity have long been known to cause band broadening and reduced separation efficiency (Giddings, 1965; Guiochon et al., 1994). A number of studies have investigated the effects of packing and flow heterogeneity in non-fouled columns using a variety of experimental techniques that measure band broadening (Coq et al., 1979; Klawiter et al., 1982; Kaminski et al., 1982; Kaminski, 1992; Moscariello et al., 2001;Williams et al., 2002) including laser anemometry (Volkov et al., 1978), magnetic resonance imaging (Ilg et al., 1990; Bayer et al., 1995; Tallarek et al., 1995 and 1998; Yuan et al., 1999), sophisticated on-line sensors (Farkas et al., 1994, 1996 and 1997), direct visualisation in the transport system with refractive index (Shalliker et al., 1999, 2000a, 200b and 2003; Broyles et al., 2000), and ultrasound (Hofmann, 2003).

It is evident that the packing of chromatographic columns are heterogeneous with an axial and radial distribution of the packing density which is largely due to the "wall effect" (Guiochon et al., 1997; Farkes et al., 1997; Shalliker et al., 2003). Theoretical calculations have shown that significant radial heterogeneity can cause marked degradation in column performance (Yun and Guiochon, 1994 and 1996). Such findings render the commonly cited plug flow model (Guiochon et al., 1994) as being too idealistic. Furthermore, different packing methods and conditions result in beds that have different structural characteristics (Kaminski et al., 1982; Klawiter et al., 1982; Guiochon et al., 1997). The packing of industrial-scale columns was investigated by Moscariello et al. (2001) and Williams et al. (2002). The first group showed, using the reverse-flow technique, that a practically homogenous bed packing in the axial direction was possible in a large-scale (44 cm diameter) column when packed using an automated slurry packing skid.

Recently, computational fluid dynamics (CFD) was used to assess the influence of packing heterogeneity and porosity on column performance (Billen et al., 2005). Simplified two-dimensional (2D) mimics of real packed bed and monolithic columns were used, where the beads in the simulated packing arrangements were not allowed to touch neighbouring beads in order to simplify the simulation of different packing arrangements. As a consequence, the pore size in the 2D mimic was slightly lower than that of a real packed bed. Also, the pore connectivity number was different: two in 2D

versus three in a 3D packed bed and three or more in a monolith (Meyers and Liapis, 1998). Despite these differences, it was assumed that the band broadening effects could be well represented with the 2D simulation since the major sources of band broadening are caused by the existence of different velocity zones and by the slowness of the radial re-equilibrium diffusion process. Their simulations showed that the presence of preferential flow due to heterogeneous packing can lead to a relatively large increase in band broadening despite a reduction in the flow resistance. Therefore, the presence of preferential flow paths always leads to an overall deterioration of the separation performance.

Additional flow heterogeneity in the column bed can also arise from non-uniform flow distribution from the column headers. This effect occurs in the ends of the packed bed until the radial gradients in axial velocity are diminished. Shalliker et al. (1999 and 2000a) showed that the inlet configuration dramatically influenced the flow distribution along the column. For small-scale columns of 1.7 cm diameter, they found that the radial flow distribution was nearly homogenous for column with headers having only a frit but not for those having also a distributor (Figure 1-2). More importantly, the frit porosity should be matched to the particle size of the bed packing. In their example, 10 μm frits produced better band profiles than 2 μm frits for packing material with an average size of 21 μm.

Quantitative information on header designs is scarce but Yuan et al. (1999) recently attempted to provide a rational basis for header design. They confirmed, using magnetic resonance imaging (MRI), that significant maldistribution is introduced by non-uniform flow in headers. Adequate flow distribution becomes more difficult as the length:diameter ratio decreases, and this warrants more careful designing of column headers.

A possible effect of fouling is packing and flow heterogeneity. This may be particularly true for loading fouling material that contains colloids, cell debris and lipids. These materials can disrupt the bed packing as well as clog column headers and ultimately cause preferential flow channels and poor flow distribution. As just described, these phenomena can have a great impact on the separation performance. Only a few reports in literature have investigated the effects of a complex biological feed stream on the bed stability in EBA (Barnfield Frej et al., 1994; Fernandez-Lahore

et al., 1999). Similar reports in literature for packed bed chromatography prove harder to find despite a vast range of techniques available to examine packing and flow heterogeneity.

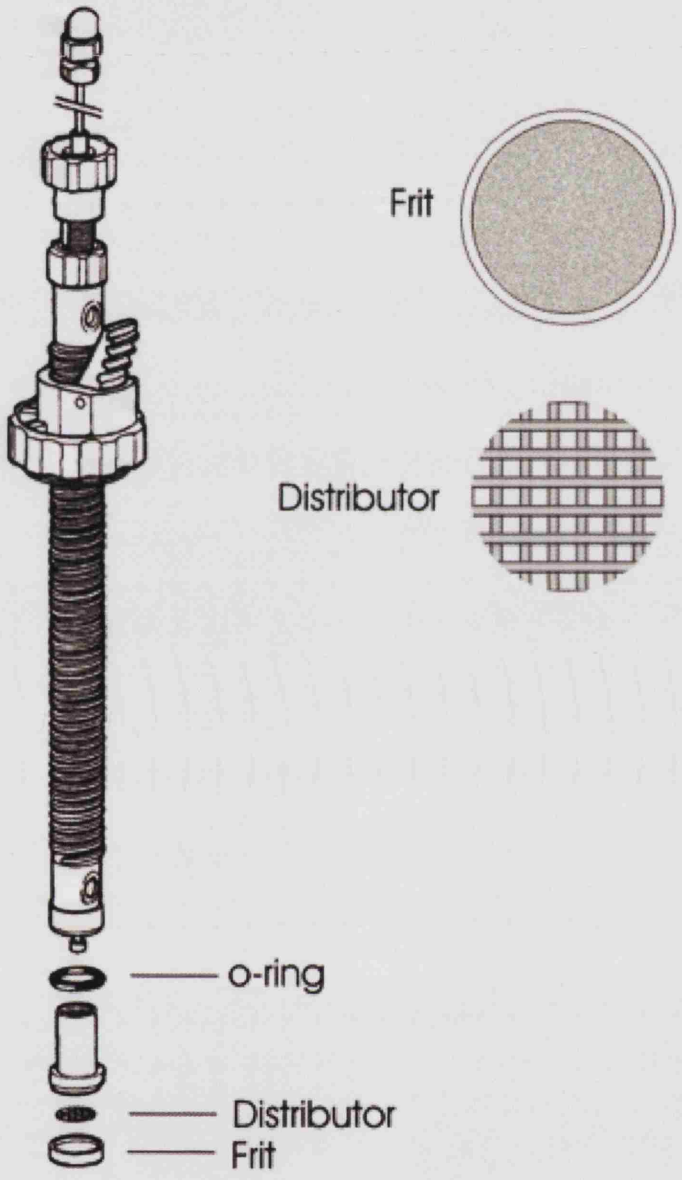

***Figure 1-2**: Illustration of column header (XK column, GE Healthcare).*

1.3.4 Pressure drop

The familiar Blake-Kozeny equation (Blake, 1922; Bird et al., 2002) describes the pressure drop as a function of flow rate for laminar flow through a packed bed of incompressible porous beads (equation 1-1):

$$\frac{dP}{dL} = \frac{150\mu}{d_p^2}\frac{(1-\varepsilon)^2}{\varepsilon^3}\cdot u \qquad (1\text{-}1)$$

It is seen from equation 1-1 that the pressure drop in a packed bed is dependent on the feed viscosity, bed porosity, flow rate, bed length and bead diameter. In the absence of bed compression, a plot of pressure drop vs. flow will be linear. For a column of a specified resin and fixed bed length, the slope of the graph is only proportional to the bed porosity and viscosity. Pressure drop is largely affected by bed porosity and also by viscosity to a lesser extent; interaction of the two factors can cause a sharp increase in pressure drop (Figure 1-3).

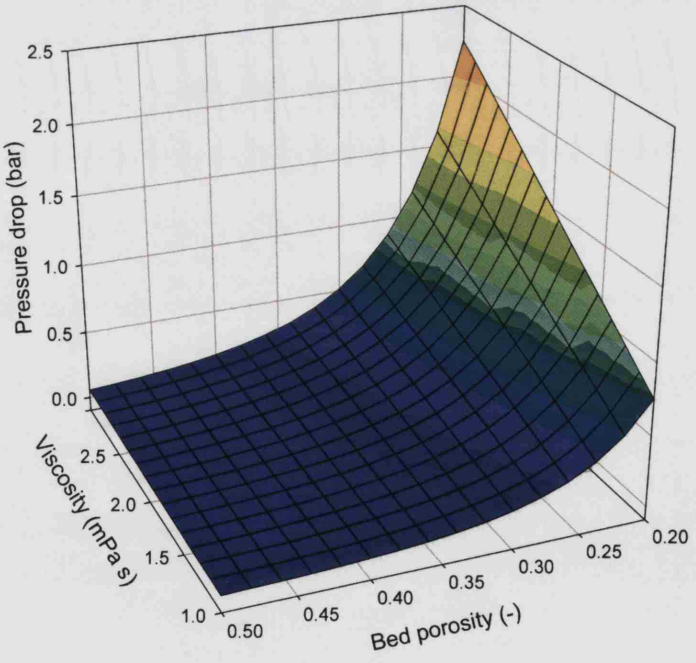

***Figure 1-3**: Effect of feed viscosity and bed porosity on column pressure drop. This graph was generated from the Blake-Kozeny equation (1-1) using the following parameter values: L = 0.15 m (15 cm), u = 4.2 x 10^{-4} m/s (150 cm/h), d_p = 0.0001 m (100 µm).*

The range of porosities typically encountered in packed beds is 0.35 – 0.5 and examples of typical viscosities seen with biological process material is listed in Table 1-3. It is important to remember that the Blake-Kozeny equation is only truly applicable to rigid particles of a single size.

Feedstock	Viscosity (mPa s)	Cell concentration
Candida kefyr	2.2	7 $g.L^{-1}$
Alkaligenes eutrophus	1.08 – 1.11	5 – 10 $g.L^{-1}$ dry mass
Bacillus cereus	1.5 – 3.0	5 – 10 $g.L^{-1}$ wet mass
BHK cell culture	1.36	10^7 cells cm^{-3}
Mammalian cells	1.3	-
E. coli homogenate (original)	40.4	19.3% bio wet mass
E. coli homogenate with DNase	12	21.3% bio wet mass
E. coli homogenate with DNase and 1:2 dilution	2.2	10.7% bio wet mass

***Table 1-3**: Typical viscosities of some cell suspensions [from Anspach et al. (1999)].*

Most chromatographic matrices are compressible to varying degrees. The extensively used agarose-based supports (e.g., Sepharose™ from GE Healthcare) are mechanically soft relative to newer ceramic-based (e.g., Ceramic HyperD™ from Pall Corporation), silica-based (e.g., Matrex™ from Millipore Corporation) and glass supports (e.g., ProSep™ from Millipore Corporation). The compressibility of the gel matrix reduces the porosity of the bed and may have detrimental effects on the separation efficiency. Excessive compression of the matrix causes the pressure-flow rate correlation to be non-linear, resulting in severe flow instability (Joustra, 1967; Verhoff and Furjanic, 1983; Parker et al., 1987; Davies and Bellhouse, 1989; Mohammad et al., 1992).

Increased pressure and bed compression can be particularly important upon scaling up to industrial-scale columns because of the large change in aspect ratio resulting in loss of wall support. Several studies have explored the effect of column scale on the pressure drop for soft or semi-rigid matrices (Mohammad et al., 1992; Aguilera Soriano et al., 1997; Stickel and Fotopoulos, 2001).

Pressure drop is not only a concern for conventional preparative chromatography of bead packings. Several articles in literature have dealt with the pressure drop in more recent chromatographic techniques: monolithic columns (Vervoot et al., 2003 and 2004; Mihelic et al., 2005), capillary columns (Li et al., 1997) and counter-current columns (van Buel et al., 1997).

Fouling can have a serious impact on pressure drop. Increases in pressure can affect the reproducibility of column performance since most operational parameters are dependent on pressure to some extent (Martin and Guiochon, 2005) and can also cause bed compression in packed bed columns. Increased viscosities in heavily fouled feed streams can cause increased pressure drop during sample loading. Furthermore, deposits of solid particulates and non-soluble foulants in the feed stream may reduce bed porosity, leading to an increased pressure drop across the column. This effect may cause long-term and progressively greater pressure drop if inadequate clean-in-place (CIP) procedures are used in between runs. It is reasonable to expect that severe particulate fouling may, in some cases, decrease pressure drop due to the creation of preferential flow or channelling in the bed structure. However, this decrease in pressure drop may not be beneficial to column performance since it will be counteracted by a relatively large increase in band broadening as previously discussed (cf. Section 1.3.3).

1.4 INDUSTRIAL CONSIDERATIONS OF FOULING

Biopharmaceutical process development is concerned with creating and optimising well-characterised processes for the production of potential therapeutic bio-molecules. Process validation is an extension of process development that verifies a process produces a product of appropriate and consistent quality when operated within

specified limits. The ultimate goal of these activities is to ensure that only efficacious, consistent and safe drug products will reach consumers.

The PDA (1992) emphasises that validation of column-based separation processes should assess packing heterogeneity, robustness, useful life of resin, impurities clearance and cleaning, among other equipment-related issues. These studies fulfil the basic requirements for use of the column in GMP manufacturing (FDA, 1987), and can be affected by fouling.

Column packings are assessed by analysing the peak shape in terms of height-equivalent-to-a-theoretical-plate (HETP) and asymmetry factor (As) (Rathore et al., 2003). The determination of HETP is performed on the basis of peak width at half-height. It is normally done for newly packed columns but can also be performed during the lifetime of the column to reassure bed integrity. The analysis only provides an overall indication of the packing heterogeneity. Whilst satisfying validation requirements, it provides only little information to the process developer for trouble-shooting. As previously mentioned, one possible cause of packing heterogeneity during the lifetime of a column may be due to fouling material reaching the column bed. Pre-treating the feed stream, to remove particulates, lipids and endotoxins, can extend the lifetime of the media but the economics of pre-treatment should be examined for each application (Sofer, 1987).

Validation should be carried out to demonstrate the robustness of the process within the normal operational range of critical process variables. Seely et al. (1999) defines a variable to be critical if "its operating range is near the edge of failure". Kelley et al. (1997) adds that extremely well-controlled variables may be dropped from consideration since it is immaterial whether those variables are critical to process performance because of their tight control. Commonly tested operating variables in chromatographic process steps include: buffer pH and ionic strength; gradient shape; temperature; flow rate; pressure drop; and load mass per resin volume. Variability in the composition of the feed stream particularly with reference to fouling material is often neglected. Moreover, the impact of long-term, time-dependent resin fouling on the robustness is ignored. Inclusion of fouling in robustness studies are often hampered by the lack of simple methods for the reliable appraisal of feed stream composition of fouling material and their effects.

The useful lifetime of chromatography resins is based on the ability of the resin, over a given number of uses, to produce product of acceptable quality and yield (O'Leary et al., 2001). The effects of fouling on the useful lifetime of the resin are of great importance since they will affect both product purity and the economics of the process. Validation studies that determine useful lifetime of a resin in essence measure the effects of long-term fouling on the resin. Parameters such as yield and purity as well as the levels of HCPs, leachables, endotoxin, DNA and certain media components are typically monitored over an extended number of runs (O'Leary et al., 2001; Breece et al., 2002a and 2002b). It is also common to incorporate the evaluation of different CIP protocols into resin lifetime studies especially at small-scale. Overall, such studies may provide little insight into underlying mechanisms of chromatographic fouling.

In impurity clearance studies, the removal of certain key contaminants from the product stream by each process step is monitored. The principle contaminants which may require clearance are media components, host cell proteins, nucleic acids, viruses, pyrogens, and material leached from bioaffinity media (PDA, 1992). It is important to distinguish between product contaminants, which are impurities in the product, from process foulants that impact process performance. However, it is clear that process fouling may affect the ability of process operations to remove these contaminants. Therefore, it is important for process developers to understand the effect of chromatographic fouling on the efficiency of impurity clearance and also understand the potential of trapped foulant material in the column subsequently to leach into the product stream over the column lifetime.

Process validation is largely concerned with monitoring the process or product to ensure that they meet predefined specifications. It is, therefore, the responsibility of early process development to design processes that are robust to fouling. Such attempts are often hampered by the lack of simple, systematic methods for reliable investigation of fouling and its effects. Knowledge of the cause and effect can be the basis of generating possible solutions to adverse fouling effects.

1.5 CLEAN-IN-PLACE (CIP)

When investigating chromatographic fouling, it is sensible also to consider column cleaning since understanding of the former will allow the design of specific and effective CIP protocols to mitigate their effects. An important challenge in process design is to develop CIP protocols to ensure removal of significant foulants from the matrix in order to extend the resin lifetime and maintain separation performance. In industry, it is common practice to clean columns, by using a clean-in-place protocol of ever increasing complexity, to target each type of contaminant with appropriate regimes, e.g., caustic, detergent or organic solvent washes.

Sodium hydroxide is the most widely used cleaning agent and is known to be very efficient in removing proteins and lipids. Levison et al. (1995) demonstrated that a CIP treatment comprising of 0.5 M NaOH treatment for 16 hours was effective for sanitisation and depyrogenation of two different ion exchange columns following gross microbial fouling. Furthermore, the NaOH treatment did not affect the separation performance of the media after re-equilibration.

However, the severity of the CIP procedure must be weighed against possible long-term deterioration in the matrix and ligand leakage which are key issues in validation (Sofer and Hagel, 1997). Ligand leakage from affinity matrices is of particular importance and clearance of any ligands from the product stream is a vital part of the overall validation effort as described previously. However, it is not limited to affinity matrices. A study by Andersson et al. (1993) found the release of amines (leachables) from the ion-exchange group in DEAE Sepharose FF when it was treated repeatedly with 1 M sodium hydroxide for a total of 672 hours. Despite this, the chromatographic separation performance and capacity appeared unaffected by the CIP treatment.

1.6 SUMMARY

The above sections have highlighted the wide breadth of material in process streams that may cause fouling to chromatographic columns as well as the possible effects of fouling. The composition of feed streams to columns are often complex and varied, and interactions between biological foulants can give rise to secondary fouling which obscures the underlying fouling mechanism.

Fouling can produce a variety of consequences such as changes to column resolution, reduced capacity, increased pressure drop and leaching of contaminants into the product stream. These are critical parameters when considering the design of a chromatographic adsorption step, and how the process stream affects these parameters has implications on the economy of the step. Therefore, it is important to select the best means of pre-treatment to use so as to minimise fouling as well as design effective clean-in-place (CIP) protocols to ensure removal of significant foulants from the matrix in order to extend the useful lifetime of the chromatographic resin. In practice the severity of a CIP protocol must be weighed against possible long-term deterioration in the matrix adsorptive performance when subjected to harsh cleaning regimes.

From an industrial perspective, regulatory authorities are aware that chromatographic fouling can ultimately affect the consistency and quality of the product which has led to the requirement of rigorous validation studies. However, these studies are mainly concern with monitoring and shed little light on how to rectify any problems. A challenge for process developers is, therefore, to design chromatographic process that are robust to fouling and can pass rigorous validation tests.

Fouling is a problem which is very often encountered during the industrial purification of proteins by process chromatography. From this point of view, any systematic investigation of the effects of column fouling can be useful to process designers.

1.7 SCOPE OF THIS THESIS

Investigation of chromatographic fouling is a challenging task – existing mathematical models that describe chromatographic separations are deemed inappropriate beyond the use of pure solutes; direct and systematic methods for evaluating fouling are lacking; and many techniques available for evaluating some of its effects may prove inapplicable under realist fouling conditions.

This thesis examines new approaches to evaluate the effects of fouling on process chromatography at three levels of increasing detail: whole-column, intra-column and single-bead level.

Though the work in this thesis focuses on fouling of ion exchange beads in packed beds or finite baths, it is hoped that the findings and some of the techniques developed can also be applicable to other types of resins and modes of chromatography. The long-term, post-fouling impact on chromatographic performance is examined, rather than the effects of having fouling material in the process stream on product adsorption during column loading. To achieve this, a particularly aggressive fouling stream was used to challenge the chromatographic resin in each study, as fouling over hundreds of cycles as typically seen in real chromatographic operations was impractical given the time constraints of a PhD. Nonetheless, realistic process material was used to produce a fouling steam that properly reflects the composition of fouling species seen by industrial columns. The use of certain single-cycle CIP protocols was also incorporated into few selected studies.

The remaining chapters of this thesis are organised as follows:

Chapter 2 gives an overview of previous work done at UCL to model chromatographic fouling and a critique of these approaches.

Chapter 3 provides details on the materials, equipment, analytical techniques and experimental methods used in this thesis.

Chapter 4 (whole-column level) examines the effects of fouling a packed bed column with yeast homogenate. The change in capacity and breakthrough characteristics for a test protein, BSA, was examined. The original data of Hearle

(1997) was re-analysed and discussed to provide qualitative inference of the changes in mass transfer properties occurring. Breakthrough curve analysis was also used to investigate the effectiveness of a rigorous CIP procedure in restoring the characteristics of a fouled column.

Chapter 5 (intra-column level) introduces a reverse-flow technique that can quantify the dispersive effect of fouling in defined sections within a packed bed column. The technique allows the band broadening effects due to reversible microscopic factors to be separated from irreversible macroscopic factors.

Chapter 6 (single-bead level) describes the use of confocal scanning laser microscopy (CSLM) as a technique to visualise directly fouling at the level of a single bead. Initially, experiments were done in finite bath mode but subsequently, the visualisation of fouling was also performed in a packed bed structure under flow conditions. The confocal images obtained provide insights to the spatial distribution of key foulant types within a single bead.

Chapter 7 will draw overall conclusions from the work reported in this thesis.

Finally, *Chapter 8* looks forward by giving recommendations for future work which will use the techniques developed in this work.

Overall, the results from this work should provide valuable insights to the likely mechanisms of fouling. The techniques developed are practical and can be easily implemented to evaluate chromatographic fouling scenarios encountered in industry.

2 CRITIQUE OF PREVIOUS WORK

2.1 INTRODUCTION

The analysis of fouling effects in chromatography columns is difficult due to the complex interactions that exist between the foulants and matrix. Furthermore, the transient nature of some fouling effects requires sensitive and non-invasive methods of analysis to avoid creating experimental artefacts. Consequently, published research on chromatographic fouling is scarce, especially in the modeling of the underlying fouling mechanisms. Chromatographic separation is governed by fundamental mass transfer properties. Many mathematical models exist that predict the output chromatogram from the fundamental mass transfer parameters (Golshan-Shirazi, 1992; Guiochon, 1994; Gu, 1995) but their applicability to fouled systems is questionable.

Attempts in using existing models to determine mass transfer parameters in fouled packed bed columns formed the basis – at least in part – of four previous research theses at UCL: Aguilera Soriano (1995), Hearle (1997), Storey (2000) and Pampel (2002). Both moment and frontal analysis have been applied to analyse chromatographic fouling in terms of changes in mass transfer properties. However, the analyses have proved to be difficult to generalise and may, in cases, be found on inappropriate assumptions (see Section 2.3).

Aguilera Soriano (1995) used moment analysis to investigate the effect of loading different concentrations of yeast homogenate on gel filtration columns. Pulses of marker proteins were sent through the columns post-fouling and the resulting statistical peak moments were fitted to a model which relates the retention time (first absolute moment) and variance (second central moment) to the physical parameters of intraparticle void volume, effective diffusivity and axial dispersion of the solute (see Section 2.2.1). The fluid film mass transfer resistance was assumed to be unaffected by fouling and was calculated using the correlation of Ohashi (1981).

An alternative method was used by Hearle (1997), who studied the breakthrough of BSA as a binding marker on anion exchange columns previously challenged with yeast homogenate clarified to varying degrees. He also investigated the effect of fouling using moment analysis and attempted to separate the fouling

occurring due to the structure of the base matrix (Sepharose 4 FF) from that due to the functional matrix (DEAE Sepharose FF). The effects of different classes of contaminants, notably lipids and particulates, on the fouling process were isolated.

Storey (2000) attempted to refine the frontal analysis approach used by Hearle (1997) by incorporating mathematical modeling of the breakthrough curves to analyse changes in column capacity, film diffusion and intraparticle diffusion. The two-film mass transfer model, as described by Cooney (1990) was employed. The model makes use of the constant pattern front (CPF) assumption to enable a near-analytical solution of the partial differential equations describing mass transfer in a column. The equation used by Cooney (1990) assumes both liquid film mass transfer and intraparticle diffusion to be significant to the overall adsorption but axial dispersion is neglected since in a CPF situation this is neutralised by the band-sharpening effects of a favourable isotherm.

Pampel (2002) used the frontal analysis method developed by Storey (2000) to study the influence of the major milk contaminants, lipid and casein, on the chromatographic capture of a model target protein, lactoperoxidase (LPO), to the cation exchanger, SP Sepharose FF. LPO was dissolved in whole or skimmed milk before loading on to the column, presenting a complex, multi-component feed material to the column.

2.2 THEORY

2.2.1 Analysis of solute concentration profiles using the method of statistical moments

Moment or pulse response analysis characterises the shape of the effluent concentration profile that develops when a small pulse of solute passes through a column. The shape of the pulse response provides information about the degree of axial dispersion, the effective diffusivity of the solute and the column porosity, which are calculated by finding the statistical moments of the curve (Schneider and Smith, 1968). The pulse analysis method is based on the statistical moment theories of Kubin (1965) and Kucera (1965). The first absolute moment of a concentration profile is

essentially the average retention time of the peak, and is calculated using the following relationships:

$$\mu_1 = \frac{\int_0^\infty C(L,t)\,t\,dt}{\int_0^\infty C(L,t)dt} - t \qquad (2\text{-}1)$$

and

$$\mu_1 = \frac{L}{u}\left[1+\frac{(1-\varepsilon)}{\varepsilon}\cdot\varepsilon_p\right]+\frac{t_0}{2} \qquad (2\text{-}2)$$

where L is the bed height, u is the interstitial fluid velocity, ε is the column void fraction, ε_p is the inclusion porosity and t_0 is the input pulse time. The second central moment of a concentration profile describes the distribution of the peak, or its variance, expressed as:

$$\mu_2 = \frac{\int_0^\infty C(L,t)(t-\mu_1)^2\,dt}{\int_0^\infty C(L,t)dt} \qquad (2\text{-}3)$$

and

$$\mu_2 = \frac{2L}{u}\left[\frac{(1-\varepsilon)}{\varepsilon}\cdot\frac{R_p^2\varepsilon_p^2}{15}\cdot\left(\frac{1}{D_e}+\frac{5}{k_f R_p}\right)+\frac{D_L}{u^2}\left(1+\frac{(1-\varepsilon)\varepsilon_p}{\varepsilon}\right)^2\right]+\frac{t_0^2}{12} \qquad (2\text{-}4)$$

Here D_L is the axial dispersion coefficient, R_p is the particle radius and k_f is the external fluid film mass transfer coefficient.

The first absolute moment is used to estimate the bead inclusion porosity, which is the volume fraction of intraparticle space available to the diffusing solute injected in the pulse. From equation 2-2, a plot of $(\mu_1 - t_0)/2$ versus L/u yields a straight line. The gradient of this line can then be used to find a value for the inclusion porosity once the void volume of the bed is determined from the average retention time

of a large, non-retained molecule such as dextran. The second central moment allows estimation of the axial dispersion, D_L, and the intraparticle diffusion coefficient, D_e. Rearranging equation 2-4 produces:

$$\frac{\left(\mu_2 - \frac{t_0^2}{12}\right)}{\frac{2L}{u}} = \frac{(1-\varepsilon)}{\varepsilon} \cdot \frac{R_p^2 \varepsilon_p^2}{15} \cdot \left(\frac{1}{D_e} + \frac{5}{k_f R_p}\right) + \frac{1}{u}\left(\frac{D_L}{u}\left(1 + \frac{(1-\varepsilon)\varepsilon_p}{\varepsilon}\right)^2\right) \qquad (2\text{-}5)$$

A plot of the left-hand side of equation 2-5 versus the reciprocal interstitial velocity (1/u) yields a linear function, the slope of which is related to the axial dispersion, with the y-intercept indicating both the external fluid film transfer coefficient, k_f, and the effective diffusivity, D_e, of the solute.

Statistical moment analysis of solute pulses has been used by several workers to obtain the transport parameters of proteins in a variety of chromatographic systems (Arnold et al., 1985; Ching et al., 1989; Boyer and Hsu, 1992; Ming and Howell, 1993) but none in fouled systems. The main difficulty it presents is the amount of error that can accrue, particularly when estimating the second central moment (Lenoff and Lightfoot, 1987). This moment is prone to variations arising from small amounts of impurities in the pulsed sample, difficulties in estimating the start and end of the pulse, noise and extra-column effects (Chesler and Cram, 1971). The reason that the method has found wide use is its general applicability to any chromatographic peak shape (making it ideal for use in a fouled column in this respect) and the lack of any requirement for specialised equipment and analytical tools.

2.2.2 Analysis of breakthrough characteristics using an analytical CPF model

In classical adsorption, under ideal (non-fouling) conditions, it is common to assume that one or other of these resistances determines the overall rate of mass transfer (Morbidelli et al., 1982). The calculation of the breakthrough curve is accordingly simplified. Such approximate methods, however, do not reveal the subtleties of flow and mass transfer within the column. Only an exact solution of the

governing flow equations can reveal such phenomena as the veracity of the isotherm model and the precise hydrodynamic performance of the packed bed.

Analytical solutions based on the constant pattern front (CPF) assumption are capable of greater refinement (Kaezmarski et al., 1997). Here, solute is assumed to move through a column as a concentration front. Rapid adsorption, like that for favourable isotherms (strong adsorption occurring at low solute concentrations), has a sharpening effect on the shape of this front. Mass transfer resistances, and dispersion effects (hydrodynamic and diffusional) tend to broaden them. Under CPF conditions, these two sets of forces are assumed to balance one another, so that the shape of the front does not change as it passes through the column. In these cases, an approximate solution to the film and pore diffusion model can be obtained analytically, yielding an explicit relationship for the concentration profile (Mazzotti et al., 1994).

Cooney (1990) developed a CPF solution method for favourable isotherm systems, where both external fluid film and pore diffusion mass transfer resistances are important, describing time *t* as a function of the fluid phase solute concentration *X*:

$$t = \left[\frac{(\varepsilon + (1-\varepsilon)K)}{\varepsilon V}\right] L + \frac{K}{k_f S_0} \int_{x_0}^{x} \frac{dX}{(X_i - X)} \qquad (2\text{-}6)$$

where ε is the porosity, V is the liquid velocity in the direction of flow, L is the bed length, S_0 is the ratio of external surface area to volume for the particle (= $3/R_p$ for spherical particles) and k_f is the external fluid film mass transfer coefficient. The parameter K is the ratio of solid and liquid phase solute concentrations ($K = q_m/c_f$). It is analogous to an equilibrium partition coefficient, and gives an indication of the relative number of free adsorption sites in the column. The integral term in equation 2-6 relates the solute concentration in the bulk liquid, X, to its concentration at the boundary between the solid and liquid phases, X_i. Equation 2-6 is underpinned by the assumption that mass transfer obeys linear driving force laws, hence the importance of this concentration difference. Another expression relating X and X_i is obtained from the isotherm data, which if assumed to be of the common Langmuir-type, is given in dimensionless form as:

$$X = X_i + \frac{K_d c_f \beta (X_i - X_i^2)}{(1 + K_d c_f X_i)} \tag{2-7}$$

where $\beta = \frac{15 D_s K}{R_p^2 k_f S_0}$ and K_d is a constant. The integration limits in equation 2-6 are obtained from the breakthrough curve centre of mass, defined by the point $[t', X_0]$, satisfying the following condition:

$$\int_0^{t'} X dt = \int_{t'}^{\infty} (1 - X) dt \tag{2-8}$$

Equation 2-7 cannot be solved explicitly for X_i. Cooney (1990) overcame this by approximating the $X = f(X_i)$ relationship (equation 2-7) with polynomial expressions of the form $X_i = aX + bX^2 + dX^3 + ...$, provided they are monotonic over the $0 < X_i < 1$ interval. Numerical solutions to these approximate curves (Cooney, 1993) compared very well with exact solutions, based on film and pore diffusion models, reported by Hand et al. (1984).

If the order of the polynomial substitution function is limited to three, $X_i = aX + bX^2 + dX^3 + ...$, then this allows an analytical solution of equation 2-6:

$$t = \left[\frac{\varepsilon + (1 - \varepsilon)K}{\varepsilon v}\right] L + \frac{K}{\gamma k_f S_0} \ln \frac{(2AX + b - \gamma)(2AX_0 + b + \gamma)}{(2AX + b + \gamma)(2AX_0 + b - \gamma)} \tag{2-9}$$

where $A = (a - 1)$ and $\gamma = \sqrt{b^2 - 4Ad}$.

The ability to fit an analytical solution to experimentally measured breakthrough data allows the values of K, D_s and k_f to be determined. These parameters define the dimensionless Biot number, Bi, given by:

$$Bi = \frac{k_f R_p}{K D_s} \tag{2-10}$$

which is a diagnostic quantity reflecting the balance between k_f and D_s in controlling overall mass transfer. Bi also reflects the relationship between X and X_i

that influences the symmetry of the breakthrough curve. It does so through its association with the Langmuir isotherm expression (equation 2-7) via the parameter β:

$$\beta = \frac{15D_s K}{R_p^2 k_f S_0} = \frac{1}{Bi}\left(\frac{15}{R_p S_0}\right) \tag{2-11}$$

Classically, K is a system constant, depending only on the adsorption capacity of the matrix and the binding equilibrium kinetics between solute and ligand. In the study by Storey (2000), which dealt with columns operated under non-ideal (fouling) conditions, the value of K was treated as a variable, testing the hypothesis that systems exposed to greater amounts of foulant would exhibit a reduction in K. The model considers the importance of both mass transfer resistances k_f and D_s.

2.3 CRITIQUE OF THE APPLICABILITY OF THE TECHNIQUES TO ANALYSE FOULING

Careful review of the approaches of using moment analysis and frontal analysis to obtain solutions for the mass transfer parameters under fouling conditions reveals critical inadequacies. The following two sections attempt to provide an overview of these and to highlight the problems of directly applying these two techniques for the analysis of chromatography under fouling conditions.

2.3.1 Moment analysis

Equations 2-2 and 2-4 provide the moments μ_1 and μ_2 of a pulse response when there is no retention of a solute by adsorption. If adsorption of a solute does occurs, then equations 2-2 and 2-4 can not be used to obtain values for ε_p from equation 2-2, and D_L and D_e from equation 2-4. This is an important issue to consider when applying moment analysis.

The use of this approach assumes that the film mass transfer coefficient, k_f, can be estimated from a correlation (e.g. Ohashi, 1981; Ruthven, 1984; Skidmore et al., 1990; Geankoplis, 1993) or measured by an independent experiment (Geankoplis,

1993) which is not an easy task. It can not be assumed that after the resin is fouled, k_f can be simply determined from established correlations that are for clean, spherical beads. Fouling material, such as lipids and cell debris, may coat the chromatographic bead surface. An example of such a geometrical change is shown by Viloria-Cols et al. (2004) where the fouling of anion exchange beads with whole cells was visualised using scanning electron microscopy (SEM).

The analysis is only valid for single solute systems. It may be arguable whether the fouled systems investigated by Aguilera Soriano (1995) and Hearle (1997) were indeed single-component or multi-component instead. However, since the fouled columns were washed with 1 M NaCl before introducing the protein test pulses to remove any loosely bound foulants, it is reasonable to assume that the changes on the column due to fouling are "permanent". In this case, one may assume that when protein pulses are introduced to the column, the system will still be single-component. This is another important issue to consider when applying moment analysis.

Analysing the moments of a pulse response assumes that the fluid is evenly distributed over the column diameter and that no preferential flow, dead zones or eddies exit. It is reasonable to expect that resin fouling may lead to the formation of "cracks" in the packed beds which can lead to channelling or preferential flow. In this case the analysis of moments of the pulse can no longer be used to determine mass transfer parameters. In order to justify the use of the simple model, one would have to demonstrate that the pre-condition of even flow distribution throughout the column is valid.

2.3.2 Frontal analysis

The application of the model of Cooney (1990) to study chromatographic fouling entails several assumptions that need verifying. Central to the model itself is the assumption that a constant pattern front (CPF) behaviour (Ruthven 1984) is present in the column. It is not simply sufficient to have a favourable isotherm in order for CPF behaviour to occur. Storey (2000) used HiTrap columns of 2.5 cm bed length in his experiments. Such a short length may or may not be sufficient to allow CPF behaviour even under a very favourable isotherm. It must be realised that the distance

required to approach CPF behaviour depends not only on how favourable the isotherm is but also on the kinetics of adsorption.

In Storey's approach, the experimental breakthrough curve data was fitted to the model to determine the value for the three parameters, K, k_f and D_s. The ability to perform mechanistic discrimination by fitting a sigmodial-type curve to obtain values for three parameters without utilising additional experimental information for determining the values of some of the three parameters from independent experiments is probably doubtful. Thus, his model discrimination (with respect to mass transfer mechanisms) and parameter estimation methodology is unlikely to be satisfactory.

If the protein of interest is in a complex feed stream and if this is loaded onto the column, as in the case of Pampel (2002), then the system examined is multi-component. The simultaneous diffusion of several solutes has to be treated by the appropriate Stefan-Maxwell relationships for multi-component mass transfer (Schluender 1984; Liapis 1990). Pampel (2002) argued that the use of these equations requires *a priori* knowledge of the diffusive properties of the individual species, and therefore, the use of single-component mass transfer equations was maintained in his work. He realised that the derived mass transfer parameters may not reflect the true mass transfer properties and so was considered as "apparent". It is important to realise that even in the case where a pure protein solution was loaded onto a column post-fouling as seen in the work of Storey (2000), the system will still be considered multi-component if the protein will compete with already-bound foulants for binding sites.

The adsorption isotherm may also be affected by fouling components even if the component is not adsorbed because the fouling component could obstruct the availability of free active sites for adsorption of the test protein. This will alter the equilibrium adsorption constant and the maximum value of the concentration of the test protein in the adsorbed phase. If the fouling components do adsorb to the resin, the analysis of the adsorption phenomenon requires the use of models for multi-component adsorption isotherms and further complicates the analysis. Both Storey (2000) and Pampel (2002) neglected the potential effects of fouling on the adsorption isotherm.

2.4 SUMMARY

Clearly, it is inadequate simply to use existing models to describe the mass transfer phenomena in fouled columns. Proper determination of the mass transfer parameters will be extremely useful in understanding the underlying fouling mechanism but is definitely a difficult task.

Chromatographic fouling is such a complex phenomenon that it certainly requires characterisation methods, which tackle the problem by adapting different and, most importantly, independent approaches.

The next section of this thesis describes the materials and methods used to develop three independent methods for the assessment of fouling and the determination of likely fouling mechanisms.

3 MATERIALS AND METHODS

This chapter provides the background information on the materials, equipment, analytical techniques and experimental methods used in this thesis. It is divided into a section devoted to the general materials and analytical methods used throughout this thesis; a section describing the method of preparation and characterisation of the fouling material used in the studies; and individual sections relating specifically to the work presented in Chapters 4, 5 and 6.

3.1 GENERAL MATERIALS AND METHODS

3.1.1 Chemicals

All chemicals, unless specified otherwise, were obtained from Sigma Chemical Co. Ltd. (Poole, Dorset, UK) and were of analytical grade. Bakers' yeast (*Saccharomyces cerevisiae*) was supplied by DCL Yeast Ltd. (Sutton, Surrey, UK). Bovine serum albumin, BSA (A-7030), was from Sigma Chemical Co. Ltd. (Poole, Dorset, UK) and of purity > 98%. Cy™3 and Cy™5.5 mono-reactive labelling kits were obtained from GE Healthcare (Uppsala, Sweden), and PicoGreen™ and BacLight™ Red were obtained from Molecular Probes Europe – Invitrogen (Leiden, The Netherlands).

3.1.2 Agarose gels

Two agarose gels were ran, one of 1.2% w/v agarose to visualise DNA fragments between the ranges 500 bp – 12 kbp. And a second agarose gel of 2% w/v to check DNA fragments between 50 bp – 2 kbp. The agarose was purchased from Sigma Chemical Co. Ltd. (Poole, Dorset, UK) (Cat No: A-9414). The general gel procedure was as described by Sambrook and Russell (2000).

DNA was isolated from crude fouling material using a Genelute Bacterial Genomic DNA Kit (Sigma Chemical Co. Ltd., Poole, Dorset, UK). The protocol

followed the manufacturer's recommended procedure except that Proteinase K and Lysis Solution C were substituted with Column Preparation Solution since the fouling material was cell homogenate so chemical lysis was not needed to extract the DNA from the cells.

The following DNA markers were used to determine DNA fragment lengths: Novagen PCR Markers (50 bp – 2 kbp, Cat No: 69278) and Novagen Perfect Markers (500 bp – 12 kbp, Cat No: 69002).

Both gels were loaded on Pharmacia LKB GNA100 Electrophoresis Gel Trays and powered by Pharmacia Electrophoresis Power Supply (EPS) 500/400 (GE Healthcare, Milton Keynes, UK). The gels ran for 1 hour at 50 V.

The gels were visualised using an Ultra-Violet Products GelDoc-It imaging system (Ultra-Violet Products Ltd., Cambridge, UK).

3.1.3 Assay techniques

3.1.3.1 Total protein assay

The protein assay was a commercially available protein assay kit from Bio-Rad Laboratories Ltd. (Hemel Hempstead, UK). The assay is based on the principal by Bradford (1976). The protocol followed the manufacturer's recommendation for the micro-assay procedure. Adsorption measurements were performed at 595 nm on a Beckmann DU 650 single-beam UV/VIS spectrophotometer (Beckmann Instruments Ltd., High Wycombe, UK). Reproducibility of the assay was typically ± 5% for duplicate samples.

3.1.3.2 Lipid Assay

The amount of lipid in the samples of yeast homogenate was assayed by chloroform extraction and weighing of the dried extract. The method used for the chloroform extraction was that of Bligh & Dyer modified by Kates (1986). A sample

of 1 mL was extracted at ambient temperature with a 2:1 v/v mixture of chloroform:methanol for 2 hours with occasional agitation. After 2 hours the sample was centrifuged with a MSE Europa 24 centrifuge (MSE UK Ltd., Beckham, Kent, UK) at 4000 rpm at 4°C in a stoppered glass vessel. The supernatant was reserved and 4.75 mL of methanol:chloroform:water in the ratio of 2:1:0.8 v/v was added to the pellet. The centrifugation was repeated and the supernatant added to that previously reserved. To the combined supernatant, a further 2.5 mL of chloroform and 2.5 mL of water were added and the mixture agitated. The resulting emulsion was broken by centrifugation with a MSE Europa 24 centrifuge (MSE UK Ltd., Beckham, Kent, UK) for 5 minutes at 4000 rpm and 4°C. The lower chloroform phase was drawn off and evaporated to dryness in a rotary vacuum evaporator. The residue was taken up in 2 mL of 1:1 chloroform:methanol v/v, and placed in a weighing bottle. A further 2 mL of chloroform-methanol mixture was used to wash the evaporator flask and this was added to the first 2 mL in the weighing bottle. The weighing bottle was dried in a desiccator over potassium hydroxide and under nitrogen to a constant weight (± 0.0005 g). Reproducibility of the samples was ± 20% for duplicate samples due to the extended nature of the method and the fact that the potential for introducing errors through phase partitioning was high.

3.1.3.3 Determination of solids dry weight

Samples of 1 mL were placed into pre-weighed Eppendorf tubes, and then spun down in a mini-centrifuge (Eppendorf Centrifuge 5415R, Hamburg, Germany) at 13,000 rpm for 5 minutes. The supernatant was carefully discarded and the recovered pellets were dried to a constant weight (± 0.0005 g) in an oven at 100 °C. Solids dry weight was estimated by the difference between the final weight and the empty Eppendorf tubes. Typically, variation between samples was ± 5%.

3.1.3.4 DNA assay

The DNA assay was a commercially available Quant-iT™ DNA Assay Kit, Broad Range (Cat. No. #Q33130) obtained from Molecular Probes Europe – Invitrogen (Leiden, The Netherlands). It is a fluorescence-based assay that is highly selective for dsDNA over RNA and uses 96-well microplates. The DNA assay was performed on samples of cell homogenate that had been spun down in a mini-centrifuge (Eppendorf Centrifuge 5415R, Hamburg, Germany) at 13,000 rpm for 5 minutes to remove any cell debris. The protocol followed the manufacturer's recommended procedure and 5 μL of clarified samples were added to each microwell. Fluorescence was measured using a FLUOstar OPTIMA microplate reader (Offenburg, Germany) at an excitation/emission maxima of 485/520 nm. Reproducibility of the assay was typically ± 5% for triplicate samples.

3.1.3.5 Particle size determination

The particle size distribution was determined using a Malvin 3600E Particle Sizer with Mastersizer™ 2000 control software (Malvern Instruments, Worcestershire, United Kingdom). The system is based on the principle of laser diffraction, where the dependence of the scattering angle on the diameter of particle passing the laser beam is used to infer the particle size. The instrument calculated a volume-based particle size distribution. Repeated measurements of these values showed variability of less than 5% for the mean particle size.

3.2 FOULING MATERIAL

3.2.1 Preparation of yeast homogenate

Fouling streams were prepared by suspending bakers' yeast (*Saccharomyces cerevisiae*) in the following proportions with buffer: 1.3 kg of yeast per litre of 20 mM phosphate buffer at pH 7 to give a yeast suspension of 600 $g.L^{-1}$ (wet basis). Typically, 12 kg of yeast was added to 9.2 L of buffer to give 20 L of yeast suspension, but this volume was adjusted depending on the requirements of the experiment. The yeast

suspension was homogenised by 5 passes through a Lab-60 high pressure homogeniser (APV Manton Gaulin, Everett, MA, USA) at a pressure of 500 bar(g). Homogenate was passed through a Westfalia SAOOH disc stack centrifuge (Westfalia Separator, Milton Keynes, UK), at a flow rate of 40 $L.h^{-1}$, corresponding to $Q/\Sigma = 1.9 \times 10^{-8}$ ms^{-1}. For some experiments, supernatant was used with no further treatment other than dilution. In other experiments, the centrifuged supernatant material was further treated to remove almost all particulates. This was achieved using the Beckman L7 ultracentrifuge (Beckman Instruments Ltd., High Wycombe, Buckinghamshire, UK) running at 40,000 rpm for 1 hr (~160,000 g; $V/(t\Sigma) = 3.5 \times 10^{-16}$ ms^{-1}).

3.2.2 Preparation of *E. coli* TOP10 homogenate

Escherichia coli TOP10 (pQR239) fermentations for biocatalyst production were performed in a 7-litre fermenter with 5-litre working volume (LH 210 fermenter, Bioprocess Engineering Services, Charing, Kent, UK) fitted with three equally spaced top driven six-bladed turbine impellers and four diametrically opposed baffles. The dissolved oxygen tension (DOT) was measured with a polarographic oxygen electrode (Ingold, Messtechnik, Urdorf, Switzerland). Cells were grown in a complex medium consisting of yeast extract and tryptone. The pH of the fermentation medium was controlled using a sterilised Ingold pH probe (Ingold, Messtechnik, Urdorf, Switzerland) at pH 7 (±0.05) by metered addition of 3 M KOH and 3 M H_3PO_4. All data logging and the exhaust gas measurements were recorded using the RT-DAS program (Acquisition System, Guildford, Surrey, UK). Ampicillin was added to the fermenter medium prior to inoculation. The fermenter was inoculated with 500 mL (10% of the total volume) seed culture grown overnight. During the growing phase, the agitation rate was maintained at 1000 rpm and varied between 250 rpm to 1500 rpm. During the fermentation process, the vessel was aerated with filtered air, sparged at 1 $L.min^{-1}$ (0.67 vvm). The fermentation profile of *E. coli* TOP10 (pQR239) has been described in detail elsewhere (Doig et al., 2001). The growth of *E. coli* was closely monitored based on the optical density of the fermentation broth. This monitoring is highly important for the induction period at approximately 3 hours after the start of the fermentation. Arabinose (2.4 $g.L^{-1}$) was used to induce the cell during the second stage of the fermentation and this was done when the optical density reached 7 – 8 OD_{670}

reading. The process was then carried out for another 3 hours after the induction period until the cell reached approximately 20 OD_{670} reading. Polypropylene glycol (PPG) 2000 was used throughout the fermentation to prevent foaming.

3.2.3 Preparation of *E. coli* Fab' broth and homogenate

The foulant was prepared from a fermentation broth expressing HumMAb4D5-8 Fab' as an antibody fragment from *E. coli* strain W3110 (pAC tAC 4d5 Fab'). The fermentation was carried out in repeated batch mode as described by Garcia-Arrazola et al. (2005). It began with a 10% v/v inoculum and was grown on SM6C media: $(NH_4)_2SO_4$ 5.00 $g.L^{-1}$, NaH_2PO_4 2.80 $g.L^{-1}$, KCl 3.87 $g.L^{-1}$, citric acid 4.00 $g.L^{-1}$, glycerol 30 $g.L^{-1}$, trace elements 10 $mL.L^{-1}$, $MgSO_4.7H_2O$ 1.00 $g.L^{-1}$, chloramphenicol 0.025 $g.L^{-1}$ and antifoam PPG 1 $mL.L^{-1}$. The trace element stock solution had the following composition: citrate, 100 $g.L^{-1}$; $CaCl.6H_2O$, 5.00 $g.L^{-1}$; $ZnSO_4.7H_2O$, 2.46 $g.L^{-1}$; $MnSO_4.4H_2O$, 2.00 $g.L^{-1}$; $CuSO_4.5H_2O$, 0.50 $g.L^{-1}$; $CoSO_4.7H_2O$, 0.427 $g.L^{-1}$; $FeCl_3.6H_2O$, 9.67 $g.L^{-1}$; H_3BO_3, 0.03 $g.L^{-1}$; and $NaMoO_4.2H_2O$, 0.024 $g.L^{-1}$. Fermentation was performed in 14-litre LH fermenters (Inceltech Ltd., Berkshire, UK). Temperature was maintained at 30°C, and pH was controlled to a set-point of 6.95 by the addition of a 15% (v/v) ammonium hydroxide solution. Agitator speed and air flow rates were varied to maintain the dissolved oxygen tension (DOT) at 20% or above. Foaming was controlled as necessary by the addition of Polypropylene glycol (PPG) 2000 antifoaming agent. A glycerol carbon source was supplemented until a biomass level corresponding to a dry cell weight concentration of 20 $g.L^{-1}$ was reached (~ 35 hours after inoculation). Plasmid expression was induced by the addition of a 50% w/w lactose solution, to bring the fermenter lactose concentration to 5% w/v. The fermentation continued for a further ~ 20 hours bringing the culture into stationary phase. The cells were then harvested and homogenised at 500 bar(g) for 5 passes. Cell homogenate was partially clarified by centrifugation in a J2-M1 laboratory centrifuge with JA-10 rotor (Beckman Instruments Ltd., High Wycombe, UK) for 1 hour at 10,000 rpm (RCF = 13,000 g). The supernatant was frozen at -20°C in 45 mL aliquots. A foulant aliquot was thawed the day of experimentation at room temperature.

3.2.4 Characterisation of fouling material

Fouling challenges were achieved using realistic process streams, in all the studies in this thesis. The protein, DNA, solids and lipid concentrations in the different foulants used are listed in Table 3-1. The particle size distribution of the particulates in the *E. coli* foulants, mainly whole cells or cell debris, are shown in Figures 3-1 and 3-2. It is apparent that the partially clarified homogenates predominantly contained cell debris of an average size of ~ 0.12 μm. A small amount of whole cells, which may have escaped total disruption under the harsh homogenisation conditions, were also present and had an average size of ~ 0.8 μm. Unprocessed *E. coli* Fab' fermentation broth was shown to contain predominantly whole cells of an average size of 0.9 μm but also contained a small amount of debris with an average size of ~ 0.1 μm as well as residual amounts of large particulates of sizes 7 – 8 μm. These larger particulates may have been external contaminants but were completely removed by subsequent centrifugation.

Foulant	Protein (mg/mL)	DNA (ng/μL)	Solids (mg/mL)	Lipids (mg/mL)
Yeast homogenate (disc stack centrifuged)	20	nd[(a)]	350	3.2
E. coli (TOP10) homogenate (partially clarified)	2.4	110	4.2	nd
E. coli (Fab') homogenate (partially clarified)	6.1	110	1.2	nd
E. coli (Fab') whole cells (non-clarified)	nd	nd	17	nd

Notes: (a) nd = Not determined.

***Table 3-1**: Concentrations of protein, DNA, solids and lipids in the foulants.*

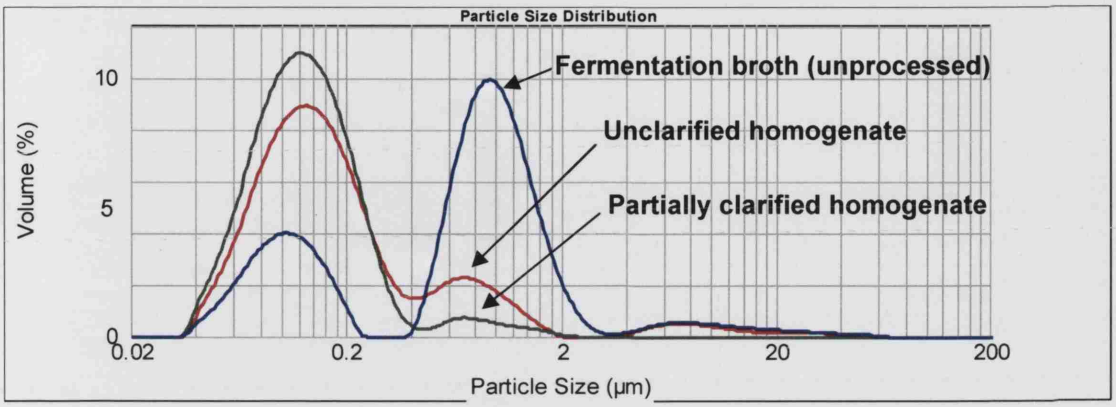

***Figure 3-1**: Particle size distribution of E. coli TOP10 foulant.*

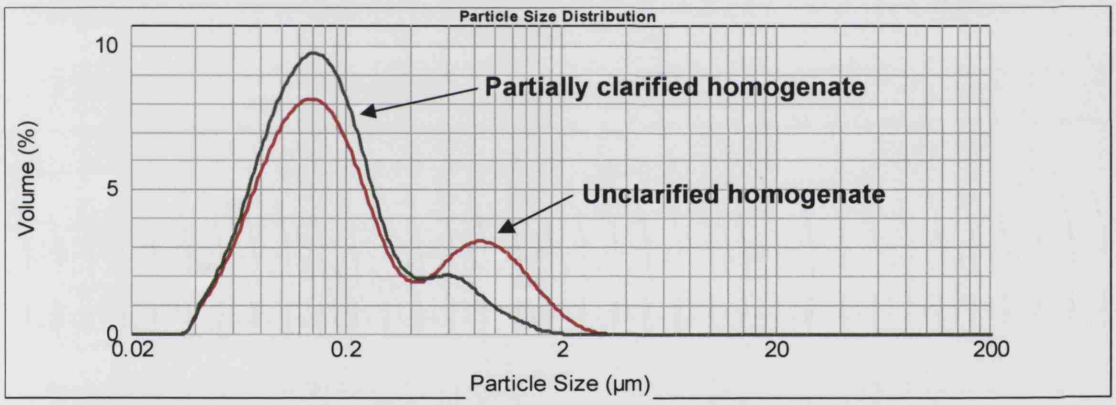

***Figure 3-2:** Particle size distribution of E. coli Fab' foulant.*

Since the homogenised fouling material applied in the studies was subjected to high shear rates in a high-pressure homogeniser during preparation, the majority of the original large genomic DNA was expected to be degraded into small fragments (Levy et al., 1999). This was confirmed by gel electrophoretic analysis (Figure 3-3) which showed the majority of fragments were in the range of 300 – 750 bp in size.

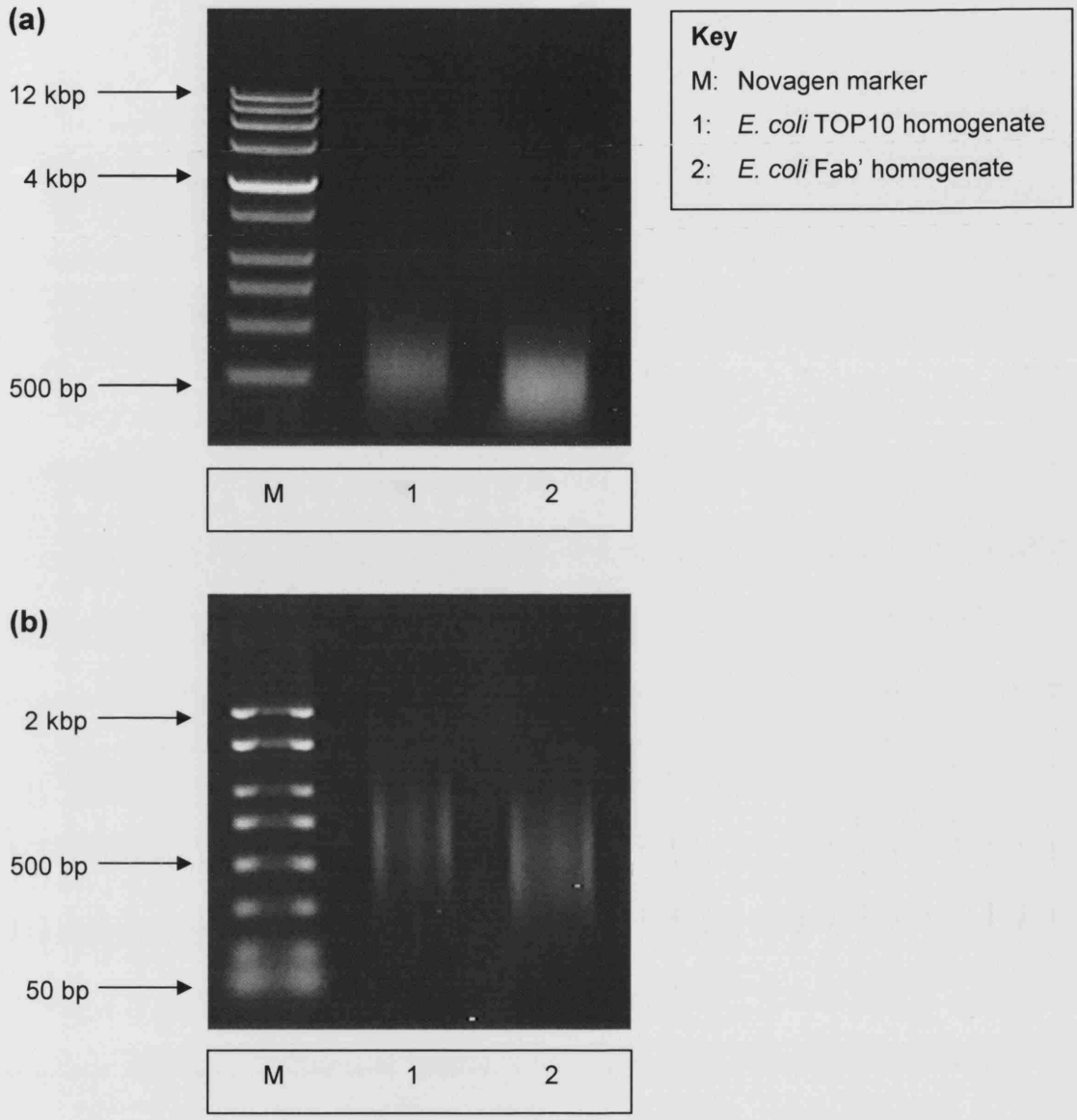

Figure 3-3: *Standard agarose gels showing the size of DNA fragments in the foulants. DNA is noted at ~ 300 – 750 bp region. (a) 1.2% agarose gel with Novagen PCR Markers (500 bp – 12 kbp); (b) 2% agarose gel with Novagen PCR Markers (50 bp – 2 kbp).*

3.3 FRONTAL ANALYSIS (CHAPTER 4)

3.3.1 Materials

3.3.1.1 Description of equipment

Chromatographic procedures were performed using an FPLC unit (GE Healthcare, Uppsala, Sweden), controlling the operation of a XK^{TM}16 column (GE Healthcare, Uppsala, Sweden), manually packed to a bed height of 5.0 ± 0.1 cm. An anion exchanger, DEAE Sepharose^{TM} Fast Flow, was used in this work and supplied by GE Healthcare (Uppsala, Sweden). The matrix has an average particle size of ~ 95 μm and a particle size distribution of 45 – 165 μm, as quoted by the manufacturer. The FPLC's built-in UV monitoring and conductivity measuring functions sent data to a PE Nelson 970 A/D converter interfaced with a computer running Turbochrom (v.2.1; Perkin Elmer, San Jose, CA, USA) data acquisition software. Spectrophotometric assays were performed using a Beckman DU 650 spectrophotometer (Beckman Instruments Ltd., High Wycombe, Buckinghamshire, UK).

3.3.2 Methods

3.3.2.1 BSA breakthrough curve determination

The following method was used to determine the breakthrough curves in all the frontal analysis tests. Before use, freshly packed columns were equilibrated with 3 column volumes (CVs) of 20 mM phosphate buffer, pH 7 (start buffer). BSA at 2 mg/mL in 20 mM phosphate buffer, pH 7 was fed to the column at a flow rate of 2 mL/min until the BSA effluent concentration, as measured by UV absorption at 280 nm (A_{280}), equalled the feed concentration. The column was washed with start buffer to remove unbound protein until the A_{280} signal returned to the baseline. Bound BSA was eluted by a step change in mobile phase composition to 1 M sodium chloride in 20 mM phosphate buffer, pH 7 and continued until the A_{280} signal returned to baseline. The column was then re-equilibrated with start buffer before further application of fouling stream. Results for the breakthrough curves are presented graphically as the ratio of output concentration of BSA to input concentration of BSA (C/C_0) versus time. The dynamic capacity at the 1% and 100% breakthrough level was calculated by calculating the amount of BSA which flowed through the column, determined as the

area below the breakthrough curve at C/C_0=0.01 and C/C_0=1 respectively, and subtracting this from the amount of BSA loaded in the equivalent time.

3.3.2.2 Method of application of fouling challenges to the column

Two modes of fouling challenge to the column were examined. In the first, the foulant challenge was presented to the column as a single volume of process material. In the second, the impact of making successive small foulant challenges to the column was investigated. The experimental conditions are summarised in Table 3-2.

Pre-treatment	Foulant volume loaded per cycle (CV)	Number of cycles	Total foulant volume loaded (CV)
Effect of repeated fouling on column breakthrough			
Ultracentrifugation	0.2	10	2
Disc stack centrifugation	0.2	10	2
Effect of loading large quantities of particulate solids to packed beds			
Disc stack centrifugation	1	1	1
Disc stack centrifugation	5	1	5
Disc stack centrifugation	10	1	10
Ultracentrifugation	10	1	10

***Table 3-2**: Experimental conditions used in fouling studies. All experiments were based on a 10 mL column.*

For the single volume foulant challenges a frontal analysis test, with BSA solution, was first carried out on a fresh column as described above. Volumes of either 10, 50 or 100 mL of fouling material were then applied to the column, after which the bed was washed to remove unbound protein from the matrix, using a gradient of NaCl from 0 M to 1 M NaCl and back to 0 M NaCl over 3 CVs. Frontal analysis was repeated for the fouled column. A different column was used for each of the different foulant volume challenges so that each column was fouled only once in this set of experiments. This fouling experiment was carried out both with yeast homogenate clarified by ultracentrifugation and by disc stack centrifugation, separately. Columns were fouled only once in this set of experiments.

Successive small fouling challenges were applied by repeatedly loading 2 mL quantities of yeast homogenate to the same column. Each cycle consisted of carrying out a frontal analysis test with BSA; loading of 2 mL of yeast homogenate onto the column; washing of unbound protein from the matrix using a gradient of NaCl from 0 M to 1 M NaCl and back to 0 M NaCl over 3 CVs; and repetition of the frontal analysis test. The total fouling procedure comprised ten such cycles. This fouling experiment was carried out both with yeast homogenate clarified by ultracentrifugation and by disc stack centrifugation, separately.

All fouling material was applied to the column at a flow rate of 2.6 mL/min (78 cm/h). Use of higher flow rates was avoided to reduce the risk of clogging of the packed bed and to avoid bed compression.

3.3.2.3 Pressure-flow measurements

The variation in pressure drop across the column was monitored as a function of flow rate both for a clean column and after challenging the column with either 50 or 100 mL of yeast homogenate which had been clarified by disc stack centrifugation. At each flow rate the pressure was allowed to stabilise and was then recorded. After fouling at a flow rate of 2.6 mL/min, the columns were washed with a gradient of NaCl in 20 mM phosphate from 0 M to 1 M NaCl and back to 0 M NaCl over 3 CVs and the pressure-flow curve was determined again.

3.3.2.4 Clean-in-place (CIP) protocol

Cleaning-in-place (CIP) was carried out using 3 CVs of 20 mM phosphate buffer at 2 mL/min, followed by 1 M sodium hydroxide at ambient temperature at 0.1 mL/min. The flow rate was designed to keep the column in contact with sodium hydroxide for a long period, whilst maintaining a flushing flow to remove dissolved foulants. This procedure was carried out for 5 hours. The column was then flushed with 20 mM phosphate buffer containing 1 M sodium chloride until the inlet and outlet pH of the buffer were the same within ± 0.5 pH units.

3.4 EXTENDED REVERSE-FLOW TECHNIQUE (CHAPTER 5)

3.4.1 Materials

3.4.1.1 Chromatography system

Chromatographic procedures were performed on an AKTA^{TM} explorer 100 (GE Healthcare, Uppsala, Sweden). System control and data acquisition was by an UNICORN^{TM} control system (GE Healthcare, Uppsala, Sweden) installed on a Pentium III computer (Compaq, Bristol, United Kingdom) with 256 MB of RAM.

3.4.1.2 Chromatography columns

The majority of the experiments were conducted using 1 mL HiTrap^{TM} SP FF columns (0.7 cm internal diameter with a bed height of 2.5 cm) pre-packed with SP Sepharose FF. Experiments were also carried out using 5 mL HiTrap^{TM} SP FF pre-packed columns (1.6 cm internal diameter with a bed height of 2.5 cm). The other columns used were XK^{TM}16 and XK^{TM}26 (1.6 cm and 2.6 cm internal diameter, respectively) glass chromatography columns. All columns were from GE Healthcare (Uppsala, Sweden).

3.4.1.3 Chromatography matrix and packing

SP Sepharose FF, a strong cation exchanger, was obtained from GE Healthcare (Uppsala, Sweden). The XK16 and XK26 columns were packed at a flow rate of 180 cm/h to a bed height of 2.5 ± 0.1 cm as per manufacturer's instructions.

3.4.2 Methods

3.4.2.1 General

For all experiments the ratio of fouling stream volume to column volume was 5:1 and was loaded at a linear flow rate of 156 cm/h. Pulse experiments were carried out at a linear flow rate of 78 cm/h with acetone tracer volumes of 15, 75 and 199 μL for 0.7 (including those arranged in series), 1.6 and 2.6 cm internal diameter columns, respectively. The UV detector was set to measure absorbance at 280 nm. An acetone tracer (2% v/v acetone in water), with a volume equivalent to 1.5% of the column volume, was use throughout the study to measure bed dispersion. The general procedure of the extended reverse-flow technique used is given in Figure 3-4.

3.4.2.2 Determining dead volume

It is necessary to determine the dead volumes of the system. To do this, the tubing leading to the top of the column was attached to the UV detector via a piece of tubing of known volume (0.19 μL). Subsequently, a 15 μL acetone tracer was applied to the system at 0.5 mL/min. By subtracting the known volume of the connecting tubing from the retention volume reading of the eluted acetone pulse, the dead volume of the system in down-flow mode was determined. Identical experiments were carried out to determine the dead volumes of the system in up-flow mode. This procedure was repeated with acetone samples of 75 μL and 199 μL at flow rates of 2.61 mL/min and 6.90 mL/min, respectively. The tubing connecting to the top and bottom flow adaptors in the XK columns were also taken into account by disconnecting them from the column and connecting them to the experimental set-up when determining their dead volumes.

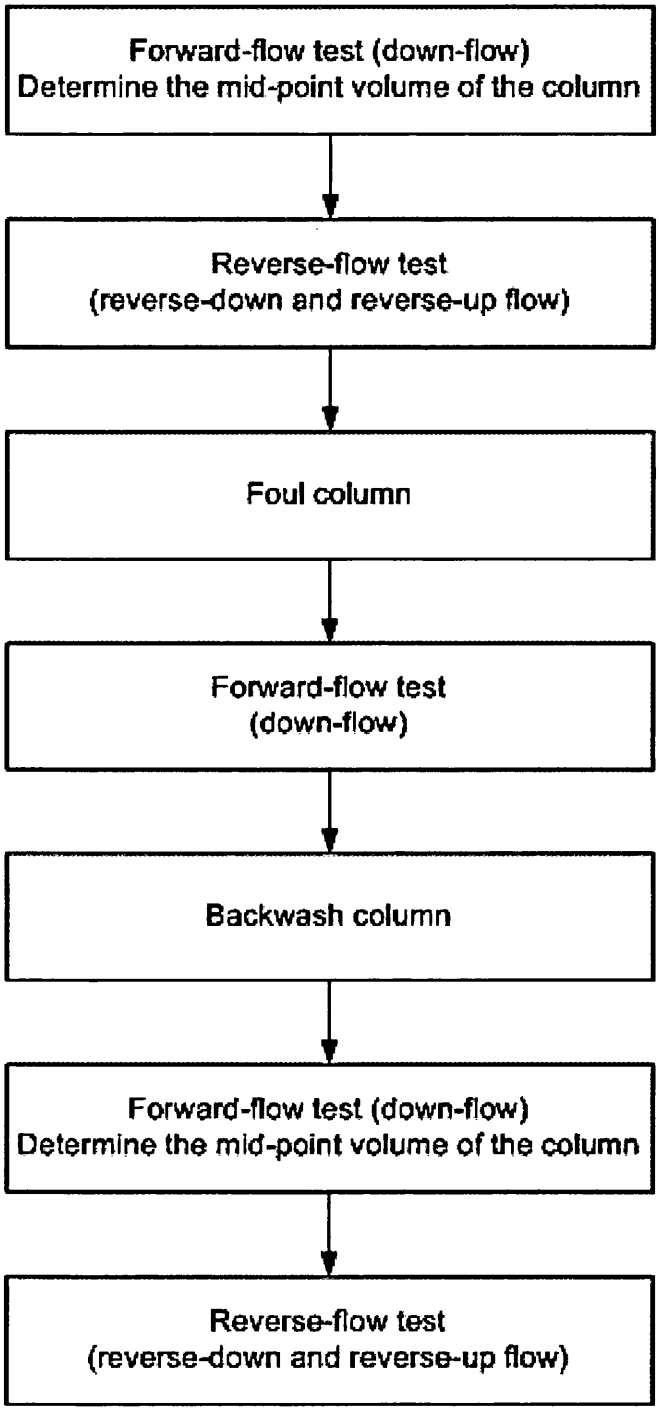

***Figure 3-4**: Outlined procedure for the extended reverse-flow technique.*

3.4.2.3 Determining dispersion due to extra-column effects

To determine the contribution of extra-column dispersion an acetone pulse was injected into the system (without the column in place) in down- and up-flow directions for the same range of flow rates and acetone pulse volumes that were used in the experiments to determine the extra-column dispersion when run in down-flow (σ^2_{sdf}) and up-flow (σ^2_{suf}), respectively (cf. Section 3.4.2.2). The extra-column dispersion when run in reverse-down-flow (σ^2_{srdf}) and reverse-up-flow (σ^2_{sruf}) were also determined by the procedure just described except that the direction of flow was reversed at the appropriate elution volume as determined from the dead volumes.

3.4.2.4 Forward-flow test (down-flow and up-flow)

An acetone tracer was applied using a sample loop at the sample valve of the AKTA system. The acetone pulse was eluted through the column (fresh or fouled) at a flow rate of 78 cm/h in down-flow direction. The resulting acetone peak was analysed in terms of residence time distribution.

3.4.2.5 Reverse-flow test (reverse-down-flow and reverse-up-flow)

An acetone tracer was applied using a sample loop at the sample valve of the AKTA system. The acetone pulse was eluted through the (fresh or fouled) column at a flow rate of 78 cm/h, in either down-flow or up-flow direction, until the axial centre of the column at which the direction of flow was reversed causing the acetone pulse to leave the column from the inlet. The resulting acetone peak was analysed in terms of residence time distribution.

3.4.2.6 Testing of fresh columns

Firstly, a forward-flow test (down-flow) was performed as per Section 3.4.2.4. The first absolute moment or mean solute residence time of the resultant acetone peak was determined and the void volume of the column was calculated. This was necessary in order to calculate the elution volume required to bring the acetone pulse from the injection value to the axial centre of the column. Reverse-flow tests (reverse-down-flow and reverse-up-flow) were then performed on the column as per Section 3.4.2.5.

3.4.2.7 Fouling and testing of fouled columns

The column was fouled with 5 CVs of partially clarified *E. coli* TOP10 homogenate that was loaded at a flow rate of 156 cm/h. The column was washed to baseline with water to remove unbound foulants.

Firstly, a forward-flow test (down-flow) was performed as per Section 3.4.2.4. Following the test the column was backwashed with water until a steady baseline was achieved, in order to remove any loosely-bound foulants that may obscure the peaks from subsequent reverse-flow tests. A further forward-flow test was performed on the backwashed column. The first absolute moment or mean solute residence time of the resultant acetone peak was determined and the void volume of the column was calculated, which was necessary in order to calculate the required elution volume to bring the acetone pulse from the injection value to the axial centre of the column. Reverse-flow tests (reverse-down-flow and reverse-up-flow) were then performed on the column as per Section 3.4.2.5.

3.4.2.8 Experimental set-up with single columns

To investigate the dispersive effects of fouling on columns with increasing diameter but identical bed heights, the following columns (their corresponding internal diameter is indicated in parentheses) were used: 1 mL HiTrap SP FF (0.7 cm); 5 mL

HiTrap SP FF (1.6 cm); XK16 (1.6 cm); and XK26 (2.6 cm). The bed lengths were 2.5 cm in all the columns. Each column was tested when fresh and after fouling.

3.4.2.9 Experimental set-up with columns in series

To investigate the dispersive effects of fouling with increasing bed length, 1 mL HiTrap SP FF pre-packed columns were used. They were arranged in series of one, two and three columns. Fresh columns were tested individually before being arranged in series, after which they were tested collectively with a forward-flow test. The column series was then fouled and another forward-flow test (down-flow) was performed. Subsequently, the columns in series were disconnected and each column was individually backwashed and tested.

3.4.3 Data processing

3.4.3.1 Calculation of first absolute moments and second central moments

The mean solute residence time, t_R, and the peak variance, σ^2, were determined by application of the method of statistical moments (McQuarrie, 1963; Grubner et al., 1967, Grubner, 1968; Dyson, 1998). The first absolute moment is the mean residence time and the second central moment is equivalent to the peak variance. The peak variance is a measure of the column efficiency and comparison of peak variances before and after fouling was used to quantify the effects of fouling (see Chapter 5).

The general formula for the nth absolute moment, M_n, and nth central moment, μ_n, is given by equations 3-1 and 3-2, respectively:

$$M_n = \frac{\int_{-\infty}^{+\infty} t^n \cdot h_t dt}{\int_{-\infty}^{+\infty} h_t dt} \qquad (3\text{-}1)$$

$$\mu_n = \frac{\int_{-\infty}^{+\infty}(t - M_1)^n \cdot h_t dt}{M_0} \qquad (3\text{-}2)$$

where h_t is the effluent concentration at time t and $M_0 = \int_{-\infty}^{+\infty} h_t dt$ (the zeroth moment). Therefore, it can be denoted that $M_1 = t_R$ and $\mu_2 = \sigma^2$.

It must be noted that elution time (t) was replaced by elution volume in the analysis of the results in Chapter 5. Accordingly, the first absolute moment corresponds to the mean residence volume (V_R) and the second central moments still corresponds to the peak variance but in units of volume (i.e., mL^2).

3.5 CONFOCAL SCANNING LASER MICROSCOPY (CHAPTER 6)

3.5.1 Materials

3.5.1.1 Description of equipment

The confocal experiments were performed with an inverted confocal laser scanning microscope (Leica SP2 DM IRBE, Leica Microsystems GmbH, Mannheim, Germany) equipped with helium/neon, krypton/argon and argon lasers. A 63x1.4 oil immersion objective was used for the experiments. Protein-Cy3 was excited at 543 nm and the emission detection range was set to 560-600 nm. Protein-Cy5.5 was excited at 633 nm and the emission detection range was set to 650-710 nm. dsDNA-PicoGreen was excited at 488 nm and the emission detection was set to 505-535 nm. BacLight Red-labelled whole cells or cell debris were excited at 568 nm and the emission detection range was set to 644-690 nm.

3.5.1.2 Chromatography matrix

Q Sepharose Fast Flow, a strong anion exchanger, was obtained from GE Healthcare (Uppsala, Sweden). The particle size distribution of the resin was determined and is shown in Figure 3-5. The mean particle size was ~ 95 μm. The inter-

decile particle size range was 55 – 145 µm, which is consistent with the particle size range of 45 – 165 µm quoted by the manufacturer.

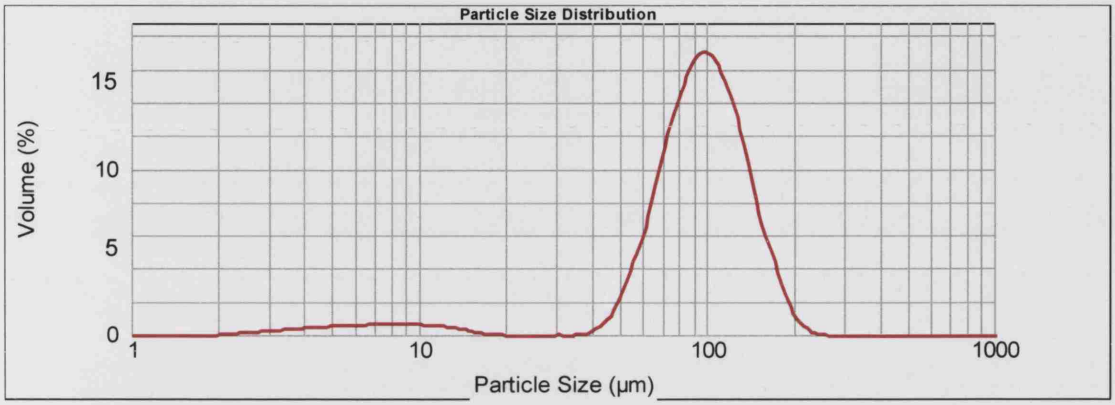

***Figure 3-5**: Particle size distribution of Q Sepharose FF resin.*

3.5.1.3 Confocal flow cell and packing

A flow cell of similar design to that used by Hubbuch et al. (2002) was used in the study (Figure 3-6). The design of the flow cell consisted of a Perspex block with precision-drilled inlets (45˚) on either side and an open channel (~ 6 mm in length) grooved into the bottom of the block. A window for observing under the microscope was created by fixing a microscope coverslip to the open channel using epoxy glue (Ciba Araldite Rapid, Casco AB, Stockholm, Sweden). The column had a total length of 22 mm and a cross-sectional area of 3 mm^2. The column volume was 0.066 mL. The flow cell was connected to a P-900 pump (GE Healthcare, Uppsala, Sweden) which allowed liquid-handling. Polypropylene frits from GE Healthcare (Uppsala, Sweden) were placed at the ends of the flow channel and were held in place using conventional screw fittings from GE Healthcare (Uppsala, Sweden). The flow cell was packed with equilibrated Q Sepharose FF by using a syringe and manually applying pressure. The packed flow cell was then equilibrated with 3 mL of 20 mM Tris-HCl, pH 8.0 at a flow rate of 0.2 mL/min.

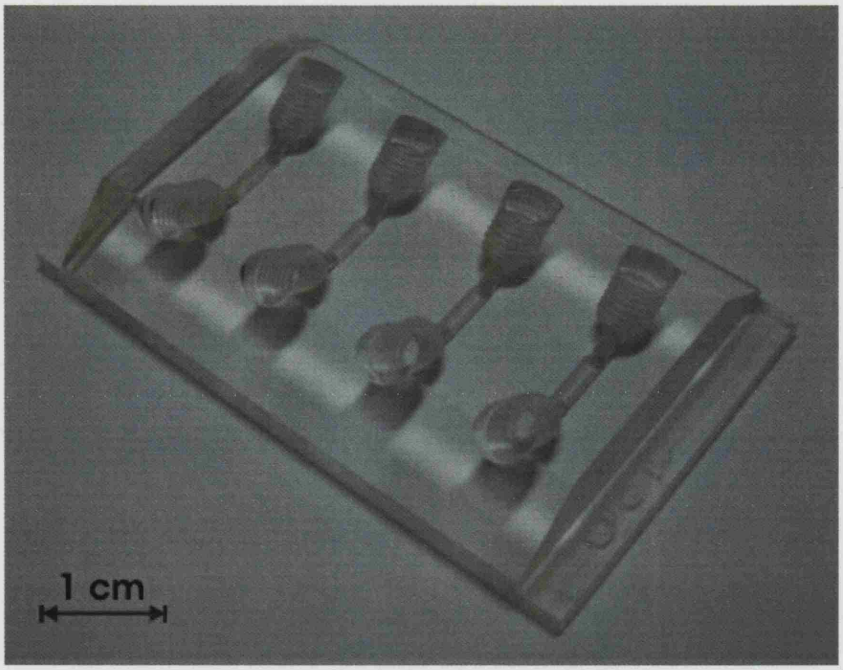

***Figure 3-6**: Picture of the confocal flow cell used in the study.*

3.5.2 Methods (general)

3.5.2.1 Fluorescent labelling of BSA with Cy5.5

BSA was dissolved in degassed conjugation buffer (100 mM Na_2CO_3, pH 9.3) to a concentration of 2 mg/mL. 1.0 mL of BSA conjugation solution was added to one vial of Cy5.5, pre-measured by the manufacturer and containing sufficient reactive dye to label 1.0 mg of protein. This mixture was incubated for 1 hour. BSA test solution was made by adding 1mL of labelled BSA to 9.0 mL of unlabelled BSA dissolved in degassed 20 mM Tris-HCl, pH 8.0.

3.5.2.2 Fluorescent labelling of E. coli host cell proteins (foulant proteins) with Cy5.5 or Cy3

0.5 mL of foulant solution was added to 0.5 mL 100 mM Na_2CO_3, pH 9.3 degassed conjugation buffer. The resultant 1.0 mL solution was added to pre-measured

Cy5.5 or Cy3 dye (capable of labelling 1 mg of protein) and incubated for 2 hours at room temperature. Foulant Cy dye-protein solution was diluted to a ratio of 1:20 (foulant Cy dye-protein to unlabelled foulant).

3.5.2.3 Normalisation of the fluorescence signal

Cyanine dye fluorophores are known to be pH insensitive (Mujumdar et al., 1993), and PicoGreen has been previously reported as being highly stable under alkaline conditions (Batel et al., 1999). Nevertheless, the fluorescent enhancement of PicoGreen has been shown to decrease at high pH conditions (Rock et al., 2003) and in the presence of sodium chloride and BSA solution (Singer et al., 1997). To avoid such effects obscuring the comparison of fluorescent intensities between experiments, the beads were always placed in the same buffer conditions (20 mM Tris-HCl, pH 8.0) before visualising under the microscope.

Any fluctuations in the laser source intensity were checked using Q Sepharose beads that had been saturated with BSA labelled with Cy5.5 before each experiment. The beads were prepared as described in Sections 3.5.2.1 and 3.5.3.2. Only relatively small fluctuations were observed.

3.5.3 Methods (finite bath experiments)

3.5.3.1 Fouling of Q Sepharose FF and fluorescent labelling of double stranded deoxyribonucleic acids (dsDNA) with PicoGreen

0.5 mL of 50% (v/v) Q Sepharose FF slurry in 20 mM Tris-HCl, pH 8.0 was added to 10 mL of foulant liquor prepared as above. In all experiments a volumetric ratio of 1:40 Q Sepharose FF to foulant was used. The resulting slurry was agitated for 5 minutes, 1 hour or 12 hours at 4°C, depending on the study. At the end of the exposure, the fouled Q Sepharose FF was washed three times with equal volumes of 20 mM Tris-HCl, pH 8.0 by repeated dilution, centrifugation (14,000 g for 30 s) and decanting. In the final step 20 mM Tris-HCl, pH 8.0 was added to give a 50% (v/v) slurry to which 10 μL of PicoGreen was added and incubated at room temperature for

30 minutes. PicoGreen shows a > 1000-fold fluorescence enhancement upon binding to dsDNA and much less fluorescence enhancement upon binding to ssDNA or dsRNA (Singer et al., 1997).

3.5.3.2 BSA adsorption time series

Protein adsorption time series studies were conducted on samples of fresh and fouled resins. In all cases samples were withdrawn and prepared for CSLM analysis at predetermined intervals. Each resin sample was washed three times by a re-suspension, centrifugation (14,000 g for 30 s) and decanting protocol using 20 mM Tris-HCl, pH 8.0 as the wash buffer. Time series experiments were started by adding 0.5 ml of 50% (v/v) Q Sepharose FF slurry in 20 mM Tris-HCl, pH 8.0 to the labelled BSA in a 20 mL sample tube and agitated using a magnetic stirrer throughout. Samples of 0.3 mL volume were withdrawn from the sample tube and diluted in 0.7 mL of 20 mM Tris-HCl, pH 8.0. These were washed three times with equal volumes of 20 mM Tris-HCl, pH 8.0 by repeated dilution, centrifugation (14,000 g for 30 s) and decanting. This was followed by re-suspension of the pellet in 20 mM Tris-HCl, pH 8.0 to a volume of 1 mL. 12 μL of the resultant Q Sepharose FF slurry was used to prepare slides for visualisation by CSLM.

3.5.3.3 Clean-in-place (CIP) time series

CIP solution – either 1M NaCl dissolved in 20 mM Tris-HCl, pH 8.0 (1 M NaCl) or 1M NaCl dissolved in 1 M NaOH (1 M NaCl + 1 M NaOH) – equal to the volume of foulant used was added to 0.25 mL of fouled Q Sepharose FF labelled for both dsDNA and foulant protein in a 20 mL sample tube which was constantly stirred. 0.3 mL samples were withdrawn at predetermined intervals and diluted in 0.7 mL of CIP solution. This was washed three times with equal volumes of 20 mM Tris-HCl, pH 8.0 by repeated dilution, centrifugation (14,000 g for 30 s) and decanting. 12 μL of the resultant Q Sepharose FF slurry was used to prepare slides for visualisation.

3.5.3.4 Post-CIP adsorption time series

The CIP procedure was repeated as above except that no samples were withdrawn and foulant protein was not labelled. After 1 hour of constant stirring with CIP solution the Q Sepharose FF beads were washed with one volume of CIP solution by dilution, centrifugation (14,000 g for 30 s), decanting. This was followed by a further three washes with 20 mM Tris-HCl, pH 8.0. A BSA adsorption time series was prepared as outlined above using 0.25 mL of fouled, post-CIP resin.

3.5.4 Methods (flow cell experiments)

3.5.4.1 Multicolour labelling of fouling material to visualise HCPs and dsDNA

0.5 mL of foulant solution was incubated with 0.5 mL 100 mM Na_2CO_3, pH 9.3 degassed conjugation buffer for 1 hour at room temperature. The resultant 1.0 mL solution was added to pre-measured Cy5.5 dye (capable of labelling 1 mg of protein) and incubated for a further 2 hours at room temperature. Foulant protein-Cy5.5 solution was diluted to a ratio of 1:20, foulant protein-Cy5.5 to unlabelled foulant. To this protein-labelled foulant mixture, PicoGreen was added to a concentration of 10 µL per mL of foulant. The mixture was allowed to incubate for a further 1 hour with frequent agitation.

3.5.4.2 Fouling of Q Sepharose FF bed in a flow cell

A flow cell packed with Q Sepharose FF was equilibrated with 20 mM Tris-HCl, pH 8.0 for 20 minutes at a flow rate of 0.08 mL/min. After equilibration, 5 CVs of partially clarified Fab' *E. coli* homogenate prepared as described in Section 3.2.3 was loaded onto the packed bed at a flow rate of 0.08 mL/min. Finally, the bed was washed and re-equilibrated with 20 mM Tris-HCl, pH 8.0 for 20 minutes at a flow rate of 0.08 mL to remove unbound foulants.

3.5.4.3 BSA adsorption time series in a flow cell

Protein adsorption time series studies were conducted on fresh, fouled and CIP-treated packed beds. Fluorescently-labelled BSA solution (2 mg/mL) was loaded onto the equilibrated bed at a flow rate of 0.08 mL/min. Visualisation of the bed by CSLM was done in real-time and *in situ*, and confocal images were taken at predetermined time intervals.

3.5.4.4 CIP time series

Flow cells packed with Q Sepharose FF were fouled as described in Section 3.5.4.2. After fouling and re-equilibrating, the bed was first washed with 15 CVs of 20 mM Tris-HCl, 1 M NaCl, pH 8.0 at a flow rate of 0.08 mL/min. During the wash, visualisation of the bed by CSLM was done in real-time and *in situ*. Confocal images were taken at predetermined time intervals. After completing the first wash, the bed was re-equilibrated with 5 CVs of 20 mM Tris-HCl, pH 8.0 to normalise the fluorescence signal (cf. Section 3.5.2.3), after which another confocal image of the bed was taken. Subsequently, the bed was washed with 15 CVs of 1 M NaOH at a flow rate of 0.08 mL/min. Again, visualisation of the bed by CSLM was done in real-time and *in situ* and confocal images were taken at predetermined time intervals during the wash. After completing the NaOH wash, the bed was re-equilibrated with 5 CVs of 20 mM Tris-HCl, pH 8.0 to normalise the fluorescence signal, after which another confocal image of the bed was taken.

3.5.5 Methods (visualising whole cells and cell debris)

3.5.5.1 General approach

CSLM was used to visualise the adsorption of whole cells and cell debris to an anion exchanger. Q Sepharose FF beads were incubated with unclarified fermentation broth containing whole *E. coli* cells or cell debris (which were homogenised on the day of use) in a finite bath. The whole cells or cell debris were labelled with BacLight Red which is a fluorescent, non-nucleic acid labelling reagent specific for bacterial cell

membranes. dsDNA in the fermentation broth was labelled with PicoGreen. As both cells/debris and dsDNA would be expected to bind to only a thin layer at the bead exterior, knowledge of their competitive adsorption may be important in understanding the interactions between the two foulants in a realist process stream.

3.5.5.2 Fouling of Q Sepharose FF and fluorescent labelling of whole cells or cell debris with BacLight Red

0.5 mL of 50% (v/v) Q Sepharose FF slurry in 20 mM Tris-HCl, pH 8.0 was added to 10 mL of foulant liquor. In all experiments a volumetric ratio of 1:40 Q Sepharose FF to foulant was used. To this mixture, 20 μL of BacLight Red was added, and the resulting slurry was agitated at ambient temperature for 30 minutes. At the end of the exposure, the fouled Q Sepharose FF was washed three times with equal volumes of 20 mM Tris-HCl, pH 8.0 by repeated dilution, centrifugation (14,000 g for 30 s) and decanting. This was followed by re-suspension of the pellet in 20 mM Tris-HCl, pH 8.0 to give a 50% (v/v) slurry.

3.5.5.3 Fouling of Q Sepharose FF and fluorescent labelling of whole cells or cell debris with BacLight Red and dsDNA with PicoGreen

0.5 mL of 50% (v/v) Q Sepharose FF slurry in 20 mM Tris-HCl, pH 8.0 was added to 10 mL of foulant liquor. In all experiments a volumetric ratio of 1:40 Q Sepharose FF to foulant was used. To this mixture, 20 μL of BacLight Red was added, and the resulting slurry was agitated at ambient temperature for 30 minutes. At the end of the exposure, the fouled Q Sepharose FF was washed three times with equal volumes of 20 mM Tris-HCl, pH 8.0 by repeated dilution, centrifugation (14,000 g for 30 s) and decanting. This was followed by re-suspension of the pellet in 20 mM Tris-HCl, pH 8.0 to a volume of 10 mL. To the resulting slurry, 10 μL of PicoGreen was added and incubated for 30 minutes at ambient temperature with mixing. At the end of the incubation, the fouled Q Sepharose FF was washed three times with equal volumes of 20 mM Tris-HCl, pH 8.0 by repeated dilution, centrifugation (14,000 g for 30 s) and

decanting. This was followed by re-suspension of the pellet in 20 mM Tris-HCl, pH 8.0 to a volume of 10 mL.

3.5.6 Data processing

3.5.6.1 Image analysis

The images of cross-sections through the centre of the beads were analysed with the supplied Leica Control Software (version 2.5) and recorded at a resolution of 512x512 pixels. To reduce the background fluorescence and noise, the images were generated by averaging 6 scans per image (or 10 scans per image for visualising whole cells and cell debris). Further image analysis was done using ImageJ software version 1.31 (National Institute of Health, Bethesda, Maryland, USA).

3.5.6.2 Calculation of volume-normalised relative intensity from CSLM

Ljunglof and Thommes (1998) calculated the overall fluorescence observed within the bead by dividing the particle radius into defined segments, and calculating the corresponding volume of a shell. By multiplying the volume by the fluorescence intensity of the segment, the total fluorescence of the shell was obtained (equation 3-3). The average intensity within each shell represents the concentration of adsorbed protein and the summation of the intensity of each segment divided by the particle volume will yield the total intensity or solid phase concentration of the particle (equation 3-4).

$$I_{\text{int egr.}}^{\text{shell}} = \bar{I}_{\text{seg}}\left[\left(r_a^3 - r_i^3\right)\frac{4}{3}\pi\right] \tag{3-3}$$

$$Q_{\text{rel}} = \frac{\sum_{\text{shells}}\left(I_{\text{int egr.}}^{\text{shell}}\right)}{V_p} \tag{3-4}$$

where $I_{int\,egr.}^{shell}$ is the integral intensity of fluorescence profile, Q_{rel} is the relative capacity of the bead, I_{seg} is the average intensity within a segment, r_a is the outer radius of the particle shell and r_i is the inner radius of the particle shell.

This calculation method only takes into account the intensity of relatively small segments along the particle radius and assumes a symmetrical intensity pattern throughout the bead. Although adequate for analysing clean beads, it may not properly approximate the total intensity for fouled beads where distributions may not be symmetrical.

An alternative method for calculating the total intensity of the bead from the optical cross-section through the centre of the bead that will better account for the potential asymmetrical and non-uniform distribution of dyed materials, and thus yield a better approximation of the total intensity of the entire bead, was adopted. In this method, the total intensity of the bead cross-section was determined. The average intensity value for half the bead cross-section (semi-circle) was then multiplied by the circumference of the bead, to achieve the intensity of the total bead. This value was normalised with respect to volume to give the relative solid phase concentration expressed as arbitrary units per volume of adsorbent (equation 3-5).

$$Q_{rel} = \frac{I_T r_p \pi}{V_p} \tag{3-5}$$

where Q_{rel} is the relative capacity of the bead, I_T is the total intensity of the bead cross-section at the centre of the bead, r_p is the radius of the particle and V_p is the particle volume.

3.5.6.3 Calculation of effective diffusivity from confocal images

If a shrinking core model can be assumed then a single lumped kinetic parameter or effective diffusivity, D_e, can be estimated directly from the confocal images by using the position of the adsorption front. The approach assumes that the adsorption layer is saturated, and the effective diffusivity is calculated from the linear regression of the

infinite volume solution of the model that takes into account external mass-transfer resistance (Teo and Ruthven, 1986) as shown in equation 3-6:

$$\frac{D_e t}{R_p^2} = \frac{\varepsilon_p D_p}{R_p^2}\frac{C_0}{q_s}t = \left[1 + \frac{\varepsilon_p D_p}{k_f R_p}\right] I_2 - I_1 \qquad (3\text{-}6)$$

where ε_p is the intraparticle porosity, D_p is the pore diffusivity, C_0 is the feed protein concentration, R_p is the particle radius, R_f is the radial position of the front, k_f is the external fluid film mass-transfer coefficient, q_s is the saturation adsorbed-phase concentrations, and:

$$I_1 = \int_1^{\eta} \eta \, d\eta = \tfrac{1}{2}\left(\eta^2 - 1\right) \qquad (3\text{-}7)$$

$$I_2 = \int_1^{\eta} \eta \, d\eta = \tfrac{1}{3}\left(\eta^3 - 1\right) \qquad (3\text{-}8)$$

where η is the fractional uptake given by (R_f/R_p).

No attempt was made to de-convolute the individual parameters, such as D_p, ε_p and k_f, in equation 3-6, as further independent experiments may be required to determine the values of some of the parameters. Physical complications that can develop by the presence of fouling material can make this less straight forward. Instead, the effective diffusivity (D_e), as described in equation 3-6, alone was used to provide an indication of the overall adsorption rate and used for comparison purposes.

3 MATERIALS AND METHODS

This chapter provides the background information on the materials, equipment, analytical techniques and experimental methods used in this thesis. It is divided into a section devoted to the general materials and analytical methods used throughout this thesis; a section describing the method of preparation and characterisation of the fouling material used in the studies; and individual sections relating specifically to the work presented in Chapters 4, 5 and 6.

3.1 GENERAL MATERIALS AND METHODS

3.1.1 Chemicals

All chemicals, unless specified otherwise, were obtained from Sigma Chemical Co. Ltd. (Poole, Dorset, UK) and were of analytical grade. Bakers' yeast (*Saccharomyces cerevisiae*) was supplied by DCL Yeast Ltd. (Sutton, Surrey, UK). Bovine serum albumin, BSA (A-7030), was from Sigma Chemical Co. Ltd. (Poole, Dorset, UK) and of purity > 98%. Cy™3 and Cy™5.5 mono-reactive labelling kits were obtained from GE Healthcare (Uppsala, Sweden), and PicoGreen™ and BacLight™ Red were obtained from Molecular Probes Europe – Invitrogen (Leiden, The Netherlands).

3.1.2 Agarose gels

Two agarose gels were ran, one of 1.2% w/v agarose to visualise DNA fragments between the ranges 500 bp – 12 kbp. And a second agarose gel of 2% w/v to check DNA fragments between 50 bp – 2 kbp. The agarose was purchased from Sigma Chemical Co. Ltd. (Poole, Dorset, UK) (Cat No: A-9414). The general gel procedure was as described by Sambrook and Russell (2000).

DNA was isolated from crude fouling material using a Genelute Bacterial Genomic DNA Kit (Sigma Chemical Co. Ltd., Poole, Dorset, UK). The protocol

followed the manufacturer's recommended procedure except that Proteinase K and Lysis Solution C were substituted with Column Preparation Solution since the fouling material was cell homogenate so chemical lysis was not needed to extract the DNA from the cells.

The following DNA markers were used to determine DNA fragment lengths: Novagen PCR Markers (50 bp – 2 kbp, Cat No: 69278) and Novagen Perfect Markers (500 bp – 12 kbp, Cat No: 69002).

Both gels were loaded on Pharmacia LKB GNA100 Electrophoresis Gel Trays and powered by Pharmacia Electrophoresis Power Supply (EPS) 500/400 (GE Healthcare, Milton Keynes, UK). The gels ran for 1 hour at 50 V.

The gels were visualised using an Ultra-Violet Products GelDoc-It imaging system (Ultra-Violet Products Ltd., Cambridge, UK).

3.1.3 Assay techniques

3.1.3.1 Total protein assay

The protein assay was a commercially available protein assay kit from Bio-Rad Laboratories Ltd. (Hemel Hempstead, UK). The assay is based on the principal by Bradford (1976). The protocol followed the manufacturer's recommendation for the micro-assay procedure. Adsorption measurements were performed at 595 nm on a Beckmann DU 650 single-beam UV/VIS spectrophotometer (Beckmann Instruments Ltd., High Wycombe, UK). Reproducibility of the assay was typically ± 5% for duplicate samples.

3.1.3.2 Lipid Assay

The amount of lipid in the samples of yeast homogenate was assayed by chloroform extraction and weighing of the dried extract. The method used for the chloroform extraction was that of Bligh & Dyer modified by Kates (1986). A sample

of 1 mL was extracted at ambient temperature with a 2:1 v/v mixture of chloroform:methanol for 2 hours with occasional agitation. After 2 hours the sample was centrifuged with a MSE Europa 24 centrifuge (MSE UK Ltd., Beckham, Kent, UK) at 4000 rpm at 4°C in a stoppered glass vessel. The supernatant was reserved and 4.75 mL of methanol:chloroform:water in the ratio of 2:1:0.8 v/v was added to the pellet. The centrifugation was repeated and the supernatant added to that previously reserved. To the combined supernatant, a further 2.5 mL of chloroform and 2.5 mL of water were added and the mixture agitated. The resulting emulsion was broken by centrifugation with a MSE Europa 24 centrifuge (MSE UK Ltd., Beckham, Kent, UK) for 5 minutes at 4000 rpm and 4°C. The lower chloroform phase was drawn off and evaporated to dryness in a rotary vacuum evaporator. The residue was taken up in 2 mL of 1:1 chloroform:methanol v/v, and placed in a weighing bottle. A further 2 mL of chloroform-methanol mixture was used to wash the evaporator flask and this was added to the first 2 mL in the weighing bottle. The weighing bottle was dried in a desiccator over potassium hydroxide and under nitrogen to a constant weight (± 0.0005 g). Reproducibility of the samples was ± 20% for duplicate samples due to the extended nature of the method and the fact that the potential for introducing errors through phase partitioning was high.

3.1.3.3 Determination of solids dry weight

Samples of 1 mL were placed into pre-weighed Eppendorf tubes, and then spun down in a mini-centrifuge (Eppendorf Centrifuge 5415R, Hamburg, Germany) at 13,000 rpm for 5 minutes. The supernatant was carefully discarded and the recovered pellets were dried to a constant weight (± 0.0005 g) in an oven at 100 °C. Solids dry weight was estimated by the difference between the final weight and the empty Eppendorf tubes. Typically, variation between samples was ± 5%.

3.1.3.4 DNA assay

The DNA assay was a commercially available Quant-iT™ DNA Assay Kit, Broad Range (Cat. No. Q33130) obtained from Molecular Probes Europe – Invitrogen (Leiden, The Netherlands). It is a fluorescence-based assay that is highly selective for dsDNA over RNA and uses 96-well microplates. The DNA assay was performed on samples of cell homogenate that had been spun down in a mini-centrifuge (Eppendorf Centrifuge 5415R, Hamburg, Germany) at 13,000 rpm for 5 minutes to remove any cell debris. The protocol followed the manufacturer's recommended procedure and 5 μL of clarified samples were added to each microwell. Fluorescence was measured using a FLUOstar OPTIMA microplate reader (Offenburg, Germany) at an excitation/emission maxima of 485/520 nm. Reproducibility of the assay was typically ± 5% for triplicate samples.

3.1.3.5 Particle size determination

The particle size distribution was determined using a Malvin 3600E Particle Sizer with Mastersizer™ 2000 control software (Malvern Instruments, Worcestershire, United Kingdom). The system is based on the principle of laser diffraction, where the dependence of the scattering angle on the diameter of particle passing the laser beam is used to infer the particle size. The instrument calculated a volume-based particle size distribution. Repeated measurements of these values showed variability of less than 5% for the mean particle size.

3.2 FOULING MATERIAL

3.2.1 Preparation of yeast homogenate

Fouling streams were prepared by suspending bakers' yeast (*Saccharomyces cerevisiae*) in the following proportions with buffer: 1.3 kg of yeast per litre of 20 mM phosphate buffer at pH 7 to give a yeast suspension of 600 $g.L^{-1}$ (wet basis). Typically, 12 kg of yeast was added to 9.2 L of buffer to give 20 L of yeast suspension, but this volume was adjusted depending on the requirements of the experiment. The yeast

suspension was homogenised by 5 passes through a Lab-60 high pressure homogeniser (APV Manton Gaulin, Everett, MA, USA) at a pressure of 500 bar(g). Homogenate was passed through a Westfalia SAOOH disc stack centrifuge (Westfalia Separator, Milton Keynes, UK), at a flow rate of 40 $L.h^{-1}$, corresponding to $Q/\Sigma = 1.9 \times 10^{-8}$ ms^{-1}. For some experiments, supernatant was used with no further treatment other than dilution. In other experiments, the centrifuged supernatant material was further treated to remove almost all particulates. This was achieved using the Beckman L7 ultracentrifuge (Beckman Instruments Ltd., High Wycombe, Buckinghamshire, UK) running at 40,000 rpm for 1 hr (~160,000 g; $V/(t\Sigma) = 3.5 \times 10^{-16}$ ms^{-1}).

3.2.2 Preparation of *E. coli* TOP10 homogenate

Escherichia coli TOP10 (pQR239) fermentations for biocatalyst production were performed in a 7-litre fermenter with 5-litre working volume (LH 210 fermenter, Bioprocess Engineering Services, Charing, Kent, UK) fitted with three equally spaced top driven six-bladed turbine impellers and four diametrically opposed baffles. The dissolved oxygen tension (DOT) was measured with a polarographic oxygen electrode (Ingold, Messtechnik, Urdorf, Switzerland). Cells were grown in a complex medium consisting of yeast extract and tryptone. The pH of the fermentation medium was controlled using a sterilised Ingold pH probe (Ingold, Messtechnik, Urdorf, Switzerland) at pH 7 (±0.05) by metered addition of 3 M KOH and 3 M H_3PO_4. All data logging and the exhaust gas measurements were recorded using the RT-DAS program (Acquisition System, Guildford, Surrey, UK). Ampicillin was added to the fermenter medium prior to inoculation. The fermenter was inoculated with 500 mL (10% of the total volume) seed culture grown overnight. During the growing phase, the agitation rate was maintained at 1000 rpm and varied between 250 rpm to 1500 rpm. During the fermentation process, the vessel was aerated with filtered air, sparged at 1 $L.min^{-1}$ (0.67 vvm). The fermentation profile of *E. coli* TOP10 (pQR239) has been described in detail elsewhere (Doig et al., 2001). The growth of *E. coli* was closely monitored based on the optical density of the fermentation broth. This monitoring is highly important for the induction period at approximately 3 hours after the start of the fermentation. Arabinose (2.4 $g.L^{-1}$) was used to induce the cell during the second stage of the fermentation and this was done when the optical density reached 7 – 8 OD_{670}

reading. The process was then carried out for another 3 hours after the induction period until the cell reached approximately 20 OD_{670} reading. Polypropylene glycol (PPG) 2000 was used throughout the fermentation to prevent foaming.

3.2.3 Preparation of *E. coli* Fab' broth and homogenate

The foulant was prepared from a fermentation broth expressing HumMAb4D5-8 Fab' as an antibody fragment from *E. coli* strain W3110 (pAC tAC 4d5 Fab'). The fermentation was carried out in repeated batch mode as described by Garcia-Arrazola et al. (2005). It began with a 10% v/v inoculum and was grown on SM6C media: $(NH_4)_2SO_4$ 5.00 $g.L^{-1}$, NaH_2PO_4 2.80 $g.L^{-1}$, KCl 3.87 $g.L^{-1}$, citric acid 4.00 $g.L^{-1}$, glycerol 30 $g.L^{-1}$, trace elements 10 $mL.L^{-1}$, $MgSO_4.7H_2O$ 1.00 $g.L^{-1}$, chloramphenicol 0.025 $g.L^{-1}$ and antifoam PPG 1 $mL.L^{-1}$. The trace element stock solution had the following composition: citrate, 100 $g.L^{-1}$; $CaCl.6H_2O$, 5.00 $g.L^{-1}$; $ZnSO_4.7H_2O$, 2.46 $g.L^{-1}$; $MnSO_4.4H_2O$, 2.00 $g.L^{-1}$; $CuSO_4.5H_2O$, 0.50 $g.L^{-1}$; $CoSO_4.7H_2O$, 0.427 $g.L^{-1}$; $FeCl_3.6H_2O$, 9.67 $g.L^{-1}$; H_3BO_3, 0.03 $g.L^{-1}$; and $NaMoO_4.2H_2O$, 0.024 $g.L^{-1}$. Fermentation was performed in 14-litre LH fermenters (Inceltech Ltd., Berkshire, UK). Temperature was maintained at 30°C, and pH was controlled to a set-point of 6.95 by the addition of a 15% (v/v) ammonium hydroxide solution. Agitator speed and air flow rates were varied to maintain the dissolved oxygen tension (DOT) at 20% or above. Foaming was controlled as necessary by the addition of Polypropylene glycol (PPG) 2000 antifoaming agent. A glycerol carbon source was supplemented until a biomass level corresponding to a dry cell weight concentration of 20 $g.L^{-1}$ was reached (~ 35 hours after inoculation). Plasmid expression was induced by the addition of a 50% w/w lactose solution, to bring the fermenter lactose concentration to 5% w/v. The fermentation continued for a further ~ 20 hours bringing the culture into stationary phase. The cells were then harvested and homogenised at 500 bar(g) for 5 passes. Cell homogenate was partially clarified by centrifugation in a J2-M1 laboratory centrifuge with JA-10 rotor (Beckman Instruments Ltd., High Wycombe, UK) for 1 hour at 10,000 rpm (RCF = 13,000 g). The supernatant was frozen at -20°C in 45 mL aliquots. A foulant aliquot was thawed the day of experimentation at room temperature.

3.2.4 Characterisation of fouling material

Fouling challenges were achieved using realistic process streams, in all the studies in this thesis. The protein, DNA, solids and lipid concentrations in the different foulants used are listed in Table 3-1. The particle size distribution of the particulates in the *E. coli* foulants, mainly whole cells or cell debris, are shown in Figures 3-1 and 3-2. It is apparent that the partially clarified homogenates predominantly contained cell debris of an average size of ~ 0.12 μm. A small amount of whole cells, which may have escaped total disruption under the harsh homogenisation conditions, were also present and had an average size of ~ 0.8 μm. Unprocessed *E. coli* Fab' fermentation broth was shown to contain predominantly whole cells of an average size of 0.9 μm but also contained a small amount of debris with an average size of ~ 0.1 μm as well as residual amounts of large particulates of sizes 7 – 8 μm. These larger particulates may have been external contaminants but were completely removed by subsequent centrifugation.

Foulant	Protein (mg/mL)	DNA (ng/μL)	Solids (mg/mL)	Lipids (mg/mL)
Yeast homogenate (disc stack centrifuged)	20	nd[(a)]	350	3.2
E. coli (TOP10) homogenate (partially clarified)	2.4	110	4.2	nd
E. coli (Fab') homogenate (partially clarified)	6.1	110	1.2	nd
E. coli (Fab') whole cells (non-clarified)	nd	nd	17	nd

Notes: (a) nd = Not determined.

***Table 3-1**: Concentrations of protein, DNA, solids and lipids in the foulants.*

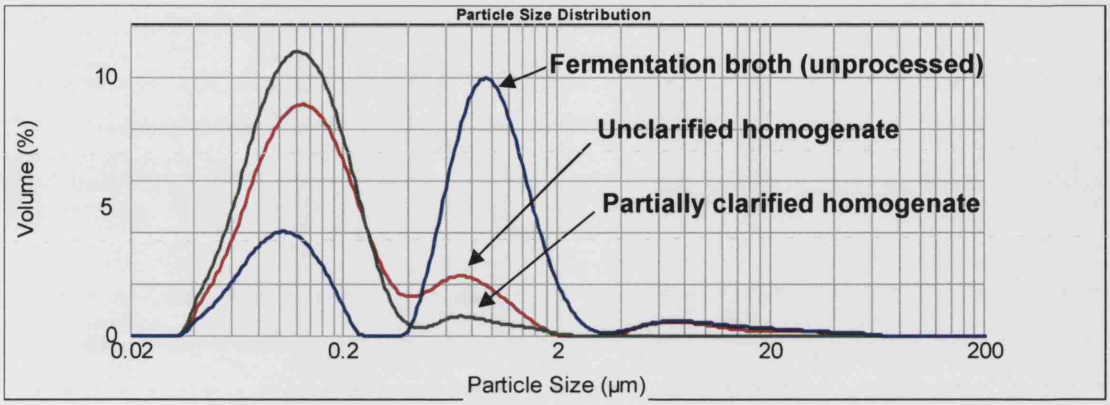

***Figure 3-1**: Particle size distribution of E. coli TOP10 foulant.*

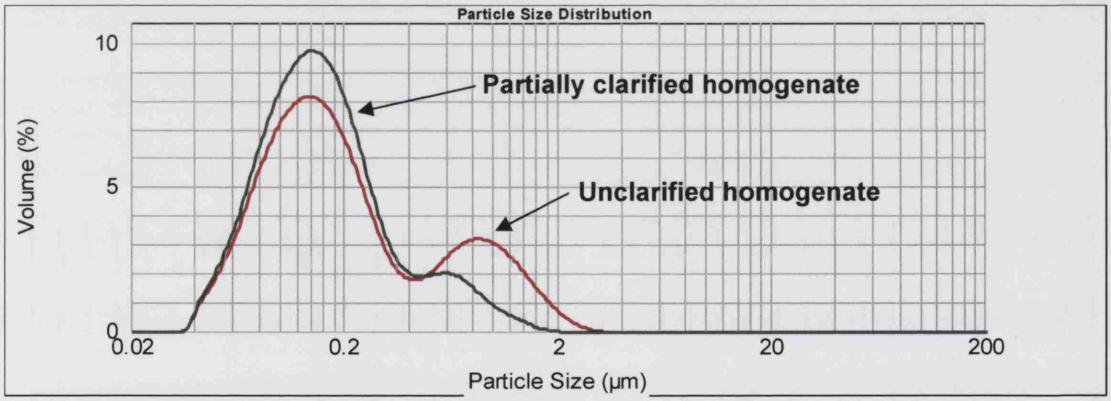

***Figure 3-2:** Particle size distribution of E. coli Fab' foulant.*

Since the homogenised fouling material applied in the studies was subjected to high shear rates in a high-pressure homogeniser during preparation, the majority of the original large genomic DNA was expected to be degraded into small fragments (Levy et al., 1999). This was confirmed by gel electrophoretic analysis (Figure 3-3) which showed the majority of fragments were in the range of 300 – 750 bp in size.

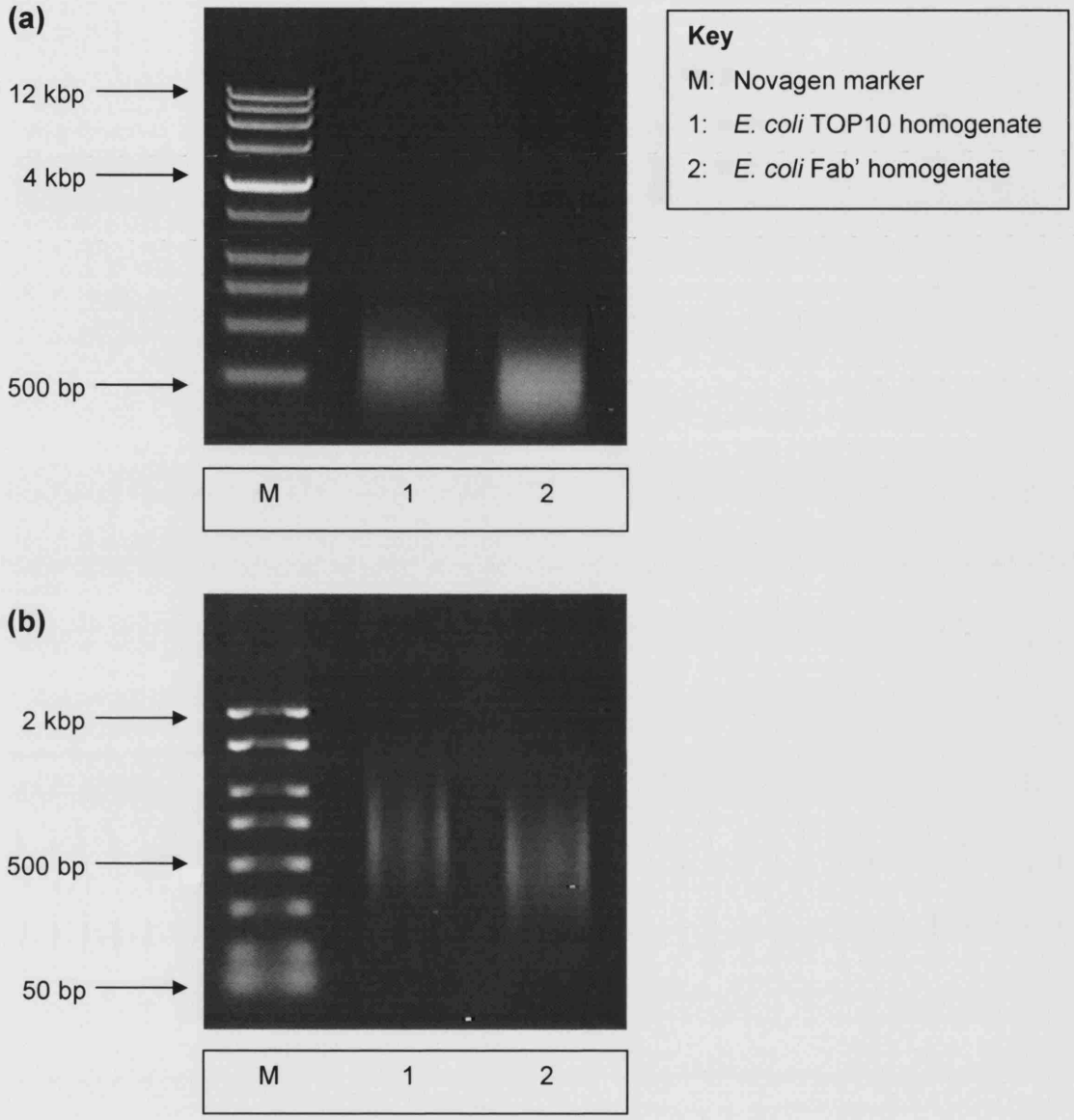

Figure 3-3: *Standard agarose gels showing the size of DNA fragments in the foulants. DNA is noted at ~ 300 – 750 bp region. (a) 1.2% agarose gel with Novagen PCR Markers (500 bp – 12 kbp); (b) 2% agarose gel with Novagen PCR Markers (50 bp – 2 kbp).*

3.3 FRONTAL ANALYSIS (CHAPTER 4)

3.3.1 Materials

3.3.1.1 Description of equipment

Chromatographic procedures were performed using an FPLC unit (GE Healthcare, Uppsala, Sweden), controlling the operation of a XK^{TM}16 column (GE Healthcare, Uppsala, Sweden), manually packed to a bed height of 5.0 ± 0.1 cm. An anion exchanger, DEAE Sepharose^{TM} Fast Flow, was used in this work and supplied by GE Healthcare (Uppsala, Sweden). The matrix has an average particle size of ~ 95 μm and a particle size distribution of 45 – 165 μm, as quoted by the manufacturer. The FPLC's built-in UV monitoring and conductivity measuring functions sent data to a PE Nelson 970 A/D converter interfaced with a computer running Turbochrom (v.2.1; Perkin Elmer, San Jose, CA, USA) data acquisition software. Spectrophotometric assays were performed using a Beckman DU 650 spectrophotometer (Beckman Instruments Ltd., High Wycombe, Buckinghamshire, UK).

3.3.2 Methods

3.3.2.1 BSA breakthrough curve determination

The following method was used to determine the breakthrough curves in all the frontal analysis tests. Before use, freshly packed columns were equilibrated with 3 column volumes (CVs) of 20 mM phosphate buffer, pH 7 (start buffer). BSA at 2 mg/mL in 20 mM phosphate buffer, pH 7 was fed to the column at a flow rate of 2 mL/min until the BSA effluent concentration, as measured by UV absorption at 280 nm (A_{280}), equalled the feed concentration. The column was washed with start buffer to remove unbound protein until the A_{280} signal returned to the baseline. Bound BSA was eluted by a step change in mobile phase composition to 1 M sodium chloride in 20 mM phosphate buffer, pH 7 and continued until the A_{280} signal returned to baseline. The column was then re-equilibrated with start buffer before further application of fouling stream. Results for the breakthrough curves are presented graphically as the ratio of output concentration of BSA to input concentration of BSA (C/C_0) versus time. The dynamic capacity at the 1% and 100% breakthrough level was calculated by calculating the amount of BSA which flowed through the column, determined as the

area below the breakthrough curve at $C/C_0=0.01$ and $C/C_0=1$ respectively, and subtracting this from the amount of BSA loaded in the equivalent time.

3.3.2.2 Method of application of fouling challenges to the column

Two modes of fouling challenge to the column were examined. In the first, the foulant challenge was presented to the column as a single volume of process material. In the second, the impact of making successive small foulant challenges to the column was investigated. The experimental conditions are summarised in Table 3-2.

Pre-treatment	Foulant volume loaded per cycle (CV)	Number of cycles	Total foulant volume loaded (CV)
Effect of repeated fouling on column breakthrough			
Ultracentrifugation	0.2	10	2
Disc stack centrifugation	0.2	10	2
Effect of loading large quantities of particulate solids to packed beds			
Disc stack centrifugation	1	1	1
Disc stack centrifugation	5	1	5
Disc stack centrifugation	10	1	10
Ultracentrifugation	10	1	10

***Table 3-2**: Experimental conditions used in fouling studies. All experiments were based on a 10 mL column.*

For the single volume foulant challenges a frontal analysis test, with BSA solution, was first carried out on a fresh column as described above. Volumes of either 10, 50 or 100 mL of fouling material were then applied to the column, after which the bed was washed to remove unbound protein from the matrix, using a gradient of NaCl from 0 M to 1 M NaCl and back to 0 M NaCl over 3 CVs. Frontal analysis was repeated for the fouled column. A different column was used for each of the different foulant volume challenges so that each column was fouled only once in this set of experiments. This fouling experiment was carried out both with yeast homogenate clarified by ultracentrifugation and by disc stack centrifugation, separately. Columns were fouled only once in this set of experiments.

Successive small fouling challenges were applied by repeatedly loading 2 mL quantities of yeast homogenate to the same column. Each cycle consisted of carrying out a frontal analysis test with BSA; loading of 2 mL of yeast homogenate onto the column; washing of unbound protein from the matrix using a gradient of NaCl from 0 M to 1 M NaCl and back to 0 M NaCl over 3 CVs; and repetition of the frontal analysis test. The total fouling procedure comprised ten such cycles. This fouling experiment was carried out both with yeast homogenate clarified by ultracentrifugation and by disc stack centrifugation, separately.

All fouling material was applied to the column at a flow rate of 2.6 mL/min (78 cm/h). Use of higher flow rates was avoided to reduce the risk of clogging of the packed bed and to avoid bed compression.

3.3.2.3 Pressure-flow measurements

The variation in pressure drop across the column was monitored as a function of flow rate both for a clean column and after challenging the column with either 50 or 100 mL of yeast homogenate which had been clarified by disc stack centrifugation. At each flow rate the pressure was allowed to stabilise and was then recorded. After fouling at a flow rate of 2.6 mL/min, the columns were washed with a gradient of NaCl in 20 mM phosphate from 0 M to 1 M NaCl and back to 0 M NaCl over 3 CVs and the pressure-flow curve was determined again.

3.3.2.4 Clean-in-place (CIP) protocol

Cleaning-in-place (CIP) was carried out using 3 CVs of 20 mM phosphate buffer at 2 mL/min, followed by 1 M sodium hydroxide at ambient temperature at 0.1 mL/min. The flow rate was designed to keep the column in contact with sodium hydroxide for a long period, whilst maintaining a flushing flow to remove dissolved foulants. This procedure was carried out for 5 hours. The column was then flushed with 20 mM phosphate buffer containing 1 M sodium chloride until the inlet and outlet pH of the buffer were the same within ± 0.5 pH units.

3.4 EXTENDED REVERSE-FLOW TECHNIQUE (CHAPTER 5)

3.4.1 Materials

3.4.1.1 Chromatography system

Chromatographic procedures were performed on an AKTA™ explorer 100 (GE Healthcare, Uppsala, Sweden). System control and data acquisition was by an UNICORN™ control system (GE Healthcare, Uppsala, Sweden) installed on a Pentium III computer (Compaq, Bristol, United Kingdom) with 256 MB of RAM.

3.4.1.2 Chromatography columns

The majority of the experiments were conducted using 1 mL HiTrap™ SP FF columns (0.7 cm internal diameter with a bed height of 2.5 cm) pre-packed with SP Sepharose FF. Experiments were also carried out using 5 mL HiTrap™ SP FF pre-packed columns (1.6 cm internal diameter with a bed height of 2.5 cm). The other columns used were XK™16 and XK™26 (1.6 cm and 2.6 cm internal diameter, respectively) glass chromatography columns. All columns were from GE Healthcare (Uppsala, Sweden).

3.4.1.3 Chromatography matrix and packing

SP Sepharose FF, a strong cation exchanger, was obtained from GE Healthcare (Uppsala, Sweden). The XK16 and XK26 columns were packed at a flow rate of 180 cm/h to a bed height of 2.5 ± 0.1 cm as per manufacturer's instructions.

3.4.2 Methods

3.4.2.1 General

For all experiments the ratio of fouling stream volume to column volume was 5:1 and was loaded at a linear flow rate of 156 cm/h. Pulse experiments were carried out at a linear flow rate of 78 cm/h with acetone tracer volumes of 15, 75 and 199 μL for 0.7 (including those arranged in series), 1.6 and 2.6 cm internal diameter columns, respectively. The UV detector was set to measure absorbance at 280 nm. An acetone tracer (2% v/v acetone in water), with a volume equivalent to 1.5% of the column volume, was use throughout the study to measure bed dispersion. The general procedure of the extended reverse-flow technique used is given in Figure 3-4.

3.4.2.2 Determining dead volume

It is necessary to determine the dead volumes of the system. To do this, the tubing leading to the top of the column was attached to the UV detector via a piece of tubing of known volume (0.19 μL). Subsequently, a 15 μL acetone tracer was applied to the system at 0.5 mL/min. By subtracting the known volume of the connecting tubing from the retention volume reading of the eluted acetone pulse, the dead volume of the system in down-flow mode was determined. Identical experiments were carried out to determine the dead volumes of the system in up-flow mode. This procedure was repeated with acetone samples of 75 μL and 199 μL at flow rates of 2.61 mL/min and 6.90 mL/min, respectively. The tubing connecting to the top and bottom flow adaptors in the XK columns were also taken into account by disconnecting them from the column and connecting them to the experimental set-up when determining their dead volumes.

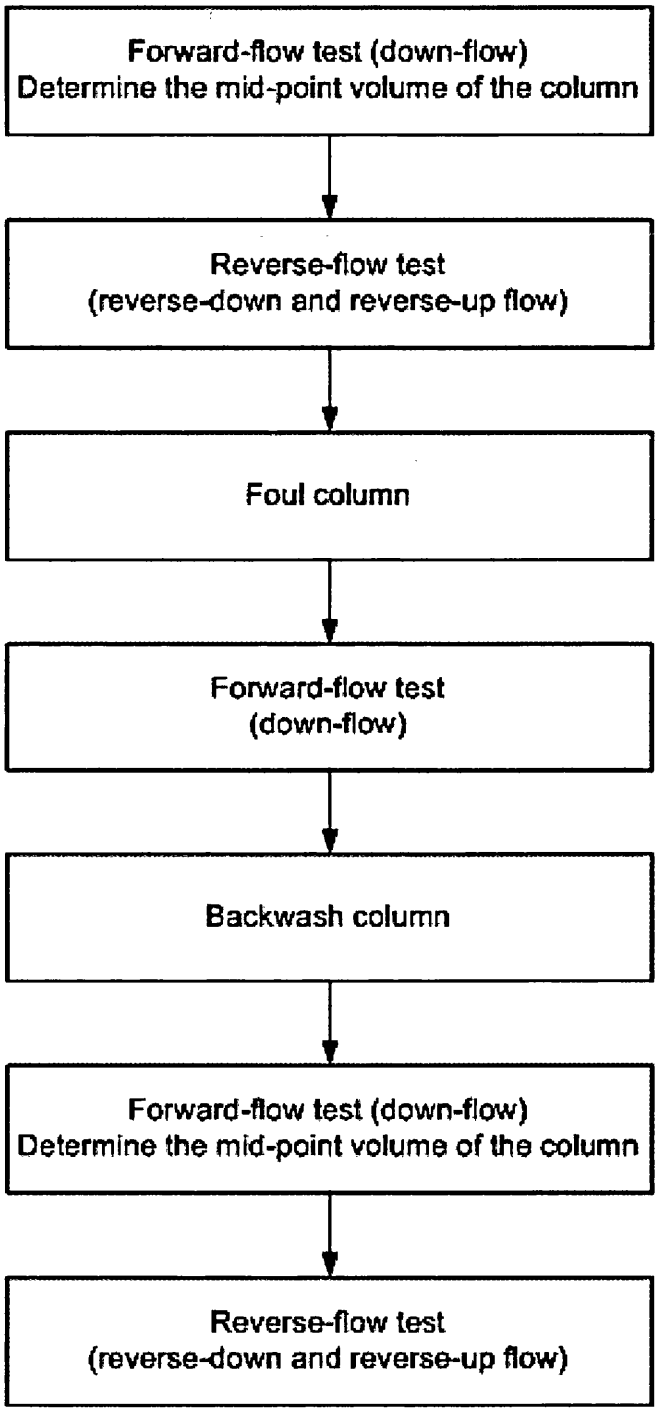

***Figure 3-4**: Outlined procedure for the extended reverse-flow technique.*

3.4.2.3 Determining dispersion due to extra-column effects

To determine the contribution of extra-column dispersion an acetone pulse was injected into the system (without the column in place) in down- and up-flow directions for the same range of flow rates and acetone pulse volumes that were used in the experiments to determine the extra-column dispersion when run in down-flow (σ^2_{sdf}) and up-flow (σ^2_{suf}), respectively (cf. Section 3.4.2.2). The extra-column dispersion when run in reverse-down-flow (σ^2_{srdf}) and reverse-up-flow (σ^2_{sruf}) were also determined by the procedure just described except that the direction of flow was reversed at the appropriate elution volume as determined from the dead volumes.

3.4.2.4 Forward-flow test (down-flow and up-flow)

An acetone tracer was applied using a sample loop at the sample valve of the AKTA system. The acetone pulse was eluted through the column (fresh or fouled) at a flow rate of 78 cm/h in down-flow direction. The resulting acetone peak was analysed in terms of residence time distribution.

3.4.2.5 Reverse-flow test (reverse-down-flow and reverse-up-flow)

An acetone tracer was applied using a sample loop at the sample valve of the AKTA system. The acetone pulse was eluted through the (fresh or fouled) column at a flow rate of 78 cm/h, in either down-flow or up-flow direction, until the axial centre of the column at which the direction of flow was reversed causing the acetone pulse to leave the column from the inlet. The resulting acetone peak was analysed in terms of residence time distribution.

3.4.2.6 Testing of fresh columns

Firstly, a forward-flow test (down-flow) was performed as per Section 3.4.2.4. The first absolute moment or mean solute residence time of the resultant acetone peak was determined and the void volume of the column was calculated. This was necessary in order to calculate the elution volume required to bring the acetone pulse from the injection value to the axial centre of the column. Reverse-flow tests (reverse-down-flow and reverse-up-flow) were then performed on the column as per Section 3.4.2.5.

3.4.2.7 Fouling and testing of fouled columns

The column was fouled with 5 CVs of partially clarified *E. coli* TOP10 homogenate that was loaded at a flow rate of 156 cm/h. The column was washed to baseline with water to remove unbound foulants.

Firstly, a forward-flow test (down-flow) was performed as per Section 3.4.2.4. Following the test the column was backwashed with water until a steady baseline was achieved, in order to remove any loosely-bound foulants that may obscure the peaks from subsequent reverse-flow tests. A further forward-flow test was performed on the backwashed column. The first absolute moment or mean solute residence time of the resultant acetone peak was determined and the void volume of the column was calculated, which was necessary in order to calculate the required elution volume to bring the acetone pulse from the injection value to the axial centre of the column. Reverse-flow tests (reverse-down-flow and reverse-up-flow) were then performed on the column as per Section 3.4.2.5.

3.4.2.8 Experimental set-up with single columns

To investigate the dispersive effects of fouling on columns with increasing diameter but identical bed heights, the following columns (their corresponding internal diameter is indicated in parentheses) were used: 1 mL HiTrap SP FF (0.7 cm); 5 mL

HiTrap SP FF (1.6 cm); XK16 (1.6 cm); and XK26 (2.6 cm). The bed lengths were 2.5 cm in all the columns. Each column was tested when fresh and after fouling.

3.4.2.9 Experimental set-up with columns in series

To investigate the dispersive effects of fouling with increasing bed length, 1 mL HiTrap SP FF pre-packed columns were used. They were arranged in series of one, two and three columns. Fresh columns were tested individually before being arranged in series, after which they were tested collectively with a forward-flow test. The column series was then fouled and another forward-flow test (down-flow) was performed. Subsequently, the columns in series were disconnected and each column was individually backwashed and tested.

3.4.3 Data processing

3.4.3.1 Calculation of first absolute moments and second central moments

The mean solute residence time, t_R, and the peak variance, σ^2, were determined by application of the method of statistical moments (McQuarrie, 1963; Grubner et al., 1967, Grubner, 1968; Dyson, 1998). The first absolute moment is the mean residence time and the second central moment is equivalent to the peak variance. The peak variance is a measure of the column efficiency and comparison of peak variances before and after fouling was used to quantify the effects of fouling (see Chapter 5).

The general formula for the nth absolute moment, M_n, and nth central moment, μ_n, is given by equations 3-1 and 3-2, respectively:

$$M_n = \frac{\int_{-\infty}^{+\infty} t^n \cdot h_t dt}{\int_{-\infty}^{+\infty} h_t dt} \qquad (3\text{-}1)$$

$$\mu_n = \frac{\int_{-\infty}^{+\infty}(t - M_1)^n \cdot h_t dt}{M_0} \qquad (3\text{-}2)$$

where h_t is the effluent concentration at time t and $M_0 = \int_{-\infty}^{+\infty} h_t dt$ (the zeroth moment). Therefore, it can be denoted that $M_1 = t_R$ and $\mu_2 = \sigma^2$.

It must be noted that elution time (t) was replaced by elution volume in the analysis of the results in Chapter 5. Accordingly, the first absolute moment corresponds to the mean residence volume (V_R) and the second central moments still corresponds to the peak variance but in units of volume (i.e., mL^2).

3.5 CONFOCAL SCANNING LASER MICROSCOPY (CHAPTER 6)

3.5.1 Materials

3.5.1.1 Description of equipment

The confocal experiments were performed with an inverted confocal laser scanning microscope (Leica SP2 DM IRBE, Leica Microsystems GmbH, Mannheim, Germany) equipped with helium/neon, krypton/argon and argon lasers. A 63x1.4 oil immersion objective was used for the experiments. Protein-Cy3 was excited at 543 nm and the emission detection range was set to 560-600 nm. Protein-Cy5.5 was excited at 633 nm and the emission detection range was set to 650-710 nm. dsDNA-PicoGreen was excited at 488 nm and the emission detection was set to 505-535 nm. BacLight Red-labelled whole cells or cell debris were excited at 568 nm and the emission detection range was set to 644-690 nm.

3.5.1.2 Chromatography matrix

Q Sepharose Fast Flow, a strong anion exchanger, was obtained from GE Healthcare (Uppsala, Sweden). The particle size distribution of the resin was determined and is shown in Figure 3-5. The mean particle size was ~ 95 μm. The inter-

decile particle size range was 55 – 145 µm, which is consistent with the particle size range of 45 – 165 µm quoted by the manufacturer.

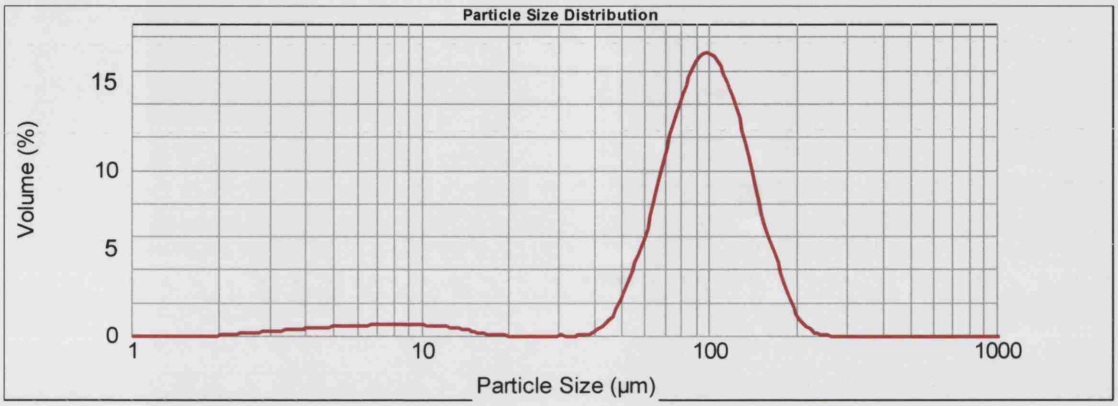

***Figure 3-5**: Particle size distribution of Q Sepharose FF resin.*

3.5.1.3 Confocal flow cell and packing

A flow cell of similar design to that used by Hubbuch et al. (2002) was used in the study (Figure 3-6). The design of the flow cell consisted of a Perspex block with precision-drilled inlets (45°) on either side and an open channel (~ 6 mm in length) grooved into the bottom of the block. A window for observing under the microscope was created by fixing a microscope coverslip to the open channel using epoxy glue (Ciba Araldite Rapid, Casco AB, Stockholm, Sweden). The column had a total length of 22 mm and a cross-sectional area of 3 mm^2. The column volume was 0.066 mL. The flow cell was connected to a P-900 pump (GE Healthcare, Uppsala, Sweden) which allowed liquid-handling. Polypropylene frits from GE Healthcare (Uppsala, Sweden) were placed at the ends of the flow channel and were held in place using conventional screw fittings from GE Healthcare (Uppsala, Sweden). The flow cell was packed with equilibrated Q Sepharose FF by using a syringe and manually applying pressure. The packed flow cell was then equilibrated with 3 mL of 20 mM Tris-HCl, pH 8.0 at a flow rate of 0.2 mL/min.

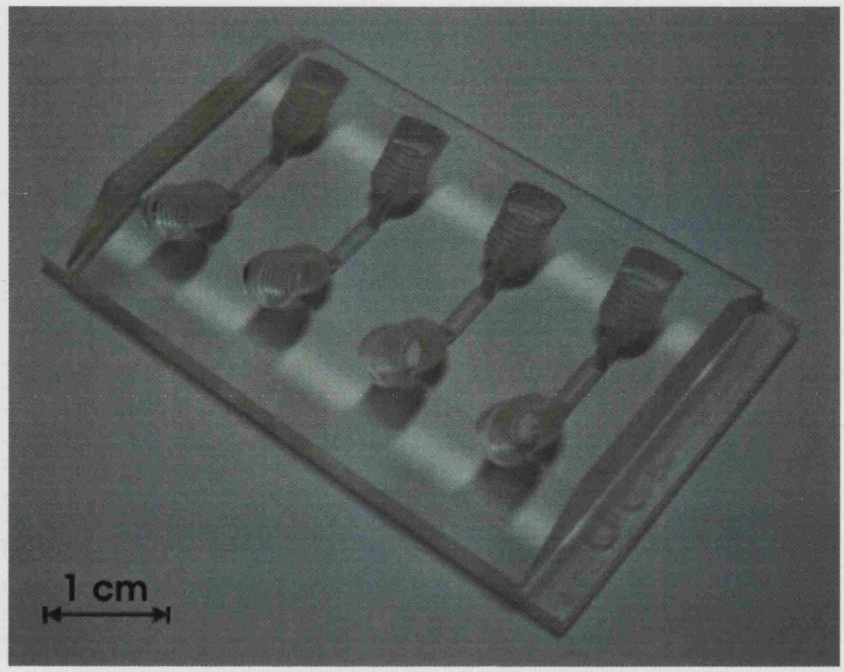

***Figure 3-6**: Picture of the confocal flow cell used in the study.*

3.5.2 Methods (general)

3.5.2.1 Fluorescent labelling of BSA with Cy5.5

BSA was dissolved in degassed conjugation buffer (100 mM Na_2CO_3, pH 9.3) to a concentration of 2 mg/mL. 1.0 mL of BSA conjugation solution was added to one vial of Cy5.5, pre-measured by the manufacturer and containing sufficient reactive dye to label 1.0 mg of protein. This mixture was incubated for 1 hour. BSA test solution was made by adding 1mL of labelled BSA to 9.0 mL of unlabelled BSA dissolved in degassed 20 mM Tris-HCl, pH 8.0.

3.5.2.2 Fluorescent labelling of E. coli host cell proteins (foulant proteins) with Cy5.5 or Cy3

0.5 mL of foulant solution was added to 0.5 mL 100 mM Na_2CO_3, pH 9.3 degassed conjugation buffer. The resultant 1.0 mL solution was added to pre-measured

Cy5.5 or Cy3 dye (capable of labelling 1 mg of protein) and incubated for 2 hours at room temperature. Foulant Cy dye-protein solution was diluted to a ratio of 1:20 (foulant Cy dye-protein to unlabelled foulant).

3.5.2.3 Normalisation of the fluorescence signal

Cyanine dye fluorophores are known to be pH insensitive (Mujumdar et al., 1993), and PicoGreen has been previously reported as being highly stable under alkaline conditions (Batel et al., 1999). Nevertheless, the fluorescent enhancement of PicoGreen has been shown to decrease at high pH conditions (Rock et al., 2003) and in the presence of sodium chloride and BSA solution (Singer et al., 1997). To avoid such effects obscuring the comparison of fluorescent intensities between experiments, the beads were always placed in the same buffer conditions (20 mM Tris-HCl, pH 8.0) before visualising under the microscope.

Any fluctuations in the laser source intensity were checked using Q Sepharose beads that had been saturated with BSA labelled with Cy5.5 before each experiment. The beads were prepared as described in Sections 3.5.2.1 and 3.5.3.2. Only relatively small fluctuations were observed.

3.5.3 Methods (finite bath experiments)

3.5.3.1 Fouling of Q Sepharose FF and fluorescent labelling of double stranded deoxyribonucleic acids (dsDNA) with PicoGreen

0.5 mL of 50% (v/v) Q Sepharose FF slurry in 20 mM Tris-HCl, pH 8.0 was added to 10 mL of foulant liquor prepared as above. In all experiments a volumetric ratio of 1:40 Q Sepharose FF to foulant was used. The resulting slurry was agitated for 5 minutes, 1 hour or 12 hours at 4°C, depending on the study. At the end of the exposure, the fouled Q Sepharose FF was washed three times with equal volumes of 20 mM Tris-HCl, pH 8.0 by repeated dilution, centrifugation (14,000 g for 30 s) and decanting. In the final step 20 mM Tris-HCl, pH 8.0 was added to give a 50% (v/v) slurry to which 10 μL of PicoGreen was added and incubated at room temperature for

30 minutes. PicoGreen shows a > 1000-fold fluorescence enhancement upon binding to dsDNA and much less fluorescence enhancement upon binding to ssDNA or dsRNA (Singer et al., 1997).

3.5.3.2 BSA adsorption time series

Protein adsorption time series studies were conducted on samples of fresh and fouled resins. In all cases samples were withdrawn and prepared for CSLM analysis at predetermined intervals. Each resin sample was washed three times by a re-suspension, centrifugation (14,000 g for 30 s) and decanting protocol using 20 mM Tris-HCl, pH 8.0 as the wash buffer. Time series experiments were started by adding 0.5 ml of 50% (v/v) Q Sepharose FF slurry in 20 mM Tris-HCl, pH 8.0 to the labelled BSA in a 20 mL sample tube and agitated using a magnetic stirrer throughout. Samples of 0.3 mL volume were withdrawn from the sample tube and diluted in 0.7 mL of 20 mM Tris-HCl, pH 8.0. These were washed three times with equal volumes of 20 mM Tris-HCl, pH 8.0 by repeated dilution, centrifugation (14,000 g for 30 s) and decanting. This was followed by re-suspension of the pellet in 20 mM Tris-HCl, pH 8.0 to a volume of 1 mL. 12 μL of the resultant Q Sepharose FF slurry was used to prepare slides for visualisation by CSLM.

3.5.3.3 Clean-in-place (CIP) time series

CIP solution – either 1M NaCl dissolved in 20 mM Tris-HCl, pH 8.0 (1 M NaCl) or 1M NaCl dissolved in 1 M NaOH (1 M NaCl + 1 M NaOH) – equal to the volume of foulant used was added to 0.25 mL of fouled Q Sepharose FF labelled for both dsDNA and foulant protein in a 20 mL sample tube which was constantly stirred. 0.3 mL samples were withdrawn at predetermined intervals and diluted in 0.7 mL of CIP solution. This was washed three times with equal volumes of 20 mM Tris-HCl, pH 8.0 by repeated dilution, centrifugation (14,000 g for 30 s) and decanting. 12 μL of the resultant Q Sepharose FF slurry was used to prepare slides for visualisation.

3.5.3.4 Post-CIP adsorption time series

The CIP procedure was repeated as above except that no samples were withdrawn and foulant protein was not labelled. After 1 hour of constant stirring with CIP solution the Q Sepharose FF beads were washed with one volume of CIP solution by dilution, centrifugation (14,000 g for 30 s), decanting. This was followed by a further three washes with 20 mM Tris-HCl, pH 8.0. A BSA adsorption time series was prepared as outlined above using 0.25 mL of fouled, post-CIP resin.

3.5.4 Methods (flow cell experiments)

3.5.4.1 Multicolour labelling of fouling material to visualise HCPs and dsDNA

0.5 mL of foulant solution was incubated with 0.5 mL 100 mM Na_2CO_3, pH 9.3 degassed conjugation buffer for 1 hour at room temperature. The resultant 1.0 mL solution was added to pre-measured Cy5.5 dye (capable of labelling 1 mg of protein) and incubated for a further 2 hours at room temperature. Foulant protein-Cy5.5 solution was diluted to a ratio of 1:20, foulant protein-Cy5.5 to unlabelled foulant. To this protein-labelled foulant mixture, PicoGreen was added to a concentration of 10 µL per mL of foulant. The mixture was allowed to incubate for a further 1 hour with frequent agitation.

3.5.4.2 Fouling of Q Sepharose FF bed in a flow cell

A flow cell packed with Q Sepharose FF was equilibrated with 20 mM Tris-HCl, pH 8.0 for 20 minutes at a flow rate of 0.08 mL/min. After equilibration, 5 CVs of partially clarified Fab' *E. coli* homogenate prepared as described in Section 3.2.3 was loaded onto the packed bed at a flow rate of 0.08 mL/min. Finally, the bed was washed and re-equilibrated with 20 mM Tris-HCl, pH 8.0 for 20 minutes at a flow rate of 0.08 mL to remove unbound foulants.

3.5.4.3 BSA adsorption time series in a flow cell

Protein adsorption time series studies were conducted on fresh, fouled and CIP-treated packed beds. Fluorescently-labelled BSA solution (2 mg/mL) was loaded onto the equilibrated bed at a flow rate of 0.08 mL/min. Visualisation of the bed by CSLM was done in real-time and *in situ*, and confocal images were taken at predetermined time intervals.

3.5.4.4 CIP time series

Flow cells packed with Q Sepharose FF were fouled as described in Section 3.5.4.2. After fouling and re-equilibrating, the bed was first washed with 15 CVs of 20 mM Tris-HCl, 1 M NaCl, pH 8.0 at a flow rate of 0.08 mL/min. During the wash, visualisation of the bed by CSLM was done in real-time and *in situ*. Confocal images were taken at predetermined time intervals. After completing the first wash, the bed was re-equilibrated with 5 CVs of 20 mM Tris-HCl, pH 8.0 to normalise the fluorescence signal (cf. Section 3.5.2.3), after which another confocal image of the bed was taken. Subsequently, the bed was washed with 15 CVs of 1 M NaOH at a flow rate of 0.08 mL/min. Again, visualisation of the bed by CSLM was done in real-time and *in situ* and confocal images were taken at predetermined time intervals during the wash. After completing the NaOH wash, the bed was re-equilibrated with 5 CVs of 20 mM Tris-HCl, pH 8.0 to normalise the fluorescence signal, after which another confocal image of the bed was taken.

3.5.5 Methods (visualising whole cells and cell debris)

3.5.5.1 General approach

CSLM was used to visualise the adsorption of whole cells and cell debris to an anion exchanger. Q Sepharose FF beads were incubated with unclarified fermentation broth containing whole *E. coli* cells or cell debris (which were homogenised on the day of use) in a finite bath. The whole cells or cell debris were labelled with BacLight Red which is a fluorescent, non-nucleic acid labelling reagent specific for bacterial cell

membranes. dsDNA in the fermentation broth was labelled with PicoGreen. As both cells/debris and dsDNA would be expected to bind to only a thin layer at the bead exterior, knowledge of their competitive adsorption may be important in understanding the interactions between the two foulants in a realist process stream.

3.5.5.2 Fouling of Q Sepharose FF and fluorescent labelling of whole cells or cell debris with BacLight Red

0.5 mL of 50% (v/v) Q Sepharose FF slurry in 20 mM Tris-HCl, pH 8.0 was added to 10 mL of foulant liquor. In all experiments a volumetric ratio of 1:40 Q Sepharose FF to foulant was used. To this mixture, 20 µL of BacLight Red was added, and the resulting slurry was agitated at ambient temperature for 30 minutes. At the end of the exposure, the fouled Q Sepharose FF was washed three times with equal volumes of 20 mM Tris-HCl, pH 8.0 by repeated dilution, centrifugation (14,000 g for 30 s) and decanting. This was followed by re-suspension of the pellet in 20 mM Tris-HCl, pH 8.0 to give a 50% (v/v) slurry.

3.5.5.3 Fouling of Q Sepharose FF and fluorescent labelling of whole cells or cell debris with BacLight Red and dsDNA with PicoGreen

0.5 mL of 50% (v/v) Q Sepharose FF slurry in 20 mM Tris-HCl, pH 8.0 was added to 10 mL of foulant liquor. In all experiments a volumetric ratio of 1:40 Q Sepharose FF to foulant was used. To this mixture, 20 µL of BacLight Red was added, and the resulting slurry was agitated at ambient temperature for 30 minutes. At the end of the exposure, the fouled Q Sepharose FF was washed three times with equal volumes of 20 mM Tris-HCl, pH 8.0 by repeated dilution, centrifugation (14,000 g for 30 s) and decanting. This was followed by re-suspension of the pellet in 20 mM Tris-HCl, pH 8.0 to a volume of 10 mL. To the resulting slurry, 10 µL of PicoGreen was added and incubated for 30 minutes at ambient temperature with mixing. At the end of the incubation, the fouled Q Sepharose FF was washed three times with equal volumes of 20 mM Tris-HCl, pH 8.0 by repeated dilution, centrifugation (14,000 g for 30 s) and

decanting. This was followed by re-suspension of the pellet in 20 mM Tris-HCl, pH 8.0 to a volume of 10 mL.

3.5.6 Data processing

3.5.6.1 Image analysis

The images of cross-sections through the centre of the beads were analysed with the supplied Leica Control Software (version 2.5) and recorded at a resolution of 512x512 pixels. To reduce the background fluorescence and noise, the images were generated by averaging 6 scans per image (or 10 scans per image for visualising whole cells and cell debris). Further image analysis was done using ImageJ software version 1.31 (National Institute of Health, Bethesda, Maryland, USA).

3.5.6.2 Calculation of volume-normalised relative intensity from CSLM

Ljunglof and Thommes (1998) calculated the overall fluorescence observed within the bead by dividing the particle radius into defined segments, and calculating the corresponding volume of a shell. By multiplying the volume by the fluorescence intensity of the segment, the total fluorescence of the shell was obtained (equation 3-3). The average intensity within each shell represents the concentration of adsorbed protein and the summation of the intensity of each segment divided by the particle volume will yield the total intensity or solid phase concentration of the particle (equation 3-4).

$$I_{\text{int egr.}}^{\text{shell}} = \bar{I}_{\text{seg}}\left[\left(r_a^3 - r_i^3\right)\frac{4}{3}\pi\right] \tag{3-3}$$

$$Q_{\text{rel}} = \frac{\sum_{\text{shells}}\left(I_{\text{int egr.}}^{\text{shell}}\right)}{V_p} \tag{3-4}$$

where $I_{int\,egr.}^{shell}$ is the integral intensity of fluorescence profile, Q_{rel} is the relative capacity of the bead, I_{seg} is the average intensity within a segment, r_a is the outer radius of the particle shell and r_i is the inner radius of the particle shell.

This calculation method only takes into account the intensity of relatively small segments along the particle radius and assumes a symmetrical intensity pattern throughout the bead. Although adequate for analysing clean beads, it may not properly approximate the total intensity for fouled beads where distributions may not be symmetrical.

An alternative method for calculating the total intensity of the bead from the optical cross-section through the centre of the bead that will better account for the potential asymmetrical and non-uniform distribution of dyed materials, and thus yield a better approximation of the total intensity of the entire bead, was adopted. In this method, the total intensity of the bead cross-section was determined. The average intensity value for half the bead cross-section (semi-circle) was then multiplied by the circumference of the bead, to achieve the intensity of the total bead. This value was normalised with respect to volume to give the relative solid phase concentration expressed as arbitrary units per volume of adsorbent (equation 3-5).

$$Q_{rel} = \frac{I_T r_p \pi}{V_p} \tag{3-5}$$

where Q_{rel} is the relative capacity of the bead, I_T is the total intensity of the bead cross-section at the centre of the bead, r_p is the radius of the particle and V_p is the particle volume.

3.5.6.3 Calculation of effective diffusivity from confocal images

If a shrinking core model can be assumed then a single lumped kinetic parameter or effective diffusivity, D_e, can be estimated directly from the confocal images by using the position of the adsorption front. The approach assumes that the adsorption layer is saturated, and the effective diffusivity is calculated from the linear regression of the

infinite volume solution of the model that takes into account external mass-transfer resistance (Teo and Ruthven, 1986) as shown in equation 3-6:

$$\frac{D_e t}{R_p^2} = \frac{\varepsilon_p D_p}{R_p^2}\frac{C_0}{q_s}t = \left[1 + \frac{\varepsilon_p D_p}{k_f R_p}\right] I_2 - I_1 \qquad (3\text{-}6)$$

where ε_p is the intraparticle porosity, D_p is the pore diffusivity, C_0 is the feed protein concentration, R_p is the particle radius, R_f is the radial position of the front, k_f is the external fluid film mass-transfer coefficient, q_s is the saturation adsorbed-phase concentrations, and:

$$I_1 = \int_1^{\eta} \eta \, d\eta = \tfrac{1}{2}\left(\eta^2 - 1\right) \qquad (3\text{-}7)$$

$$I_2 = \int_1^{\eta} \eta \, d\eta = \tfrac{1}{3}\left(\eta^3 - 1\right) \qquad (3\text{-}8)$$

where η is the fractional uptake given by (R_f/R_p).

No attempt was made to de-convolute the individual parameters, such as D_p, ε_p and k_f, in equation 3-6, as further independent experiments may be required to determine the values of some of the parameters. Physical complications that can develop by the presence of fouling material can make this less straight forward. Instead, the effective diffusivity (D_e), as described in equation 3-6, alone was used to provide an indication of the overall adsorption rate and used for comparison purposes.

4 FRONTAL ANALYSIS OF CAPACITY AND BREAKTHROUGH CHARACTERISTICS OF FOULED PACKED BED COLUMNS

ABSTRACT

This study examines the impact of fouling on the dynamic capacity and breakthrough behaviour of packed bed chromatography columns. Columns packed with DEAE Sepharose FF were challenged with yeast homogenate feed material which had been clarified by centrifugation to varying extents. Change in column performance was assessed by analysis of breakthrough curves obtained with BSA as a test protein. The fouling effects of repeated loading of small quantities of poorly clarified yeast homogenate was compared to effects of loading the same total quantity of yeast homogenate to the column as a single challenge. The impact of solid particulates in the foulant stream on the change in column breakthrough behaviour was investigated as well as the reversibility of the most severe fouling effects by application of a clean-in-place (CIP) protocol comprising a column wash with 1 M sodium hydroxide for five hours.

4.1 INTRODUCTION

Chromatographic separations are critical in downstream processing of biopharmaceuticals due to their excellent selectivity and relatively straight forward scaling (Hammond and Scawen, 1989). Several chromatographic steps are usually used to achieve the high levels of final product purity required (Walsh, 2003). During manufacturing, time-dependent and process-specific degradation in the performance of chromatography columns must be monitored and controlled to satisfy stringent regulatory requirements on product consistency between batches (Larson et al., 2003). A number of components in process feed streams to chromatography columns may exert deleterious effects on the matrix bed characteristics, particularly under repeated or prolonged exposure. Colloidal material such as lipids, cell debris and carbohydrates, as well as soluble components such as contaminant proteins and nucleic acids can give rise to this phenomenon, which is generally referred to as fouling. These components may act by blocking matrix bead pores, selectively absorbing to the matrix active groups (Feuser et al., 1999) or by occupying interparticle void volume in the column. These effects can cause changes in column capacity (Staby et al., 1998) and column resolution as well as increased pressure drop, all of which are critical process parameters that determine the economics of a separation step. Analysis of how these process parameters are affected by feed stream properties is of particular importance and will aid in optimal choice of method of feed pre-treatment. Prior to chromatography steps, process streams are typically clarified to remove particulate material such as cell debris either by centrifugation or filtration, or a combination of both. Knowledge of the trade-offs between additional processing effort to clean up a process stream and the benefits in terms of performance of the subsequent chromatographic steps is key to achieving efficient bioprocess operation. Ideally one would aim to minimise the extent of feed pre-treatment prior to column-based separation without affecting chromatographic performance and column lifetime.

Only a few investigations on the effect of fouling of packed bed chromatography columns have been reported in the literature (Levison et al., 1990; Shepard et al., 2000; Staby et al., 1998), which show how binding capacity for the protein product can be reduced in the presence of contaminants in the feed material, and how foulants can affect matrix lifetime. A qualitative analysis of the components of fermentation broths that can give rise to fouling of chromatography columns has

been presented by Pirotta (1985). Effects of fouling have, however, been investigated for expanded bed adsorption operations (Anspach et al. 1999; Fernandez-Lahore et al., 1999; Feuser et al., 1999; Smith et al., 2002) and filtration operations (Belfort et al., 1994), since in such systems the feed material contains a high load of potentially fouling components. Detailed elucidation of fouling mechanisms requires complete characterisation of fouling components in the feed stream and in depth knowledge of specific interactions which occur between these components and the matrix chemistry (Maa and Hsu, 1998; Yiantsios and Karabelas, 1998). Due to the complexity of most realistic process streams, such as yeast homogenate, this would be practically impossible to achieve. However, comparison of the breakthrough curves for clean and fouled columns can be informative in determining the effect of foulants on the performance of the chromatography column. The shape and position of the breakthrough curve with respect to the volume of material processed are dependent on the capacity of the adsorbent, the binding kinetics and mass transfer characteristics of the solute in the system (Chase, 1984; Cooney, 1990; Cooney 1993). The leading edge of the breakthrough curve, $C/C_0 < 0.5$, is dominated by the mass transfer of solute in the fluid film, whereas the tailing edge, $C/C_0 > 0.5$, is dominated by diffusion of the solute in the matrix pores (Helfferich and Carr, 1993). The diffusive transport of molecules through the external liquid film to the bead surface can be subject to obstruction through deposit formation around matrix particles (Stewart, 1998). External mass transfer limitations can cause premature breakthrough of adsorbing species (Jungbauer, 1993; Li et al., 1995). Colloidal material may obstruct bead pores, and for large adsorbents, narrowing of bead pores due to the presence of bound species has also been suggested as a limiting mechanism to intraparticle diffusion (Linden et al., 1999). Specific binding of some fouling species to adsorption sites both on the bead surface and internal to the pore could alter the capacity of the adsorbent for the target protein and affect the position of the breakthrough curve (Staby et al., 1998).

In this work we examined the change in performance of a packed bed chromatographic column which was challenged with *S. cerevisiae* homogenate, representing a realistic process stream. Change in column performance was evaluated by comparing breakthrough curves, obtained using BSA as a test protein, generated on fresh and on fouled columns. Feed material of differing fouling severity was loaded to the column. Change in performance was assessed as a function of the total amount of homogenate loaded, which was either presented to the column as a single challenge or

as the summation of successive smaller loads, with intermittent salt washes between loads. The effectiveness of a typical CIP protocol in restoring the characteristics of fouled columns was also determined.

4.2 RESULTS

In this work, column performance was monitored as a function of foulant challenge to the column. Performance was assessed in terms of the breakthrough characteristics obtained for binding of a test protein, BSA. The foulant material was yeast homogenate which was clarified either simply by disc stack centrifugation, giving a poorly clarified feed stream, or with further clarification by ultracentrifugation to give a highly clarified feed stream. Material clarified by disc stack centrifugation was characterised for content of its major components. The soluble protein concentration was found to be 20 mg/mL, the lipid content was 3.2 mg/mL and particulate solid concentration was 350 mg/mL. The supernatant prepared by ultracentrifugation was assumed to differ only in solids content, being essentially particulate-free. Testing the fouling effect of these two different feed streams allowed determining the influence of particulates (e.g., cell debris) on column performance.

The load volume of material during a chromatography cycle is usually determined by the yield or throughput desired for the particular step. The length of the wash step after loading is usually tailored to remove sufficient unbound protein before elution is commenced. When loading potentially fouling material to the column, the use of different load/wash strategies may be beneficial in maintaining acceptable column performance. To address this, we investigated the effect on column performance of loading fouling feed material both in an incremental fashion with small volume loads followed immediately by a column wash, or by loading the same volume of feed in one single challenge.

Maintaining column performance over more feed cycles is also of importance and thus appropriate CIP protocols must be designed to accommodate less clarified feeds to the column. The reversibility of fouling effects was investigated for material with highest fouling potential.

4.2.1 Effect of repeated loading of small volumes of fouling material on column breakthrough behaviour

The capacity of a fresh column was determined to be 318 ± 47 (95% C.I.) mg BSA at 1% breakthrough and 480 ± 80 (95% C.I.) mg BSA at 100% breakthrough, based on determinations of breakthrough curves on 5 different fresh columns. The determination of binding capacity on the same column was found to repeatable within 5% (95% C.I.) of the mean based on ten repeated determinations, so that changes in binding capacity greater than 5% were judged as significant.

Yeast homogenate was clarified by ultracentrifugation to obtain a particulate-free process stream. The effect of repeated loading of small volumes of this foulant material on column performance was determined by analysing changes in breakthrough curves obtained after each cycle of foulant challenge to the column (Figure 4-1). As evident from the similar positions of the breakthrough curves it is clear that there was no significant variation in the dynamic capacity at the 1% and 100% breakthrough levels with the number of fouling cycles carried out.

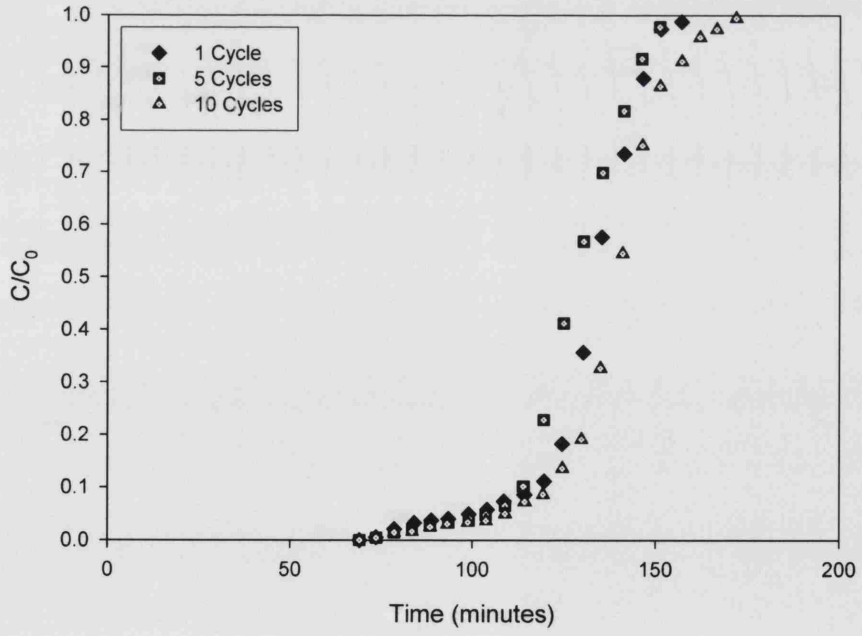

***Figure 4-1**: The effect of repeatedly fouling a DEAE Sepharose Fast Flow column with ultracentrifuged yeast homogenate on breakthrough curves of the test protein BSA. For each cycle, 2 mL of clarified homogenate were loaded, column was washed with 1 M NaCl and a breakthrough test was carried out. Breakthrough curves for the first, fifth, and tenth cycle are shown. C_0= 2 mg/mL.*

Repeatedly loading small volumes of yeast homogenate clarified only by disc stack centrifugation, containing a higher particulate solids concentration, had a more pronounced effect on binding capacity (Figure 4-2). With respect to the average capacity of a fresh column the decrease in binding capacity at the 1% breakthrough level was judged as significant, but the drop at the 100 % breakthrough level was not.

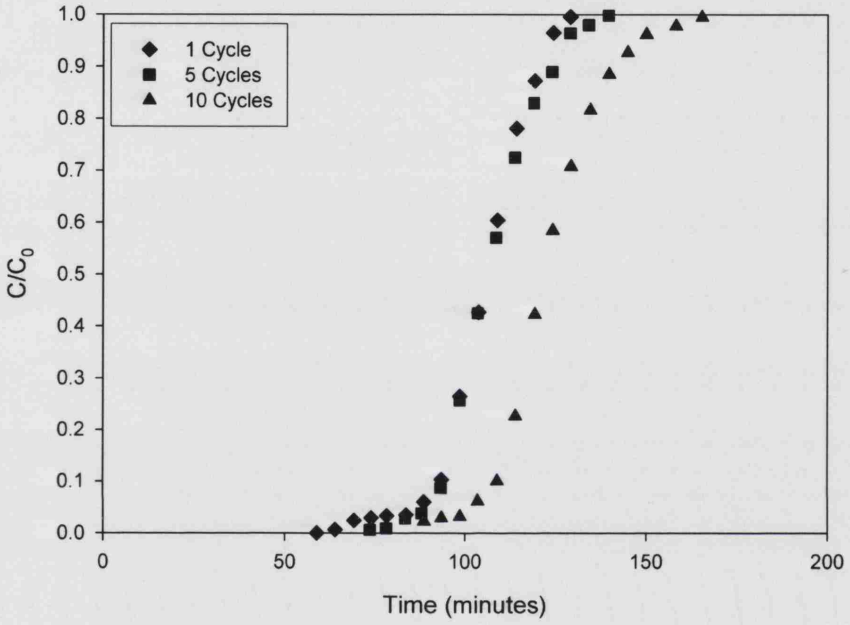

Figure 4-2: *The effect of repeatedly fouling a DEAE Sepharose Fast Flow column with disc stack centrifuged yeast homogenate on breakthrough curves of the test protein BSA. For each cycle, 2 mL of homogenate were loaded, column was washed with 1 M NaCl and a breakthrough test was carried out. Breakthrough curves for the first, fifth, and tenth cycle are shown.* C_0*= 2 mg/mL.*

With increasing number of fouling cycles there was a gradual and significant increase in the binding capacity at both the 1% and 100% breakthrough level, with respect to the binding capacity determined after the first fouling cycle (Figure 4-3). After the tenth fouling cycle the column dynamic capacity at 100% breakthrough had increased by approximately 15% compared to after cycle 1, and the capacity at the 1% breakthrough level increased by 50 % compare to after the first fouling application. The changes in binding capacity were due to shift of breakthrough with loading time but the shape of the curves and the gradient at 50% breakthrough remained unchanged

with respect to a fresh column. Nevertheless, after the tenth cycle the binding capacities were not significantly different to those of a fresh column.

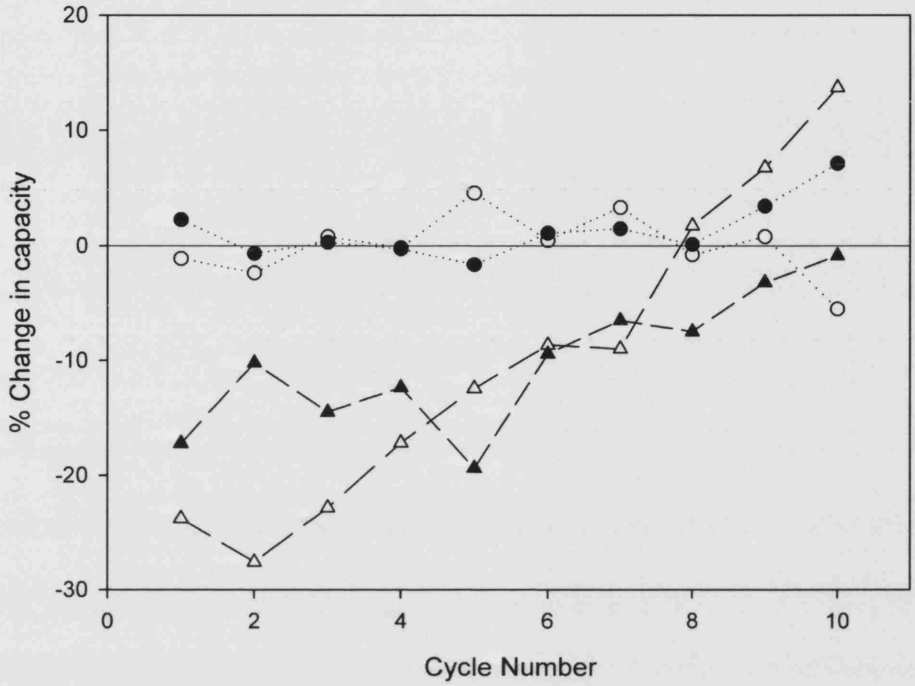

***Figure 4-3**: The effect of repeatedly fouling a DEAE Sepharose Fast Flow column with either ultracentrifuged (○,●) or disc stack centrifuged (Δ,▲) yeast homogenate on column binding capacity. For each cycle, 2 mL of clarified homogenate were loaded, column was washed with 1 M NaCl and a breakthrough test was carried out. Capacity at 1% breakthrough (○,Δ) and capacity at 100% breakthrough (●,▲) are shown.*

4.2.2 Effect of loading large quantities of fouling material on column breakthrough

The effect of loading large volumes of fouling material with high solids concentration onto the column, prepared by disc stack centrifugation alone, on the breakthrough characteristics was more significant than that observed when small loads were applied with intermittent salt washing of the column bed. After fouling, breakthrough occurred significantly earlier and the shape of the breakthrough curve was altered compared to the same column before it was fouled. The severity of the changes depended on the volume of fouling material loaded (Figure 4-4).

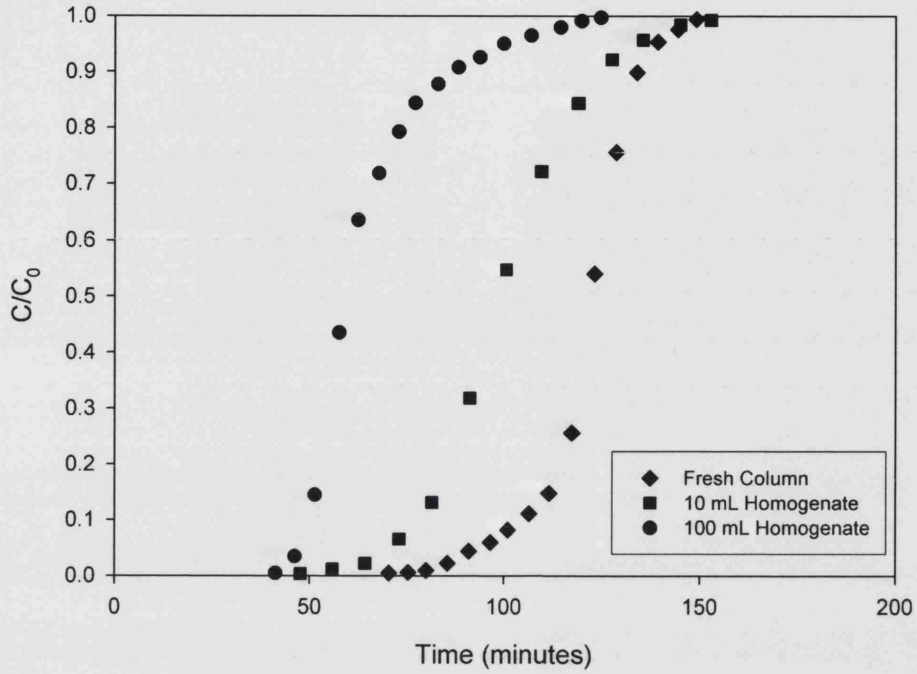

***Figure 4-4**: The effect of fouling a DEAE Sepharose Fast Flow column with disc stack centrifuged yeast homogenate on breakthrough curves of the test protein BSA. The effect of single loadings of 10 mL and 100 mL compared to the fresh column breakthrough curves are shown.*

The relative capacity values and amounts of solids fed to the column for each fouling challenge are listed in Table 4-1, and the effect of solids deposition on the column capacity is illustrated in Figure 4-5. For a 10 mL load, which equates to the whole of the amount of material added over five cycles of small fouling loads, there was a 50% reduction in the dynamic capacity of the column both at the 1% and 100% breakthrough level. The dynamic capacity was not significantly lower for a challenge of 50 mL of fouling material but decreased by a further 15% and 20% for the 1% and 100% levels, respectively, when the column was challenged with 100 mL of homogenate. After fouling, the breakthrough curves were characterised by a steeper slope in the initial phase of breakthrough ($C/C_0<0.2$) and also showed severe tailing. Both these effects were more pronounced for higher loads of fouling material.

Volume of yeast homogenate challenge (mL)	Solids loaded (wet weight) (mg)	Solids retained in column [b] (wet weight) (mg)	1% breakthrough relative capacity (arbitrary units)	100% breakthrough relative capacity (arbitrary units)
0 [a]	0	0	1	1
10	3500	50	0.53	0.5
50	17500	115	0.49	0.54
100	35000	2514	0.33	0.35

[a] Denotes a freshly-packed, clean column.

[b] Calculated by subtracting solids concentration in column effluent from solids concentration in column feed.

***Table 4-1**: Effect of loading yeast homogenate clarified with a disc stack centrifuge onto a packed bed of DEAE Sepharose FF on the dynamic capacity of the column.*

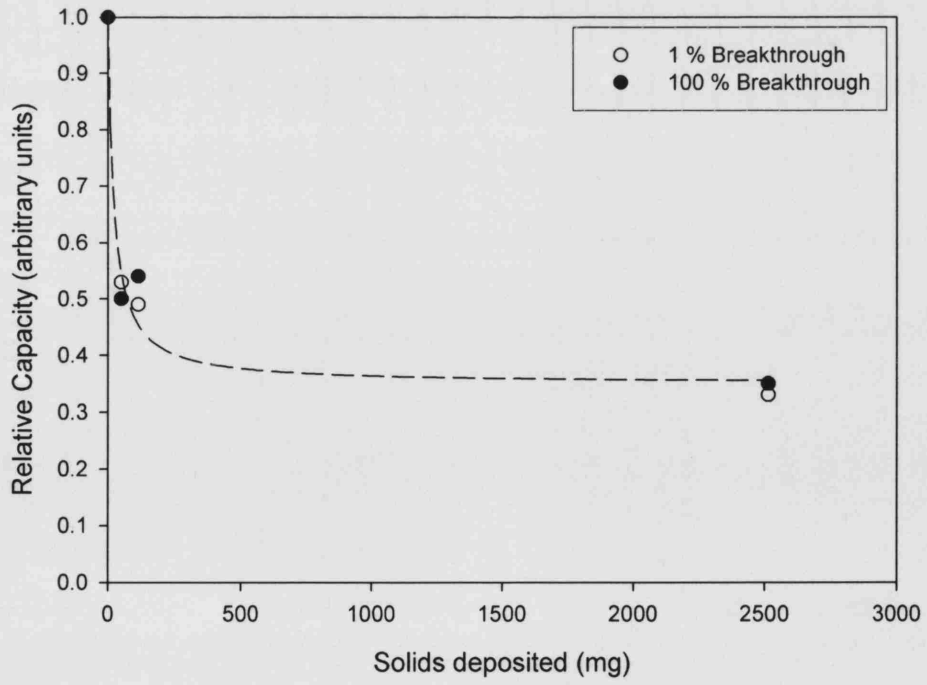

***Figure 4-5**: Effect of solids deposition on the column capacity. Different volumes of disc stack centrifuged homogenate were load onto the column and the capacity at 1% and 100% were determined.*

To determine whether loading of large volumes of homogenate containing high concentration of solids could alter the column bed structure and lead to bed compression as a result of solids deposition in void spaces between matrix beads, the pressure drop over the column as a function of operating flow rate was monitored for fresh and fouled columns (Figure 4-6). Loading yeast homogenate with high solids content onto the column caused a transient increase in pressure drop over the column. This was partly ascribed to the higher viscosity of the homogenate compared to the equilibration/wash buffers. Pressure-flow tests indicated that a small amount of bed clogging did occur, however no bed compression was observed visually. The linearity of the pressure vs. flow curves confirmed the absence of bed compression at the flow rates investigated for both the fresh and fouled columns. From the Blake-Kozeny equation, which describes the pressure drop as function of flow rate for packed beds of rigid particles under laminar flow, the increased pressure drop at a fixed flow rate and the increase in the slope of the pressure-flow lines which is observed for the fouled columns compared to the fresh column, suggests that a decrease in the bed porosity occurred upon fouling (Stickel and Fotopoulos, 2001). This may have been caused by cell debris occupying the interstices of the packed bed. There was a slight increase in slope of the pressure-flow curve for the column fouled with 100 mL of yeast homogenate compared to the column fouled with 50 mL of homogenate. This suggests that there is only a small difference in the amount of material deposited in the void spaces of the bed after the additional 50 mL load of fouling material. Given the relatively small increase in pressure drop despite the large amount of solid particulates loaded to the column, most of the particulates apparently flowed straight through the column. The mass of solids retained in the column was determined from a mass balance over the column (Table 4-1), but it proved difficult to determine this accurately due to the small mass of material retained. Data (not shown) revealed that the size distribution of solids transported through the bed was indistinguishable from that of the feed homogenate.

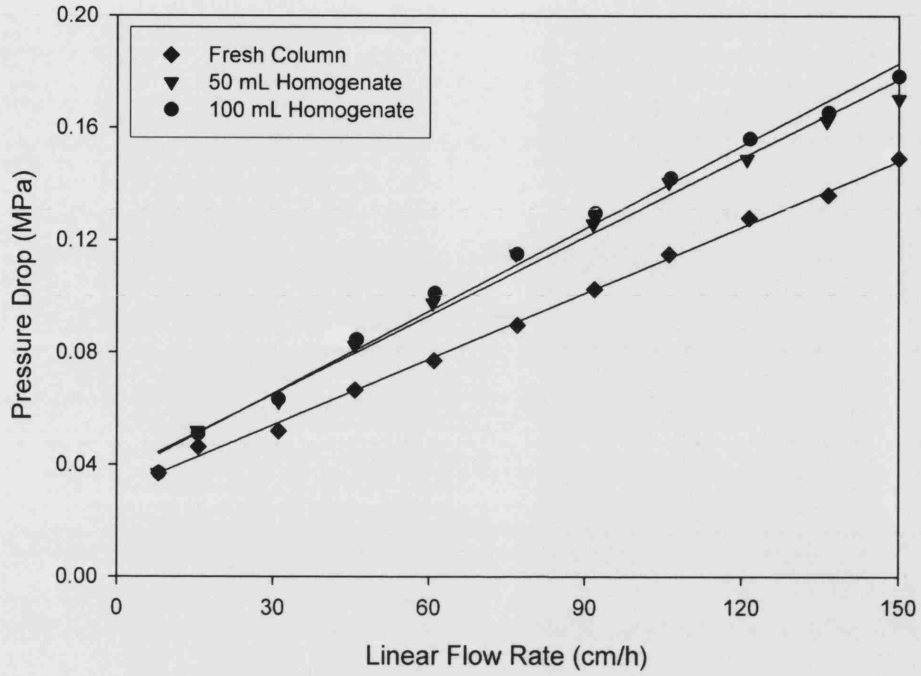

***Figure 4-6**: Variation in pressure drop across column as a function of flow rate for a freshly packed column and columns which had been fouled with 50 and 100 mL of yeast homogenate clarified by disc stack centrifugation.*

To examine the role of particulate solids contained in the feed material in the observed fouling effects, a comparison was made between the loading of 100 mL of the highly clarified yeast homogenate prepared by ultracentrifugation (Figure 4-7) compared to 100 mL of the disc stack centrifuged homogenate (Figure 4-4). When the particulate-free homogenate was applied to the column, there was very little difference between the breakthrough curves obtained with the fouled and fresh columns. The dynamic binding capacity was unchanged, and only a slight tailing of the breakthrough curves for the fouled column was observed. This result was similar to that observed when the same highly clarified yeast homogenate was applied to the column in repeated cycles of 2 mL feed volumes (Figure 4-1).

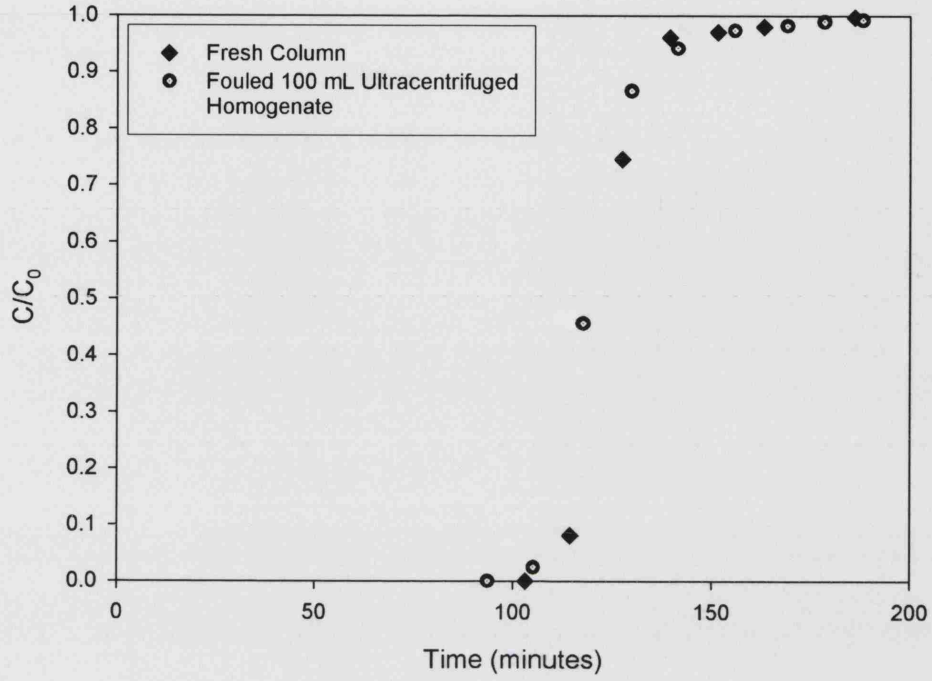

***Figure 4-7**: Effect of loading 100 mL of ultracentrifuged yeast homogenate to the DEAE Sepharose Fast Flow column in a single load, on breakthrough of the test protein BSA. Graph shows breakthrough curves for the freshly packed and the fouled column.*

4.2.3 Impact of CIP on column performance

The ability to clean a column in-situ without the requirement to re-pack is an important consideration for the economics of a process involving packed bed chromatography. With stable agarose-based matrices, reasonably harsh caustic wash treatments can be performed in order to remove foulants and to re-generate the column bed. To determine the reversibility of fouling effects, a common CIP protocol (cf. Section 3.3.2.4) was performed on a column that was fouled with 50 mL of yeast homogenate prepared by disc stack centrifugation so as to represent a severe fouling challenge. The column breakthrough curve was measured pre- and post-fouling and post CIP (Figure 4-8). Although the fouling caused a significant change in the breakthrough curve, the fouling effects were reversible as the CIP protocol was effective in restoring the column characteristics. There was no significant difference in

the breakthrough curves between the fresh column and the fouled column after cleaning.

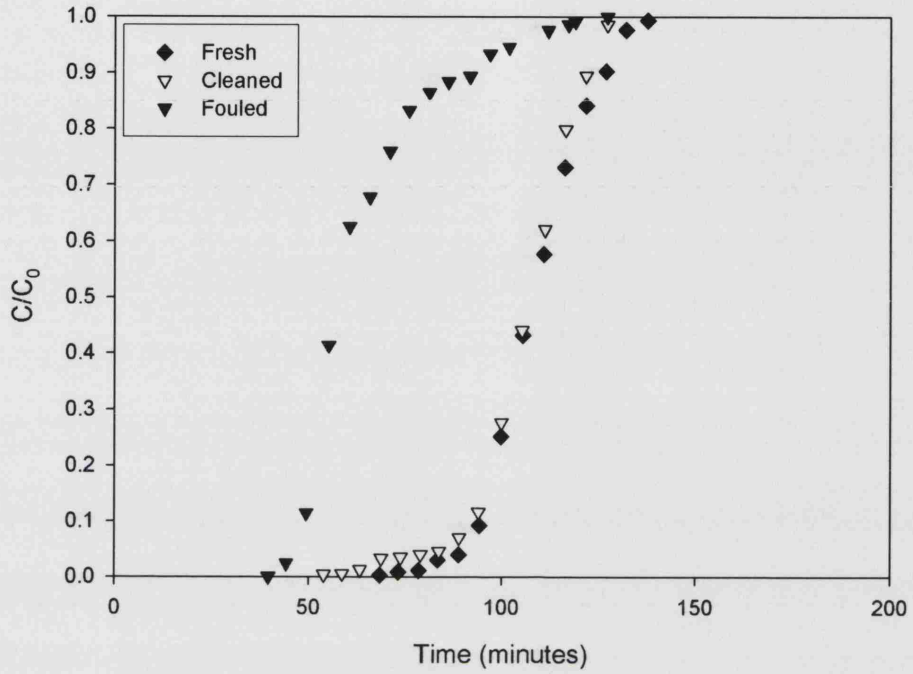

***Figure 4-8**: Efficacy of CIP treatment to clean a column fouled with 50 mL of yeast homogenate prepared by disc stack centrifugation. The breakthrough curves were determined with BSA for the fresh column, after fouling and after cleaning with 1 M NaOH at a flow rate of 0.1 mL/min for five hours.*

4.3 DISCUSSION

Loading of highly clarified homogenate to the column did not cause appreciable change in column capacity or shape of breakthrough profiles regardless of mode of application to the column. This was in contrast to the results obtained with poorly clarified homogenate suggesting that fouling effects were directly attributable to cell debris in the feed material.

The application of poorly clarified material to the column caused a decrease in column capacity regardless of the fouling protocol used. However, loading small volumes of material with intermittent salt washes of the column not only limited the overall decrease in capacity but also caused a recovery of column capacity to the levels

of a fresh column. The immediate decrease in binding capacity with the first fouling cycle is likely to be caused either by cell debris deposition at the surface of the matrix particles or blockage of particle pores or a combination of both. Cells and cell debris are negatively charged and have been shown to foul anion exchange matrices by selectively binding to the chromatographic bead surface (Feuser et al., 1999, Viloria-Cols et al., 2004). The salt wash employed between loading cycles may have been insufficient to remove all such particulate material bound to the matrix so that with each fouling cycle further cell debris may have bound to particulate material already in the column. The gradual recovery in binding capacity can only be rationalised if fouling material which remained in the column after washing provided additional surface area for binding of BSA. Binding of proteins to yeast cell debris through electrostatic interactions has been reported (Shaeiwitz et al., 1989). In this study, however, this would be unlikely at the pH employed since both BSA and cell debris would be negatively charged. It is possible, however, that hydrophobic patches on the cell debris attached to the matrix may have provided extra surface for binding of BSA, thus contributing to the increase in column capacity observed. Kelly and Zydney (1997) have shown that proteins in solution can bind to already-adsorbed protein deposits on ultrafiltration membranes through intermolecular disulphide bond formation or hydrophobic interactions, giving rise to secondary fouling.

A single large challenge of poorly clarified homogenate to the column resulted in a greater reduction of column capacity for equal amount of material loaded in repeated fouling cycles. In addition an increased slope of the curve at low breakthrough values and significant tailing of the breakthrough curve was observed. In this loading method, washing of unbound contaminants from the column occurred only for a short time after the extended loading. Again, the reduced binding capacity must be due to unavailability of binding sites to BSA both on the bead surface and inside the bead pores. In this case it appears that the increased loading time exacerbates this effect possibly by further cell debris deposition in the column through cell-cell interactions in addition to cell-matrix attachment (cf. Section 6.3.6). Significant deposition of particulates around matrix beads would also increase the severity of external mass transfer limitations causing faster breakthrough from the column as observed. Severe clogging of the column could also give rise to uneven flow distribution in the column and channelling of flow resulting in increased axial

dispersion in the column; however, the pressure-flow curves determined were not indicative of severe blockage.

A reduction in the rate of mass transfer of the BSA to binding sites inside the pores of the matrix beads after fouling is supported by the dramatic tailing observed of the breakthrough curves. Intraparticle mass transfer limitations seemed to have played an increasing role in modifying breakthrough characteristics as more fouling material was loaded to the column. The small increase in slope of the pressure-flow curves after fouling with 100 mL of poorly clarified homogenate compared to only 50 mL indicated that bed porosity was not reduced significantly; however, the total binding capacity was reduced by a further 20%. This suggests that the reduction in effective intraparticle diffusivity of the BSA was a major contributing factor of the reduced binding capacity. Loading of fouling material over a long period may have allowed colloidal contaminants to diffuse into matrix pores to a greater extent.

4.4 CONCLUSIONS

In this work we have characterised the effect of fouling with yeast homogenate on capacity and breakthrough performance of an ion exchange packed bed. The overall impact of fouling on bed performance depended heavily on the level of solids concentration in the feed stream. Frequent salt washes were effective in allowing recovery of column capacity, probably due to non-specific binding of BSA to cell debris deposits on the chromatography matrix. When large volumes of poorly clarified homogenate was fed to the column, dynamic binding capacity decreased and changes in breakthrough curves suggested increased intraparticle and external mass transfer limitations. These changes were ascribed to deposition of solid particulates in void spaces in the bed and colloidal contaminants in the bead pores.

The methodology employed in this study can be used to determine the fouling potential of industrial feed streams applied to protein capture steps and inform on the minimum clarification required before the packed bed purification step.

5 QUANTIFYING THE DISPERSIVE EFFECTS OF FOULING ON A PACKED BED COLUMN USING AN EXTENDED REVERSE-FLOW TECHNIQUE

ABSTRACT

An extended reverse-flow technique using an acetone tracer has been developed to investigate the effects of fouling on a packed bed column. The technique allows the band broadening effects due to reversible macroscopic factors, such as flow maldistribution in the flow distributor and inside the packed bed caused by packing heterogeneity, to be separated from irreversible microscopic factors, such as intraparticle diffusion, boundary layer mass transfer and interparticle axial dispersion. This method was used to assess the extent of fouling of a packed bed as a function of axial position.

5.1 INTRODUCTION

Chromatographic resins can be very expensive and therefore considerable effort and money will normally be spent on improving column performance and maximising the number of re-uses of the resin. In industry, it is common practise to clean columns by back-washing and/or by using a clean-in-place protocol of ever increasing complexity to target each type of contaminant with caustic, detergent or organic solvent washes. Repacking of the top section of column is also done to remove visible discoloration caused by fouling. Conventional approaches used in industry for diagnosing the condition of a packed bed column (O'Leary et al., 2001; Williams et al., 2002; Rathore et al., 2003) only provides an indication of the overall condition of the column, and will not necessarily identify where the fouling effects are most severe or the mechanism of fouling. This missing information can be extremely useful during process development and when designing clean-in-place protocols to mitigate fouling effects. This chapter sets out to examine a simple, non-destructive approach that can provide information on the band broadening effects due to fouling within a packed bed column which can not be gained by using conventional approaches.

5.1.1 Techniques for studying the effects of packing and flow heterogeneity

Packing and flow heterogeneity have been long known to cause band broadening and reduced separation efficiency (Giddings, 1965; Guiochon et al., 1994), and recently have been demonstrated via computational fluid dynamics (Billen et al., 2005). A variety of insightful techniques have been used by researchers to study the effects of such flow disturbances. The techniques that have been used are, however, often disruptive to the column packing (Coq et al., 1979; Klawiter et al., 1982; Kaminski et al, 1982) or are complicated and requiring expensive equipment. Examples of such elaborate methods include laser anemometry (Volkov et al, 1978), magnetic resonance imaging (Ilg et al., 1990; Bayer et al., 1995; Tallarek et al., 1995 and 1998; Yuan et al., 1999), direct visualisation in the transport systems via refractive index (Shalliker et al., 1999, 2000a, 2000b and 2003; Broyles et al., 2000) and ultrasound (Hofmann, 2003). However, none of the above techniques can be readily

applied to large columns and have not been widely used in industry due to their complexity and often intrusive nature.

A simple, non-destructive test based on reversing the flow of a non-binding test pulse when travelling down a column has been developed (Kaminski, 1992; Roper and Lightfoot, 1995; Moscariello et al., 2001; Teeters et al., 2002) and shown to be applicable to large-scale columns (Moscariello et al., 2001). It can be used as a quick test to diagnose the flow disturbances in a column, providing a more detailed description of the flow maldistribution than with using conventional forward-flow test methods (Rathore et al., 2003), and can be used for industrial applications. The application of the technique is described in the next section and detailed in Section 3.4.

5.1.2 Reverse-flow technique

A reverse-flow or bidirectional test allowing the diagnosis of the major reasons for unsatisfactory column efficiency was first developed by Kaminski (1992). The test consists of two stages. The first stage is a standard test of column efficiency using a single, non-binding substance or an easily separable mixture under conditions where no overloading occurs. The second step involves the bidirectional elution of a single test substance, initially as in the first stage, but only until a predetermined fraction of column length has been reached. Then the direction of flow is reversed and the tracer is eluted back through the column inlet. The test takes advantage of the reversible nature of macroscopic flow distribution. For well designed columns where the proper operation of the distributor head is certain, the differences between the height-equivalent-to-a-theoretical-plate (HETP) values obtained from the two stages indicates the degree of deviation of the flow profile from plug flow. The HETP value obtained from the reverse-flow stage characterises the potentially attainable column efficiency in the applied chromatographic system. However, when the proper operation of the distributor head is doubtful, the difference in the HETP values in favour of the reverse-flow stage can indicate excessive resistance of radial flow in the distributor head and a difference in HETP values in favour of the conventional stage can confirm the existence of large diffusion spaces in the column heads or large extra-column band broadening effects (e.g., the existence of void volumes and/or blockage of the frit).

Roper and Lightfoot (1995) performed the reverse-flow technique to evaluate the separation performance of stacked-membrane chromatography. Reversing the flow eliminated the distortion of effluent profiles generated by non-uniform flow. They suggested that the obtained performance estimates are more reliable than those based on moments or bandwidth measurements when non-uniform or extra-column effects are significant. More recently, Teeters et al. (2002) tested the separation efficiency and scalability of the new Mustang™ (Pall Corporation, Ann Arbor, MI, USA) stacked-membrane chromatographic devices under various conditions and sizes. At 10 mL and 1 L scale the test was insensitive to tracer size and flow rate. Stacked-membrane chromatography gave sharper peaks than would have been expected from conventional packed bed using 15 μm beads.

Development of the reverse-flow technique by Kiminski (1992) and Roper and Lightfoot (1995) provided a basis for Moscariello et al. (2001) to qualify a slurry-packed, process-scale column. An IsoPak™ column with an internal diameter of 44 cm (Millipore Corporation, Bedford, MA, USA) was packed with Cellufine GC 700 media using an IsoPak™ slurry transfer skid. It was noted that the technique allowed the quantification of the relative effects of macroscopic flow maldistribution from the microscopic sources and also allowed the separation of band broadening effects induced by header design, packing non-uniformity and the column peripherals. Additivity of peak moments as described by Lightfoot et al. (1997 and 2003), allowed Moscariello et al. (2001) to derive the following equation that describes the total dispersion as a linear function of the bed length (cf. Section 5.2.5):

$$\mu_{2,\text{total}} = \mu_{2,\text{header}} + \frac{H_{\text{bed}}}{v^2} L \qquad (5\text{-}1)$$

where μ_2 is the second central moment, H_{bed} is the height of the theoretical plate, L is the bed depth and v is the superficial flow velocity. For this analysis, the height of the theoretical plate inside the packed bed, H_{bed}, is assumed to be independent of the bed length, L. Therefore, by varying the depth of the packed bed and implementing equation 5-1, it is possible to examine the contributions of the packing heterogeneity and the header maldistribution individually. If the plot of $\mu_{2,\text{total}}$ vs. L yields a linear correlation, one may assume the bed is homogeneous in the

direction of flow, and that the y-intercept represents $\mu_{2,header}$. For reverse-flow operation, $\mu_{2,header}$ should be zero due to the reversible nature of macroscopic flow maldistribution. They found that the slurry-packed columns were very uniform and no significant macroscopic flow maldistribution was observed in the column. Dispersion in the flow distributors was significant, corresponding to 15 – 25% of the intra-column dispersion when the full 24 cm bed length was used, and this proportion increased with shorter bed lengths. The study illustrated the effectiveness of the reverse-flow technique in investigating industrially important column systems.

5.1.3 Objectives

The studies described have demonstrated the ability of the reverse-flow technique to examine band broadening in both packed-bed chromatography and membrane chromatography but in both cases only for clean, non-fouled systems. The technique has been shown to be simple and non-destructive. It has found applications in industry, especially for qualifying column packing at large scale, and plausibly may be used to investigate other band broadening problems associated with process chromatography.

The work reported in this chapter seeks to extend the reverse-flow technique so as to enable the extent of fouling of a packed bed as a function of axial position to be assessed and to isolate the dispersive effects of fouling caused by changes in mass transfer parameters from that of macroscopic maldistribution of the feed stream.

5.2 THEORY

5.2.1 Chromatographic separation performance

A common description of column performance is the concept of theoretical plates which was adopted by Martin and Synge (1941) from the analysis of distillation columns. They recognised that vapour-liquid equilibria are analogous to adsorption isotherms, which describe the partitioning of a solute between the liquid and solid phases. The chromatographic bed can be considered as consisting of a series of

conceptual plates stacked perpendicular to the direction of flow. Lee et al. (1993) discussed the analysis of chromatographic separation by plate theory in detail.

These conceptual plates are termed "theoretical plates" and the thickness of each plate is called the "height-equivalent-to-a-theoretical-plate" (HETP or H). Explicitly, HETP can be expressed by equation 5-2 (Giddings, 1965):

$$H = \frac{\sigma_L^2}{R_D v t_R} = \frac{\sigma_L^2}{L} \tag{5-2}$$

where R_D is the retardation factor, t_R is the retention time, v is the superficial flow velocity, σ_L is the standard deviation of the eluted solute concentration profile in column length terms, and L is the length of the bed. The standard deviation can be expressed in time or volume units, resulting in the following expression for the plate height (equation 5-3):

$$H = \frac{\sigma_T^2 R_D v}{t_R} = \frac{\sigma_v^2 R_D v}{V_R Q} \tag{5-3}$$

where V_R is the retention volume and Q is the volumetric flow rate of the mobile phase. The number of theoretical plates, N, is simply the bed length, L, divided by H. A high number of plates (i.e. short HETP) produce sharp solute peaks, therefore allowing better separation efficiency in chromatographic operations.

5.2.2 Band broadening

Several practical factors work towards dispersing solute bands as they move through a column, thus increasing the value of HETP. Solute band broadening can result from inhomogeneities in the streamline flow of the mobile phase, deviations in the adsorption equilibrium due to mass transfer resistance between the mobile and stationary phases, and axial molecular diffusion driven by solute concentration gradients. Band broadening can happen within the column itself (intra-column) and also in ancillary parts of the system (extra-column).

5.2.2.1 Intra-column band broadening

In chromatographic systems, it is desirable to maximise mass transfer rates while minimising momentum transfer or pressure drops. Several relationships that describe band broadening or dispersion in gas and liquid chromatography have been previously proposed (Lee et al., 1993), including the widely cited model by van Deemter et al. (1965). Furthermore, Lightfoot et al. (2003) recently reviewed five ways to improve mass transfer, and Kirkup et al. (2004) compared some of the models that describe band broadening. The studies performed have been limited to the context of pure, single-component samples and do not address the varied and complex mechanisms of fouling. In fouling situations, diffusive transport of molecules through the external liquid film and into the bead pores can be obstructed through deposit formation around the matrix particles, or even inside the bead pores (cf. Chapter 1). For the case of large absorbents, narrowing of the bead pores due to the presence of bound species has been suggested as a limiting mechanism to transport (Linden et al., 1999; cf. Chapter 6). Mass transfer limitations can directly influence the performance of the column by causing band broadening. Evidently, an understanding of the mechanisms underlying band broadening will allow better column design as well as predicting the conditions that allows the minimisation of band broadening for any given column.

The flow distributor or header design is commonly believed to contribute significantly to the flow maldistribution. This has led to a large number of patented header designs (Mott, 1983; McNeil, 1982; Munk, 1984; Saxena and Andersen, 1989; Saxena and Young, 1995; LePlang and Charbol, 1992; Colvin and Hanley, 1990; Kearney et al., 1994; Joseph et al., 1994; Jungbauer and Letters, 1995). Quantitative information on header designs is scarce but Yuan et al. (1999) recently attempted to provide a rational basis for header designing and confirmed, using magnetic resonance imaging (MRI), that significant maldistribution is introduced by non-uniform flow in headers. Shalliker et al. (1999 and 2000a) showed that the inlet configuration dramatically influenced the flow distribution along the column. For small-scale columns of 1.7 cm diameter, they found that the radial flow distribution was nearly homogenous for columns with headers having only a frit but not for those having also

a distributor. More importantly, the frit porosity should be matched to the particle size of the bed packing.

5.2.2.2 Extra-column band broadening

Studies of extra column band broadening have been reported by Sternberg (1966), Huber and Rizzi (1987) and Dose and Guiochon (1990). Sternberg et al. (1966) provided a comprehensive account of extra-column band broadening for gas chromatography and Jonsson (1987) verified that most of the descriptions are applicable for liquid chromatography. Models that predict the peak profiles (Mao et al., 1995; Yu and Wang, 1989; Golshan-Shirazi and Guiochon; 1994; Gallant et al., 1995) often neglect extra-column dispersion.

Extra-column effects can be subdivided into dispersion in tubes, contributions of dead volumes, finite detector volume and dynamic behaviour of transducers and electronics. Tubes introduce a symmetrical Gaussian-type broadening (σ_t^2) to the sample (Taylor, 1953); the finite sensing volume of a detector introduces symmetrical, rectangular broadening(σ_d^2)(Cram and Glenn, 1975; Sternberg, 1966); dead volumes introduce an exponential broadening (τ_{dead}^2) (Cram and Glenn, 1975); and the finite response rate of electronics introduces an exponential contribution that is independent of the flow rate (τ_{elec}^2)(Cram and Glenn, 1975; Poppe, 1980). Assuming addivity of the variances, the total extra-column broadening can be expressed as (Kaltenbrunner et al., 1997):

$$\sigma_{ex}^2 = \sigma_s^2 + \sigma_t^2 + \sigma_d^2 + \tau_{dead}^2 + \tau_{elec}^2 \qquad (5\text{-}4)$$

where σ_{ex}^2 is the lumped extra-column dispersion and σ_s^2 is the variance of the initial injection profile.

Kaltenbrunner et al. (1997) showed that extra-column dispersion can contribute significantly to band broadening especially when using very small columns. Extra-column broadening was shown to account for over 60% of the total broadening in 2

mL columns, whilst the contribution decreases sharply to about 5% for 10 mL columns. It can be concluded from their observations that extra-column effects may overwhelm all band broadening effects when using very small columns and this must be considered when seeking to use scaled-down column studies to predict performance of larger-scale columns.

5.2.3 Macroscopic and microscopic factors that influence band broadening

Solute band broadening occurs as a result of inhomogeneities in the streamline flow of the mobile phase, axial molecular diffusion driven by solute concentration gradients and deviations in the adsorption equilibrium due to mass transfer resistances between the mobile phase and stationary phase. These three effects are independent and the total band broadening can be expressed as a sum of the three band broadening for each of these processes. This band broadening can be expressed as plate heights and is given by equation 5-5 (van Deemter et al., 1965):

$$H = H_{flow} + H_{diffusion} + H_{mass\ transfer} \tag{5-5}$$

Morscariello et al. (2001) categorised the factors that cause band broadening in a packed bed of porous media into two groups: macroscopic factors and microscopic factors. Macroscopic factors contribute to the first term on the right-hand side of equation 5-5 and arise through dispersion due to (Lode et al., 1998):

- Packing heterogeneity of the column bed,
- Non-uniform flow from the column flow distributor or header.

Microscopic factors contribute to the remaining two terms on the right-hand side of equation 5-5. These factors are:

- Intraparticle diffusion,
- External fluid film mass transfer,
- Interparticle axial dispersion,
- Adsorption-desorption kinetics.

Furthermore, the effects of these four microscopic processes are simply additive (Klinkenberg and Sjenitzer, 1956). If the solute used is non-reactive and non-adsorptive (such as acetone to agarose-based matrices) then adsorption-desorption kinetics can be disregarded.

5.2.4 The reversibility of macroscopic flow distribution

Key to the reverse-flow technique is the reversible nature of macroscopic flow maldistribution. Under typical process conditions, flow in a chromatography system is characterised by a very low Reynolds number (Re) as shown in equation 5-6:

$$\mathrm{Re} = \frac{d_p \nu \rho}{\mu} \langle\langle 1 \tag{5-6}$$

where d_p is the diameter of a chromatographic bead, ν is the interstitial fluid velocity, ρ is the density of the fluid and μ is the viscosity of the fluid. For an incompressible fluid, the creeping flow equations of continuity and motion (equations 5-7 and 5-8) (Bird et al., 2002) show that the flow in such systems are proportional to velocity and if the flow was reversed, e.g., by reversing the driving pressure, the fluid element would retrace its path in the opposite direction.

$$\nabla \bullet \nu = 0 \tag{5-7}$$

$$\left(\nabla^2 [\nabla \times \nu]\right) = 0 \tag{5-8}$$

Furthermore the Blake-Kozeny equation (5-9) (Blake, 1922; Bird et al., 2002) for flow through a bed of porous beads suggests that changing the magnitude of the velocity, or driving pressure, will change only the speed at which this retracing takes place.

$$\frac{dP}{dL} = \frac{150\mu}{d_p^2} \frac{(1-\varepsilon)^2}{\varepsilon^3} \cdot \nu \tag{5-9}$$

Lightfoot et al. (2003) states that: "All contributions to plate height in one-dimensional models, all localised to the size scale of the packing particle diameter, are

irreversible, whereas fluid motion on a size scale of the packing particle diameter is reversible."

5.2.5 Additivity of moments

The additivity of moments described by Lightfoot et al. (1997 and 2003) allows the characterisation of the system in terms of variance of an elution peak of a short pulse of non-adsorptive tracer with respect to residence time or volume. In the reverse-flow technique it is important that these variances are additive, thereby allowing the total dispersion to be described simply as a linear sum of the individual dispersive contributions of different components.

The additivity of the first absolute moment and the second central moments can be very useful in chromatographic systems.

These can be expressed as equations 5-10 and 5-11, respectively:

$$M_{1,total} = M_{1,header} + M_{1,bed} \tag{5-10}$$

$$\sigma^2_{total} = \sigma^2_{header} + \sigma^2_{bed} \tag{5-11}$$

Knowing that:

$$H_{bed} = \frac{L}{N} = L \cdot \left(\frac{\sigma_{bed}}{t_R} \right)^2 = L \cdot \left(\frac{\sigma^2_{bed}}{M^2_{1,bed}} \right) \tag{5-12}$$

where N is the plate number and t_R is the mean solute residence time.

Also,

$$M_{1,bed} = \frac{L}{v} \tag{5-13}$$

Equation 5-13 can be substituted into equation 5-12 giving equation 5-14:

$$\sigma^2_{bed} = \frac{H_{bed} L}{v^2} \tag{5-14}$$

Substituting equation 5-14 into equation 5-11 yields equation 5-1 (which is shown again below as equation 5-15):

$$\mu_{2,total} = \mu_{2,header} + \frac{H_{bed}}{v^2} L \tag{5-15}$$

Equation 5-15 assumes the height of a theoretical plate inside the packed bed, H_{bed}, is independent of the bed depth, L.

5.2.6 Extended reverse-flow technique

Extending the reverse-flow technique allows the investigation of band broadening in fouled columns in addition to fresh columns. The following equations provide the basis for analysis used in the work of this chapter.

For general a column system, band broadening in the outlet is defined as:

$$\sigma^2_{total} = \sigma^2_{ex} + \sigma^2_{macro,total} + \sigma^2_{micro,total} \tag{5-16}$$

where σ^2_{total} is the cumulative variance, and $\sigma^2_{ex}, \sigma^2_{macro,total}, \sigma^2_{micro,total}$, are the variances due to the extra-column effects, macroscopic factors and microscopic factors, respectively.

The usefulness of the reverse flow techniques is that macroscopic disturbances to flow are eliminated when the flow is reversed and the microscopic variations are simply doubled. If a pulse of tracer was introduced into the system in the normal (down-flow) direction until it is at the centre of the packed bed, the flow then reversed (reverse-down-flow) and the distribution of the tracer peak measured, any band broadening effects due to macroscopic flow variations would have been eliminated. Similarly, the bottom 50% of the bed can be investigated simply by pumping the tracer

from the bottom of the column (up-flow) until it is at the centre of the column and then reversing the flow (reverse-up-flow). Therefore we are able to further separate $\sigma^2_{micro,total}$, such that:

$$\sigma^2_{micro,total} = \sigma^2_{micro,top} + \sigma^2_{micro,bottom} \quad (5\text{-}17)$$

where $\sigma^2_{micro,top}$ and $\sigma^2_{micro,bottom}$ are the variance attributed to the top and bottom 50% of the column respectively. By substituting (5-17) into (5-16),

$$\sigma^2_{total} = \sigma^2_{ex} + \sigma^2_{macro,total} + \sigma^2_{micro,top} + \sigma^2_{micro,bottom} \quad (5\text{-}18)$$

For clarity, σ^2_{tdf}, σ^2_{tuf}, σ^2_{trdf} and σ^2_{truf} are defined as the cumulative variance when the system and column is run in down-flow, up-flow, reverse-down-flow and reverse-up-flow, respectively. Therefore the contribution of the top half of the column to band broadening can be determined from

$$\sigma^2_{micro,top} = \frac{1}{2}\left(\sigma^2_{trdf} - \sigma^2_{srdf}\right) \quad (5\text{-}19)$$

where is σ^2_{srdf} the variance attributed to the system run in reverse-down-flow mode. Similarly, the contribution of the bottom half of the column to band broadening can be determined from:

$$\sigma^2_{micro,bottom} = \frac{1}{2}\left(\sigma^2_{truf} - \sigma^2_{sruf}\right) \quad (5\text{-}20)$$

where σ^2_{sruf} is the variance attributed to the system only, run in reverse-up-flow mode.

Due to the additive nature of peak variances, it follows that this technique can be applied to determine the contribution of any proportion of the column to band broadening by reversing the flow at the appropriate axial position in the column. Practically, however, this may be limited by the precision of the pump and instrumentation.

5.3 RESULTS AMD DISCUSSION

5.3.1 Experimental errors

A considerable amount of variability may have been introduced when disconnecting and reconnecting HiTrap columns in series. Care was taken to minimise this variability as much as possible. (All error values shown in the figures and tables in this chapter represent 95% C.I.)

When connecting HiTrap columns in series to obtain longer bed lengths (cf. Section 5.3.4), it is recognised that the additional column headers/ends and the small dead volume in the connection between columns may introduce additional band broadening. This superfluous dispersion is shown to be relative small and considering the fact that most fouling effects occur at the very top of the column, the column headers/ends in the second or third HiTrap columns in series can be assumed to be practically "clean" even after fouling. In this case, each "clean" column header/end is predicted to contribute to less than 10% of the total dispersion in fresh columns and less than 6% of the total dispersion in fouled columns. Furthermore, in reverse-flow mode, these macroscopic distributions are eliminated and so will not affect the analysis of microscopic dispersion within defined axial sections of the bed.

It is also recognised that by connecting the HiTrap columns in series, a stacked column (commonly used in large-scale gel filtration) is essentially formed and so the pressure drop that each section experience will be less than if the bed was one continuous packing. However, it must be remembered that the most important objective of this study was to demonstrate the effectiveness of the reverse-flow technique to diagnose the fouling effects within a column. Therefore, the convenience and reproducibility of the packing in HiTrap columns, which allowed rapid development of the technique, may outweigh the resulting discrepancies in pressure drop.

5.3.2 Dispersion attributed to extra-column effects

Table 5-1 summarises the band broadening due to extra-column effects under different flow conditions. The volume of the acetone tracer applied was kept proportional to the size of the column (1.5% v/v). The AKTA system was set up to ensure similar flow distances and extra-column dispersion in both the down-flow and up-flow direction. This is reflected in the results in Table 5-1.

Applicable Column	Volumetric flow rate (mL/min)	Sample Volume (µL)	σ^2_{sdf} (mL^2)	σ^2_{suf} (mL^2)	σ^2_{srdf} (mL^2)	σ^2_{sruf} (mL^2)
HiTrap (1 mL)	0.50	15	0.029 (± 0.001)	0.027 (± 0.001)	0.023 (± 0.002)	0.028 (± 0.002)
HiTrap (5 mL)	2.61	75	0.037 (± 0.001)	0.033 (± 0.001)	0.034 (± 0.004)	0.035 (± 0.003)
XK16	2.61	75	0.065 (± 0.004)	0.061 (± 0.005)	0.057 (± 0.004)	0.057 (± 0.002)
XK26	6.90	199	0.075 (± 0.01)	0.073 (± 0.02)	0.075 (± 0.02)	0.081 (± 0.01)

Table 5-1: *Band broadening due to extra-column effects.*

Kaltenbrunner et al. (1997) claimed that extra-column broadening can have a large influence on the total broadening especially when using small columns. Therefore, the extra-column dispersion must be carefully considered when scaling-down to predict the performance of large-scale chromatographic process. Figure 5-1, shows the influence of extra-column broadening at the different column scales used in this work. The results obtained are compared with that reported by Kaltenbrunner et al. (1997) for fresh, non-fouled columns. The extra-column broadening accounted for about 75% of the total broadening for a fresh 1 mL column but it decreased to about 10% for a 10 mL column. This observation is consistent with that reported by Kaltenbrunner et al. (1997). The ratios of $\left(\sigma^2_{ex}/\sigma^2_{total}\right)$ for fouled columns were lower than that for the corresponding fresh columns but followed the same exponential

decrease relationship as that for fresh columns. This is expected as the total broadening, σ^2_{total}, increases after fouling.

At 5 mL scale both HiTrap and XK columns were used, allowing the impact of different header designs on band broadening to be investigated. As seen in Figure 5-1, the ratio of $\left(\sigma^2_{ex}/\sigma^2_{total}\right)$ appeared to be similar for both columns under fresh (~ 0.12 - 0.15) and fouled conditions (~ 0.06). Therefore, it may be suggested that header design, unlike column volume, does not have a large influence on the ratio $\left(\sigma^2_{ex}/\sigma^2_{total}\right)$.

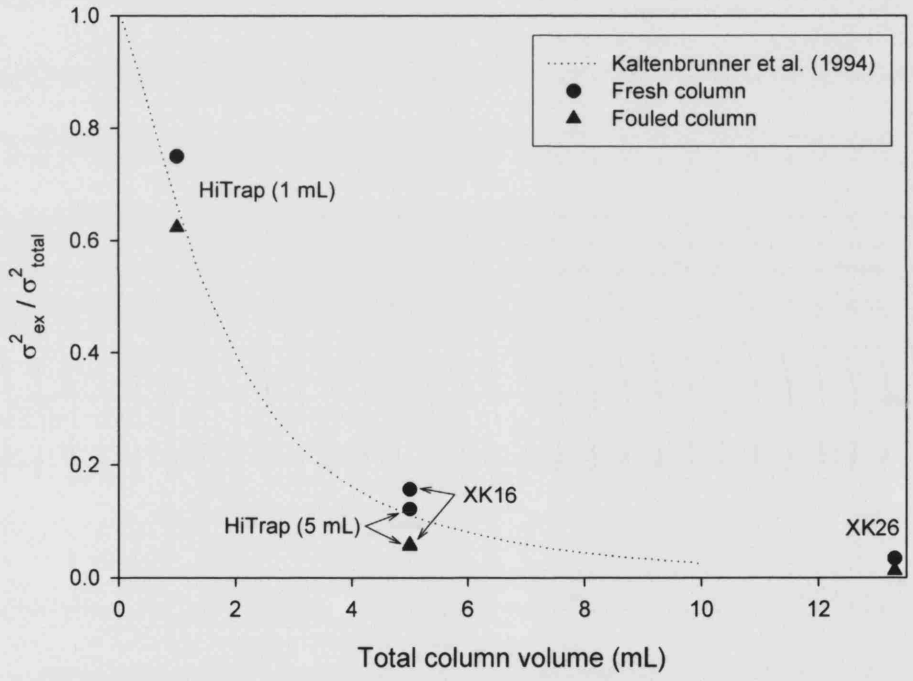

***Figure 5-1**: Ratio of extra-column band broadening $\left(\sigma^2_{ex}\right)$ to the total broadening $\left(\sigma^2_{total}\right)$ as a function of the total column volume. The ratios obtained for fresh and fouled columns of different volumes are in good agreement with those predicted by Kaltenbrunner et al. (1997).*

5.3.3 Effects of fouling with columns of increasing diameter

The dispersive effects of fouling were investigated as a function of column diameter. Pre-packed HiTrap columns of diameters 0.7 cm (1 mL) and 1.6 cm (5 mL) were used as well as XK columns of diameters 1.6 cm (XK16) and 2.6 cm (XK26). Comparison of the 5 mL HiTrap column with the XK16 column, which has the same physical dimensions, was used to infer the impact of header design on fouling of the packed bed. An example of typical peaks obtained in forward-flow and reverse-flow modes are shown in Figure 5-2.

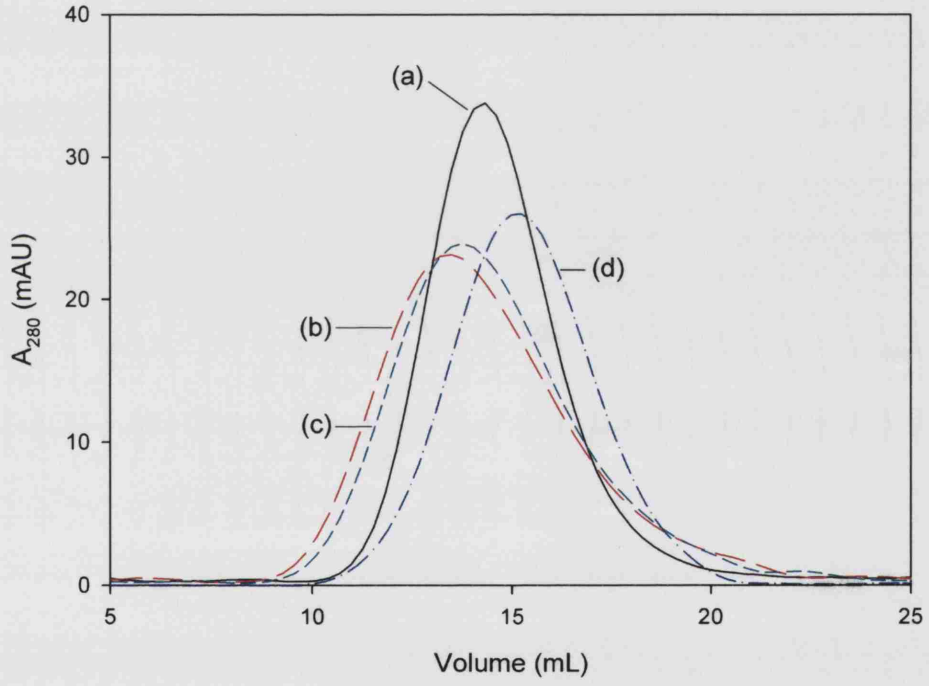

***Figure 5-2**: Comparison of peaks obtained from the reverse-flow experiments. The peaks were obtained by loading acetone pulses onto an XK26 column packed with Q Sepharose FF to a bed height of 2.5 cm. (a) fresh column under forward-flow (normal operation); (b) fouled column before backwashing under forward-flow; (c) fouled column after backwashing under forward flow; (d) fouled column under reverse-flow.*

Table 5-2 and Figure 5-3 summarises the change in $(\sigma^2_{total} - \sigma^2_{ex})$ and $\sigma^2_{micro,total}$ for fresh, fouled and backwashed columns. The total band broadening, $(\sigma^2_{total} - \sigma^2_{ex})$, increased significantly after fouling (approximately by 100% to 300%). Subsequent to fouling, backwashing with water decreased the band broadening only marginally (~ 2 - 10%), and the effect seemed to be dependent on the column diameter for a given header design. Backwashing is used to remove solid particulates and other fouling material that had deposited near the top of the bed or at the column header. The total microscopic dispersion ($\sigma^2_{micro,total}$) significantly increased after fouling for all the columns tested (Table 5-2). There does not appear to be a clear relationship between the percentage increase in $\sigma^2_{micro,total}$ and the column diameter for fouled columns but generally, the percentage increase seen in XK columns (~ 90 – 250%) was substantially greater than those seen in the HiTrap columns (~ 15 – 50%).

Column	Column diameter (cm)	$(\sigma^2_{total} - \sigma^2_{ex})$ (mL^2)			σ^2_{micro} (mL^2)	
		Fresh column	Fouled column (pre-backwash)	Fouled column (post-backwash)	Fresh column	Fouled column
HiTrap (1 mL)	0.7	0.010 (± 0.002)	0.018 (± 0.001)	0.017 (± 0.002)	0.009 (± 0.001)	0.014 (± 0.002)
HiTrap (5 mL)	1.6	0.26 (± 0.03)	0.62 (± 0.05)	0.55 (± 0.03)	0.18 (± 0.02)	0.21 (± 0.04)
XK16	1.6	0.35 (± 0.02)	1.0 (± 0.3)	0.98 (± 0.3)	0.20 (± 0.02)	0.7 (± 0.1)
XK26	2.6	2.2 (± 0.2)	6.1 (± 0.6)	5.7 (± 0.4)	1.4 (± 0.4)	2.7 (± 0.8)

***Table 5-2**: Total and microscopic band broadening for fresh and fouled columns of various diameters.*

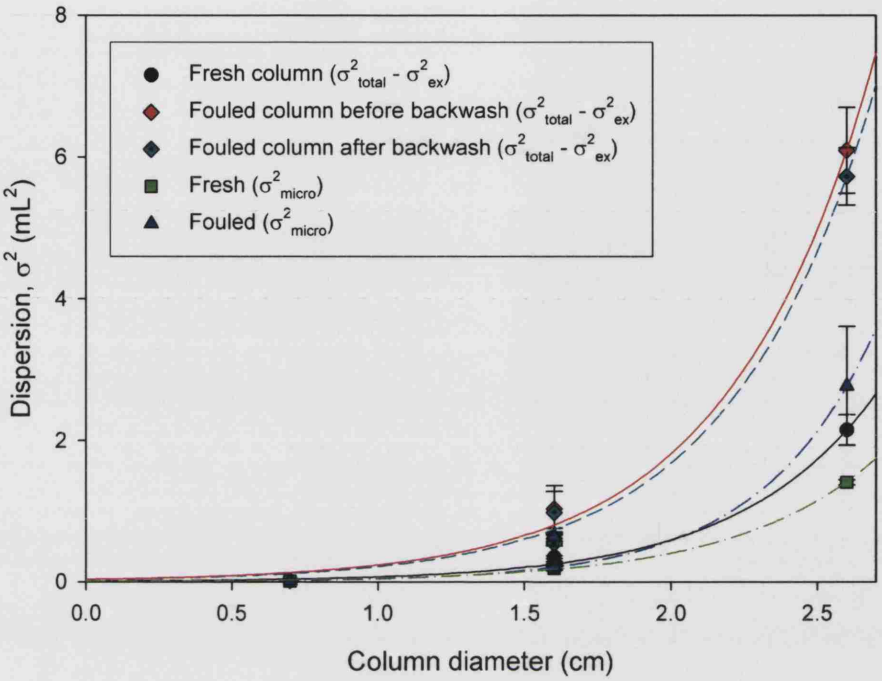

***Figure 5-3**: Total and microscopic band broadening for fresh and fouled columns as a function of column diameter. All columns were packed with Q Sepharose FF to a bed height of 2.5 cm. Columns were fouled with 5 CVs of partially clarified E. coli homogenate.*

Running in reverse-flow mode allows isolation of the dispersion due to microscopic factors at selected axial positions within a column bed. Figures 5-4 to 5-7 show the percentage contributions of the top and bottom halves of a column (pre- and post-fouling) to the total microscopic dispersion $\left(\sigma^2_{micro,total}\right)$. Prior to fouling, $\sigma^2_{micro,top}$ and $\sigma^2_{micro,bottom}$ were approximately equal in all the columns and conditions examined. This suggests that the microscopic mass transfer conditions were practically uniform throughout the packed bed. After fouling, a significant increase in the contribution from the top half of the bed was observed. Visual inspection of the fouled bed in the XK16 and XK26 columns revealed discoloration predominantly in the top half of the bed (Figure 5-8) which is consistent with the results determined by the reverse-flow method. (Similar observations were notice during visual inspection of a fouled mini-scale bed described in Section 6.3.5). Generally, the increase was more pronounced for XK columns than for HiTrap columns. Comparison of the fouled XK16 column

with the fouled 5 mL HiTrap confirms this observation, and it is seen that both $\sigma^2_{micro,total}$ and $\sigma^2_{micro,top}$ increases more dramatically in the XK16 column. Clearly, the header design can greatly influence the extent and pattern of microscopic dispersion caused by fouling within the packed bed. A possible reason for this is that the header design in HiTrap columns is more prone to trapping fouling material than the design in the XK columns, in which more fouling material is able to reach the bed.

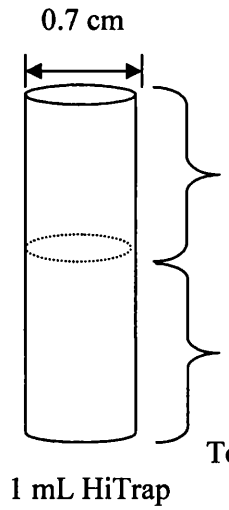

	Fresh Column		Fouled Column	
	$\sigma^2_{micro}(mL^2)$	Contribution (%)	$\sigma^2_{micro}(mL^2)$	Contribution (%)
	0.0042 (± 0.0006)	48	0.0079 (± 0.0008)	57
	0.0046 (± 0.0009)	52	0.006 (± 0.001)	43
Total	0.009 (± 0.001)	100	0.014 (± 0.002)	100

***Figure 5-4**: Microscopic dispersion within fresh and fouled 1 mL HiTrap columns.*

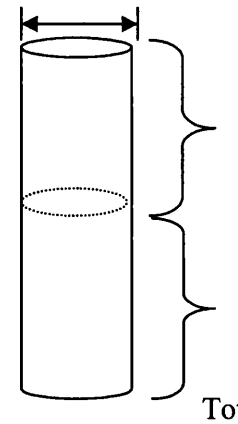

	Fresh Column		Fouled Column	
	$\sigma^2_{micro}(mL^2)$	Contribution (%)	$\sigma^2_{micro}(mL^2)$	Contribution (%)
	0.09 (± 0.03)	49	0.11 (± 0.02)	52
	0.094 (± 0.007)	51	0.10 (± 0.03)	48
Total	0.18 (± 0.02)	100	0.21 (± 0.04)	100

***Figure 5-5**: Microscopic dispersion within fresh and fouled 5 mL HiTrap columns.*

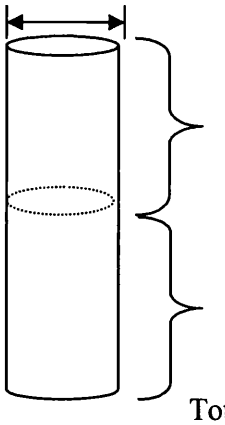

	Fresh Column		Fouled Column	
	$\sigma^2_{micro}(mL^2)$	Contribution (%)	$\sigma^2_{micro}(mL^2)$	Contribution (%)
	0.10 (± 0.01)	50	0.5 (± 0.1)	76
	0.10 (± 0.01)	50	0.16 (± 0.02)	24
Total	0.20 (± 0.02)	100	0.7 (± 0.1)	100

***Figure 5-6**: Microscopic dispersion within fresh and fouled XK16 columns.*

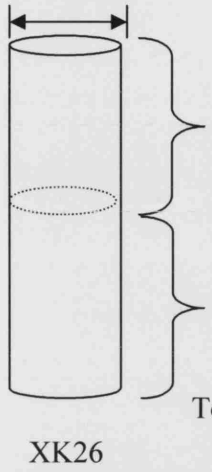

	Fresh Column		Fouled Column	
	$\sigma^2_{micro}(mL^2)$	Contribution (%)	$\sigma^2_{micro}(mL^2)$	Contribution (%)
	0.69 (± 0.2)	49	2.0 (± 0.4)	74
	0.73 (± 0.2)	51	0.7 (± 0.3)	26
Total	1.4 (± 0.4)	100	2.7 (± 0.8)	100

***Figure 5-7**: Microscopic dispersion within fresh and fouled XK26 columns.*

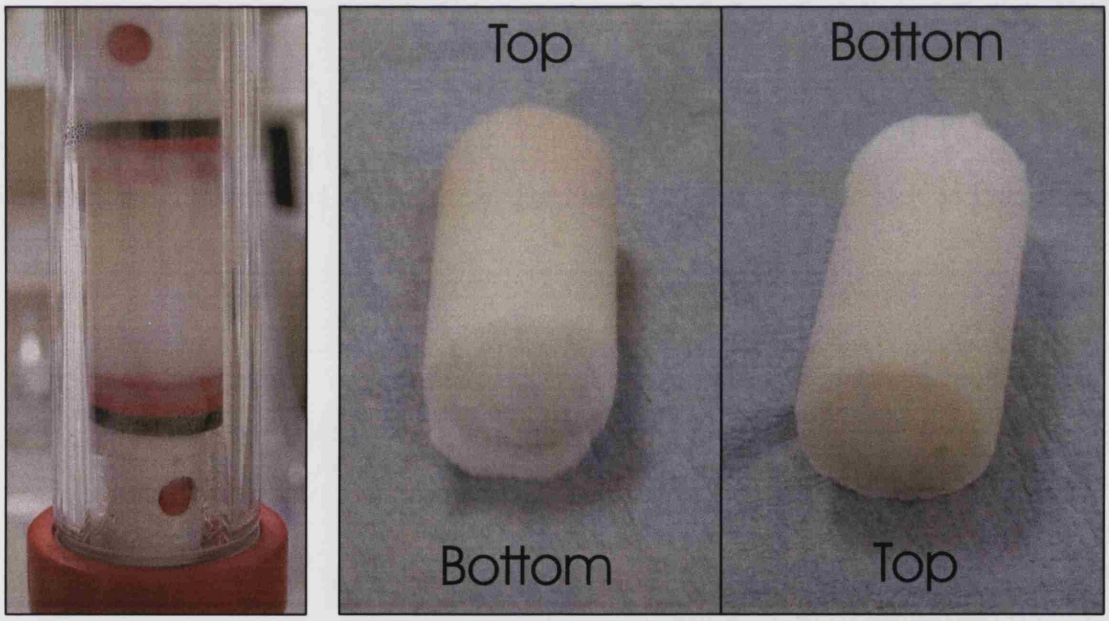

***Figure 5-8**: Picture of a fouled XK16 column. This XK16 column was packed with Q Sepharose FF to a bed height of 2.5 cm and used for reverse-flow experiments. It was fouled with 5 CVs of partially clarified E. coli homogenate. The fouled column is shown on the left. The bed was carefully removed from the column and is shown in the pictures on the right. Most discoloration appears in the top half of the packed bed.*

The change in the macroscopic dispersion before and after fouling (post-backwashing) is listed in Table 5-3. The macroscopic band broadening $\left(\sigma^2_{macro,total}\right)$ for the columns tested increased by 200 – 400% after fouling. There does not appear to clear relationship between the change in the post-fouling macroscopic dispersion $\left(\sigma^2_{macro,total}\right)$ and the column diameter. The increase in macroscopic dispersion may be attributed to both augmented flow maldistribution in the column header due to partial blockage by fouling material and disruption of the bed packing due to fouling.

Column	Column diameter	σ^2_{macro} (mL)	
		Fresh column	Fouled column
HiTrap (1 mL)	0.7	0.001 (± 0.001)	0.003 (± 0.001)
HiTrap (5 mL)	1.6	0.077 (± 0.04)	0.3 (± 0.1)
XK16	1.6	0.14 (± 0.05)	0.3 (± 0.3)
XK26	2.6	0.7 (± 0.2)	3.0 (± 0.8)

***Table 5-3**: Macroscopic band broadening for fresh and fouled columns of various* diameters.

5.3.4 Effects of fouling with increasing column length

Figures 5-4, 5-9, 5-10 and 5-11 illustrate the microscopic dispersion in defined axial sections within packed beds of increasing total length. For fresh columns, the microscopic dispersion in each section of the column was approximately equal. After fouling and then backwashing, microscopic band broadening $\left(\sigma^2_{micro,total}\right)$ was noticeably more severe within the top 1.25 cm section of the bed and became gradually less significant in the lower sections. Biological foulants may have a great affinity with

already-adsorbed impurities giving rise to secondary fouling. For example, Kelly and Zydney (1997) reported that proteins in solution can bind to already-adsorbed protein deposits on ultrafiltration membranes. It may be that a similar secondary fouling mechanism in combination with steric hindrance due to the tight packing arrangement of the beads in the bed have caused foulants to accumulate at the very top of the column. (Another example of foulant-foulant interactions in chromatographic processes was seen with cell debris and is described in Section 6.3.6.)

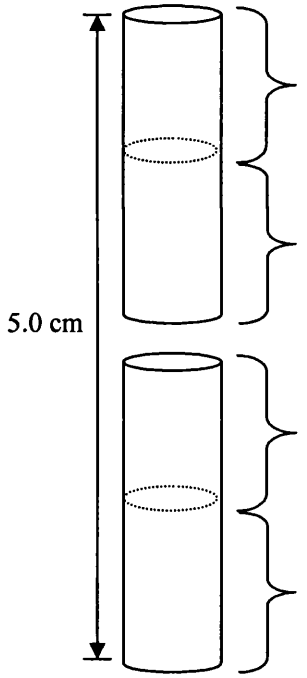

	Fresh Column		Fouled Column	
	σ^2_{micro} (mL^2)	Contribution (%)	σ^2_{micro} (mL^2)	Contribution (%)
	0.0043 (± 0.0009)	26	0.012 (± 0.002)	49
	0.0042 (± 0.0005)	26	0.0044 (± 0.0005)	18
	0.0040 (± 0.0005)	25	0.0044 (± 0.0005)	18
	0.0038 (± 0.0004)	23	0.0039 (± 0.0005)	15
Total	0.016 (± 0.002)	100	0.025 (± 0.003)	100

***Figure 5-9**: Microscopic dispersion within a column consisting of two 1 mL HiTrap columns connected in series.*

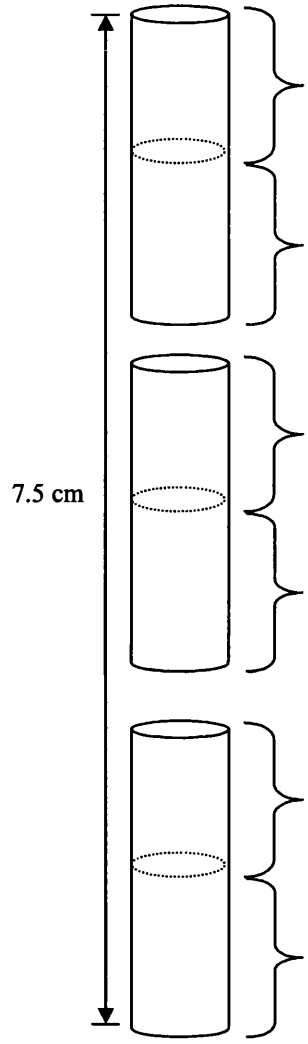

	Clean Column		Fouled Column	
	$\sigma^2_{micro}(mL^2)$	Contribution (%)	$\sigma^2_{micro}(mL^2)$	Contribution (%)
	0.0040 (± 0.0007)	17	0.012 (± 0.003)	33
	0.0028 (± 0.0009)	12	0.0061 (± 0.0005)	17
	0.0052 (± 0.0008)	22	0.006 (± 0.001)	17
	0.0034 (± 0.0007)	14	0.0039 (± 0.0009)	11
	0.0050 (± 0.0006)	21	0.0048 (± 0.0008)	13
	0.0033 (± 0.0008)	14	0.0033 (± 0.0008)	9
Total	0.024 (± 0.005)	100	0.036 (± 0.006)	100

***Figure 5-10**: Microscopic dispersion within a column consisting of three 1 mL HiTrap columns connected in series.*

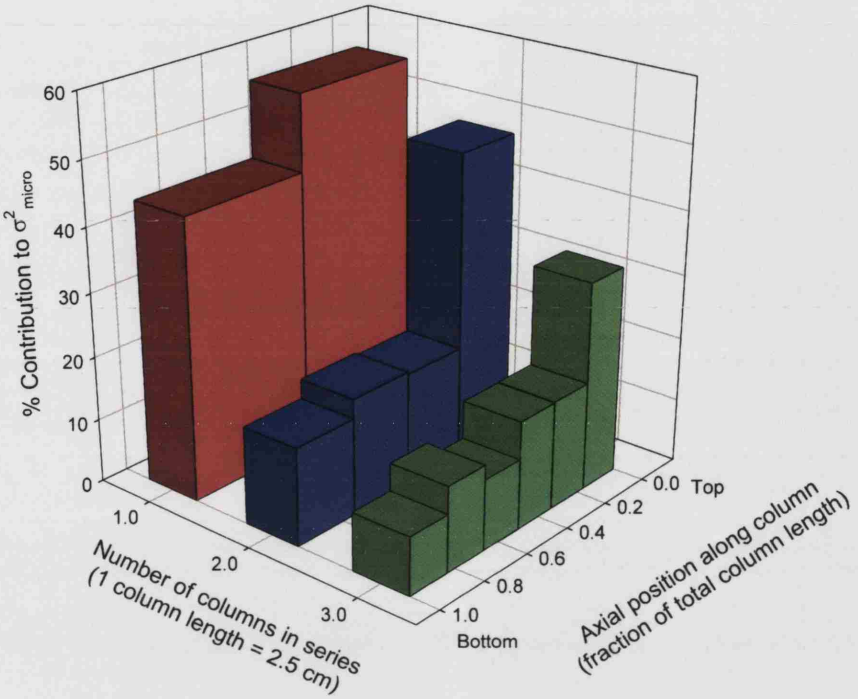

***Figure 5-11**: Percentage contribution of different axial sections to the total microscopic band broadening. Up to three 1 mL HiTrap columns were connected in series to obtain total beds lengths of 2.5 cm, 5.0 cm and 7.5 cm. Each bar represents 1.25 cm bed length (or half of a 1 mL HiTrap column).*

Moscariello et al. (2001) suggests plotting the total dispersion $\left(\sigma^2_{total}\right)$ vs. bed length for forward- and reverse-flow tests to analyse the packing heterogeneity in a bed (cf. Section 5.1.2). From this graph, it is possible to examine the macroscopic contributions of header misdistribution and packing heterogeneity separately by implementing equation 5-15. In Figure 5-12, dispersion $\left(\sigma^2\right)$ is plotted against the total bed length, L. Extra-column dispersion has been accounted for since it can significantly contribute to the total dispersion in small columns. The good linear correlation between $\left(\sigma^2_{total} - \sigma^2_{ex}\right)$ and bed length as well as between $\sigma^2_{micro,total}$ and bed length, confirm that the bed is homogenous in the direction of flow within the range of bed lengths examined. This agrees with the results shown in Figures 5-4, 5-9 and 5-10. The y-intercept for $\left(\sigma^2_{total} - \sigma^2_{ex}\right)$ is very close to zero and this reflects the low total

macroscopic dispersion $\left(\sigma^2_{macro,total}\right)$ observed in fresh 1 mL HiTrap columns (Table 5-4). As expected, the y-intercept for $\sigma^2_{micro,total}$ is not significantly different from zero (t-test, d.f. = 1, $P < 0.05$), since in reverse-flow mode all header dispersion will have refocused. The difference in the slopes gives an indication of the contribution of packing heterogeneity to the total macroscopic dispersion $\left(\sigma^2_{macro,total}\right)$. The slope of $\left(\sigma^2_{total} - \sigma^2_{ex}\right)$ vs. L is 0.0042 ± 0.0001 (± std. error), and the slope of $\sigma^2_{micro,total}$ vs. L is 0.00299 ± 0.00008 (± std. error). The slopes are significantly different (t-test, n = 3, d.f. = 1, $P < 0.05$) from one another. Comparison of the two slopes indicate that the microscopic band broadening accounts for ~ 70% of the total dispersion found in the column bed, leaving macroscopic packing heterogeneity to account for ~ 30% of the total dispersion.

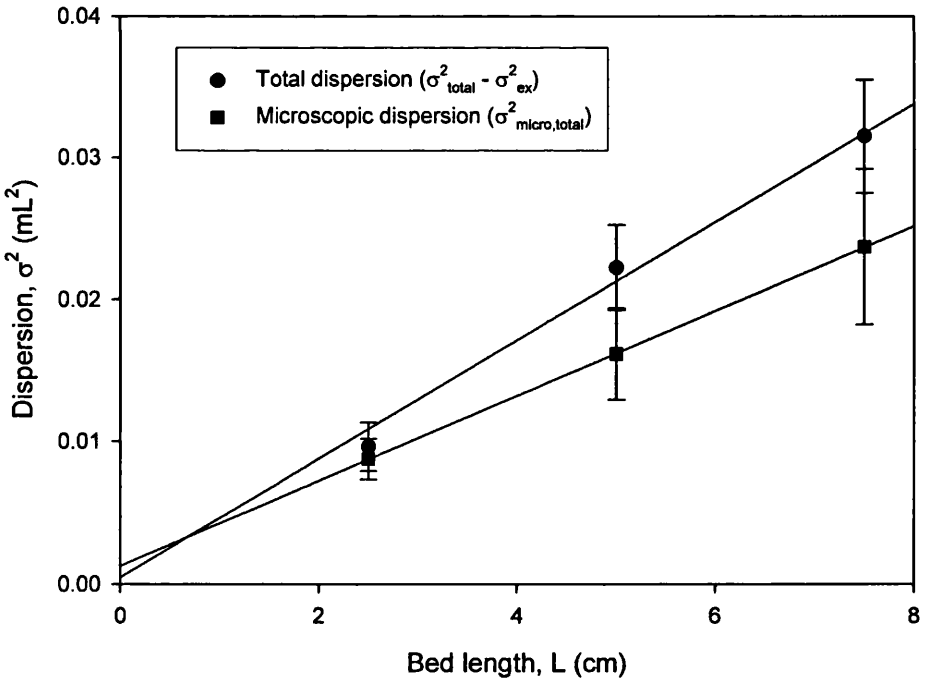

***Figure 5-12**: Band broadening as a function of bed length for fresh columns. 1 mL HiTrap columns (0.7 cm diameter) were connected in series to obtain bed lengths of 2.5 cm, 5.0 cm and 7.5 cm.*

Column length (cm)	$(\sigma^2_{total} - \sigma^2_{ex})$ (mL²)		$\sigma^2_{micro,total}$ (mL²)		$\sigma^2_{macro,total}$ (mL²)	
	Fresh column	Fouled column (post-backwash)	Fresh column	Fouled column	Fresh column	Fouled column
2.5	0.010 (± 0.002)	0.017 (± 0.002)	0.009 (± 0.001)	0.014 (± 0.002)	0.001 (± 0.001)	0.003 (± 0.001)
5.0	0.022 (± 0.003)	0.031 (± 0.003)	0.016 (± 0.003)	0.024 (± 0.002)	0.006 (± 0.004)	0.007 (± 0.004)
7.5	0.032 (± 0.004)	0.059 (± 0.008)	0.024 (± 0.005)	0.036 (± 0.006)	0.008 (± 0.006)	0.02 (± 0.01)

***Table 5-4**: Total, microscopic and macroscopic band broadening for fresh and fouled columns of various lengths.*

Unfortunately the interpretation of the same plot for fouled columns (Figure 5-13) is less clear than that for fresh columns. The total dispersion $(\sigma^2_{total} - \sigma^2_{ex})$ for the fouled columns does not increase linearly with bed length, rendering equation 5-15 inappropriate for describing the dispersive effects. On the other hand, the total microscopic dispersion was linearly proportional to the bed length. The y-intercept was shown to be not significantly different from zero (t-test, n = 3, d.f. = 1, $P < 0.05$) as expected. However, unlike with fresh columns this linearity in the slope can not be interpreted as showing microscopic homogeneity throughout the bed, since the results from Figures 5-4, 5-9 and 5-10 show that σ^2_{micro} is noticeably higher at the top of the bed in all the columns tested after fouling. Given that the microscopic dispersion is linearly proportional to the bed length and that the total dispersion $(\sigma^2_{total} - \sigma^2_{ex})$ is equal to sum of microscopic and macroscopic dispersion $(\sigma^2_{macro,total} + \sigma^2_{micro,total})$ (see

equation 5-16), it is evident that the correlation between total macroscopic dispersion $\left(\sigma^2_{macro,total}\right)$ and bed length, L, is non-linear (also see Table 5-4) and causes the diversion of $\left(\sigma^2_{total} - \sigma^2_{ex}\right)$ vs. L from linearity. Furthermore, since it may be reasonable to assume that most foulants accumulate near the top of bed, $\left(\sigma^2_{total} - \sigma^2_{ex}\right)$, $\sigma^2_{macro,total}$ and $\sigma^2_{micro,total}$ may be proportional to the amount of foulant loaded rather than fundamentally related to the bed length under the fouling conditions used. (It is important to remember that the columns tested have the same diameter and the amount of foulant loaded was kept proportional to the total column volume and so also proportional to the column length). This is proved to be the case in the following section.

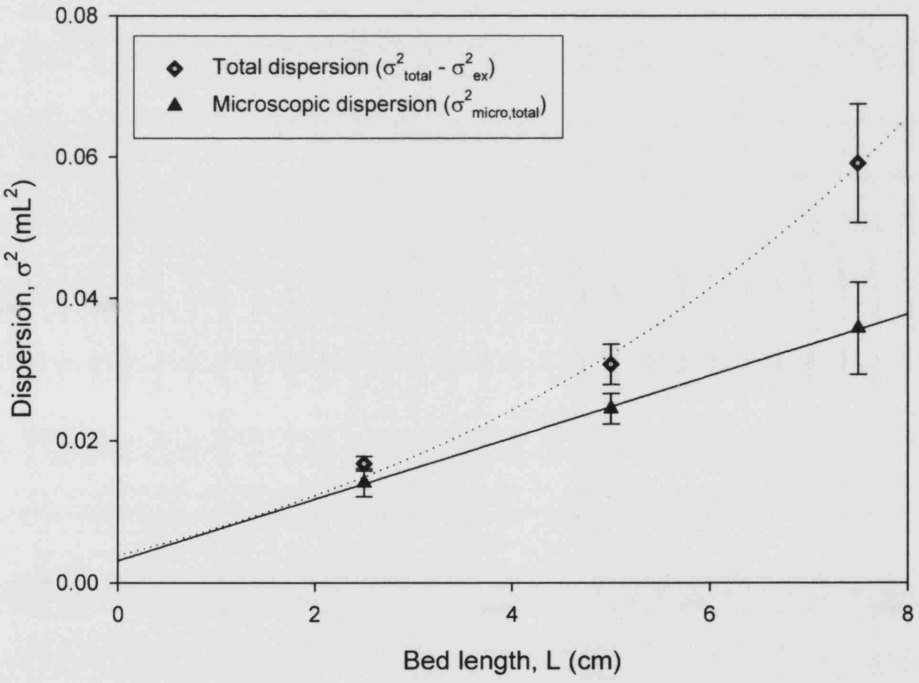

***Figure 5-13**: Band broadening as a function of bed length for fouled columns. 1 mL HiTrap columns (0.7 cm diameter) were connected in series to obtain bed lengths of 2.5 cm, 5.0 cm and 7.5 cm.*

5.3.5 Effects of foulant load

Figure 5-14 is a plot of $\left(\sigma^2_{total} - \sigma^2_{ex}\right)$ against the volume of foulant loaded onto a 1 mL HiTrap column. Figure 5-15 is a plot of $\sigma^2_{micro,total}$ against the volume of foulant loaded onto a 1 mL HiTrap column. The data points were obtained from considering only the top column in Figures 5-4, 5-9 and 5-10.

Figure 5-14 clearly shows that the total dispersion $\left(\sigma^2_{total} - \sigma^2_{ex}\right)$ increases in an exponential fashion with the volume of foulant. However, from Figure 5-15 it can be seen that the total microscopic dispersion $\left(\sigma^2_{micro,total}\right)$ of the entire 1 mL bed increases almost linearly between bed lengths of 2.5 – 7.5 cm. This further suggests that the total dispersion $\left(\sigma^2_{total} - \sigma^2_{ex}\right)$ and $\sigma^2_{macro,total}$ may, in fact, be proportional to the amount of foulant loaded rather than fundamentally related to the bed length.

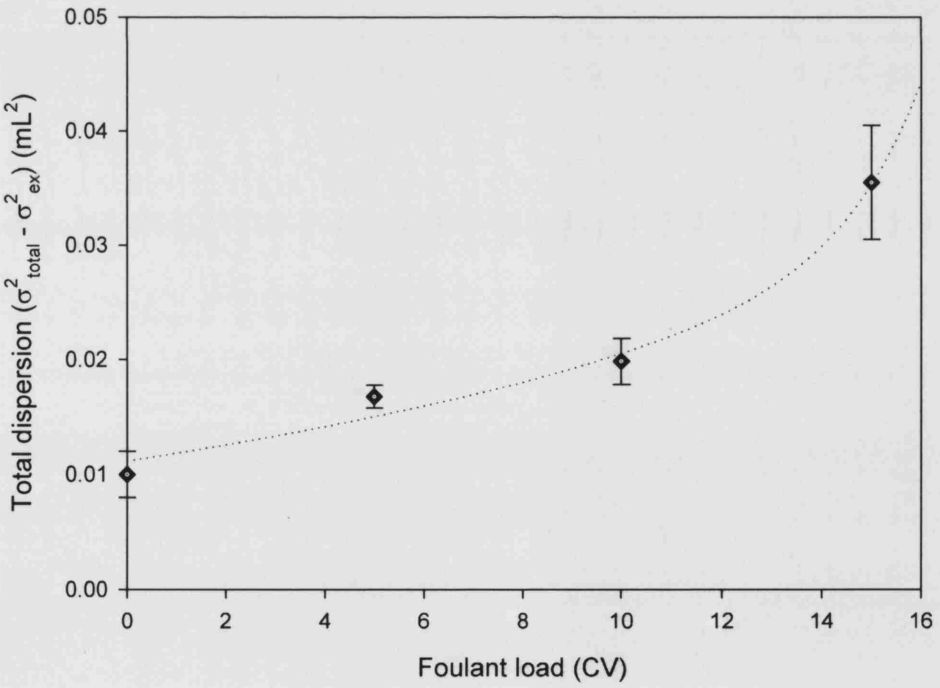

***Figure 5-14**: Effect of foulant load on the extent of total band broadening. 1 mL HiTrap columns were exposed to different volumes of foulant loading.*

Figure 5-15 focuses on the relationship between the microscopic dispersion and the volume of foulant load. There is an increase in the total microscopic dispersion with increasing volume of foulant loading. However, increasing the foulant load caused the microscopic dispersion of the top 1.25 cm of the bed to increase but only up to a saturation load after which there was no further increase in band broadening in this top section whilst the total microscopic dispersion continued to gradually increase. This suggests that fouling effects occur predominantly at the top section of the column and progresses down the column as fouling material is loaded.

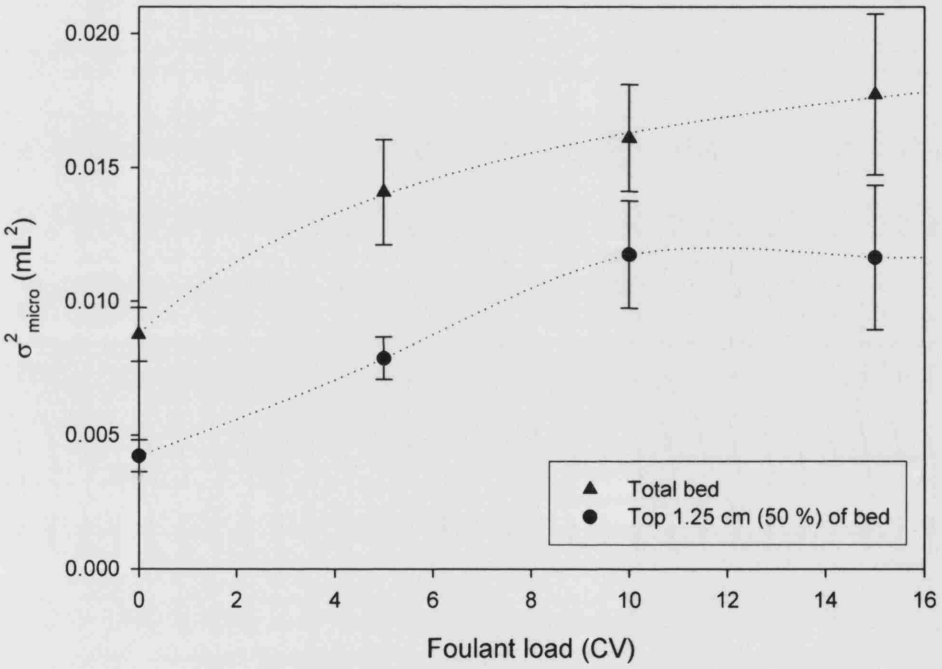

***Figure 5-15**: Effect of foulant load on the extent of microscopic band broadening. 1 mL HiTrap columns were exposed to different volumes of foulant loading.*

5.4 CONCLUSIONS

This study supports a number of conclusions. Primarily, it demonstrates the utility of the reverse-flow technique to investigate the dispersive effects of fouling on a packed bed column. The technique allows the band broadening effects due to reversible macroscopic factors (flow maldistribution and packing heterogeneity) to be

separated from irreversible microscopic factors (interparticle axial dispersion, external fluid film mass transfer and intraparticle diffusion). It is a simple and non-destructive technique that can be used to diagnose both small-scale and large-scale columns. In addition, the use of an inert tracer, acetone, allows the technique to be applied to industrial columns used in GMP production.

Backwashing is often part of a CIP protocol to remove solid particulates and other fouling material that deposit near the top of the bed or at the column header. In this study, backwashing with water only marginally reduced the total dispersion after fouling. This low cleaning effectiveness of water is, in fact, beneficial to the use of the reverse-flow technique to diagnose the true fouling conditions of a column especially if the fouled column is not normally subjected to backwashing. On the other hand, it is interesting to point out that if backwashing is used as part of a cleaning procedure then using water alone may not be adequate.

It was found that band broadening due to macroscopic effects can account for ~ 10 – 40% of the total band broadening in fresh columns. After fouling, the macroscopic band broadening increased by ~ 20 – 50%. The percentage increase in macroscopic dispersion after fouling does not appear to be dependent on the column (or header) diameter for the range of diameters examined in this study (0.7 – 2.6 cm).

The design of the header may have more impact than its diameter on the extent of fouling. Comparison between the XK and HiTrap columns (especially between the 5 mL HiTrap and XK16 columns) showed that header design can greatly influence the degree of microscopic dispersion after fouling - even though microscopic dispersion occurs inside the packed bed.

The reverse-flow technique allowed the extent of band broadening due to microscopic factors to be quantified as a function of the axial position within a column. For the fouling conditions used in this study, the effects of fouling were noticeably greater within the top 1.25 cm of the bed. This information may be extremely useful in designing appropriate cleaning procedures and guard columns.

Under the fouling conditions studied, there was not a clear correlation between the percentage change in total dispersion $\left(\sigma^2_{total} - \sigma^2_{ex}\right)$, total macroscopic dispersion

$\left(\sigma^2_{macro,total}\right)$ or total microscopic dispersion $\left(\sigma^2_{micro,total}\right)$ and column diameter. However, $\left(\sigma^2_{total} - \sigma^2_{ex}\right)$, $\sigma^2_{macro,total}$ or $\sigma^2_{micro,total}$ were found to be apparently proportional to the bed length (when the foulant load to bed volume ratio is kept constant), though only $\sigma^2_{micro,total}$ was linearly proportional to bed length. From a practical point of view, knowing the influence of column dimensions on fouling can reduce unpredictability when scaling up chromatographic processes and can also help in the design of appropriate small-scale mimics for predicting the effects of fouling.

Moreover, the study has provided circumstantial evidence on the mechanism of fouling. The amount of fouling material was shown to greatly impact the dispersive effects, and the effects occur predominantly at the top section of the column before progressing down the column axis if fouling material continues to be loaded.

Conventional approaches, such as analysing breakthrough characteristics described in Chapter 4, rely on measuring changes in overall performance indicators (e.g., binding capacity) to provide a quantitative assessment of the general extent of fouling. The reverse-flow technique described in this chapter improves the diagnosis of chromatographic fouling by allowing examination at an intra-column level. By using this technique, it is possible to identify where the fouling effects are most severe and provides potential insights into the mechanism of fouling. The work described in the subsequent section (Chapter 6) advances the knowledge of chromatographic fouling even further by allowing visualisation of fouling at a single-bead level.

6 VISUALISING FOULING OF A CHROMATOGRAPHIC MATRIX USING CONFOCAL SCANNING LASER MICROSCOPY

ABSTRACT

The purpose of the work in this chapter was to investigate the use of confocal scanning laser microscopy (CSLM) in analysing fouled chromatographic media and in determining the effectiveness of clean-in-place (CIP) procedures. A particularly aggressive fouling stream of partially clarified *E. coli* homogenate was used to challenge an anion exchange resin in a finite bath, and subsequently in a packed structure under flow conditions. It was expected that the extent of fouling produced would be high, due to the combined presence of nucleic acid and proteinaceous material as well as debris and lipids (Fernandez-Lahore et al., 1999). The fouling caused by the material was visualised by fluorescently-labelling DNA and protein in the foulant stream and by testing the adsorptive capacity for a test protein, to the resin pre- and post-fouling and following the application of various CIP procedures. The effects of fouling on the binding capacity and uptake rate for BSA were measured. Confocal images were obtained to provide insight of the spatial distribution of key foulants types at the single-bead level. The competitive adsorption of whole cells or cell debris and DNA to an anion exchange resin has also been visualised.

6.1 INTRODUCTION

6.1.1 CSLM to visualise beads in finite baths

Confocal scanning laser microscopy (CSLM) has become an increasingly important tool in chromatography research. The technique was first outlined by Marvin Minsky in 1958 (Minsky, 1961; Minsky, 1988). Less than a decade ago, Kim et al. (1996) showed that it is possible to view, at the level of a single bead, the adsorption of a fluorescent molecule on a polymeric cation exchanger using confocal microscopy. Since then, the development of confocal microscopy and its combination with finite bath uptake experiments (Ljunglof and Hjorth, 1996; Ljunglof and Thommes, 1998) has allowed the investigation of a wide breadth of chromatographic adsorption phenomena (Ljunglof et al., 1999; Malmsten et al., 1999; Ahmed and Pyle, 1999; Laca et al, 1999; Linden et al., 1999 and 2002; Ljunglof et al., 2000; Dziennik et al., 2003; Kasche et al., 2003) as well as spatially-resolved pH measurements in absorbent particles (Heinemann et al., 2004). The technique allows the determination of fluid phase information and the intra-particle adsorption profile over time. The use of different dyes furthermore allows investigation of the adsorption behaviour of protein mixtures (Linden et al., 1999) and other adsorbing species besides protein, such as nucleic acids (Ljunglof et al., 1999).

6.1.1.1 Development of CSLM for visualising chromatographic matrices

Ljunglof and Hjorth (1996) performed the first extensive confocal investigation into chromatographic resin adsorption. They investigated the binding of fluorescently-labelled Protein A to an immuno-affinity resin. The study showed that at low concentrations of absorbate relative to resin (1:10) absorbate only binds to a thin outer layer on the beads. As the concentration of absorbate is increased this layer becomes progressively thicker, and at high concentrations (5:1) Protein A was seen throughout the bead. Furthermore, the study demonstrated that by increasing incubation time absorption depth increased.

The relationship between indirect measurements of solid-phase concentration from finite bath experiments and direct measurements of individual bead from

confocal images was investigated by Ljunglof and Thommes (1998). They constructed a batch uptake curve from finite batch experiments based on the measurement of the fluid phase protein concentration. Intensity profiles of the protein distribution within a single bead were also obtained with CSLM. After integration of the profiles the overall fluorescence within the bead could be calculated. The group investigated four different experimental systems and showed excellent correlation between direct measurements of adsorption kinetics by CSLM and indirect measurements in the fluid phase. Furthermore, the study proved that CSLM can be used as a reliable tool for studying of protein adsorption to porous media.

6.1.1.2 Phenomenon of inner radial concentration rings

For single protein adsorption to certain ion exchange matrices at specific conditions of ionic strength and pH, the presence of inner radial concentration rings have been observed in CSLM experiments (Dziennik and Lenoff, 1999; Dziennik and Lenoff, 2000; Ljunglof, 2002). One example was demonstrated by Ljunglof (2002) for the adsorption of IgG to SP Sepharose FF. He showed that concentration rings gradually disappeared with an increase in the buffer concentration from 50 mM to 150 mM. Similar results have been reported by Dziennik and Lenoff (1999 and 2000). They also noted that no concentration rings appeared at low ionic strengths of 2 – 5 mM acetate buffer and speculated that this was due to protein-protein repulsion. Furthermore, they confirmed that the concentration rings are also formed without fluorescence labelling, thus excluding the possibility of the rings being an artefact. One possible explanation of this interesting phenomenon is that it may be due to variation of the electrostatic potential along the radial direction of the particles (Dziennik and Lenoff, 1999; Dziennik and Lenoff, 2000; Liapis et al., 2001). Recently, a theoretical model for adsorption that accounts for the presence of an electrical double layer in the pores of adsorbent particles and can qualitatively explain the development of the concentration rings has been solved (Liapis et al., 2001).

6.1.1.3 Competitive adsorption of protein matrices

Development of CSLM for visualising adsorption processes at the single-bead level has allowed a greater understanding of the fundamental mechanisms for industrially relevant chromatographic separations. With monoclonal antibody (MAb) sales exceeding US$ 2 billion in year 2000 and over 225 companies developing antibody-based therapeutics (Reed and Flanigan, 2001), MAbs are becoming an increasingly important drug class. A major challenge in bioseparation during MAb purification processes is the separation of the antibodies from albumin. In order to investigate this complex two-component system Linden et al. (1999) visualised the competitive adsorption of BSA and human IgG to cationic media using CSLM. By using appropriate dichroic beam splitters and band-pass filters with a confocal microscope it is possible to detect different fluorescence emissions simultaneously. Linden's group showed, both qualitatively and quantitatively, that in equilibrium BSA would bind to the outer regions of the ion exchange absorbent while human IgG would be displaced to the internal regions. This finding contradicts the conventional picture of an equal equilibrium distribution of all proteins adsorbed.

In another study, Linden et al. (2002) labelled reference proteins (BSA and mIgG 2a) with three different fluorescent dyes (Alexa^{TM} 488, Cy^{TM}3 and Cy^{TM}5). SP Sepharose FF, a porous cation exchanger, was then sequentially incubated with these protein-dye conjugates. The confocal images showed that at low pH and ionic strength conditions, protein adsorption was consistent with a classical shrinking core pattern (Dedrick and Beckmann, 1967; Brauch and Schlunder, 1975; Ruthven, 1984; Teo and Ruthven, 1986; Weaver and Carta, 1996) where the beads are gradually saturated from the edge to the core. However, changes in the mobile phase pH and ionic strength can lead to significant shifts in the uptake pattern. Specifically, initially bound molecules travelled further to the core, thus making binding sites at the rim available for adsorption of new molecules. During the adsorption of a mIgG 2a, a change in pH was shown to be sufficient to change completely the uptake pattern during finite bath adsorption.

The information gathered from these types of studies can be used to model, optimise and design real protein adsorption processes that often involve complex multi-component mass transfer phenomena. Multicolour labelling experiments have

been successfully used to monitor simultaneously the adsorption of multiple proteins to porous media.

6.1.1.4 Direct visualisation of plasmid DNA adsorption

The binding of plasmid DNA (pDNA) to anion exchange matrices have also been visualised with CSLM. pDNA is the primary constituent of gene therapy and DNA vaccines. It is manufactured by bacterial fermentation and chromatography is often a fundamental step in the purification of pDNA from other cellular components present in the cell lysate (Diogo et al., 2005). A major problem with this separation process is the lower capacity of adsorbent particles compared to protein purification systems. Prazeres et al. (1998) postulated that only a small fraction of the internal void volume of the chromatographic resin was accessible to the long thin plasmid molecules. Ljunglof et al. (1999) confirmed this reduced binding capacity observation by confocal microscopy. The confocal images obtained showed that pDNA only bound to the surface of both anion-exchange and oligonucleotide affinity resins. This study again demonstrates the effectiveness of confocal microscopy to investigate industrially important adsorption systems and the potential to visualise other binding species besides proteins.

6.1.2 CSLM to visualise packed bed flow cells

The understanding of adsorption mechanisms of molecules within a porous support during chromatographic separations has long been restricted to information gained from finite bath uptake (Horstmann and Chase, 1998; Hunter and Carta, 2000; Weaver and Carta, 2000) and packed bed breakthrough experiments (Chase, 1984; Cooney, 1990; McCoy and Liapis, 1991). Recently, the use of CSLM in combination with finite bath uptake have proved to be a powerful tool for investigating transport and adsorption mechanisms within a single chromatography bead (as described in Section 6.1.1). However, it does not allow real-time, *in situ* observations within a packed bed, which is more relevant to industrial chromatographic processes. Recently,

two scientific papers were published describing the use of flow cells in conjunction with CSLM to investigate adsorption phenomena in a packed bed and in real-time (Hubbach et al., 2002; Dziennik et al., 2002).

Hubbach et al. (2002) developed a flow cell that could be packed with chromatography media and operated it as a fully functional mini-scale column. Using this flow cell in combination with CSLM, they visualised on-line and in real-time the dynamics of protein adsorption to porous stationary phases in packed bed mode. Specifically, they obtained adsorption profiles of single- and two-component mixtures containing BSA and IgG 2a during cation exchange chromatography. The classical shrinking core model with pore diffusion as the dominant transport mechanism was found to be adequate for describing the adsorption of BSA. IgG 2a, on the other hand, appeared to exhibit a different transport mechanism where an initial concentration overshoot of bound IgG 2a was detected at the centre of the bead. For the two-component system, adsorption can be described as a superposition of the transport adsorption mechanism of the single-component systems with a classical displacement of the weaker bound protein species. In general, they observed that even for adsorption to the same chromatographic matrix, the uptake kinetics can vary greatly depending on the actual protein adsorbed. They have also illustrated the usefulness of the flow cell for *in situ* quantitative investigations of protein adsorption dynamics within a single chromatographic bead. The design of the flow cell consisted of a Perspex block with precision-drilled inlets (45°) on either side and an open channel (~ 8 mm in length) grooved into the bottom of the block. A microscope coverslip can be attached to the open channel to create a window for observing under the microscope. The column had a total length of 22 mm and a cross-sectional area of 3 mm^2. The column volume was 0.066 mL. The flow cell was connected to an AKTA Basic 10 System (GE Healthcare, Uppsala, Sweden) which allowed liquid-handling and data monitoring.

Dziennik et al. (2002) used CSLM to show that mechanisms other than diffusion may contribute to protein transport in ion exchange chromatography and that this may be exploited to achieve rapid uptake in process chromatography. The real-time studies were done using a flow cell into which chromatographic particles were packed behind microscope coverslip. The design of the flow cell is different from that of Hubbach et al. (2002) but similar in principle. The flow cell consisted of a solid

Delrin block (51 x 55 x19 mm) with a 1/16-inch-diameter channel drilled through either side of the block at the same angle from the horizontal. The channels meet and penetrate through one face of the block to which a coverslip can be attached to create a window for observing under the microscope. A stainless steel frit was installed in one of the channels to hold the particles. The confocal images obtained verified that protein diffusion at low ionic strength conditions in all the adsorbents examined could be adequately described by classical shrinking core behaviour, but at relatively high salt concentrations ($\geq$ 100 mM) diffuse adsorption fronts were seen in some adsorbents. Consequently, pore diffusivities from the confocal images were calculated from estimates of fractional uptake using linear regression of the finite volume solution of the shrinking core model as described by Teo and Ruthven (1986). This was based on the radial position of the adsorption front and the assumption that the adsorption layer was saturated.

6.1.3 Cell/adsorbent interactions

A problem associated with process chromatography is the degradation of performance due to fouling of the adsorbent particles with whole cells or cell debris present early in the process stream (Fernandez-Lahore et al., 1999; Viloria-Cols et al., 2004; cf. Chapter 4). It is particularly important in expanded bed adsorption (Fernandez-Lahore et al., 1999) and with anion exchange matrices which bind the negatively charged cell surface (Chase et al., 1992; Feuser et al., 1999). Viloria-Cols et al. (2004) suggested coating anion exchangers with agarose to prevent cell-adsorbent interactions, and visualised the adsorption of *E. coli*, *S. cerevisiae* and *L. casei* cells to various anion exchange resins using scanning electron microscopy (SEM).

SEM has proved to be a useful tool for visualising cells. However, sample preparation for SEM can often be elaborate and tedious, involving multiple fixing, rinsing, dehydrating, critical point drying and gold staining steps. Generally, the harsh sample preparation procedure may also risk altering the structure of the sample, thus creating experimental artefacts (Roos and Morgan, 1990).

6.1.4 Objectives

The studies described have demonstrated the ability of scanning confocal microscopy to analyse the adsorption kinetics of protein and DNA. The results of such experiments could be used to improve the design and parameters of operation for large scale chromatographic processes.

The techniques developed have found applications in industry, especially for characterising novel adsorbent particles and in the quality control of resin manufacturing. Numerous new industrially-relevant applications of CSLM are possible, including the use of CSLM as a tool for investigating fouling in chromatography and in particular in examining the effectiveness of clean-in-place protocols. The work reported in this chapter seeks to develop methodologies to allow visualisation of the fouling of chromatographic matrices using CSLM, and in doing so, to provide new insights into the mechanism of chromatographic fouling.

6.2 THEORY

6.2.1 Shrinking Core Model

Protein adsorption to porous chromatographic beads is often described by the classical shrinking core model. The model has been discussed in detail by Dedrick and Beckmann (1967), Brauch and Schlunder (1975), Ruthven (1984), Teo and Ruthven (1986), and Weaver and Carta (1996). In this model, the adsorbent particle is gradually saturated from the edge to the core. All adsorption occurs at the front (radius $R_f < R_p$) which divides the sorbate-free core from the saturated external layer. Over the region, $R_p > R > R_f$, the total flux of sorbate is constant and the sorbate concentration falls from c_0 at the surface ($R = R_p$) to 0 at R_f. The sorbate profile through the saturation layer is given by

$$c = k\left[\frac{1}{R_f} - \frac{1}{R}\right] \tag{6-1}$$

and at the particle surface,

$$c_0 = k\left[\frac{1}{R_f} - \frac{1}{R_p}\right] \tag{6-2}$$

The total flux may be equated to the net uptake rate:

$$4\pi R^2 \varepsilon_p D_p \left(\frac{\partial C}{\partial R}\right) = 4\pi\varepsilon_p D_p k = \frac{4\pi\varepsilon_p D_p c_0}{\left[\frac{1}{R_f} - \frac{1}{R_p}\right]} = -4\pi R_f^2 q_s \frac{dR_f}{dt} \tag{6-3}$$

Rearranging equation 6-3 gives,

$$\frac{\varepsilon_p D_p}{R_p^2}\frac{c_0}{q_s} = (\eta^2 - \eta)\frac{d\eta}{dt} \tag{6-4}$$

where $\eta = \frac{R_f}{R_p}$.

The sorbate concentration in the external fluid phase, c_0, varies with time and is related to η by an overall mass balance

$$c_0(\eta) = C_0[1 - \Lambda(q/q_s)] = C_0\left[1 - \Lambda\left(1 - \eta^3\right)\right] \tag{6-5}$$

where C_0 is the initial sorbate concentration in the external fluid phase, Λ is the fraction of the sorbate initially present in the system which is eventually taken up by the adsorbent, and $(q/q_s) = Q$ is the fractional uptake by the adsorbent at time t. Combining equations 6-4 and 6-5 and integrating, we obtain

$$\frac{\varepsilon_p D_p}{R_p^2}\frac{C_0}{q_s} t = \int_1^{\eta} \frac{(\eta^2 - \eta)}{1 - \Lambda + \Lambda\eta^3} d\eta = I_2 - I_1 \tag{6-6}$$

where

$$I_1 = \int_1^{\eta} \frac{\eta}{1 - \Lambda - \Lambda\eta^3} d\eta \tag{6-7}$$

$$I_2 = \int_1^{\eta} \frac{\eta^2}{1-\Lambda-\Lambda\eta^3}\, d\eta \qquad (6\text{-}8)$$

Equations 6-7 and 6-8 can be integrated to give:

$$I_1 = \frac{1}{3\Lambda\lambda}\left\{\tfrac{1}{2}\ln\left[\frac{(1-\Lambda-\Lambda\eta^3)(\lambda+1)^3}{(\eta+\lambda)^3}\right]\right\} + \sqrt{3}\tan^{-1}\left\{\frac{2\eta-\lambda}{\lambda\sqrt{3}}\right\} - \sqrt{3}\tan^{-1}\left[\frac{2-\lambda}{\lambda\sqrt{3}}\right] \qquad (6\text{-}9)$$

and

$$I_2 = \frac{1}{3\Lambda}\ln\left[1-\Lambda-\Lambda\eta^3\right] \qquad (6\text{-}10)$$

where $\lambda = [(1-\Lambda)/\Lambda]^{1/3}$. Since $\eta^3 = 1-(q/q_s) = 1-Q$, it is evident that both I_1 and I_2 may be expressed as functions of Λ and Q, so that equation 6-6 may be written in the form:

$$\frac{D_e t}{R_p^2} = \frac{\varepsilon_p D_p}{R_p^2}\frac{C_0}{q_s}t = (I_2 - I_1)(Q,\Lambda) \qquad (6\text{-}11)$$

Equation 6-11 suggests that a plot of $(I_2\text{-}I_1)$ vs. t should give a straight line through the origin with slope D_e/R_p^2.

If the reservoir of fluid is effectively infinite, that is $\Lambda \rightarrow 0$ and $c_0 = C_0 =$ constant then equations 6-7 and 6-8 become:

$$I_1 = \int_1^{\eta} \eta\, d\eta = \tfrac{1}{2}(\eta^2 - 1) \qquad (6\text{-}12)$$

$$I_2 = \int_1^{\eta} \eta^2\, d\eta = \tfrac{1}{3}(\eta^3 - 1) \qquad (6\text{-}13)$$

and equation 6-11 reduces to the familiar form derived by Dedrick and Beckmann (1967):

$$\frac{\varepsilon_p D_p}{R_p^2}\frac{C_0}{q_s}t = \frac{1}{6} - \frac{1}{2}\eta^2 + \frac{1}{3}\eta^3$$
$$= \frac{1}{2} - \frac{1}{2}(1-Q)^{2/3} + \frac{Q}{3} \qquad (6\text{-}14)$$

If external mass-transfer resistance cannot be neglected, the relationship between the particle surface, c_s, and the bulk concentration, c_0, may be derived from a mass balance at the particle surface

$$\frac{4}{3}\pi R_p^3\left(\frac{dq}{dt}\right)_{R_p} = 4\pi R_p^2 k_f (c_0 - c_s) = 4\pi R^2 \varepsilon_p D_p \frac{dc}{dR} = 4\pi R^2 \varepsilon_p D_p \frac{c_s}{\left[\frac{1}{R_f} - \frac{1}{R_p}\right]} \qquad (6\text{-}15)$$

which may be rearranged to give

$$\frac{c_0}{c_s} = 1 + \frac{\varepsilon_p D_p}{k_f R_p^2\left[\frac{1}{R_f} - \frac{1}{R_p}\right]} \qquad (6\text{-}16)$$

Following the same analysis as shown earlier for equation 6-11, the expression for the uptake curve becomes

$$\frac{D_e t}{R_p^2} = \frac{\varepsilon_p D_p}{R_p^2}\frac{C_0}{q_s}t = \left[1 + \frac{\varepsilon_p D_p}{k_f R_p}\right] I_2(Q,\Lambda) - I_1(Q,\Lambda) \qquad (6\text{-}17)$$

This equation suggests that a plot of I_1/I_2 vs. $-t/I_2$ should be linear with intercept $\left(1 + \varepsilon_p D_p / k_f R_p\right)$ and slope D_e / R_p^2.

6.2.2 Technical overview of confocal scanning laser microscopy

In confocal microscopy, laser light is focused on one spot on the specimen as opposed to conventional microscopy where the entire field of view of a specimen is simultaneously illuminated. Reflected light or emitted fluorescent light from this single point is refocused and allowed to pass through a pinhole aperture as illustrated in

Figure 6-1. The pinhole aperture effectively blocks light from out-of-focus planes from reaching the detector, and this depth discriminating property allows the specimen to be sliced optically into thin sections. Scanning a plane at a given depth provides a two-dimensional optical section of the sample at that depth, and by moving the acquisition plane to different depths within the sample allows a stack of confocal images to be obtained that will describe a three-dimensional volume. (In depth discussions of this technique have been given by Wilson (1990), Pawley (1995), Masters (1996), and Sheppard and Shotton (1997)).

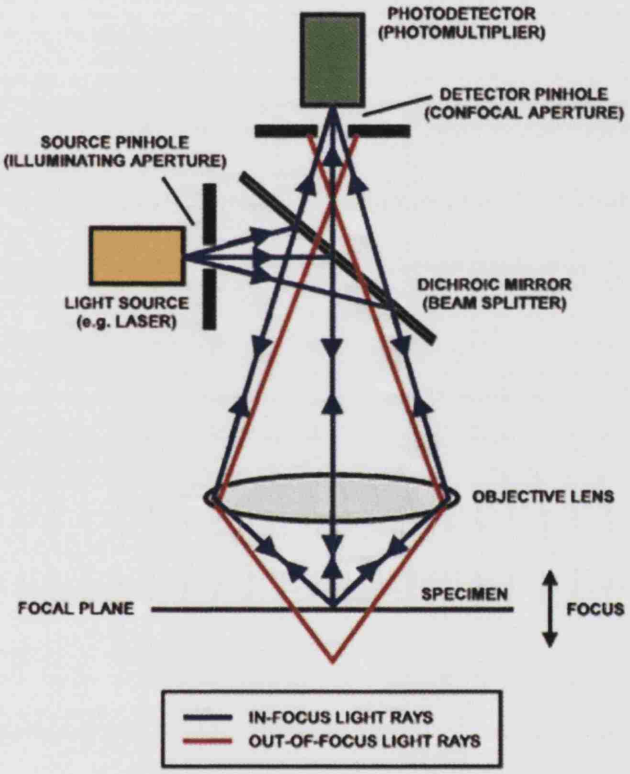

Figure 6-1: *Simplified ray paths in a confocal microscope. The pinhole aperture blocks light from out-of-focus planes to reach the detector, allowing the specimen to be optically sectioned.*

6.2.3 Fluorophores and Fluorescence

Fluorophores are molecules (generally polyaromatic hydrocarbons or heterocycles) where adsorption of light causes the molecule to emit photons. This process is known as fluorescence and can be viewed as a three-stage process:

excitation, excited-state lifetime, and fluorescence mission. The electronic-state diagram (Jablonski diagram) in Figure 6-2 illustrates these stages.

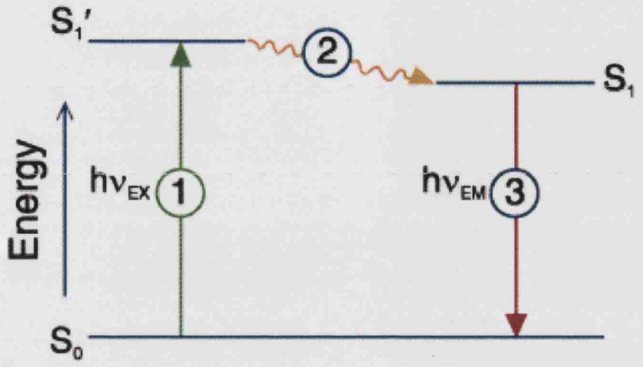

***Figure 6-2**: Jablonski diagram illustrating the different energy-levels in fluorescence. There are three stages: (1) excitation, (2) excited-state lifetime, and (3) fluorescence emission.*

1) Excitation

When an external source, such as a laser, supplies a photon of energy $h\nu_{ex}$ to a fluorophore, the light is absorbed very quickly (~10^{-15} seconds) and creates an excited electronic singlet state (S_1'). This process is different from chemiluminescence, in which the excited state is populated by a chemical reaction.

2) Excited-state lifetime

The excited state exists only for approximately 10^{-9} seconds. During this time, energy is partially dissipated to the environment and relaxation to the lowest level of the excited state (S_1) occurs.

3) Fluorescence Emission

Further relaxation from the excited state S_1 to the ground state (S_0) emits a photon of energy $h\nu_{em}$. This is referred to as fluorescence. Due to energy dissipation during the excited state, the energy of $h\nu_{em}$ is lower than that of $h\nu_{ex}$, and therefore, also of longer wavelength. The difference in energy or wavelength can be represented by ($h\nu_{ex}$-$h\nu_{em}$) and is called the Stokes shift.

Fluorophores can undergo the excitation/emission process repeatedly. However, a problem associated with some fluorophores under prolonged high-intensity conditions is photobleaching, or fading, due to the finite capacity of fluorophores to give off photons on excitation. Song et al. (1995 and 1996) investigated the photobleaching kinetics of fluorescein, a widely used dye, and described in detail the multiple photochemical reaction pathways responsible for photobleaching. The rate of photobleaching varies between different fluorophores, and it is recommended to avoid fluorophores that fade quickly.

Background fluorescence, which may originate from the specimen itself (autofluorescence) or from unbound or non-specifically bound fluorophores (reagent background), can obscure the obtained confocal image. Autofluorescence can be minimised by narrowing the fluorescence detection bandwidth, using fluorescent dyes that absorb and emit at longer wavelengths or by reducing the laser intensity since autofluorescence is normally very weak.

A wide selection of commercially available fluorescent dyes has been listed by Haughland (2002). An overview of some fluorescent dyes, including those used in this work, is given in Section 6.2.5.

6.2.4 Multicolour labelling experiments

Multicolour labelling involves the use of two or more fluorescent dyes to monitor simultaneously different specimens or biochemical functions. This technique has major applications in flow cytometry, DNA sequencing, fluorescence *in situ* hybridisation and fluorescence microscopy (Haugland, 2002). In the context of using CSLM to visualise adsorption to chromatographic beads, it has been demonstrated by Linden et al. (1999), Linden et al. (2002) and Hubbach et al. (2002). In these studies, selected fluorescent dyes were used for labelling different proteins in order to visualise their competitive adsorption to chromatographic beads.

When choosing the appropriate dyes to use simultaneously, it is important to consider avoiding energy transfer between the fluorophores and cross-talk

(bleedthrough) between different detector channels. Therefore, the choice of fluorophores is normally based on the absorption/emission spectra of the individual dyes. Maximising the spectral separation of the multiple emissions will help in signal isolation. One way of avoiding cross-talk is to record the images in succession. Computer software can then be used to obtain a true overlay of the individual images. (An example of this is given in Figure 6-3). Another way is to limit the emission spectrum that is detected for each dye, provided that the spectral separation of each emission spectrum is large enough to ensure the detection of the individual fluorophores using band-pass filters in front of the detectors. The latter method may be practically difficult when simultaneously using more than two fluorophores.

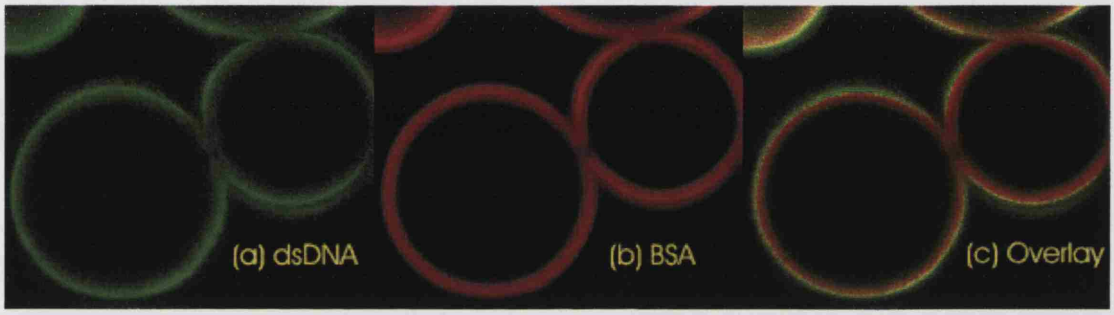

***Figure 6-3**: An example of overlaying individual images in CSLM. This allows cross-talking to be minimised in multicolour labelling experiments. A flow cell packed with Q Sepharose FF was successively loaded with partially clarified E. coli homogenate (foulant) then 2 mg/mL BSA. The images show a snapshot of after loading BSA for 10 minutes. (a) dsDNA-PicoGreen; (b) BSA-Cy5.5; (c) overlay of (a) & (b).*

6.2.5 Fluorescent dyes

6.2.5.1 Amine-reactive dyes

Amine probes are commonly used to label proteins, peptides, ligands, synthetic oligonucleotides and other biomolecules. The cyanine dyes Cy3, Cy5 and Cy5.5 are such probes. They are available in three chemistries: N-hydroxysuccinimide (NHS) ester, maleimide and hyrazide for labelling different biomolecules. The NHS-esters were used in this study. Under the correct buffer conditions they will covalently bind to amino groups by an acylation reaction as shown by the reaction schematic in Figure

6-4. Cyanine dye fluorophores are known to be relatively photo-stable and pH insensitive (Mujumdar et al., 1993). The structure of these cyanine dyes are illustrated in Figure 6-5. The absorbance and emission spectra of the dyes are given in Figure 6-6 and shows the following maximum excitation and emission wavelengths, respectively: Cy3 - 550 nm and 570 nm; Cy5 - 649 nm and 670 nm; Cy5.5 – 675 nm and 694 nm.

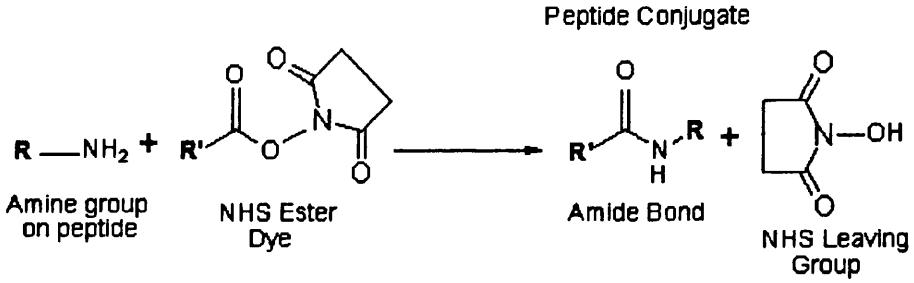

***Figure 6-4**: Reaction schematic of the acylation reaction in protein-dye conjugate formation for the cyanine NHS-ester dyes.*

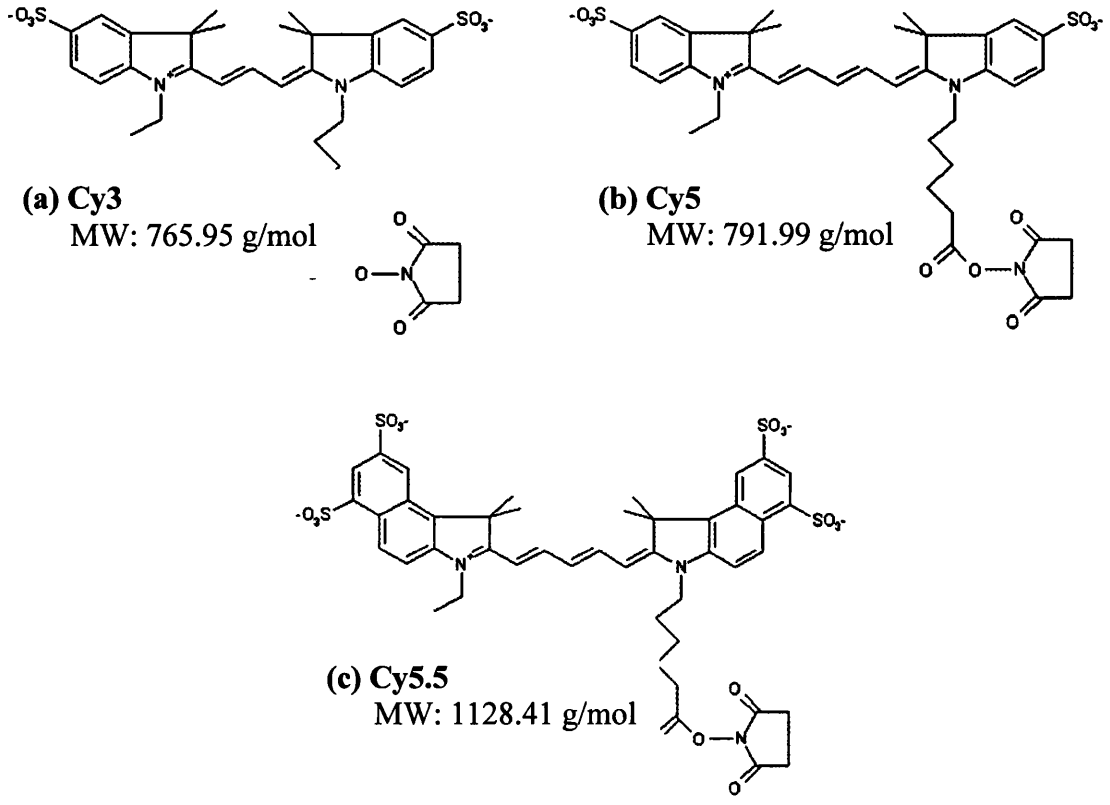

Figure 6-5: Molecular structures of (a) Cy3, (b) Cy5, and (c) Cy5.5. These CyDye™ NHS-esters are used for labelling the primary amino group in proteins.

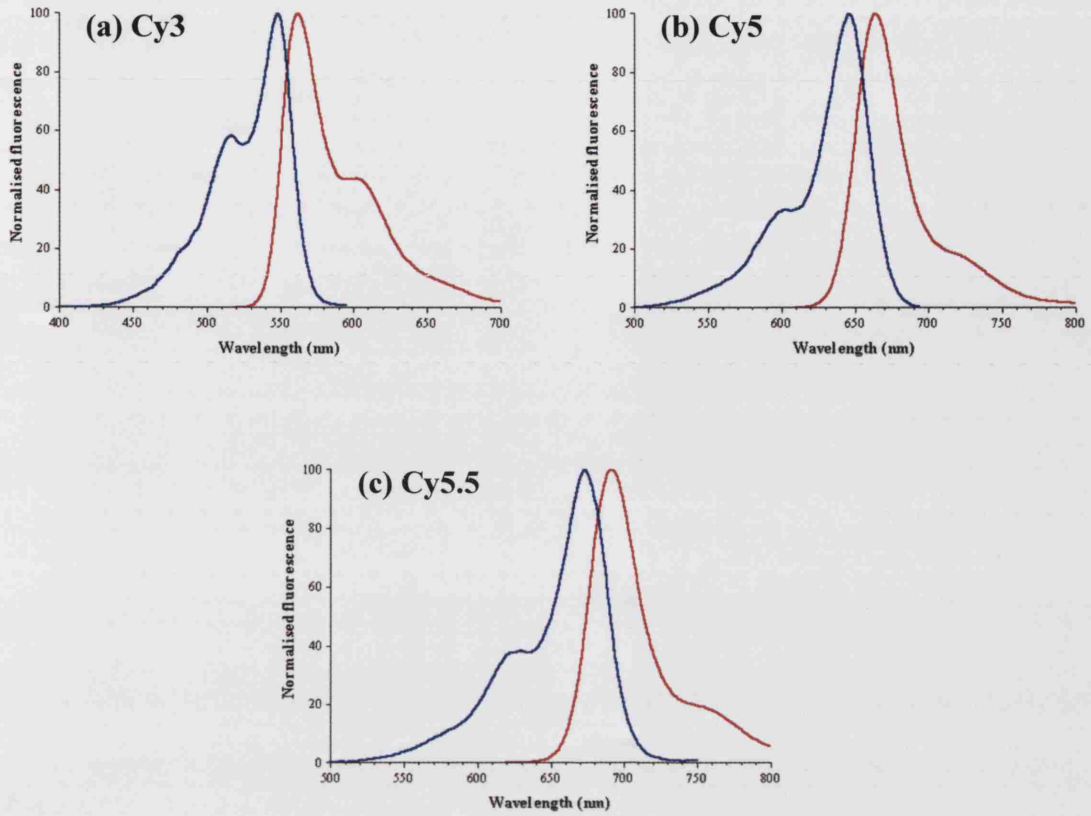

***Figure 6-6**: Absorbance and emission spectra of Cy3, Cy5 and Cy5.5. The absorbance spectra are in blue and the emission spectra are in red. Ex_{max}/Em_{max} (nm): Cy3 550/570; Cy5 649/670; Cy5.5 675/694.*

6.2.5.2 Nucleic acid detection

The characteristics of PicoGreen have been recently described by Singer et al. (1997). It forms highly fluorescent complexes with double stranded DNA. Although it is not specific for dsDNA, PicoGreen shows a >1000-fold fluorescence enhancement upon binding to dsDNA, and much less fluorescence enhancement upon binding to ssDNA or dsRNA (Singer et al., 1997). It has been previously reported as being highly stable under alkaline conditions (Batal et al., 1999). Nevertheless, the fluorescent enhancement of PicoGreen has been shown to decrease at high pH conditions (Rock et al., 2003) and also decrease slightly with increasing NaCl and BSA concentrations in solution (Singer et al., 1997). The maximum fluorescence excitation and emission for PicoGreen occurs at wavelengths of 581 nm and 644 nm, respectively (Figure 6-7).

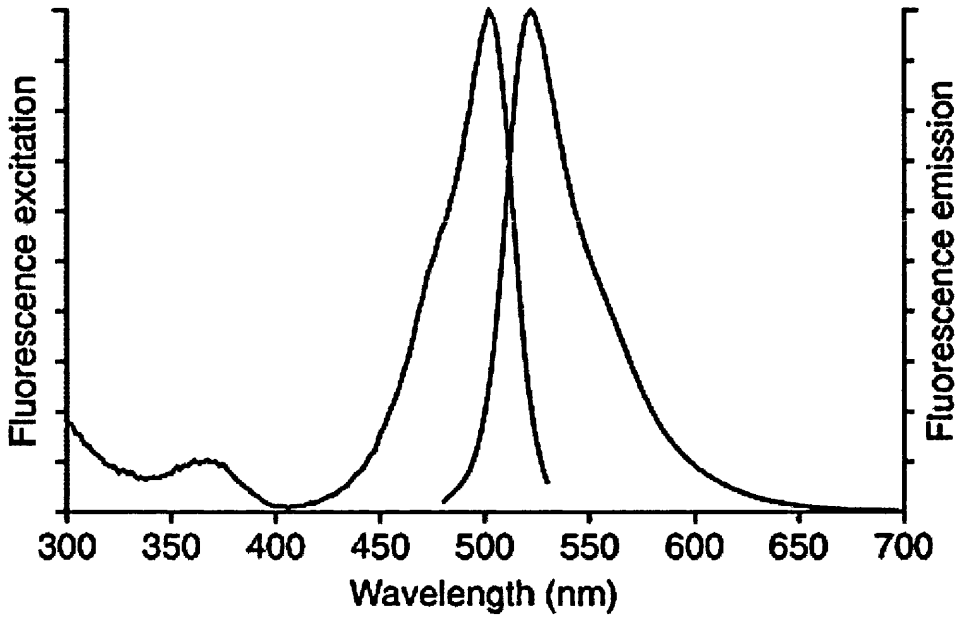

***Figure 6-7**: Absorbance and emission spectra of PicoGreen bound to dsDNA. Ex_{max}/Em_{max} (nm): 502/523.*

6.2.5.3 Bacterial stains

BacLight Red and BacLight Green bacterial stains are fluorescent, non-nucleic acid labelling reagents for detecting bacteria. They can efficiently label a variety of different bacteria species. The intensity of the staining appears to depend on several factors, including gram character, outer membrane composition and overall membrane integrity. BacLight Red and BacLight Green have molecular weights of 724 and 671, respectively. Their molecular structures are given in Figure 6-8. The maximum fluorescence excitation and emission for BacLight Red occurs at wavelengths of 581 nm and 644 nm, respectively. For BacLight Green they occur at 480 nm and 516 nm, respectively.

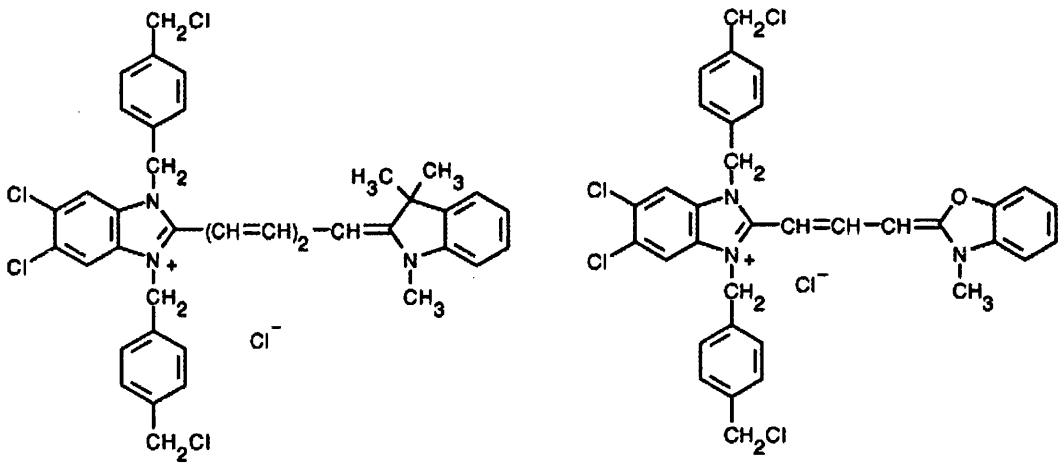

(a) BacLight Red **(b) BacLight Green**

Figure 6-8: *Molecular structures of BacLight Red and BacLight Green. These are fluorescent, non-nucleic acid labelling bacterial stains.*

6.3 RESULTS AND DISCUSSION

6.3.1 Experimental errors

Photobleaching can be caused by surrounding light during the experiments. This can result in an unsystematic decrease in the fluorescent signal over time, and such variability may obscure quantitative comparison of fluorescence intensities between samples. An example of photobleaching is described by Singer et al. (1997) where a large decrease in signal stability was observed over time when dsDNA-PicoGreen samples were exposed to room light. Conversely, they found that this decrease was minimal when the samples were protected from light using aluminium foil or by storing them in a drawer. Because of this, care was taken to minimise the exposure of samples to surrounding light and all samples containing fluorophores where wrapped with aluminium foil.

The uptake rate of protein in porous beads is determined by the diffusional time constant (D/r_p^2) (Ruthven, 1984). Clearly, the uptake rate is dependent on the bead size. Q Sepharose FF contains beads with a particle size distribution of 45 – 165 μm in diameter, as quoted by the manufacturer. In the finite bath experiments, different

beads of varying diameters where measured at each sampling time. Similarly for the packed bed experiments, the size of the selected bead can vary between experiments. Effort was given to select beads of roughly the same size but often this was not practically possible. The typical range of beads sizes used for analysis in the finite bath experiments was ~ 90 – 115 μm in diameter, and that for the packed bed experiments was ~ 67 – 72 μm in diameter. This variation in bead sizes may have contributed to the variability in the determined capacity values.

Contact points between beads have been shown to be areas of restricted transport (Hubbach et al., 2002). As discussed in Section 6.3.4.1, these dead zones were, obviously, only seen during packed bed experiments and not in those using a finite bath. The degree of restriction appeared to vary which suggests that it may be dependent upon by the homogeneity of the bed packing. Hubbach et al. (2002) found that the variation in intensity for shells near the contact points may be twice as much as for shells situated in the inner part of the bead, where the influence of the contact points between neighbouring beads is greatly reduced. This variation of the intensity at contact points may have also been a source of variation in the determined capacity values.

6.3.2 Experimental controls

Table 6-3 lists the control experiments that were done to eliminate any autofluorescence or reagent fluorescence.

Tables 6-4 to 6-7 list the control experiments that were done to eliminate any crosstalk when simultaneously using Cy3, Cy5.5, PicoGreen and BacLight Red.

Control Experiment	Purpose	Results
All experiments were repeated without the addition of fluorescent dyes.	To check for autofluorescence or reagent fluorescence.	No fluorescence signal detected.
Q Sepharose FF was incubated with PicoGreen and Cy5.5 but in the absence of any protein or DNA.	To verify that the dyes do not bind directly to Q Sepharose FF (reagent fluorescence).	No fluorescence signal detected.
Q Sepharose was incubated with Cy3 but in the absence of any protein or DNA.	To verify that the dye does not bind directly to Q Sepharose FF (reagent fluorescence).	No fluorescence signal detected.
Q Sepharose FF was incubated with BacLight Red but in the absence of any cells/debris, protein or DNA.	To verify that the dye does not bind directly to Q Sepharose FF (reagent fluorescence).	No fluorescence signal detected.
Foulant was centrifuged to remove all cells and debris before adding BacLight Red. This was subsequently used to incubate Q Sepharose FF.	To check if BacLight Red will bind to other fouling material (reagent fluorescence).	No fluorescence signal detected.
Sepharose CL-6B (base matrix) was incubated with BSA-Cy5.5.	To check for non-specific binding of BSA.	No fluorescence signal detected.

***Table 6-1**: Control experiments performed to eliminate autofluorescence or reagent fluorescence.*

Excitation	FLUORESCENT SIGNAL Detection bandwidth		
	505 – 535 nm	560 – 600 nm	644 – 710 nm
488 nm	✓	✓	✗
543 nm	✗	✗	✗
633 nm	✗	✗	✗

***Table 6-2**: Control experiments performed to eliminate any crosstalking of PicoGreen.*

Excitation	FLUORESCENT SIGNAL Detection bandwidth		
	505 – 535 nm	560 – 600 nm	650 – 710 nm
488 nm	✗	✓	✗
543 nm	✗	✓	✗
633 nm	✗	✗	✗

***Table 6-3**: Control experiments performed to eliminate any cross talking of Cy3.*

Excitation	FLUORESCENT SIGNAL Detection bandwidth		
	505 – 535 nm	560 – 600 nm	650 – 710 nm
488 nm	✗	✗	✗
543 nm	✗	✗	✗
633 nm	✗	✗	✓

***Table 6-4**: Control experiments performed to eliminate any crosstalking of Cy5.5.*

Excitation	FLUORESCENT SIGNAL Detection bandwidth	
	505 – 535 nm	644 – 690 nm
488 nm	✗	✗
568 nm	✗	✓

***Table 6-5**: Control experiments performed to eliminate any crosstalking of BacLight Red.*

Notes:
✓ = detectable fluorescent signal

✗ = no detectable fluorescent signal

6.3.3 Fouling of a chromatographic matrix in finite baths

6.3.3.1 Correlation between fluorescence intensity and protein capacity

Ljunglof et al. (1998) have shown that there is a linear correlation between the protein capacity taken directly from fluorescence intensity measurements of confocal images and the protein capacity calculated indirectly from fluid phase measurements. A good linear correlation was found for four different protein/adsorbent combinations. This proved their assumption that the measurement of fluorescence profiles gives a realistic picture of the kinetics of protein uptake to porous adsorbents.

The direct, linear correlation between the fluorescence intensity and the uptake capacity was reconfirmed under the conditions of study in this thesis (Figure 6-9). In order to calculate the corresponding calculated capacities, fresh Q Sepharose FF beads were incubated in 2mg/mL BSA with mixing and the solid phase concentration was calculated indirectly by mass balance at appropriate times from:

$$q = \frac{V_M(C_0 - C)}{V_s} \qquad (6\text{-}18)$$

where q = solid phase concentration, V_M = volume of mobile phase, V_S = volume of solid phase, C_0 = initial protein concentration.

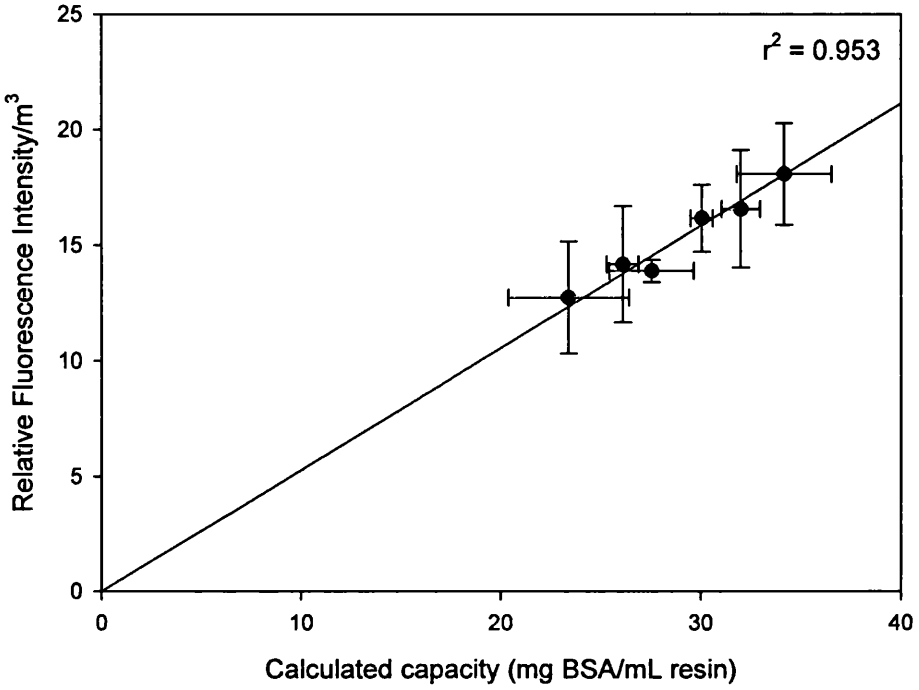

Figure 6-9: *Parity plot correlating the fluorescence intensity to the BSA capacity. (Error bars show 95% C.I.)*

6.3.3.2 Adsorption of BSA to fresh Q Sepharose FF

The adsorption of 2 mg/mL BSA to fresh Q Sepharose FF beads is shown in Figure 6-10. Shrinking core behavior, as described by a number of authors (Dedrick and Beckmann, 1967; Brauch and Schlunder, 1975; Ruthven, 1984; Teo and Ruthven, 1986; Weaver and Carta, 1996), was observed. This phenomenon is a classical example of the self-sharpening front that results from particulate pore diffusion with local adsorption equilibrium. Translation of the confocal images to fluorescence intensity profiles over the particle diameter, as illustrated in Figure 6-11, shows the expected flattening of the intensity profile over time. After 160 minutes there was no discernible change in the amount of BSA adsorbed and adsorption equilibrium was assumed to be practically achieved.

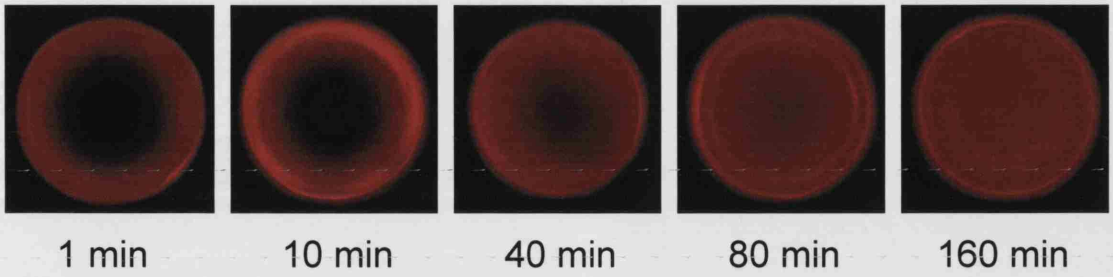

***Figure 6-10**: Adsorption of BSA to fresh Q Sepharose FF. 2 mg/mL BSA-Cy5.5 (labelling ratio = 1:20) was incubated with 0.25 mL Q Sepharose FF in 20 mM Tris-HCl, pH 8.0 with mixing. Classical shrinking core pattern of protein adsorption was observed.*

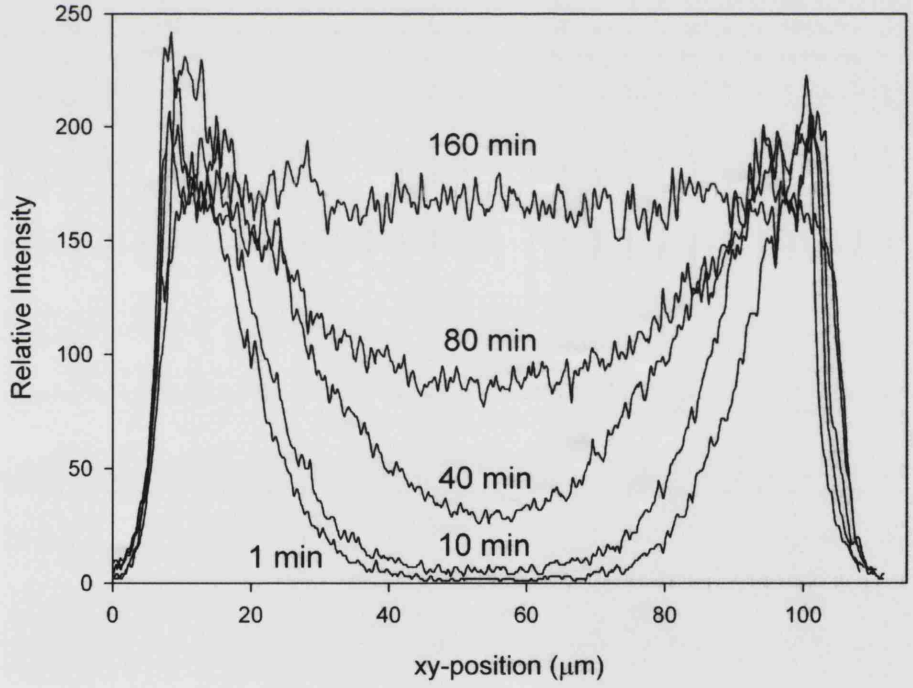

***Figure 6-11**: Fluorescence intensity profiles obtained from the adsorption of BSA to fresh Q Sepharose FF. 0.25 mL of fresh Q Sepharose FF was incubated with 2 mg/mL BSA-Cy5.5 in 20 mM Tris-HCl, pH 8.0. The profiles show the fluorescence intensity across the bead diameter through the bead centre (cf. Figure 6-10).*

6.3.3.3 *Effect of severe fouling of Q Sepharose FF beads on subsequent BSA adsorption*

As Q Sepharose FF is an anion exchanger, genomic nucleic acids in the *E .coli* homogenate, used as the foulant challenge, would be expected to act as a major fouling species due to attraction between their intrinsic negative charge and the positive charge of the quaternary amine groups on the resin. To investigate this, PicoGreen was used to label fluorescently the dsDNA in the foulant material that bound to the resin. Figure 6-12 (0 min) shows that after incubating the fresh Q Sepharose FF resin in foulant material for 12 hours, the foulant dsDNA remains absorbed to only a thin layer at the bead exterior and had not penetrated the core of the bead. Similar observations have been seen with pure solutions of plasmid DNA by Prazeres et al. (1998) and Ljunglof et al. (1999). Plasmid DNA was unable to diffuse further into the bead presumably due to its size.

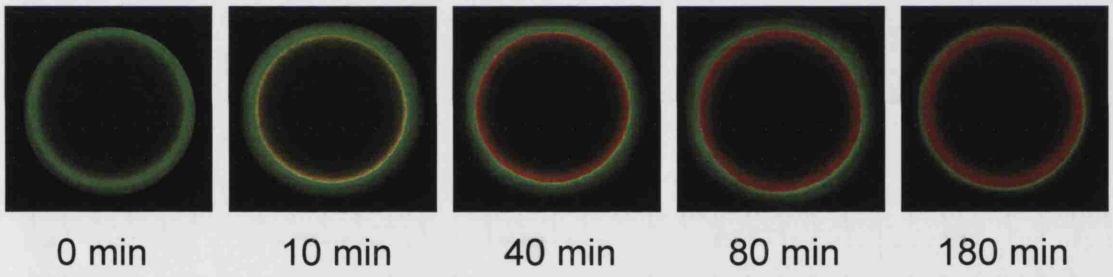

***Figure 6-12**: Effect of severe bead pre-fouling on the subsequent uptake of BSA to Q Sepharose FF. Fresh Q Sepharose FF beads were fouled by incubating in partially clarified E. coli homogenate for 12 hours. dsDNA (green) was labelled with PicoGreen. 2 mg/mL BSA-Cy5.5 (red) (labelling ratio = 1:20) was incubated with 0.25 mL of fouled Q Sepharose FF in 20 mM Tris-HCl, pH 8.0 with mixing.*

A BSA adsorption time series following the same procedure as that for fresh beads is shown in the confocal images in Figure 6-12 (0-180mins) with their corresponding intensity profiles in Figure 6-13. These show that initially BSA does not occupy the outer layer where dsDNA was bound but penetrates and binds past this outer layer. Over time the BSA appeared to displace the dsDNA, but not completely, so that even after 180 minutes an even thinner dsDNA layer (~ 2 μm) at the bead

exterior was observed. Even beyond 180 minutes, the BSA does not penetrate the core of the bead. This is in sharp contrast when compared to BSA adsorption to fresh beads. It is presumed that foulants besides dsDNA which will be present in the *E. coli* foulant may have prevented BSA from binding or penetrating to the core of the bead.

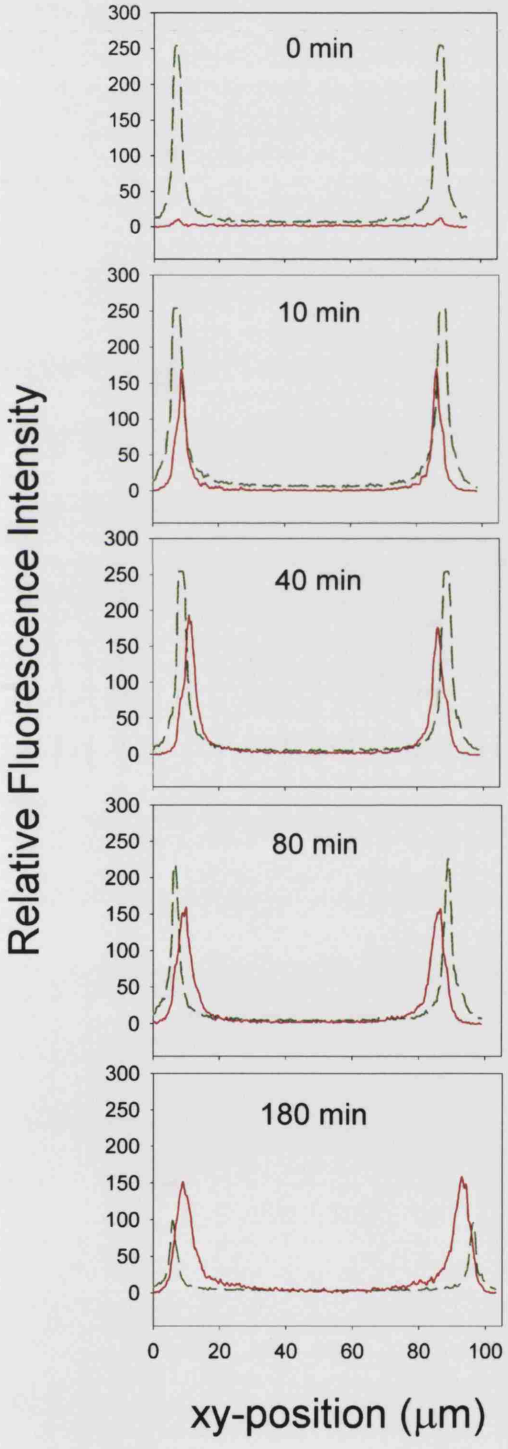

***Figure 6-13**: Fluorescence intensity profiles obtained from the adsorption of BSA to fouled Q Sepharose FF. Fouled Q Sepharose FF was incubated with 2 mg/mL BSA-Cy5.5 in 20 mM Tris-HCl, pH 8.0 with mixing. dsDNA (---); BSA-Cy5.5 (–). The fresh Q Sepharose FF beads were fouled by incubating in partially clarified E. coli homogenate for 12 hours (cf. Figure 6-12).*

6.3.3.4 Effectiveness of CIP solutions

Two CIP treatments were investigated for their abilities to recover the bead capacity for binding of protein (BSA) and for the removal of foulants as determined by CSLM visualisation. The two protocols were based on standard industrial practices: (A) 1 M NaCl, and (B) 1 M NaCl with 1M NaOH. The former CIP solution is commonly used during column regeneration for removing ionically-bound protein by disrupting ionic interactions between the adsorbents and immobilised charged groups on the resin. 1 M NaOH on the other hand is known to remove strongly-bound hydrophobic proteins or lipoproteins and to hydrolyse bound proteins by virtue of the strong alkali conditions.

After gross fouling, a layer of nucleic acid was observed bound to the exterior of the beads (Figure 6-14a). Within 15 minutes of incubation of the beads in 1 M NaCl, virtually all dsDNA was removed (Figure 6-14b). However, there was no significant removal of HCPs even after 180 minutes of incubation. Similar to when using 1 M NaCl, virtually all dsDNA was removed within 15 minutes of incubating the beads in 1 M NaCl + 1 M NaOH (Figure 6-14c). Again no significant removal of HCPs occurred even after 180 minutes of incubation. The corresponding fluorescence intensity profiles in Figure 6-15 show no significant change in the spatial distribution of HCPs within the bead. They show that HCPs penetrated throughout the interior of the bead but does not saturate the core of the beads, thus suggesting the presence of other fouling species, other than protein, occupy the core region.

The time series of BSA adsorption to fouled Q Sepharose FF post-treated with CIP of 1 M NaCl for 60 minutes (Figure 6-16a) reveals that BSA was only able to bind near the exterior of the bead and could not bind to the core of the bead even after 120 minutes of incubation. The time series of BSA adsorption to fouled Q Sepharose FF post-treated with the more aggressive CIP of 1 M NaCl + 1 M NaOH for 60 minutes is very different from that obtained after treatment with 1 M NaCl alone. Following the harsher CIP protocol, the BSA adsorption behavior (Figure 6-16b) was much more like that seen for fresh matrix where BSA does penetrate and bind throughout the entire bead over time. As with fresh matrix a shrinking core behavior of BSA adsorption is seen but the total amount of BSA bound to the beads is considerably lower than when

the beads are fresh, indicating that a degree of irreversible loss in binding capacity had occurred due to the severe fouling challenge.

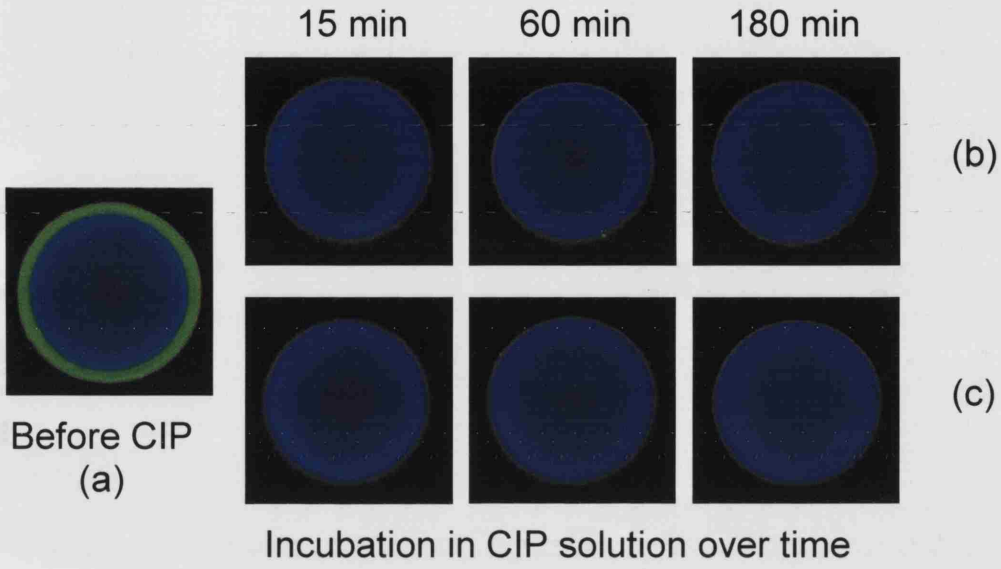

***Figure 6-14**: The effectiveness of CIP washing on the removal of foulant dsDNA and protein. Fresh Q Sepharose FF beads were fouled by incubating in partially clarified E. coli homogenate for 12 hours. dsDNA-Pico(Green); HCPs-Cy5.5 (blue). (a) pre-CIP; (b) CIP using 1 M NaCl for 180 min; (c) CIP using 1 M NaCl + 1 M NaOH for 180 min.*

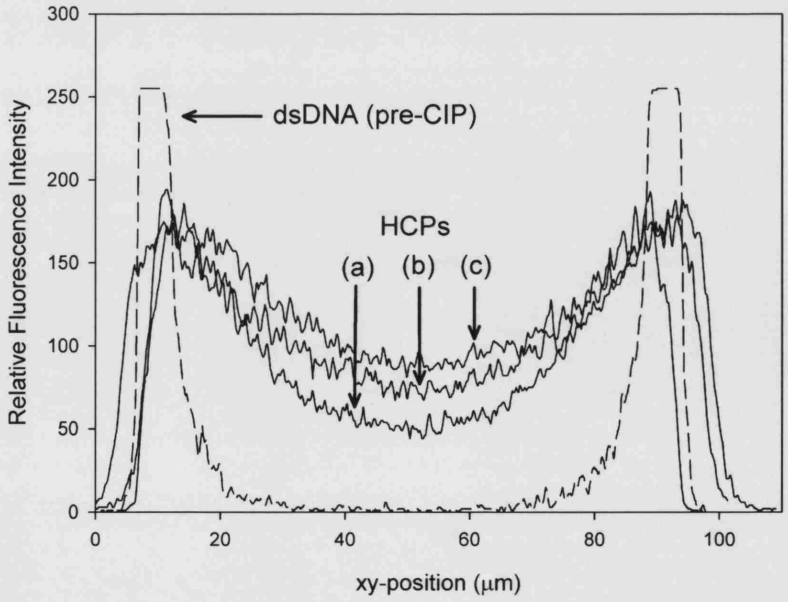

***Figure 6-15**: Fluorescence intensity profiles for fouled Q Sepharose FF beads (cf. Figure 6-14).*

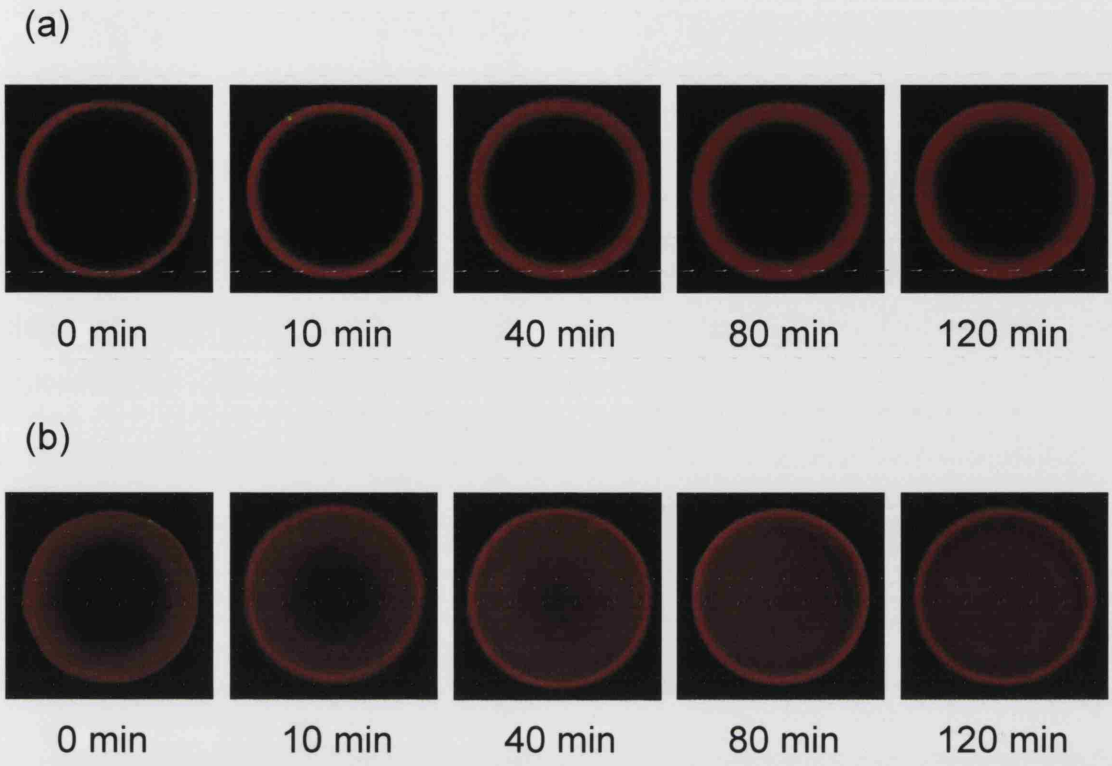

***Figure 6-16**: Adsorption of BSA to fouled Q Sepharose FF beads that were CIP-treated. The beads were first fouled by incubating in partially clarified E. coli homogenate for 12 hours. dsDNA (green) was labelled with PicoGreen and only trace amounts of dsDNA remained after CIP treatment. 2 mg/mL BSA-Cy5.5 (red) (labelling ratio = 1:20) was incubated with 0.25 mL of CIP-treated Q Sepharose FF in 20 mM Tris-HCl, pH 8.0 with mixing. (a) CIP with 1 M NaCl; (b) CIP with 1 M NaCl + 1 M NaOH.*

It is not surprising that a combination of NaOH + NaCl proved to be more effective at cleaning the beads than NaCl alone. The fact that not all HCPs were entirely removed by 1 M NaCl + 1 M NaOH may be as a consequence of only partially removing other fouling species, the presence of which may hinder subsequent protein transport or displacement. Complex interactions between biological foulants can exist. For example, Kelly and Zydney (1997) have shown that proteins in solution can bind to already-adsorbed protein deposits on ultrafiltration membranes through intermolecular disulphide bond formation or hydrophobic interactions, giving rise to secondary fouling. Such a fouling mechanism as well as interactions between HCPs

and other fouling species may also be occurring in this case leading to grossly fouled beads which are extremely difficult to clean thoroughly even with a combined high salt and harsh caustic wash.

Although 1 M NaCl + 1 M NaOH proved to be the more effective agent, it must be noted that in practice, such caustic washes may have a deleterious effect on the long-term stability and lifetime of certain matrices especially since in its operational life a column may be expected to go through hundreds of cycles. An examination of long-term matrix degradation was beyond the scope of the current study but could be a subject of future work (see Chapter 8).

6.3.3.5 Comparison of total BSA binding capacity and BSA uptake rate

The adsorption curves of BSA to fresh, fouled and CIP-treated beads are illustrated in Figure 6-17 and the approximate BSA binding capacities listed in Table 6-1. After fouling for 12 hours, the binding capacity of Q Sepharose FF was reduced 15-fold. After a CIP with 1 M NaCl, the capacity reduction was 4-fold. Even though 1 M NaCl + 1 M NaOH provides a harsher, and hence more effective, cleaning regime the reduction in capacity compared to the original condition was still 2.5-fold.

The uptake rate of BSA was calculated as a function of the foulant challenge and the CIP protocol applied. These were determined by taking the first derivative of the uptake curves in Figure 6-17. The resulting uptake rate curves are shown in Figure 6-18, and the maximum rate of BSA uptake for the different bead conditions is listed in Table 6-1. There is a clear reduction in uptake rate as the degree of exposure to fouling increases. After cleaning with 1 M NaCl + 1 M NaOH, the maximum uptake rate did improve but was still only a third of the original rate seen for fresh beads. Fouling species occupying binding sites or hindering the diffusion of BSA into the bead core may have caused the reduced uptake of BSA.

Bead condition	Relative binding capacity (arbitrary units)	Initial relative uptake rate $x10^{-1}$ (min^{-1})
Fresh	15	12
Fouled (12 hours)	1	0.5
Fouled (1 hour)	6	4
Fouled (5 minutes)	6	7
CIP A[(1)] applied to material fouled for 12 hour	4	2
CIP B[(2)] applied to material fouled for 12 hour	6	4

Notes: (1) CIP A: 1 M NaCl for 60 minutes
(2) CIP B: 1 M NaCl + 1 M NaOH for 60 minutes

***Table 6-6**: Comparison of BSA binding capacities and uptake rates for Q Sepharose FF beads subjected to different conditions of fouling and cleaning.*

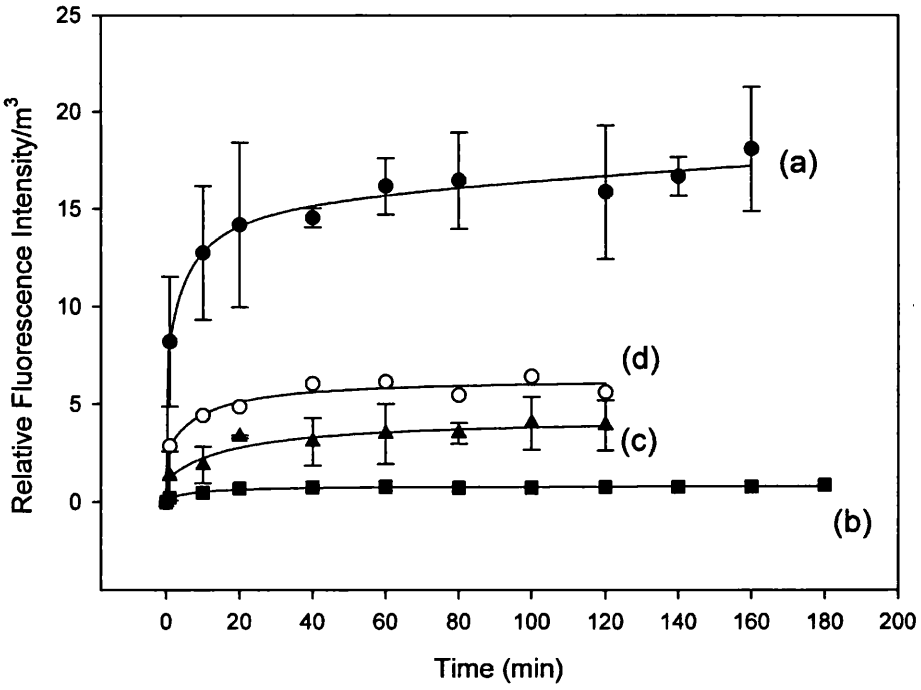

***Figure 6-17**: Comparison of BSA adsorption for different states of Q Sepharose FF beads. (a) fresh beads; (b) fouled beads; (c) fouled beads treated with CIP of 1 M NaCl; (d) fouled beads treated with CIP of 1 M NaCl + 1 M NaOH. (Error bars show 95% C.I. Error bars were omitted for curves (b) and (d) for clarity.)*

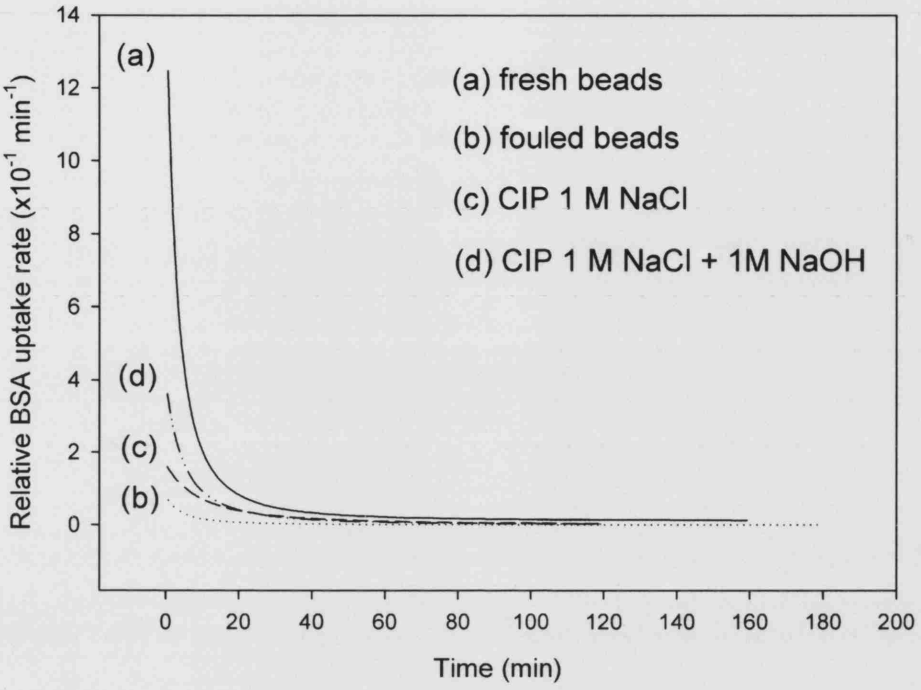

***Figure 6-18**: Relative BSA uptake rate for different bead conditions. These curves were generated by taking the 1st derivative of the uptake curves in Figure 6-17.*

6.3.3.6 Effect of fouling time on BSA adsorption

The effect of bead:foulant contact time on the degree of fouling was investigated. The beads were incubated with foulant for periods of 5 minutes, 1 hour or 12 hours. A BSA adsorption time series was then performed on the fouled beads. The confocal images (Figure 6-19) show that BSA was unable to bind to the core of the Q Sepharose FF bead even for the best-case scenario where the beads were fouled for 5 minutes. In both cases, BSA was predominantly only able to bind ~ 10 μm into the bead even after 180 minutes of incubation. This is similar to the BSA adsorption pattern for beads exposed to foulant for 12 hours (Figure 6-12). Beads that were fouled for 5 minutes and those for 1 hour had similar binding capacities, which were 2.5-fold less than that of fresh beads (Table 6-1). However, the amount of BSA bound when fouled for 12 hours was 6-fold less than when the beads were fouled for 5 minutes or 1 hour (Table 6-1). The results suggest that even a relatively short exposure time of the beads to foulant can cause a significant, immediate decrease in their capacity. Any

further reduction in capacity only occurs when the beads are fouled for a significantly longer time. This result may indicate that components in the foulant stream impact the binding capacity at two different rates – presumably by virtue of size and diffusional limitations.

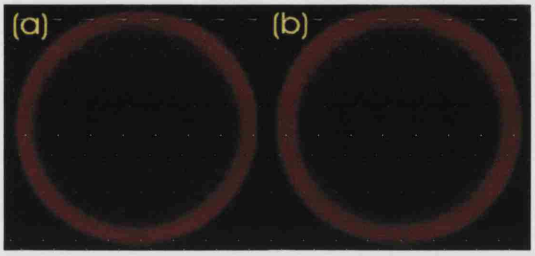

Figure 6-19: *Effect of fouling time on the uptake of BSA to Q Sepharose FF. Fresh Q Sepharose FF beads were fouled by incubating in partially clarified E. coli homogenate for (a) 5 minutes and (b) 1 hour. 2 mg/mL BSA-Cy5.5 (red) (labelling ratio = 1:20) was incubated with 0.25 mL of fouled Q Sepharose FF in 20 mM Tris-HCl, pH 8.0 with mixing. The above images were taken after 180 minutes of incubation with the BSA solution.*

The foulant contact time does affect the subsequent maximum adsorption rate of BSA (Table 6-1) with an increase in the contact time causing a decrease in the initial adsorption rate. It may be speculated that certain fouling species, possibly lipids and nucleic acids, may reduce the diffusivity of BSA and these fouling species may build up over time.

6.3.4 Fouling of a chromatographic matrix in a packed flow cell

6.3.4.1 Homogeneity of adsorption

Foulant, buffers and BSA solution were loaded onto the packed flow cell at a flow rate of 150 cm/h which is typical for Q Sepharose FF (Amersham Biosciences, 1999). The mini-bed had a total bed length of 2.2 cm, giving a residence time of less than 1 minute when compared to conventional chromatographic columns, and the

"window" for viewing under the microscope only allowed observations around the axial centre of the unit.

It is expected that the bead surface facing the loading front may initially see a higher concentration of adsorbent. However, this was not seen during the confocal studies, and the adsorption profile was relatively homogenous throughout the adsorption process for the conditions used. Interestingly, the effect of contact between neighbouring beads within the tightly packed bed did restrict adsorption close to the contact spots. This was seen for both protein and dsDNA as clearly shown in Figure 6-20. Hubbach et al. (2002) also noticed this affect during the adsorption of BSA and β-Lactoglobulin to a packed bed of SP Sepharose beads. They confirmed that the restricted transport in these areas leads not only to restriction in protein transport but also to a lower total amount of protein being adsorbed. This restricted transport was more pronounced early during adsorption causing visible dead zones but the intensity variation became less significant as the adsorption progressed. Dead zones were, as expected, not seen during finite bath experiments (cf. Section 6.3.3).

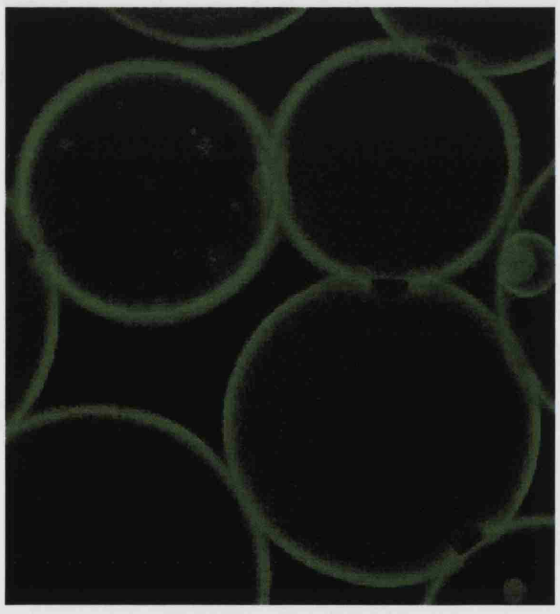

***Figure 6-20**: Dead zones of restricted transport at contact points between beads in a packed bed. A packed bed of Q Sepharose FF was fouled with 5 CVs of partially clarified E. coli homogenate. The dsDNA in the foulant was labelled with PicoGreen.*

6.3.4.2 Fresh Q Sepharose FF bed

The adsorption of 2 mg/mL BSA to a single Q Sepharose FF bead in a packed bed is illustrated in Figure 6-21a, and provides a basis for comparison. Classical shrinking core behaviour, as described by a number of authors (Brauch and Schlunder, 1975; Ruthven, 1984; Teo and Ruthven, 1986; Weaver and Carta, 1996), was observed. This finding is in agreement with the adsorption pattern found in the finite bath experiments (cf. Section 6.3.3.2). The shrinking core pattern for the adsorption of BSA to the cation exchanger, SP Sepharose FF, was first visualised by Linden et al. (1999) and subsequently by Linden et al. (2000) and Hubbach et al. (2002).

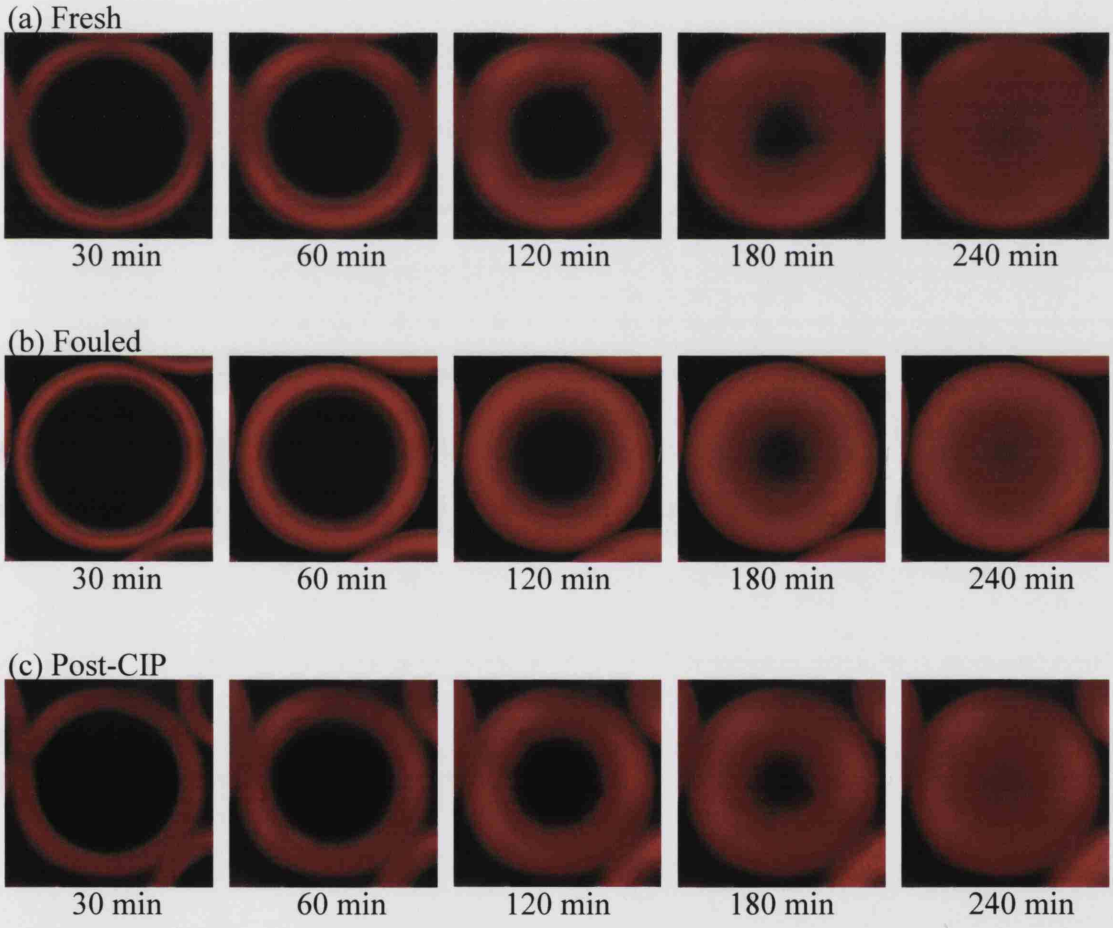

***Figure 6-21**: Adsorption of BSA to fresh, fouled and CIP-treated beds. The beds were packed with Q Sepharose FF and BSA (2mg/mL) was loaded onto the beds at a flow rate of 150 cm/h. (a) fresh bed; (b) bed fouled with 5 CVs of partially clarified E. coli homogenate; (c) fouled bed that was subsequently cleaned with 15 CVs of 1 NaCl followed by 15 CVs of 1 M NaOH.*

Translation of the confocal images to fluorescence intensity profiles over the particle diameter, as shown in Figure 6-22, shows the expected flattening of the intensity profile over time; although even after 240 minutes of adsorption equilibrium was not completely achieved as indicated by the unsaturated bead core.

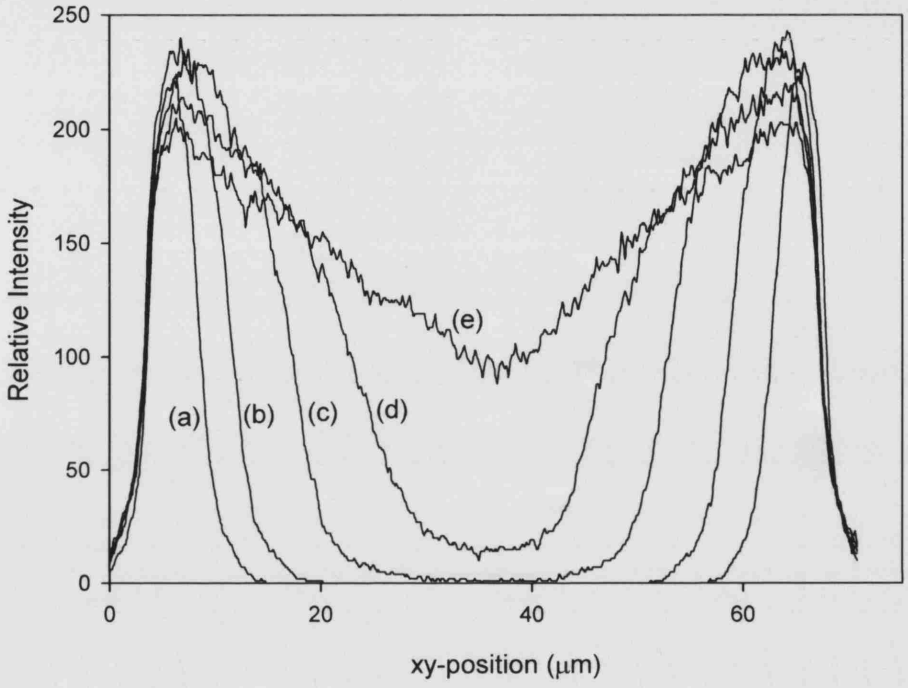

***Figure 6-22**: Fluorescence intensity profiles for the adsorption of BSA to a fresh bed. The bed was packed with Q Sepharose FF and BSA (2mg/mL) was loaded onto the bed at a flow rate of 150 cm/h. The profiles show the fluorescence intensity of BSA across the bead diameter through the bead centre over time. (a) 30 min; (b) 60 min; (c) 120 min; (d) 180 min; (e) 240 min.*

6.3.4.3 Fouling of the packed bed

Q Sepharose FF is an anion exchanger with quaternary amine groups carrying a positive charge. Genomic DNA and HCPs (with pI values below 8.0) in the *E. coli* homogenate, used as the foulant challenge, would be expected to act as major fouling species. To investigate this, PicoGreen was used to label fluorescently dsDNA and Cy3 was used to label HCPs in the foulant material before loading 5 column volumes

(CVs) of the material onto the bed. Figure 6-23 (0 min) shows the dsDNA and HCPs distribution within single beads in the bed after fouling. The intensity profiles of the two foulants within the selected bead are shown in Figure 6-24. The results show that dsDNA adsorption only takes place at the bead exterior as a thin layer of approximately 3 μm deep. Similar observations were seen when fouling of the beads with the same fouling material in finite baths (cf. Section 6.3.3.3) and have also been reported for pure solutions of plasmid DNA by Prazeres et al. (1998) and Ljunglof et al. (1999). In contrast, HCPs absorbed virtually evenly throughout the bead as confirmed by a relatively flat intensity profile in Figure 6-24. Severe fouling for a prolonged period of time can cause a non-uniform binding of HCPs as discussed in Section 6.3.3.4. Under those fouling conditions, HCPs did not saturate to the centre of the bead, thus suggesting the presence of other fouling species, other than protein, occupy the core region.

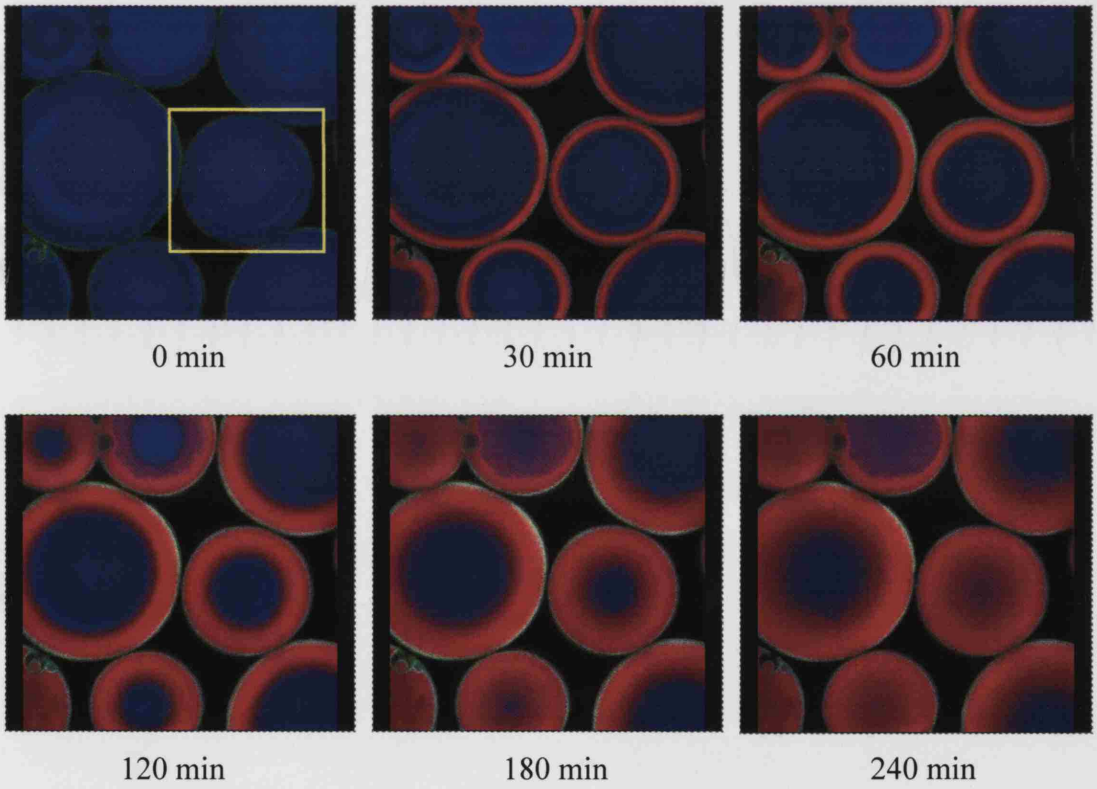

***Figure 6-23**: The adsorption of BSA to Q Sepharose FF beads in a packed bed. A fresh bed was fouled with 5 CVs of partially clarified E. coli homogenate. BSA (2 mg/mL) was subsequently loaded on to the bed at 150 cm/h. dsDNA and HCPs in the foulant were labelled with Pico(Green) and Cy3 (blue), respectively. The bead analysed is highlighted with the yellow box.*

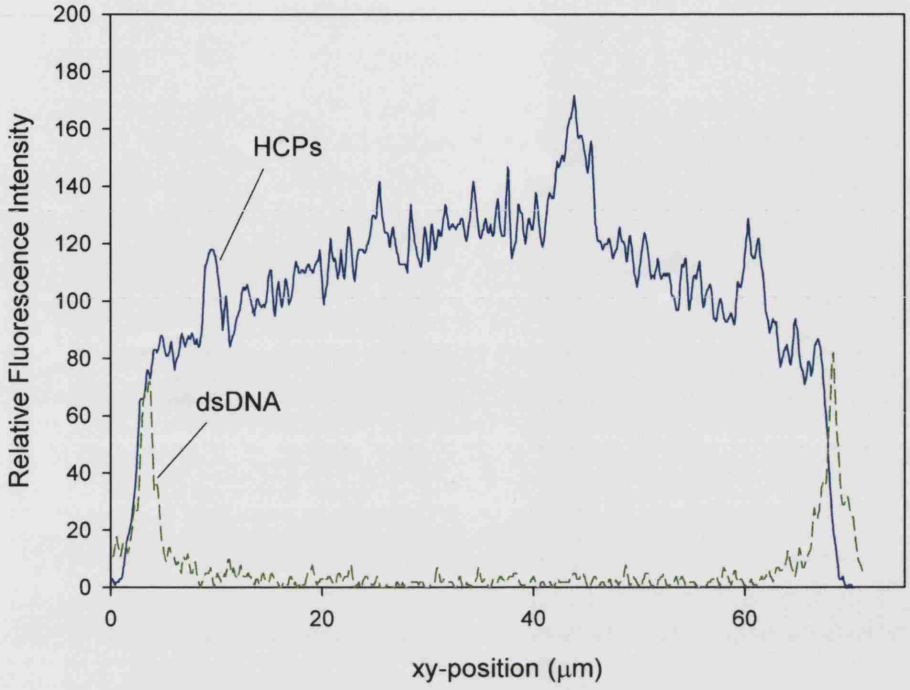

***Figure 6-24**: Fluorescence intensity profiles for beads fouled in a packed bed. A fresh Q Sepharose FF bed was fouled with 5 CVs of partially clarified E. coli homogenate. BSA (2 mg/mL) was subsequently loaded onto the bed at 150 cm/h. dsDNA and HCPs in the foulant were labelled with Pico(Green) and Cy3 (blue), respectively.*

A solution of 2 mg/mL BSA was loaded onto the fouled bed following the same procedure as that for the fresh bed (cf. Section 6.3.4.2). Fouling did not appear to affect the adsorption behaviour as a shrinking core pattern, like that seen in the fresh bed, was observed (Figures 6-21b and 6-25). The images in Figure 6-25 take advantage of the ability of CSLM to detect simultaneously multiple fluorescence emissions. They clearly show that BSA does not occupy the outer layer where dsDNA was bound but penetrates and binds past this outer layer. Even after 240 minutes, BSA does not appear to displace completely the dsDNA layer. This observation is in agreement to that seen in a finite bath (Section 6.3.3.3).

HCPs are a mixture of proteins with different binding affinities for Q Sepharose FF. As expected, BSA partially displaced HCPs as the adsorption front moved towards the bead core; giving rise to a slight "hump" in the intensity profile

(Figure 6-26) but eventually flattening out indicating that the HCPs concentration was relatively constant throughout the bead after 240 minutes. The relative concentration of HCPs in the bead against time is plotted in Figure 6-27, and shows a 50% decrease in HCPs concentration after 240 minutes. Such classical competitive adsorption behaviour is not always seen with protein mixtures. For the competitive adsorption of a pure protein mixture of hIgG and BSA to SP Sepharose FF, hIgG was found more in the centre of the bead while BSA was predominantly bound at the edge (Linden et al. 1999). In our case, HCPs and BSA were both approaching an even distribution throughout the bead.

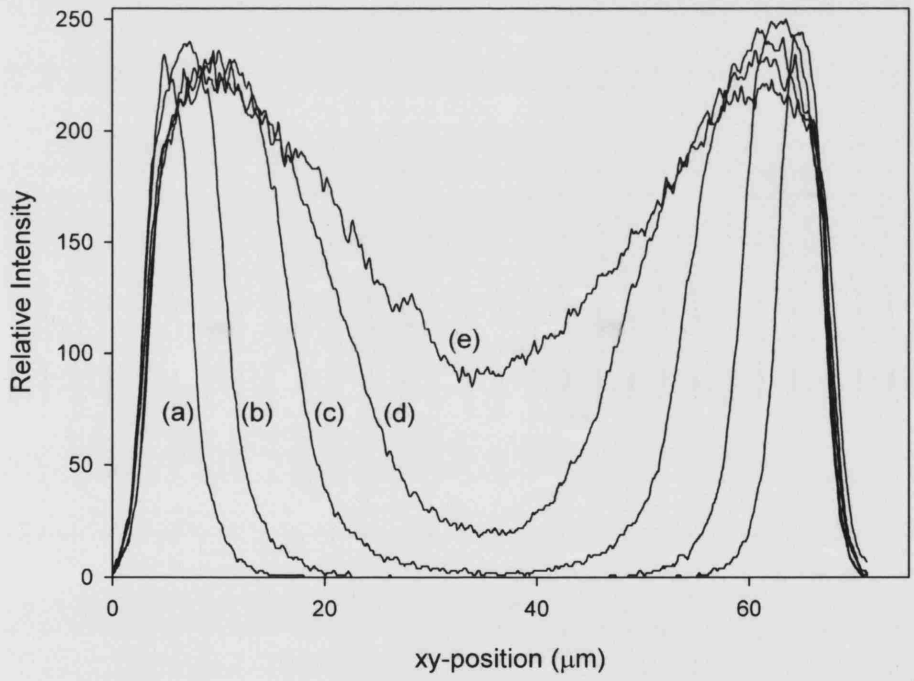

***Figure 6-25**: Fluorescence intensity profiles for the adsorption of BSA to a fouled bed. A fresh Q Sepharose FF bed was fouled with 5 CVs of partially clarified E. coli homogenate. BSA (2 mg/mL) was subsequently loaded onto the bed at 150 cm/h. The profiles show the fluorescence intensity of BSA across the bead diameter through the bead centre over time. (a) 30 min; (b) 60 min; (c) 120 min; (d) 180 min; (e) 240 min.*

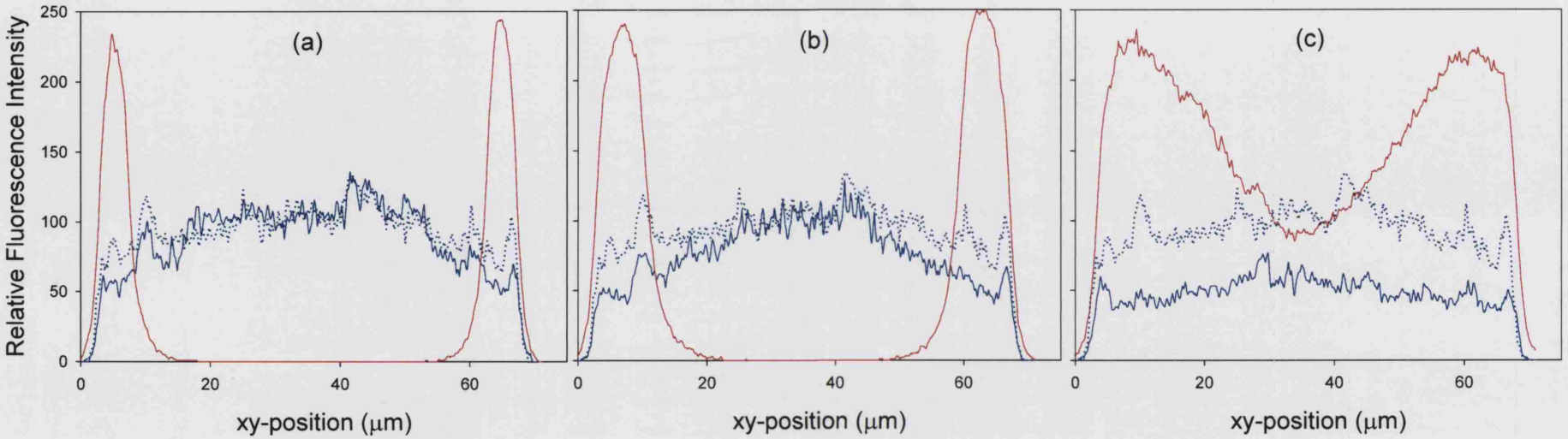

Figure 6-26: *Intensity profiles for BSA and HCPs in a fouled bed. A fresh Q Sepharose FF bed was fouled with 5 CVs of partially clarified E. coli homogenate. BSA (2 mg/mL) was subsequently loaded onto the bed at 150 cm/h. A classical displacement of HCPs is seen over time as the BSA adsorption front moves towards the bead core. (a) 30 min; (b) 60 min, (c) 240 min. (····) HCPs profile at 2 min; (–) HCPs (blue); (–) BSA (red).*

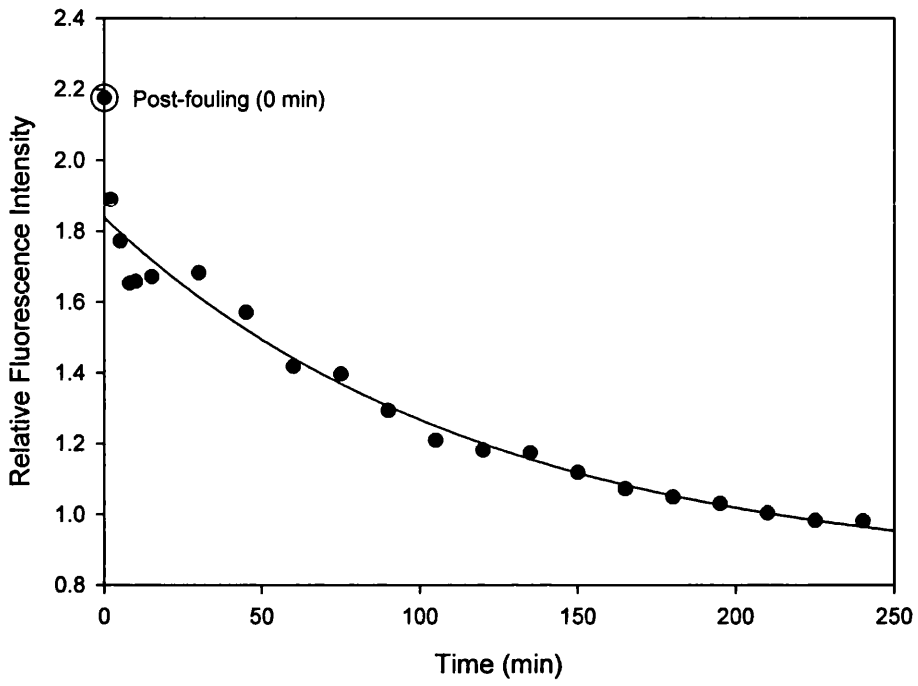

***Figure 6-27**: Reduction of HCPs concentration over time. A fresh Q Sepharose FF bed was fouled with 5 CVs of partially clarified E. coli homogenate. BSA (2 mg/mL) was subsequently loaded onto the bed at 150 cm/h. A classical displacement of HCPs is seen over time as the BSA adsorption front moves towards the bead core.*

6.3.4.4 CIP of fouled bed

The ability to clean a column *in-situ* without the requirement to re-pack is an important consideration for the economics of a process involving packed bed chromatography. For this experiment, a column was fouled with 5 CVs of foulant as in Section 6.3.4.3. The column was then cleaned using 15 CVs of 1 M NaCl followed by 15 CVs of 1 M NaOH, both commonly used in industry. The course of the cleaning was followed using CSLM and is shown in Figure 6-28.

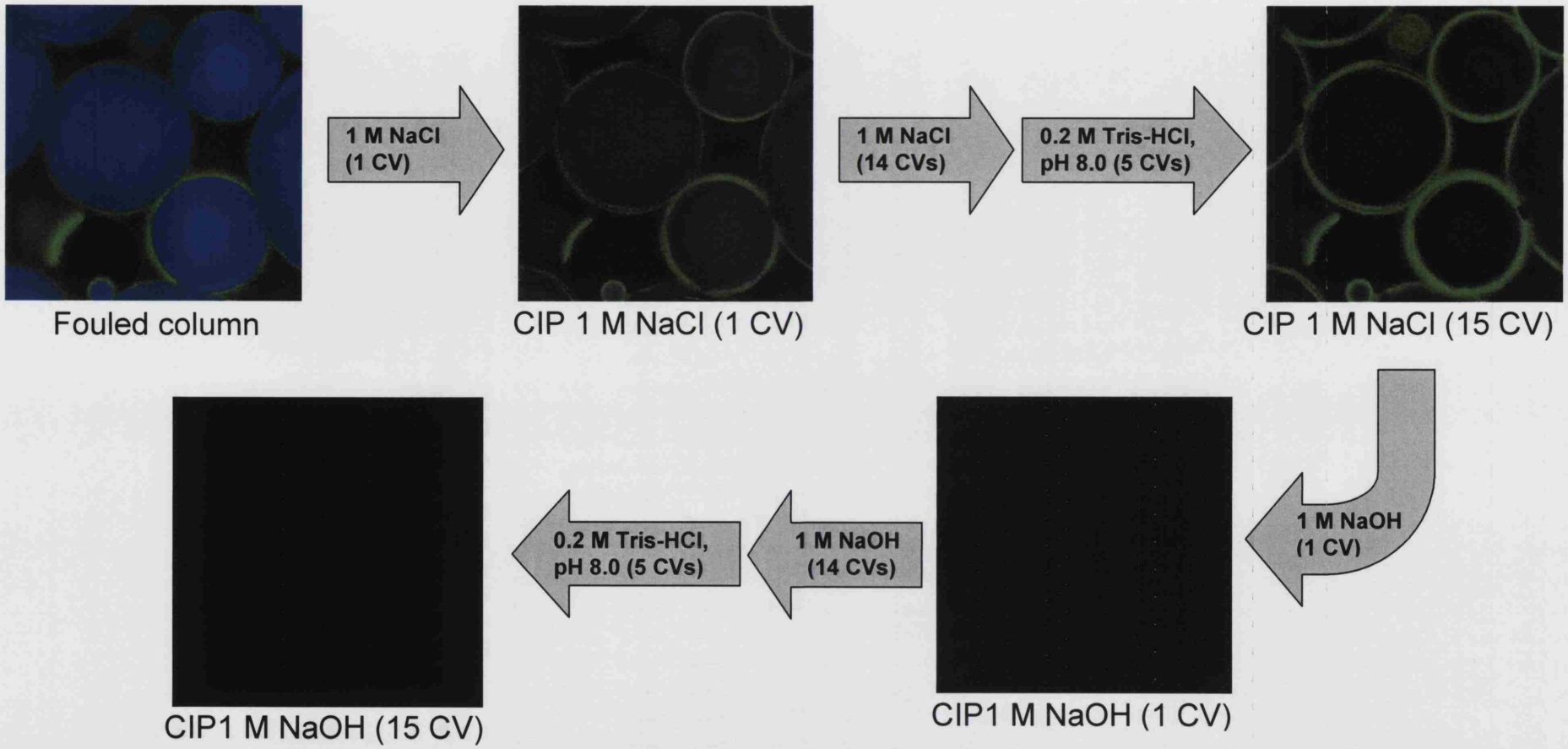

***Figure 6-28**: CIP of a fouled bed. A fresh Q Sepharose FF bed was fouled with 5 CVs of partially clarified E. coli homogenate and then washed with 5 CVs of 20 mM Tris-HCl, pH 8.0. A CIP procedure consisting of 15 CVs of 1 M NaCl (in 20 mM Tris-HCl, pH 8.0) followed by 15 CVs of 1 M NaOH was then performed. dsDNA was labelled with Pico(Green) and HCPs were labelled with Cy5.5 (blue).*

Most of the HCPs appeared to be removed with loading just 1 CV of 1 M NaCl, and only a residual amount remained after 15 CVs. However, even 15 CVs of 1 M NaCl appeared ineffective in removing dsDNA. This is surprising since previous studies in finite baths had shown 1 M NaCl to be effective in removing dsDNA from fouled beads (cf. Section 6.3.3.4). Also Prazeres et al. (1998) have demonstrated that NaCl concentrations of around 0.7 M were able to elute pDNA from small-scale Q Sepharose FF columns loaded with a pure pDNA solution. A combination of the complex fouling nature of realistic process streams combined with the dynamic effects of a packed bed may be responsible for this unexpected observation. A higher concentration of NaCl may be required to remove dsDNA from a fouled packed bed but further studies are required to prove this.

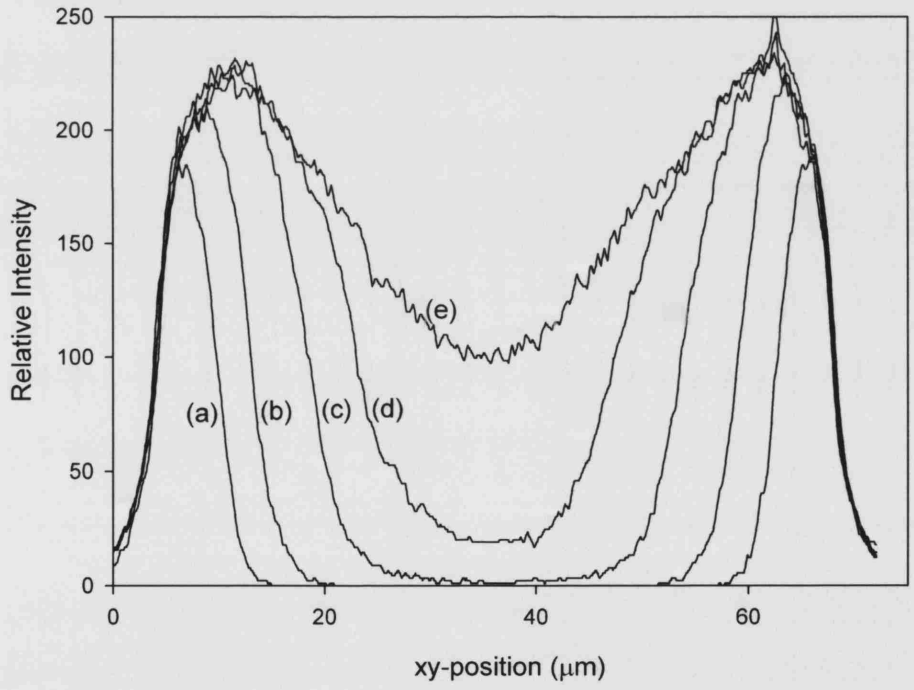

***Figure 6-29**: Fluorescence intensity profiles for the adsorption of BSA to a CIP-treated bed. A fresh Q Sepharose FF bed was fouled with 5 CVs of partially clarified E. coli homogenate. The fouled bed was then cleaned with a 15 CVs of 1 M NaCl followed by 15 CVs of 1 M NaOH. Subsequently, BSA (2 mg/mL) was loaded onto the bed at 150 cm/h. The profiles show the fluorescence intensity of BSA across the bead diameter through the bead centre over time. (a) 30 min; (b) 60 min; (c) 120 min; (d) 180 min; (e) 240 min.*

Subsequently, 1 M NaOH was used to further clean the column and proved to be an effective cleaning agent. All dsDNA and residual HCPs were removed after loading just 1 CV of NaOH. The cleaning was continued for a further 14 CVs to remove any other fouling species such as lipids and lipopolysaccharides etc.

A BSA adsorption time series following the same procedure as that for fresh beads was performed on the CIP-treated bed. The confocal images are shown in Figure 6-21c, and the corresponding fluorescence intensity profiles are shown in Figure 6-29. Shrinking core behaviour similar to that of fresh beads was observed.

6.3.4.5 Comparison of BSA binding capacity

The adsorption curve of BSA to fresh, fouled and CIP-treated beds are displayed in Figure 6-30, and the approximate BSA binding capacities listed in Table 6-7. The binding capacity of Q Sepharose FF was reduced by 20% after fouling. Cleaning the fouled column using 15 CVs of 1 M NaCl followed by 15 CVs of 1 M NaOH proved effective in restoring the capacity of the column to its fresh state.

Bead condition	**D_e (x 10^{-10} cm^2/s)**	**$\left[1+\frac{\varepsilon_p D_p}{k_f R_p}\right]$ (Intercept term)**	**Relative Binding Capacity (arbitrary units)**
Fresh beads	1.5 ± 0.9 (95% C.I.)	1.06 ± 0.1 (95% C.I.)	5 ± 0.5 (95% C.I.)
Fouled beads	1.5	1.03	4
CIP-treated beads	1.4	1.06	5

***Table 6-7** : Comparison of BSA diffusivity and binding capacities for Q Sepharose FF beds subjected to different conditions of fouling and cleaning.*

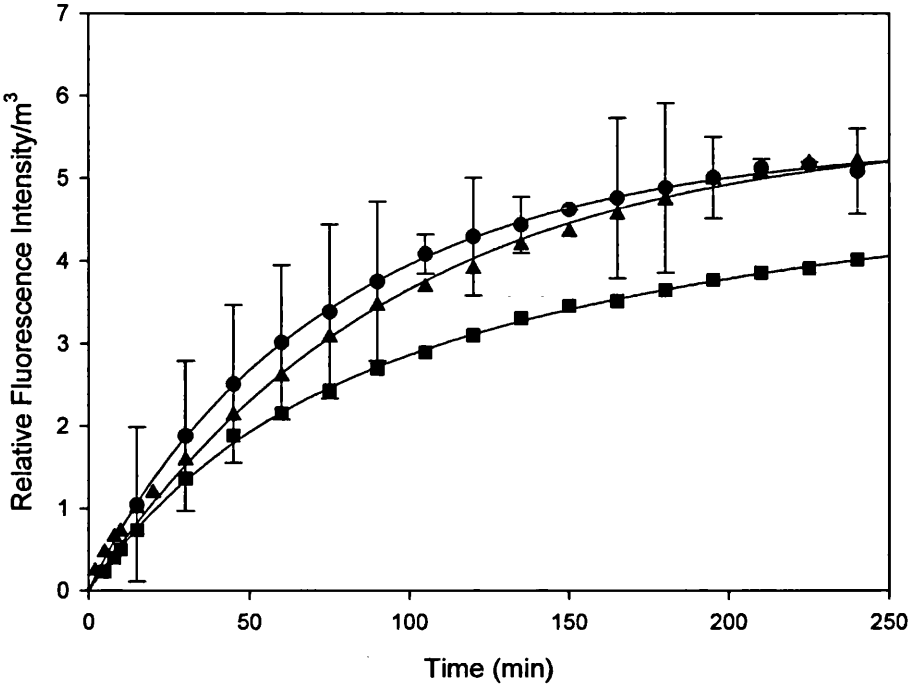

***Figure 6-30**: Comparison of BSA adsorption for different states of Q Sepharose FF beds. A 20% reduction was experienced after fouling. The CIP treatment was effective in regenerating the fouled bed to its fresh state. (●) fresh bed; (■) fouled bed; (▲) fouled bed treated with CIP of 1 M NaCl followed by 1M NaOH. (Error bars show 95% C.I.)*

6.3.4.6 Comparison of BSA uptake rate and effective diffusivity

The confocal images in Figure 6-21 suggest that the shrinking core model may be appropriate for describing the adsorption process in all cases. In all conditions examined, sharp adsorption fronts that gradually moved from the rim of the bead to the centre were seen. A single lumped kinetic parameter or effective diffusivity, D_e, can be estimated directly from the confocal images by assuming that the adsorption layer is saturated. The approach uses the position of the adsorption front and linear regression of the infinite volume solution of the model that takes into account external mass-transfer resistance (Teo and Ruthven, 1986) as shown in equation 6-17.

Figure 6-31 shows the results plotted as I_1/I_2 against $-t/I_2$ for the fresh, fouled and CIP-treated beds. It is evident that for each condition there is a good linear correlation with an intercept value ≥ 1, as required by the mathematical model. The derived D_e and intercept values are listed in Table 6-7. The intercepts of the plots were in all cases close to but greater than unity, suggesting that external mass transfer resistance may be significant but small. The effective diffusivities, D_e, for the three conditions were not significantly different from each other, suggesting that fouling did not have a significant impact on the overall protein mass transfer.

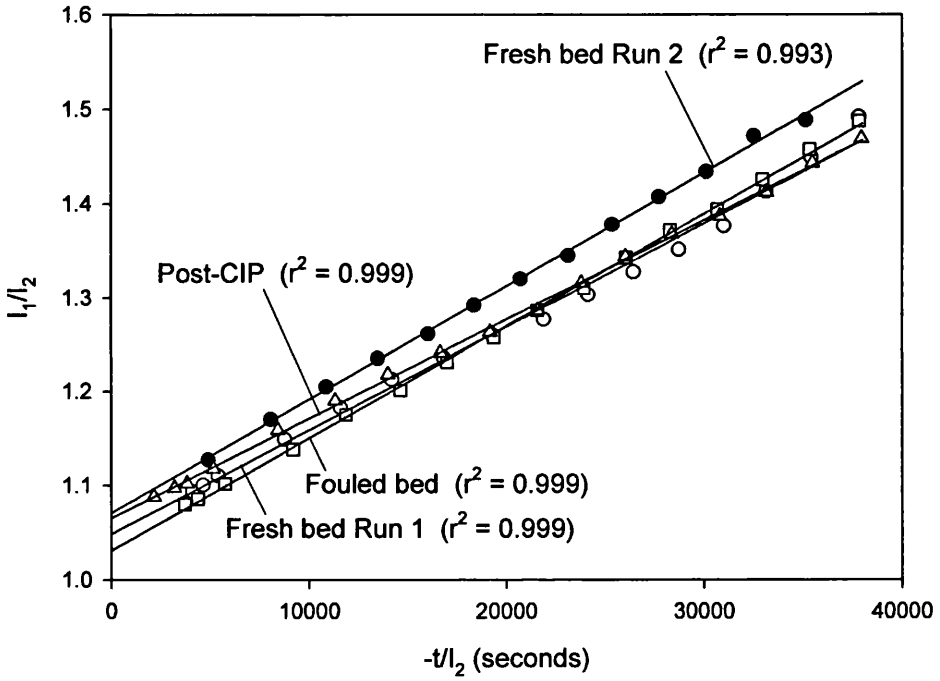

***Figure 6-31**: Plot I_1/I_2 vs. $-t/I_2$ for determining the effective diffusivity. The results show a good linear correlation as required by the mathematical model of shrinking core behaviour of protein adsorption.*

To validate our approach, D_p for fresh beads were calculated using equation 3-6 by using the mean value of D_e determined from Figure 6-31 and assuming values of ε_p (0.55) and q_s (137 mg/mL) taken from Boyer and Hsu (1992) and Section 6.3.1.1, respectively. The intraparticle diffusivity was determined to be 1.9×10^{-8} cm^2/s which is reasonably close to the value of 5.6×10^{-8} cm^2/s quoted by Boyer and Hsu (1992) for

an agarose matrix. This should also be compared to the free diffusivity, D_0, of BSA as reported by Boyer and Hsu (1992) of about 3.6 x 10^{-7} cm^2/s.

6.3.5 Comparison of fouling in finite baths and pack bed columns

Comparing the effects of subjecting beads to the same fouling material for approximately the same contact time in both finite baths and in packed beds has shed light on how the degree of fouling can be affected by the physical and hydrodynamic properties of the packed bed. In the first case, beads were incubated in fouling material for 5 minutes with mixing (cf. Section 6.3.3.6); and in the latter case, 5 CVs of fouling material was loaded to the mini-bed at a flow rate of 150 cm/h giving an exposure time of 4.5 minutes (cf. Section 6.3.4.3). The capacity of the beads fouled in the finite bath was reduced by 60% whereas those fouled in the column only experienced a 20% reduction after fouling. The subsequent BSA adsorption patterns showed even greater differences between the two modes of fouling (Figures 6-19 and 6-21b). In the finite bath, BSA was unable to penetrate into the core of the fouled beads. In contrast, in a packed bed BSA was able to penetrate the bead core and exhibited classical shrinking core adsorption behaviour. Clearly, it has been demonstrated that fouling is more severe for beads in a finite bath than those in a packed bed. Visual inspection of the fouled mini-bed revealed that most of the cell debris in the foulant was trapped near the top of the bed. The top portion of the bead may have acted as a "pre-filter" for the remaining bed length. This observation is consistent with that generally seen during the reverse-flow experiments in Chapter 5. It may be reasonable to suspect that other fouling species may have also bound to this top portion of the bed, so that the beads in the middle and lower bed sections would have been exposed to a lower concentration of fouling materials. In a well-mixed finite bath, the entire surface area of the bead would be exposed to the same concentration of fouling material.

6.3.6 Visualising whole cell- and cell debris-adsorbent interactions

CSLM was used to visualise the adsorption of whole cells and cell debris to an anion exchanger. Q Sepharose FF beads were incubated with freshly thawed, unclarified fermentation broth containing whole *E. coli* cells or cell debris (high-pressure homogenised) in a finite bath. Figure 6-32 shows the competitive adsorption of cell debris and dsDNA to Q Sepharose FF beads. Similar images were obtained with whole cells and dsDNA. As expected, cells/debris bound only to the exterior of the bead. Unlike dsDNA, however, cells/debris did not appear to coat the bead exterior uniformly. Inspection of the images reveals that for both cells and debris the adsorbed layer in the thicker regions was ~ 1 – 2 μm in depth. In the case for cell debris this suggests that there may have been debris-debris interactions resulting in multi-layer adsorption. It is apparent that the bound cells or debris did not exclude dsDNA from binding at the same location.

***Figure 6-32**: Binding of cell debris and dsDNA to Q Sepharose FF beads. Q Sepharose FF beads were incubated in fresh unclarified E. coli homogenate for 1 hour with mixing. Cell debris was labelled with BacLight Red and dsDNA was labelled with PicoGreen. Similar images were obtained with whole cells.*

In all the images obtained, there was a variable but considerable amount of background noise surrounding the beads. This was due to labelled cells or debris in free solution that did not bind to the beads. In order to reduce this background noise

and to distinguish between bound cells/debris from those in free solution, the images were generated by averaging 10 scans per image. An example of this is given in Figure 6-33. Due to the large particle size difference between Q Sepharose FF beads (~ 95 μm diameter) and the cells (~ 1 – 2 μm) or cell debris (< 1 μm), it may have also been possible to remove any unbound cells or cell debris using a filter with an appropriate pore size.

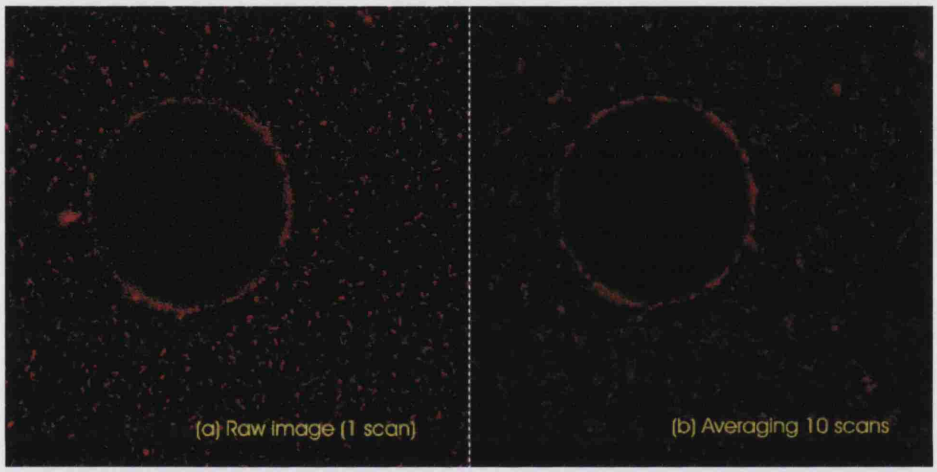

***Figure 6-33**: Effect of averaging 10 scans to reduce background noise. The bead in the two images was incubated in E. coli fermentation broth for 1 hour with mixing. The E. coli cells were labelled with BacLight Red.*

It was found that PicoGreen would label whole cells that were not immediately used after thawing but stored at 4 – 8°C for 24 hours before addition of the dye (results not shown). This may be rationalised by a loss of cell membrane integrity and increased membrane permeability upon aging of the whole cells. Such structural changes are generally seen during apoptosis (Wyllie et al., 1980) and DNA-binding fluorescent dyes such as 7-amino-actinomycin D (7-AAD) are commonly used in flow cytometry to discriminate between dead and live cells (Schmid et al., 1992). PicoGreen did not appear to label cell debris at all. Therefore, it is imperative that fresh whole cells are used when using PicoGreen to label dsDNA in the presence of whole cells.

6.4 CONCLUSIONS

Fouling can have a serious, negative impact on the performance of chromatography and considerable effort is normally spent to prevent fouling species reaching the column, or in developing effective CIP procedures to recover performance after fouling. Conventional approaches to investigate chromatographic fouling by analysing deterioration in column performance (Staby et al., 1998; Shepard et al., 2000; O'Leary et al., 2001; cf. Chapter 4) or changes in the residence time distribution (Fernandez-Lahore et al., 1999) can only provide an overall indication of the state of fouling.

Development of CSLM in the field of chromatography now provides a basis for the direct visualisation of fouling and for potentially providing new insights into the mechanisms of fouling. The method is both quantitative and qualitative, giving not only information on the effect of fouling on capacity and uptake rates but also a direct picture of the spatial distribution of foulants at a single-bead level. This information can be extremely useful in optimising adsorption processes and in designing novel chromatographic matrices.

6.4.1 Finite bath experiments

CSLM has proved to be a simple, effective tool for visualising foulant-adsorbent interactions between Q Sepharose FF and the following foulant types: HCPs, dsDNA, whole cells and cell debris. In the present study, severe fouling of a chromatographic matrix was shown, using CSLM, to have detrimental effects on its capacity and on the subsequent post-challenge BSA uptake rate. Even after cleaning the fouled beads with a harsh CIP treatment of 1 M NaCl dissolved in 1 M NaOH for 1 hour, there was still a substantial reduction in capacity and uptake rate.

There are components in the fouling stream that affect the capacity of the resin. These appear to have a rapid impact on the capacity and prevent protein from binding into the core of the bead. Further deterioration in capacity is seen when the beads are exposed to foulant for a prolonged time. Components in the fouling stream may also

affect the protein adsorption rate which appears to be proportional to the contact time. We conclude that such fouling species may accumulate over time during incubation with foulants, and that this may affect the subsequent diffusion rate of binding target proteins.

6.4.2 Confocal flow cell

A flow cell, similar in design to that used by Hubbach et al. (2002), was successfully used in combination with CSLM to visualise fouling in a packed bed column. This allowed the effect of physical and dynamic effects of a packed bed on the degree of fouling to be investigated.

The confocal images for BSA adsorption confirmed that for fresh, fouled and CIP-treated columns, shrinking core behaviour existed. Subsequently, it was possible to determine a single lumped kinetic parameter or effective diffusivity, D_e, directly from the confocal images using the shrinking core model. Although it is recognised that this approach does not allow the mechanistic discrimination of the intrinsic mass transfers parameters (D_p, K_f and ε_p), it may be useful for comparisons when combined with the confocal images.

Fouling under the conditions examined, caused a 20% reduction in capacity when compared to a fresh column. However, the effective diffusivity of the test protein, BSA, did not appear to be affected by the fouling conditions. Sequential CIP using 15CVs of 1 M NaCl then 15 CVs of 1 M NaOH was shown to be effective in removing any dsDNA and HCPs. Subsequent testing using BSA showed that such a cleaning regime successfully restored the column capacity to its fresh state. 15 CVs of 1 M NaCl alone was ineffective in removing dsDNA but did substantially remove HCPs.

The mode of the chromatographic adsorption (i.e. finite bath verses packed bed) can influence the extent of fouling. Comparing the effects of fouling in the two different modes has shown that fouling is less severe for beads in a packed bed. This may be due to the top portion of the packed bed acting as a "pre-filter for the remaining bed length.

6.4.3 Visualising whole cell- and cell debris-adsorbent interactions

The adsorption of whole cells and cell debris to Q Sepharose FF beads in finite baths were successfully visualised using CSLM. This has never been reported previously. The images reveal that, like dsDNA, cells/debris adsorbed only to the exterior of the bead, but do not bind to the bead surface uniformly. Debris-debris interactions may have also occurred causing multi-layer debris adsorption at certain regions on the bead surface. CSLM has proved to be a simple yet effective tool for visualising cell-adsorbent interactions.

The next section of this thesis provides an overall conclusion and describes the limitations of the three independent approaches for evaluating chromatographic fouling.

7 OVERALL CONCLUSIONS

Fouling was examined at three different levels: whole-column, intra-column and single-bead level. Each level provided unique insights into the effects and likely mechanisms of fouling.

7.1 FRONTAL ANALYSIS (CHAPTER 4)

Frontal analysis was used to determine the effects of fouling on a packed bed in terms of changes in capacity and underlying mass transfer properties. The impact of fouling was found to be dependent on the mode of application of the fouling stream but only when it contained solid particulates. When the column was challenged with particulate-free yeast homogenate, prepared by ultracentrifugation, there was only a small change in column capacity compared to the fresh column, regardless of how the material was applied to the column.

Interestingly, repeated loading of small quantities of poorly clarified yeast homogenate caused a gradual increase in binding capacity over the number of loading cycles. This was attributed to hydrophobic interaction between the cell debris in the fouling material and the test protein. Binding of proteins to yeast cell debris was also observed by Shaeiwitz et al. (1989) but through electrostatic interactions in their case.

Frontal analysis is a simple technique that can give quantitative information on the capacity and qualitative information on the change in the underlying mass transfer properties after fouling. Quantitative analysis of the change in mass transfer properties is a difficult task as discussed in Chapter 2 and requires a greater understanding of the underlying mechanism. This is where the techniques of reverse-flow (cf. Chapter 5) and confocal microscopy (cf. Chapter 6) may prove useful.

7.2 EXTENDED REVERSE-FLOW TECHNIQUE (CHAPTER 5)

The reverse-flow technique was shown to be effective in quantifying the band broadening effects of fouling within a packed bed column. By using the technique, band broadening due to macroscopic factors was distinguished from that due to microscopic factors. Furthermore, the reverse-flow technique enables the extent of microscopic band broadening within a packed bed to be assessed as a function of the axial position.

Both macroscopic and microscopic band broadening are significant before and after column fouling, and both increase significantly after fouling. As expected, the extent of microscopic band broadening was most severe at the very top of the packed bed. In fact, the top 1.25 cm of a 7.5 cm bed was shown to account for 33% of the total microscopic band broadening after fouling.

The header design of the column appeared to have a great influence on the degree of microscopic dispersion after fouling. Quantitative information on header design is scarce with only a few reports in the literature (Yuan et al., 1999; Shalliker et al., 1999 and 2000a). Certainly, the impact of header design on fouling effects might warrant further research.

The reverse-flow technique does have its limitations. It requires reversing the flow direction of the mobile phase. In essence, the column will be subjected to backwashing. If the column is not normally subjected to backwashing during its normal operation then this may change the fouling conditions in the column when performing the reverse-flow test. Beneficially, backwashing with water appeared to only marginally change the total dispersive effects (cf. section 5.3.3). Having to reverse the flow also prevents this technique to be used for testing columns that contain a buffer head space between the top of the bed and the column header (top adaptor). The top adapter must be fitted tightly against the top of the bed which is, however, standard practice in well-packed columns.

In addition, the reverse-flow technique can only quantify microscopic dispersion within a packed bed. Quantifying the macroscopic dispersion within a bed will require more complex methods (cf. Section 5.1.1). Also, this technique only

allows examination of microscopic dispersion in the axial direction along the bed length but not in the radial direction (across the bed diameter). Shalliker et al. (2003) developed a method using the refractive index to visualise the axial and radial diffusion of a band of iodine in a chromatographic column. However, the technique was only demonstrated for columns in their fresh, non-fouled state and seems unlikely to provide a simple, widely-applicable test for studying the dispersive effects in process-fouled columns.

Finally, the reverse-flow technique can not provide any information on the binding capacity of the column. This is in contrast to the frontal analysis method as described in Chapter 4 and to the use of confocal scanning laser microscopy as described in Chapter 6.

Despite these limitations, the reverse-flow technique proved to be an effective, widely-applicable test that can distinguish between macroscopic and microscopic dispersion within a packed-bed column. It provided valuable insights to the mechanism of fouling which was discussed in Chapter 5.

7.3 CONFOCAL SCANNING LASER MICROSCOPY (CHAPTER 6)

Confocal microscopy permits even greater insights into the mechanism of fouling than the two above-mentioned techniques by allowing direct visualisation of the spatial distribution of fouling species at the single-bead level and has the potential for visualisation of the foulant distribution within packed bed structures. The foulant-matrix interactions between foulant protein, dsDNA and whole cells/debris were visualised by CSLM, and the effectiveness of CIP procedures were evaluated. Furthermore, the adsorption of BSA to the chromatographic beads pre- and post-fouling provided a quantitative means of evaluating the degree of fouling.

Physical and hydrodynamic properties of the system have been shown to influence fouling. Experiments were conducted in both finite bath and packed bed modes. In general, fouling was more severe in a finite bath than in a packed bed. Also, CSLM revealed the presence of restricted protein and dsDNA adsorption close to

bead-to-bead contact spots in a packed bed. There was also a difference in the ability of a high salt wash to remove dsDNA between the two modes.

However, visualisation by CSLM can not be used to examine *in situ* a chromatography column, unlike frontal analysis and the use of the reverse-flow technique. With CSLM, fouling must be studied off-line in a finite bath or in a flow cell.

The dynamics of the packing structure in the flow cell may not exactly reflect that of a packed bed column. Hubbach et al. (2002) found a significantly lower dynamic capacity and shallower breakthrough in the flow cell when compared to conventional chromatography columns but stated that measured adsorption profiles or mass transfer rates should be independent of the hydrodynamic conditions outside the bead assuming intra-particle mass transfer control. Despite this, the packing dynamics may affect fouling as shown in the results of Chapter 6.

Another limitation of using CSLM to visualise fouling in a packed bed is due to the design of the flow cell. The "window" for viewing under the microscope only allows observations around the axial centre of the unit. As confirmed using the reverse-flow technique in Chapters 5, fouling effects are most severe at the top of the packed bed. New designs of appropriate flow cells are required and this is recommended in Chapter 8 as future work.

Lastly, the different foulant types that can be visualised by CSLM are limited by the availability of appropriate fluorescent dyes. The dyes must label specifically the foulant type of interest and must not affect the adsorption process of the foulant to the chromatographic matrix. A vast selection of fluorescent dyes is already commercially available (Haughland, 2002) but as CSLM gains importance in chromatography research, increasingly more dyes that are appropriate should become available. In contrast, performing frontal analysis and the reverse-flow method require only commonly available materials which are less expensive.

7.4 FINAL REMARKS

It is hoped that the work in this thesis has laid the groundwork for studying chromatographic fouling. The focus has been to develop and demonstrate practical, systematic techniques that can be used to evaluate the effects of fouling regardless of column scale and that can be easily implemented in industrial situations.

While developing these techniques, valuable insights into the mechanisms of fouling have been gained. It is hoped that the techniques will be further improved and will allow investigation of other fouling scenarios. Ultimately, to model mathematically the effects of fouling in an accurate fashion requires a deeper understanding of underlying physical and chemical mechanisms.

The work in this thesis is just one step towards tackling the important problem of chromatographic fouling which is often encountered in process chromatography but is rarely studied.

8 RECOMMENDATIONS FOR FUTURE WORK

The techniques examined in this thesis can be used to investigate a multitude of fouling phenomena. Suggestions of possible future work which will seek to develop the techniques further and to extend the knowledge of fouling are given below.

As previously mentioned, fouling over hundreds of cycles as typically seen in real chromatographic operations was not examined as it was impractical given the time constraints of a PhD. Consequently, the effect of CIP was studied for only one cycle and may not truly reveal the long-term impact of the CIP procedure. The techniques developed in this thesis could be applied to real chromatographic process that had been subjected to numerous loading cycles, and it would be interesting to compare the obtained results with those in this thesis.

Throughout the work of this thesis realistic process material was used to foul the chromatographic matrix. This allowed any complex interactions between foulants to be generated and observed. However, it may also be interesting to isolate the fouling effects of individual foulant types. An attempt to isolate the contribution of solid particulates to the overall fouling effect was carried out in the work of Chapter 4 (frontal analysis). Solids were removed from the complex feed stream using ultracentrifugation. Alternatively, feed material of a defined foulant composition could be prepared and used to foul the chromatographic matrix. Evaluation of the fouling effects could then be done with the reverse-flow method (cf. Chapter 5) or CSLM (cf. Chapter 6) which should provide more information than by frontal analysis alone.

The reverse-flow technique was demonstrated at laboratory-scale. The technique is simple and non-destructive making it applicable even to large-scale columns. Commercially available chromatography liquid-handling systems, which are used in conjunction with large-scale columns, are capable of controlling fluid flow direction; and modern data acquisition systems that allow real-time monitoring and peak analysis are commonly available. Despite this, large-scale verification of the effectiveness of the reverse-flow technique should be done to expose any unforeseen scale-dependent difficulties in applying the technique.

Development of CSLM to visualise fouling (cf. Chapter 6), allowed the chromatographic adsorption of protein, dsDNA, whole cells and cell debris to be visualised. Other foulant types commonly found in the feed material to columns, e.g., lipids and metals ions, may possibly be visualised and their fouling behaviour analysed. For example, Caudron et al. (2005) used 1,6-dipheneyl-1,3,5-hexatriene (DPH) (Molecular Probes – Invitrogen, Eugene, USA) to label various lipid classes for post-column fluorescence detection in liquid chromatography. A comprehensive search to find suitable dyes to specifically label other foulant types would be required.

Finally, the design of the flow cell used in conjunction with CSLM (cf. Chapter 6) must be modified so that all sections along the mini-bed can be viewed under the confocal microscope. This is practically possible but will, of course, require more sophisticated construction. The material of construction should preferably be resistant to strong base and, unlike Perspex, resistant to alcohol since these are commonly used for CIP or storage. A suggestion of such a material with these properties is glass. Furthermore, the physical and hydrodynamic properties of the packed bed in the flow cell should be thoroughly characterised and compared to that of conventional columns, in order to be able to translate the results obtained using the flow cell to that in the conventional columns.

APPENDIX

ADDITIVITY OF MOMENTS

Consider two systems in series with a sharp tracer pulse applied to the first component of the system at time zero. The response functions are defined as h_1 and h_2 for the two components, respectively. The output from the first system becomes the input for the second system. The behaviour of both systems is linear in concentration (each described by the diffusion equation with diffusivity and velocity independent of concentration) and both systems have a constant flow rate, Q. The outlet concentration from the second system can then be expressed as equation A-1:

$$c(t) = \int_0^t h_1(t-\tau)h_2(\tau)d\tau \equiv h_1 \cdot h_2 \qquad \text{(A-1)}$$

In other words, the exit concentration is the sum of the differential inputs from the first system. Furthermore, the distribution of such pulses in time is given by $h_1(t)$.

Taking the Fourier transform of equation A-1 and its moments, equation A-2 is obtained:

$$\frac{M_1}{M'_2} = \langle t^2 \rangle = \frac{\int_{-\infty}^{\infty} t^2 f(t)}{\int_{-\infty}^{\infty} f(t)} = \frac{F''(0)}{4\pi^2 F(0)} \qquad \text{(A-2)}$$

where F(*s*) is the Fourier transform of f(t) and the single and double prime are the first and second order derivatives with respect to s. It then follows that,

$$M_2 = \int_{-\infty}^{\infty} t^2 c(t)dt = \int_{-\infty}^{\infty} t^2 (h_1 h_2)dt = \frac{(H_1 H_2)''\big|_{s=0}}{4\pi^2} \qquad \text{(A-3)}$$

where $H_i(s)$ is the Fourier transform of $h_i(t)$ and

$$(H_1 H_2)'' = H_1'' H_2 + 2H_1' H_2' + H_1 H_2'' \qquad \text{(A-4)}$$

It follows that,

$$M_2(h_1h_2) = M_2(h_1) + M_2(h_2) - \frac{2H_1'(0)H_2'(0)}{4\pi^2 H_1(0)H_2(0)} M_1(h_1h_2) \qquad \text{(A-5)}$$

If the second moment is the variance of the elution peak taken about the mean residence time (first moment), the last term in equation A-5 is zero and simplifies to,

$$\sigma^2_{total} = \sigma^2_1 + \sigma^2_2 \qquad \text{(A-6)}$$

where σ^2 is the second central moment or variance of the distribution. This shows that normalised variances are additive. Reasonably, this may also be extended to any number of systems in series.

CONFOCAL FLOW CELL

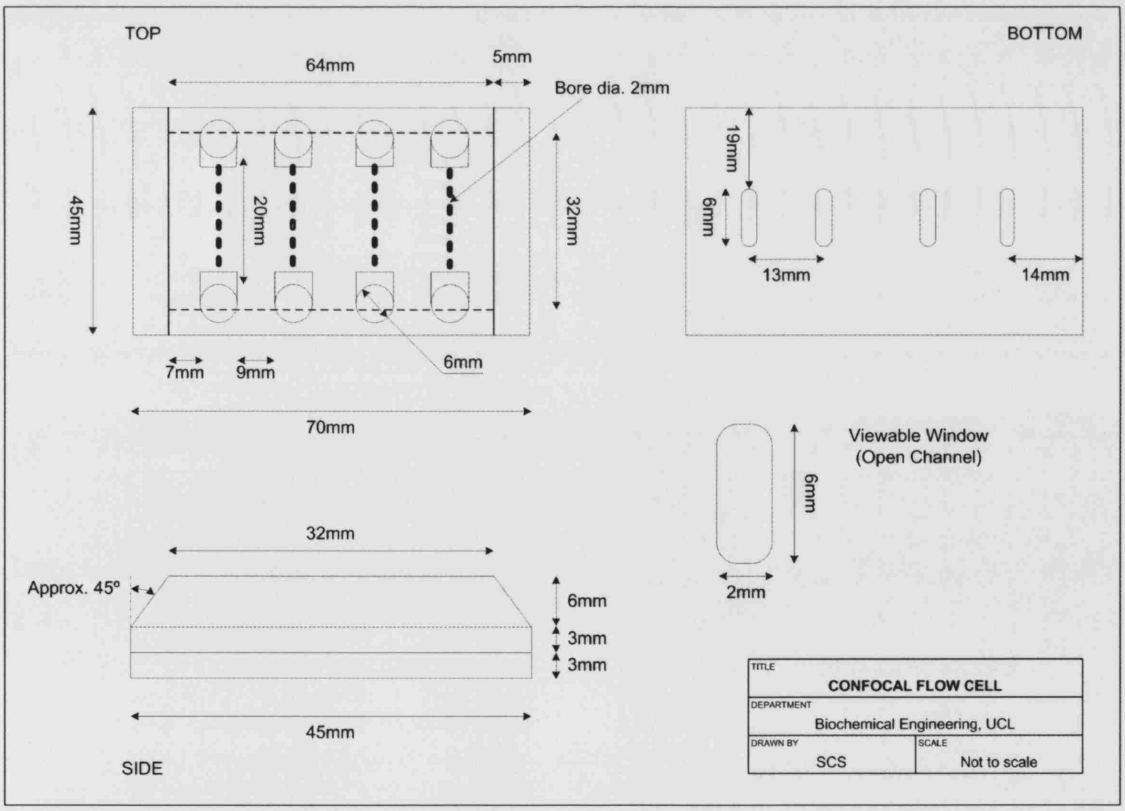

Figure A-1: Schematic diagram of the confocal flow cell.

SYMBOLS AND ABBREVIATIONS

a	constant in polynomial approximation of equation 2-9	-
A	constant in equation 2-9	-
b	constant in polynomial approximation of equation 2-9	-
Bi	Biot number	-
BSA	bovine serum albumin	
C	concentration of solute in fluid phase	$mg.mL^{-1}$
c	concentration of solute in fluid phase	$mg.mL^{-1}$
c_0	inlet solute concentration	$mg.mL^{-1}$
C_0	initial value of c_0	$mg.mL^{-1}$
c_f	concentration of solute in feed	$mg.mL^{-1}$
C.I.	confidence interval	
CIP	clean-in-place	
c_s	concentrations of sorbate in liquid phase at surface of adsorbent particle	$mg.mL^{-1}$
CSLM	confocal scanning laser microscopy	
d	constant in polynomial approximation of equation 2-9	-
D	diffusivity	cm^2s^{-1}
D_e	effective diffusivity of solute	cm^2s^{-1}
D_L	axial dispersion coefficient	cm^2s^{-1}
DNA	deoxyribonucleic acid	
D_0	free diffusivity in bulk fluid phase	cm^2s^{-1}
d_p	diameter of adsorbent particles	m
D_p	pore diffusion coefficient (defined on pore sectional area basis)	cm^2s^{-1}
D_s	effective diffusivity of solute	cm^2s^{-1}
f(X)	time function describing experimental breakthrough	s
FDA	Food and Drug Administration	
g	gravitational constant, g = 9.81 ms^{-1}	$m.s^{-1}$
g(X')	time function describing modelled breakthrough	s
GMP	Good Manufacturing Practice	
H	height-equivalent-to-a-theoretical-plate	m

H_{bed}	height of the theoretical plate for a column bed	m
$H_{diffuion}$	contribution to H by diffusion	m
HETP	height-equivalent-to-a-theoretical-plate	m
H_{flow}	contribution to H by hydrodynamic factors	m
$H_{mass\ transfer}$	contribution to H by mass transfer resistance	m
h_x	response function of system x to a pulse input	-
I_1, I_2	integrals defined in equations 6-12 and 6-13	-
$I_{integr.}$	integral intensity of fluorescence profile	-
I_{seg}	average intensity within a segment	-
I_T	total intensity of bead cross-section at centre	-
K	equal to q_m/c_f, fluid phase volume per solid phase volume	-
k	constant	-
K_d	constant in Langmuir isotherm expression	$mL.mg^{-1}$
k_f	external fluid film mass transfer coefficient	$cm.s^{-1}$
L	bed length	cm
M_n	*n*th absolute moment	-
MW	molecular weight	kDa
N	number of theoretical plates	-
PDA	Parenteral Drug Association	
P_x	pressure at position x	$kg.m^{-2}$
Q	volumetric flow rate	m^3s^{-1}
Q	fractional approach to equilibrium = q/q_s (Section 6.2.1)	-
Q_{rel}	relative capacity	m^{-3}
q	adsorbed-phase concentration averaged over a particle	$mg.mL^{-1}$
q_m	constant in Langmuir isotherm equation	$mg.mL^{-1}$
q_s	saturation adsorbed-phase concentrations (particle volume basis)	$mg.mL^{-1}$
R_D	retardation factor in equation 5-2	-
R	radial coordinate	m
r_a	outer radius of particle shell	m
RCF	relative centrifugal force	-
Re	Reynolds Number	-
R_f	radius of adsorption front	m

r_i	inner radius of particle shell	m
RNA	ribonucleic acid	
r_p	radius of particle	m
R_p	radius of adsorbent particles	μ
S_0	particle surface area per particle volume	cm^2
t	time	s
t_R	retention time	s
t′	value of t at which $X = X_0$	s
u	superficial flow velocity of mobile phase	$cm.s^{-1}$
UCL	University College London	
V	volume of material in ultracentrifuge tubes	m^3
V_m	volume of mobile phase	mL
V_p	particle volume	m^3
V_R	retention volume	mL
V_s	volume of solid phase	mL
X	dimensionless concentration of solute in the fluid phase	-
X_0	value of X corresponding to the centre of gravity of the front	-
X_i	interfacial value of X at solid-fluid boundary	-
Y	dimensionless average concentration of solute in the adsorbent phase	-
Y_i	interfacial value of Y at solid-fluid boundary	-
Z	axial distance measured from bed inlet	cm
β	constant defined by equation 2-7	-
ε	void fraction in bed	-
ε_p	inclusion porosity	-
γ	constant in equations 2-9 and 6-9	-
η	the ratio R_f/R_p	-
Λ	fraction of sorbate initially present in solution which is eventually taken up by adsorbent	-
μ	viscosity of the fluid	$kg.m^{-1}s^{-1}$
μ_1	first absolute moment	s^2 or mL^2
μ_2	second central moment	s^2 or mL^2

ν	superficial flow velocity of mobile phase	ms^{-1}
ρ	density of the fluid	$kg.m^{-3}$
Σ	centrifuge equivalent settling area	m^2
τ	increment in time	s
τ^2_{dead}	extra-column band broadening due to dead volumes	mL^2
τ^2_{elec}	extra-column band broadening due to the finite response rate of electronics	mL^2
σ^2_{bed}	variance due to column bed	mL^2
σ^2_{d}	extra-column band broadening due to the finite sensing volume of the detector	mL^2
σ^2_{ex}	lumped extra-column band broadening	mL^2
σ^2_{header}	variance due to column header	mL^2
σ^2_{i}	variance of the *i*th sub-system	mL^2
σ^2_{L}	variance of the eluted solute concentration profile in column lengths term	mL^2
$\sigma^2_{macro,total}$	variance due to the macroscopic factors	mL^2
σ^2_{micro}	variance due to microscopic factors	mL^2
$\sigma^2_{micro,top}$	variance due to microscopic factors for the top half of the packed bed	mL^2
$\sigma^2_{micro,bottom}$	variance due to microscopic factors for the bottom half of the packed bed	mL^2
σ^2_{s}	extra-column band broadening of the initial injection profile	mL^2
σ^2_{sdf}	variance due to system peripherals (extra-column band broadening) when pulse is run in down-flow mode	mL^2
σ^2_{srdf}	variance due to system peripherals (extra-column band broadening) when pulse is run in reverse-down-flow mode	mL^2
σ^2_{sruf}	variance due to system peripherals (extra-column band broadening) when pulse is run in reverse-up-flow mode	mL^2
σ^2_{suf}	variance due to system peripherals (extra-column band broadening) when pulse is run in up-flow mode	mL^2

σ_t^2	extra-column band broadening due to tubes	mL^2
σ_T^2	variance of the eluted solute concentration profile in time term	mL^2
σ_{tdf}^2	cumulative variance when pulse is run in down-flow mode	mL^2
σ_{total}^2	cumulative variance of all sub-systems	mL^2
σ_{trdf}^2	cumulative variance when pulse is run in reverse-down-flow mode	mL^2
σ_{truf}^2	cumulative variance when pulse is run in reverse-up-flow mode	mL^2
σ_{tuf}^2	cumulative variance when pulse is run in up-flow mode	mL^2
σ_V^2	variance of the eluted solute concentration profile in volume term	mL^2

REFERENCES

Aguilera Soriano, G. (1995) "An engineering study of compression and fouling of chromatographic matrices" PhD Thesis. University of London, UK.

Aguilera Soriano, G., Titchener-Hooker, N. J., and Ayazi Shamlou, P. (1997) "The effects of processing scale on the pressure drop of compressible gel supports in liquid chromatographic columns" *Bioprocess Eng.* 17: 115-119.

Ahmed, M. and Pyle, D. L. (1999) "Investigation of single protein adsorption on ion exchangers using confocal laser scanning microscopy" *J.Chem.Technol.Biotechnol.* 74: 193-198.

Amersham Biosciences (2004) "Ion Exchange Chromatography & Chromatofocusing. Principles and Methods" Uppsala, Sweden.

Andersson, M., Drevin, I., and Johansson, B.-L. (1993) "Characterization of the chemical and functional stability of DEAE Sepharose fast flow" *Process Biochem.* 28: 223-230.

Anspach, F. B., Curbelo, D., Hartmann, R., Garke, G., and Decker, W.-D. (1999) "Expanded-bed chromatography in primary protein purification" *J.Chromatogr.A* 865: 129-144.

Arnold, F. H., Blanch, H. W., and Wilke, C. R. (1985) "Analysis of affinity separations II: The characterisation of affinity columns by pulse techniques" *Chem.Eng.J.* 30: B25-B36.

Barnfield Frej, A.-K., Hjorth, R., and Hammarstrom, A. (1994) "Pilot scale recovery of recombinant Annexin V from unclarified *Escherichia coli* homogenate using expanded bed adsorption" *Biotechnol.Bioeng.* 44: 922-929.

Batel, R., Jaksic, Z., Bilhari, N., Hamer, B., Fafande, M., Chauvin, H. C., Schroder, H. C., Muller, W. E. G., and Zahn, R. (1999) "A microplate assay for DNA damage determination (fast micromethod) in cell suspensions and solid tissues" *Anal.Biochem.* 270: 195-200.

Bayer, E., Baumeister, E., Tallarek, U., Albert, K., and Guiochon, G. (1995) "NMR imaging of the chromatographic process. Deposition and removal of gadolinium ions on a reversed-phase liquid chromatographic column" *J.Chromatogr.A* 704: 37-44.

Belfort, G., Davies, R. H., and Zydney, A. L. (1994) "The behavior of suspensions and macromolecular solutions in crossflow microfiltration" *J.Membr.Sci.* 96: 1-58.

Billen, J., Gzil, P., Vervoot, N., Baron, G. V., and Desmet, G. (2005) "Influence of the packing heterogeneity on the performance of liquid chromatography supports" *J.Chromatogr.A* 1073: 53-61.

Bird, R. B., Stewart, W. E., and Lightfoot, E. N. (2002) "Transport Phenomena" Wiley, New York, 2nd edition.

Blake, F. C. (1922) "The resistance of packing to flow" *Trans.Inst.Chem.Engrs.* 14: 415-421.

Boyer, P. M. and Hsu, J. T. (1992) "Experimental studies of restricted protein diffusion in an agarose matrix" *AIChE J.* 38: 259-272.

Bradford, M. (1976) "A rapid and sensitive method for the quantification of microgram quantities of protein utilizing the principles of protein dye binding" *Anal.Biochem.* 72: 248-254.

Brauch, V. and Schlunder, E. U. (1975) "The scale-up of activated carbon columns for water purification based on results from batch tests-II: theoretical and experimental determination of breakthrough curves in activated carbon columns" *Chem.Eng.Sci.* 30: 539-548.

Breece, T. N., Gilkerson, E., and Schelzer, C. (2002a) "Validation of large-scale chromatographic processes, part 1. Case study of Neuleze capture on Macroprep High-S" *Biopharm* (May): 16-20.

Breece, T. N., Gilkerson, E., and Schelzer, C. (2002b) "Validation of large-scale chromatographic processes, part 2. Results from the case study of Neuleze capture on Macroprep High-S" *Biopharm* (July): 35-42.

Broyles, B. S., Shalliker, R. A., and Guiochon, G. (2000) "Visualization of solute migration in chromatographic columns. Quantitation of the concentration in a migrating zone" *J.Chromatogr.A* 867: 71-92.

Caudron, E., Zhou, J. Y., Chaminade, P., Baillet, A., and Prognon, P. (2005) "Fluorescence probe assisted post-column detection for lipid analysis in microbore-LC" *J.Chromatogr.A* 1072: 149-157.

Chase, H. A. (1984) "Prediction of the performance of preparative affinity chromatography" *J.Chromatogr.A* 297: 179-202.

Chase, H. A. and Draeger, N. M. (1992) "Expanded bed adsorption of proteins using ion-exchangers" *Separation Sci.Technol.* 27: 2021-2039.

Chelser, S. N. and Cram, S. P. (1971) "Effect of peak sensing and random noise on the precision and accuracy of statistical moment analysis from digital chromatographic data" *Anal.Chem.* 43: 1922-1933.

Ching, C. B., Uddin, M. S., and Hidajat, K. (1989) "Diffusional kinetics of monoclonal antibody, transferrin and bovine serum albumin on Sephacryl s-200 HR gel" *Chem.Eng.J.* 42: B47-B52.

Colvin Jr., A. E. and Hanley, M. W., US Pat. 4894152 (1990).

Cooney, D. O. (1990) "Rapid approximate solutions for adsorption bed concentration profile and breakthrough curve behavior: favorable isotherms and both phase resistances important" *Chem.Eng.Comm.* 91: 1-9.

Cooney, D. O. (1993) "Comparison of simple adsorber breakthrough curve method with exact solution" *AIChE J.* 39: 355-358.

Coq, B., Cretier, G., and Rocca, J. L. (1979) "End-effects and band spreading in liquid column chromatography" *J.Chromatogr.* 178: 41-61.

Cram, S. P. and Glenn, T. H. (1975) "Instrumental contributions to band broadening in gas chromatography" *J.Chromatogr.* 112: 329-341.

Davies, P. A. and Bellhouse, B. J. (1989) "Permeability of beds of agarose-based particles" *Chem.Eng.Sci.* 44: 452-455.

Dedrick, R. L. and Beckmann, R. B. (1967) "Kinetics of adsorption by activated carbon from dilute aqueous solution" *Chem.Eng.Prog., Symp.Ser.* 63: 68-78.

Diogo, M. M., Queiro, J. A., and Prazeres, D. M. F. (2005) "Chromatography of plasmid DNA" *J.Chromatogr.A* 1069: 3-22.

Doig, S. D., Lisa, M., O'Sullivan, M., Patel, S., Ward, J. M., and Woodley, J. M. (2001) "Large scale production of cyclohexanone monooxygenase from *Escherichia coli* TOP10 pQR239" *Enzyme Microb.Technol.* 28: 265-274.

Dose, E. V. and Guiochon, G. (1990) "Effects of extracolumn convolution on preparative chromatographic peak shapes" *Anal.Chem.* 62: 1723-1730.

Dyson, N. (1998) "Chromatographic integration methods" The Royal Society of Chemistry, Cambridge, 2nd edition.

Dziennik, S. R. and Lenhoff, A M. (1999) "Use of confocal microscopy to resolve protein transport mechanisms in chromatographic particles" *AIChE meeting*, Dallas, paper 22b.

Dziennik, S. R. and Lenhoff, A M. (2000) "Use of confocal microscopy to resolve protein transport mechanisms in chromatographic particles" *PREP 2000*, Washington, DC, paper L-302.

Dziennik, S. R., Belcher, E. B., Barker, G. A., DeBergalis, M. J., Fernandez, S. E., and Lenhoff, A M. (2002) "Nondiffusive mechanisms enhance protein uptake rates in ion exchange particles" *PNAS* 100: 420-425.

Farkas, T., Chambers, J. Q., and Guiochon, G. (1994) "Column efficiency and radial homogeneity in liquid chromatography" *J.Chromatogr.A* 679: 231-245.

Farkas, T., Sepaniak, M. J., and Guiochon, G. (1996) "Column radial homogeneity in high-performance liquid chromatography" *J.Chromatogr.A* 740: 169-181.

Farkas, T., Sepaniak, M. J., and Guiochon, G. (1997) "Radial distribution of the flow velocity, efficiency and concentration in a wide HPLC column" *AIChE J.* 43: 1964-1974.

Fernandez-Lahore, H M., Kleef, R., Kula, M.-R. S. R., and Thommes, J. (1999) "The influence of complex biological feedstock on the fluidization and bed stability in expanded bed adsorption" *Biotechnol.Bioeng.* 64: 484-496.

Feuser, J. W., Kula, M.-R., and Thommes, J. (1999) "Cell/adsorbent interactions in expanded bed adsorption of proteins" *Bioseparation* 8: 99-109.

Food and Drug Administration (1987) "Guideline on General Principles of Process Validation" Rockville, Maryland.

Garcia-Arrazola, R., Siu, S. C., Chan, G., Buchanan, I., Doyle, B., Titchener-Hooker, N. J., and Baganz, F. (2005) "Evaluation of a pH-stat feeding strategy on the production and recovery of Fab' fragments from *E. coli*" *Biochem.Eng.J.* 23: 221-230.

Geankoplis, C. J. (2003) "Transport Processes and Unit Operations" Prentice Hall, New Jersey, 3rd edition.

Giddings, J. C. (1965) "Dynamics of Chromatography. Part I: Principles and Theory" Marcel Dekker, New York.

Golshan-Shirazi, S. and Guiochon, G. (1992) "Comparison of the various kinetic models of non-linear chromatography" *J.Chromatogr.A* 603: 1-11.

Grubner, O., Zikanova, A., and Ralek, M. (1967) "Statistical moments theory of gas-solid chromatography. Diffusional controlled kinetics" *J.Chromatogr.* 28: 209-218.

Grubner, O. (1968) "Advances in Chromatography" Marcel Dekker, New York, Vol. 6.

Gu, T. (1995) "Mathematical Modeling and Scale-up of Liquid Chromatography" Springer, Berlin.

Guiochon, G., Shirazi, S. G., and Katti, A. M. (1994) "Fundamentals of Preparative and Nonlinear Chromatography" Academic Press, London.

Guiochon, G., Farkas, T., Guan-Sajonz, H., Koh, J.-H., Sarker, M., Stanley, B. J., and Yun, T. (1997) "Consolidation of particle beds and packing of chromatographic columns" *J.Chromatogr.A* 762: 83-88.

Hammond, P. M. and Scawen, M. D. (1989) "High resolution fractionation of proteins in downstream processing" *J.Biotechnol.* 11: 119-134.

Hand, D. W., Crittendon, J. C., and Thacker, W. E. (1984) "Simplified models for design of fixed-bed adsorption systems" *J.Env.Eng., ASCE* 110: 440-

Hansen, E. and Mollerup, J. (1998) "Application of the two-film theory to the determination of mass transfer coefficients for bovine serum albumin on anion-exchange columns" *J.Chromatogr.A* 827: 259-267.

Haugland, R. P. (2002) "Handbook of Fluorescent Probes and Research Products" Molecular Probes, Inc., 9th edition.

Hearle, D. C. (1997) "An investigation into process related fouling of chromatographic supports" PhD Thesis. University of London, UK.

Heinemann, M., Limper, U., and Buchs, J. (2004) "New insights in the spatially resolved pH measurement in macroscopic large absorbent particles by confocal laser scanning microscopy" *J.Chromatogr.A* 1024: 45-53.

Helfferich, F. G. and Carr, P. W. (1993) "Non-linear waves in chromatography I. Waves, shocks, and shapes" *J.Chromatogr.A* 629: 97-122.

Hochuli, E., Dobeli, H., and Schacher, A. (1987) "New metal chelate adsorbent selective for proteins and peptides containing neighbouring histidine residues" *J.Chromatogr.A* 411: 177-184.

Hofmann, M. (2003) "Use of ultrasound to monitor the packing of large-scale columns, the monitoring of media compression and passage of molecules, such as monoclonal antibodies, through the column bed during chromatography" *J.Chromatogr.A* 989: 79-94.

Horstman, B. J. and Chase, H. A. (1989) "Modelling the affinity adsorption of immunoglobulin G to Protein A immobilized to agarose matrixes" *Chem.Eng.Res.Des.* 67: 243-254.

Hubbach, J., Linden, T., Knieps, E., Thommes, J., and Kula, M-R. (2002) "Dynamics of protein uptake within the adsorbent particle during packed bed chromatography" *Biotechnol.Bioeng.* 80: 359-368.

Huber, J. F. K. and Rizzi, A. (1987) "Influence of the accuracy of the extra-column peak-width determination on the verification of theoretical plate-height equations" *J.Chromatogr.* 384: 337-348.

Hunter, A. K. and Carta, G. (2000) "Protein adsorption on novel acrylamido-based polymeric ion exchanger. II. Adsorption rates and column behavior" *J.Chromatogr.A* 897: 81-97.

Ilg, M., Maier-Rosenkranz, J., Muller, W., and Bayer, E. (1990) "Magnetic resonance imaging in reversed-phase liquid chromatography" *J.Chromatogr.A* 517: 263-268.

Jonsson, A. S. (1987) "Dispersion and Peak Shapes in Chromatography" in: "Chromatographic Theory and Basic Principles" Jonsson, A. S. (ed.), Marcel Dekker, Inc., New York, Chapter 2, pp. 27-102.

Joseph, T., Pearson, A. J., Adams, R. C., and Swift, O. A., US Pat. 5324426 (1994).

Joustra, M. K., Emneus, A., and Tibbling, P. (1967) "Large-scale gel filtration" *Protides Biol.Fluids* 15: 575-579.

Jungbauer, A. (1993) "Preparative chromatography of biomolecules" *J.Chromatogr.A* 639: 3-16.

Jungbauer, A. and Letter, H. P., US Pat. 5423982 (1995).

Kaezmarski, K., Mazzotti, M., Storti, G., and Morbidelli, M. (1997) "Modeling fixed-bed adsorption columns through orthogonal collocations on moving finite elements" *Com.Chem.Engng.* 21: 641-660.

Kaltenbrunner, O., Jungbauer, A., and Yamamoto, S. (1997) "Prediction of the preparative chromatography performance with a very small column" *J.Chromatogr.A* 760: 41-53.

Kaminski, M., Klawiter, J., and Kowalczyk, J. S. (1982) "Investigation of the relationship between packing methods and efficiency of preparative columns: II. Characteristics of the slurry method of packing chromatographic columns" *J.Chromatogr.A* 243: 225-244.

Kaminski, M. (1992) "Simple test for determination of the degree of distortion of the liquid-phase flow profile in columns for preparative liquid chromatography" *J.Chromatogr.* 589: 61-70.

Kasche, V., de Boer, M., Lazo, C., and Gad, M. (2003) "Direct observation of intraparticle equilibration and the rate-limiting step in adsorption of proteins in chromatographic adsorbents with confocal laser scanning microscopy" *J.Chromatogr.B* 790: 115-129.

Kates, M. (1986) "Techniques in Lipidology" in: "Laboratory Techniques in Biochemistry and Molecular Biology" van der Vliet, P.C. and Pillai, S. (eds.), Elsevier, New York, Vol. 2 Part 2.

Kearney, M. M., Peterson, K. R., Vervloet, T., and Munn, M. W., US Pat. 5354460 (1994).

Kelley, B. D., Jennings, P., Wright, P., and Briasco, C. (1997) "Demonstrating process robustness for chromatographic purification of a recombinant protein" *Biopharm* (October): 36-47.

Kelly, S. T. and Zydney, A. L. (1997) "Protein fouling during microfiltration: comparative behaviour of different proteins" *Biotechnol.Bioeng.* 55: 91-100.

Kim, H.-B., Hayashi, M., Nakatani, K., and Kitamura, N. (1996) "*In situ* measurements of ion-exchange processes in single polymer particles: laser trapping microscopy and confocal fluorescence microscopy" *Anal.Chem.* 68: 409-414.

Kirkup, L., Foot, M., and Mulholland, M. (2004) "Comparison of equations describing band broadening in high-performance liquid chromatography" *J.Chromatogr.A* 1030: 25-31.

Klawiter, J., Kaminski, M., and Kowalczyk, J. S. (1982) "Investigation of the relationship between packing methods and efficiency of preparative columns: I. Characteristics of the tamping method for preparative columns" *J.Chromatogr.A* 243: 207-224.

Klinkenberg, A. and Sjenitzer, F. (1956) "Holding-time distributions of the Gaussian type" *Chem.Eng.Sci.* 5: 258-270.

Kubin, M. (1965) "Beiag zur theorie der chromatographie" *Collection Czechoslav.Chem.Commun.* 30: 1104-1118.

Kucera, E. (1965) "Contribution to the theory of chromatography: linear non-equilibrium elution chromatography" *J.Chromatogr.* 19: 237-248.

Laca, A., Garcia, L. A., Argueso, F., and Diaz, M. (1999) "Protein diffusion in alginate beads monitored by confocal microscopy. The application of wavelets for data reconstruction and analysis" *J.Ind.Microbiol.Biotechnol.* 23: 155-165.

Larson, T. M., Davis, J., Lam, H., and Cacia, J. (2003) "Use of process data to assess chromatographic performance in production-scale protein purification columns" *Biotechnol.Bioeng.* 19: 486-492.

Lee, W.-C., Tsai, G.-L, and Tsao, G. T. (1993) "Analysis of chromatography by plate theory" *Sep.Technol.* 3: 178-197.

Lenhoff, A. M. and Lightfoot, E. N. (1987) "Significance and estimation of chromatographic parameters" *J.Chromatogr.A* 384: 285-299.

LePlang, M. and Charbol, D., US Pat. 5141635 (1992).

Levison, P. R., Koscielny, L. M., and Butts, E. T. (1990) "A simplified process for large-scale isolation of IgG from goat serum" *Bioseparation* 1: 59-67.

Levison, P. R., Badger, S. E., Jones, R. M. H., Toome, D. W., Streater, M., Pathirana, N. D., and Wheeler, S. (1995) "Validation studies in the regeneration of ion-exchange celluloses" *J.Chromatogr.A* 702: 59-68.

Levy, M. S., Collins, I. J., Yim, S. S., Ward, J. M., Titchener-Hooker, N. J., Ayazi Shamlou, P., and Dunnill, P. (1999) "Effect of shear on plasmid DNA in solution" *Bioprocess Eng.* 20: 7-13.

Li, Q., Grandmaison, E. W., Hsu, C. C., Taylor, D., and Goosen, M. F. A. (1995) "Interparticle and intraparticle mass transfer in chromatographic separation" *Bioseparation* 5: 189-202.

Li, W., Malik, A., and Lee, M. L. (1997) "Pressure drop effects in packed capillary column supercritical fluid chromatography" *J.Chromatogr.A* 758: 117-123.

Liapis, A. I. (1990) "Modeling affinity chromatography" *Sep.Purif.Methods* 19: 133-210.

Liapis, A. I., Grimes, B. A., Lacki, K., and Neretnieks, I. (2001) "Modeling and analysis of the dynamic behavior of mechanisms that result in the development of inner radial humps in the concentration of a single adsorbate in the adsorbed phase of porous adsorbent particles observed in confocal scanning laser microscopy experiments: diffusional mass transfer and adsorption in the presence of an electrical double layer" *J.Chromatogr.A* 921: 135-145.

Lightfoot, E. N., Coffman, J. L., Lode, F., Yuan, Q. S., Perkins, T. W., and Root, T. W. (1997) "Refining the description of protein chromatography" *J.Chromatogr.A* 760: 139-149.

Lightfoot, E. N., Moscariello, J. S., Teeters, M. A., and Root, T. W. (2003) "Mass Transfer and Fluid Mechanics" in: "Scale-up and Optimization in Preparative

Chromatography" Rathore, A. S and Velayudhan, A. (eds.), Marcel Dekker, Inc., New York, Chapter 2, pp. 33-75.

Linden, T., Ljunglof, A., Kula, M.-R., and Thommes, J. (1999) "Visualizing two-component protein diffusion in porous adsorbents by confocal scanning laser microscopy" *Biotechnol.Bioeng.* 65: 622-630.

Linden, T., Ljunglof, A., Hagel, L., Kula, M.-R., and Thommes, J. (2002) "Visualizing patterns of protein uptake to porous media using confocal scanning laser microscopy" *Sep.Sci.Technol.* 37: 1-32.

Ljunglof, A. and Hjorth, R. (1996) "Confocal microscopy as a tool for studying protein adsorption to chromatographic matrices" *J.Chromatogr.A* 743: 75-83.

Ljunglof, A. and Thommes, J. (1998) "Visualising intraparticle protein transport in porous adsorbents by confocal microscopy" *J.Chromatogr.A* 813: 387-395.

Ljunglof, A., Bergvall, P., Bhikhabhai, R., and Hjorth, R. (1999) "Direct visualisation of plasmid DNA in individual chromatography adsorbent particles by confocal scanning laser microscopy" *J.Chromatogr.A* 844: 129-135.

Ljunglof, A., Larsson, M., Knuuttila, K.-G., and Lingren, J. (2000) "Measurement of ligand distribution in individual adsorbent particles using confocal scanning laser microscopy and confocal micro-Raman spectroscopy" *J.Chromatogr.A* 893: 235-244.

Ljunglof, A. (2002) "Direct observation of biomolecule adsorption and spatial distribution of functional groups in chromatographic adsorbent particles" PhD Thesis. Uppsala University, Sweden.

Maa, Y-F. and Hsu, C. C. (1998) "Investigation of fouling mechanisms for recombinant human growth hormone sterile filtration" *J.Pharm.Sci* 87: 808-812.

Malmsten, M., Xing, K., and Ljunglof, A. (1999) "Confocal microscopy studies of trypsin immobilization on porous glycidyl methacrylate beads" *J.Colloid Interface Sci.* 220: 436-442.

Mao, Q. M., Prince, I. G., and Hearn, M. T. W. (1995) "High-performance liquid chromatography of amino acids, peptides and proteins CXXXIX. Impact of operating parameters in large-scale chromatography of proteins" *J.Chromatogr.A* 691: 273-283.

Martin, A. J. P. and Synge, R. L. H. (1941) "A new form of chromatogram employing 2 liquid phases" *Biochem.J.* 35: 1358-1368.

Martin, M. and Guiochon, G. (2005) "Effects of high pressure in liquid chromatography" *J.Chromatogr.A* 1090: 16-38.

Master, B. R. (ed.) (1996) "Selected Papers on Confocal Microscopy" The International Society for Optical Engineering, Washington.

Mazzotti, M., Storti, G., and Morbidelli, M. (1994) "Shock layer analysis in multicomponent chromatography and countercurrent adsorption" *Chem.Eng.Sci.* 49: 1337-1355.

McCoy, M. A. and Liapis, A. I. (1991) "Evaluation of kinetic models for biospecific adsorption and its implications for finite bath and column performance" *J.Chromatogr.* 548: 25-60.

McNeil, R. J., US Pat. 4354932 (1982).

McQuarrie, D. A. (1963) "On the stochastic theory of chromatography" *J.Chem.Phys.* 38: 437-445.

Meyers, J. J. and Liapis, A. I. (1998) "Network modeling of the intraparticle convection and diffusion of molecules in porous particles packed in a chromatographic column" *J.Chromatogr.A* 827: 197-213.

Mihelic, I., Nemec, D., Podgornik, A., and Koloini, T. (2005) "Pressure drop in CIM disk monolithic columns" *J.Chromatogr.A* 1065: 59-67.

Ming, F. and Howell, J. A. (1993) "Parameter estimation for a column adsorption model incorporating axial dispersion - application to a novel monolithic ion-exchange column" *Trans.Inst.Chem.Engrs.* 71: 267-272.

Minsky, M., US Pat. 3,013,467 (1961).

Minsky, M. (1988) "Memoir on inventing the confocal scanning microscope" *Scanning* 10: 128-138.

Mohammad, A. W., Stevenson, D. G., and Wankat, P. C. (1992) "Pressure drop correlations and scale-up of size exclusion chromatography with compressible packings" *Ind.Eng.Chem.Res.* 31: 549-561.

Morbidelli, M., Servida, A., Storti, G., and Carra, S. (1982) "Simulation of multicomponent adsorption beds. Model analysis and numerical solution" *Ind.Eng.Chem.Fundamen.* 21: 123-131.

Moscariello, J. S., Purdom, G., Coffman, J., Root, T. W., and Lightfoot, E. N. (2001) "Characterizing the performance of industrial-scale columns" *J.Chromatogr.A* 908: 131-141.

Mott, L. H., US Pat. 4399032 (1983).

Mujumdar, R. B., Ernst, L. A., Mujumdar, S. R., Lewis, C. J., and Waggoner, A. S. (1993) "Cyanine dye labelling reagents: sulfoindocyanine succinimidyl esters" *Bioconjugate Chem.* 4: 105-111.

Munk, M. N., US Pat. 4457846 (1984).

Nordstrom, T., Senkas, A., Eriksson, S., Pontynen, N., Nordstrom, E., and Lindqvist, C. (1999) "Generation of a new protein purification matrix by loading ceramic hydroxyapatite with metal ions - demonstration with poly-histidine tagged green fluorescent protein" *J.Biotechnol.* 69: 125-133.

O'Leary, R. M., Feuerhelm, D., Peers, D., Xu, Y., and Blank, G. S. (2001) "Determining the useful lifetime of chromatography resins" *Biopharm* (September): 10-18.

Ohashi, H., Sugawa, T., Kikuchi, K.-I., and Konno, H. (1981) "Correlation of liquid-side mass-transfer coefficient for single particles and fixed beds" *J.Chem.Eng.Japan* 14: 433-438.

Pampel, L. W. (2002) "A scale-down study of process sequences for the recovery of proteins from transgenic milk" PhD Thesis. University of London, UK.

Pawley, J. B. (ed.) (1995) "Handbook of Biological Confocal Microscopy" Plenum Press, New York.

PDA (1992) "Technical Report No. 14: Industry Perspective on the validation of column-based separation processes for the purification of proteins" *PDA Journal of Pharmaceutical Science and Technology* 46 (Supplement): S1-S11.

Pessela, B. C. C., Torres, R., Fuentes, M., Mateo, C., Munilla, R., Vian, A., Carrascosa, A. V., Garcia, J. L., Guisan, J. M., and Fernandez-Lafuente, R. (2004) "Selective and mild adsorption of large proteins on lowly activated immobilized metal ion affinity chromatography matrices. Purification of multimeric thermophilic enzymes overexpressed in *Escherichia coli*" *J.Chromatogr.A* 1055: 93-98.

Pirotta, M. (1985) "Ion-Exchange Resins and Adsorbents in the Extraction of Antibiotics" in: "Discovery and Isolation of Microbial Products" Verrall, M. S. (ed.), Ellis Horwood Ltd., Chichester, UK, pp. 98-114.

Poppe, H. (1980) "Characterization and design of liquid phase flow-through detector systems" *Anal.Chim.Acta* 114: 59-70.

Prazeres, D. M. F., Schluep, T., and Cooney, C. (1998) "Preparative purification of supercoiled plasmid DNA using anion-exchange chromatography" *J.Chromatogr.A* 806: 31-45.

Rathore, A. S, Kennedy, R M., O'Donnell, J. K., Bemberis, I., and Kaltenbrunner, O. (2003) "Qualification of a chromatographic column: why and how we do it" *Biopharm International* (March): 30-40.

Reed, F. and Flanigan, P. (2001) "Therapeutic monoclonal antibody industry overview" Adams, Harkness and Hill, Boston.

Rober L.Fahrner and Gregory S.Blank (1999) "Real-time monitoring of recombinant antibody breakthrough during Protein A affinity chromatography" *Biotechnol.Appl.Biochem.* 29: 109-112.

Rock, C., Shamlou, P. A., and Levy, M. S. (2003) "An automated microplate-based method for monitoring DNA strand breaks in plasmid and bacterial artificial chromosomes" *Nucleic Acids Res.* 31: e65-e65(1).

Roos, N. and Morgan, A. J. (1990) "Cryopreparation of Thin Biological Specimens for Electron Microscopy: Methods and Applications" Oxford University Press, Oxford, pp 1-8.

Roper, D. K. and Lightfoot, E. N. (1995) "Estimating plate heights in stacked-membrane chromatography by flow reversal" *J.Chromatogr.A* 702: 69-80.

Ruthven, D. M. (1984) "Principles of adsorption and adsorption processes" John Wiley & Sons, New York, pp. 166-205.

Sambrook, J. and Russell, D. W. (2001) "Molecular Cloning: A Laboratory Manual" Cold Spring Harbor Laboratory Press, New York, 3rd edition.

Saxena, V. and Andresen, B. D., US Pat. 4865729 (1989).

Saxena, V. and Young, P., US Pat. 5462659 (1995).

Scheider, P. and Smith, J. M. (1968) "Adsorption rate constants from chromatography" *AIChE J.* 14: 763-771.

Schmid, I., Krall, W. J., Uittenbogaart, C. H., Braun, J., and Giorgi, J. V. (1992) "Dead cell discrimination with 7-amino-actinomycin-D in combination with dual color immunofluorescence in single laser flow cytometry" *Cytometry* 13: 204-208.

Seely, R. J., Hutchins, H. V., Luscher, M. P., Sniff, K. S., and Hassler, R. (1999) "Defining critical variables in well-characterised biotechnology processes" *Biopharm* (April): 33-36.

Shaeiwitz, J. A., Blair, J. B., and Ruaan, R. C. (1989) "Evidence that yeast cell wall debris can separate proteins by ion-exchange during cell lysis" *Biotechnol.Bioeng.* 34: 137-140.

Shalliker, R. A., Broyles, B. S., and Guiochon, G. (1999) "Visualisation of sample introduction in liquid chromatographic columns. Contribution of a flow distributor on the sample band shape" *J.Chromatogr.A* 865: 83-95.

Shalliker, R. A., Broyles, B. S., and Guiochon, G. (2000a) "On-column visualization of sample migration in liquid chromatography" *Anal.Chem.* 72: 323-332.

Shalliker, R. A., Broyles, B. S., and Guiochon, G. (2000b) "Physical evidence of two wall effects in liquid chromatography" *J.Chromatogr.A* 888: 1-12.

Shalliker, R. A., Broyles, B. S., and Guiochon, G. (2003) "Axial and radial diffusion coefficients in a liquid chromatography column and bed heterogeneity" *J.Chromatogr.A* 994: 1-12.

Shepard, S. R., Brickman-Stone, C., Schrimsher, J. L., and Koch, G. (2000) "Discoloration of ceramic hydroxyapatite used for protein chromatography" *J.Chromatogr.A* 891: 93-98.

Sheppard, C. J. R. and Shotton, D. M. (1997) "Confocal Laser Scanning Microscopy" BIOS Scientific Publishers, Oxford.

Singer, V. L., Jones, L. J., Yue, S. T., and Haugland, R. P. (1997) "Characterisation of PicoGreen reagent and development of a fluorescence-based solution assay for double stranded DNA quantification" *Anal.Biochem.* 249: 228-233.

Slattery, J. C. (1999) "Advanced Transport Phenomena" Cambridge University Press, Cambridge.

Smith, M. P., Bulmer, M. A., Hjorth, R., and Titchener-Hooker, N. J. (2002) "Hydrophobic interaction ligand selection and scale-up of an expanded bed separation of an intracellular enzyme from *Saccharomyces cerevisiae*" *J.Chromatogr.A* 968: 121-128.

Sofer, G. K. (1987) "Increasing media lifetime for cost-effective chromatography" *Bio/Technology* 5: 341-342.

Sofer, G. K. and Hagel, L. (1997) "Handbook of Process Chromatography: A Guide to Optimization, Scale-up and Validation" Academic Press, London, pp 132-171.

Song, L., Hennink, E. J., Young, I. T., and Tanke, H. J. (1995) "Photobleaching kinetics of fluorescein in quantitative fluorescence microscopy" *Biophys.J.* 68: 2588-2600.

Song, L., Varma, C. A., Verhoeven, J. W., and Tanke, H. J. (1996) "Influence of the triplet excited state on the photobleaching kinetics of fluorescein in microscopy" *Biophys.J.* 70: 2959-2968.

Staby, A., Jonasen, N., Wahlstom, H., and Mollerup, I. (1998) "Comparison of loading capacities of various proteins and peptides in culture medium and in pure state" *J.Chromatogr.A* 827: 311-318.

Sternberg, J. C. (1966) "Extra Column Contributions to Chromatographic Band Broadening" in: "Advances in Chromatography, Volume 2" Giddings, J. C. and Keller, R. A. (eds.) Marcel Dekker, New York, pp. 205-270.

Stewart, P. S. (1998) "A review of experimental measurements of effective diffusive permeabilities and effective diffusion coefficients in biofilms" *Biotechnol.Bioeng.* 59: 262-271.

Stickel, J. J. and Fotopoulos, A. (2001) "Pressure-flow relationships for packed beds of compressible chromatography media at laboratory and production scale" *Biotechnol.Prog.* 17: 744-751.

Storey, S. A. (2000) "Physical property indices to aid bioprocess synthesis and design" PhD Thesis. University of London, UK.

Suen, R.-B., Lin, S.-C., and Hsu, W.-H. (2004) "Hydroxyapatite-based immobilized metal affinity adsorbents for protein purification" *J.Chromatogr.A* 1048: 31-39.

Tallarek, U., Baumeister, E., Albert, K., Bayer, E., and Guiochon, G. (1995) "NMR imaging of the chromatographic process. Migration and separation of bands of gadolinium chelates" *J.Chromatogr.A* 696: 1-18.

Tallarek, U., Bayer, E., and Guiochon, G. (1998) "Study of dispersion in packed chromatography columns by pulsed field gradient nuclear magnetic resonance" *J.Am.Chem.Soc.* 120: 1494-1505.

Taylor, G. (1953) "Dispersion of soluble matter in solvent flowing slowly through a tube" *Proc.Roy.Soc.London, Ser.A* 219: 186-203.

Teeters, M. A., Root, T. W., and Lightfoot, E. N. (2002) "Performance and scale-up of adsorptive membrane chromatography" *J.Chromatogr.A* 944: 129-139.

Teo, W. K. and Ruthven, D. M. (1986) "Adsorption of water from aqueous ethanol using 3-A molecular sieves" *Ind.Eng.Chem.Process Des.Dev.* 25: 17-21.

Tice, P. A., Mazsaroff, I., Lin, N. T., and Regnier, F. E. (1987) "Effects of large sample loads on column lifetime in preparative-scale liquid chromatography" *J.Chromatogr.A* 410: 43-51.

van Buel, M. J., van der Wielen, L. A. M., and Luyben, K. Ch. A. M. (1997) "Pressure drop in centrifugal partition chromatography" *J.Chromatogr.A* 773: 1-12.

van Deemter, J J., Zuiderweg, F. J., and Klinkenberg, A. (1956) "Longitudinal diffusion and resistance to mass transfer as causes of non-ideality in chromatography" *J.Chem.Eng.Sci.* 5: 271-289.

Vervoot, N., Gzil, P., Baron, G. V., and Desmet, G. (2003) "A correlation for the pressure drop in monolithic silica columns" *Anal.Chem.* 75: 843-850.

Vervoot, N., Gzil, P., Baron, G. V., and Desmet, G. (2004) "Model column structure for the analysis of the flow and band-broadening characteristics of silica monoliths" *J.Chromatogr.A* 1030: 177-186.

Viloria-Cols, M. E., Hatti-Kaul, R., and Mattiasson, B. (2004) "Agarose-coated anion exchanger prevents cell-adsorbent interactions" *J.Chromatogr.A* 1043: 195-200.

Volkov, S. A., Reznikov, V. I., Smirnov, V. I., Zel'vensky, U. Yu., Rinkevichus, B. S., Sakodynsky, K. I., and Frolov, F. Ya. (1977) "Investigation of the fluid dynamics of gas flow in large-diameter columns" *J.Chromatogr.A* 156: 225-232.

Walsh, G. (2003) "Biopharmaceuticals: Biochemistry and Biotechnology" John Wiley & Sons Ltd., Chichester, 2nd edition.

Weaver, L. E. and Carta, G. (1996) "Protein adsorption on cation exchangers: comparison of macroporous and gel-composition media" *Biotechnol.Prog.* 12: 342-355.

Williams, A., Taylor, K., Dambuleff, K., Persson, O., and Kennedy, R M. (2002) "Maintenance of column performance at scale" *J.Chromatogr.A* 944: 69-75.

Wilson, T. (ed.) (1990) "Confocal Microscopy" Academic Press Inc., San Diego.

Wyllie, A. H., Kerr, J. K. R., and Currie, A. R. (1980) "Cell death: the significance of apoptosis" *Int.Rev.Cytol.* 68: 251-305.

Yaintsios, S. G. and Karabelas, A. J. (1998) "The effect of colloid stability on membrane fouling" *Desalination* 118: 143-152.

Yuan, Q. S., Rosenfeld, A., Root, T. W., Klingenberg, D. J., and Lightfoot, E. N. (1999) "Flow distribution in chromatographic columns" *J.Chromatogr.A* 831: 149-165.

Yun, T. and Guiochon, G. (1994) "Modeling of radial heterogeneity in chromatographic columns. Columns with cylindrical symmetry and ideal model" *J.Chromatogr.A* 672: 1-10.

Yun, T. and Guiochon, G. (1996) "Modeling of radial heterogeneity in chromatographic columns II. Separation of a two-component mixture on a column with cylindrical symmetry" *J.Chromatogr.*A 734: 97-103.